Indice

ALLEGATI

Allegato I

Mauro M, Crosera M, Bianco C, Adami G, Montini T, Fornasiero P, Jaganjac M, Bovenzi M, Filon FL. Permeation of platinum and rhodium nanoparticles through intact and damaged human skin. J Nanopart Res (2015) 17:253.

Allegato II

Crosera M, Prodi A, Mauro M, Pelin M, Florio C, Bellomo F, Adami G, Apostoli P, De Palma G, Bovenzi M, Campanini M, Filon FL. Titanium Dioxide Nanoparticle Penetration into the Skin and Effects on HaCaT Cells. Int J Environ Res Public Health. 2015 Aug 7; 12 (8):9282-97.

Allegato III

Mauro M, Crosera M, Pelin M, Florio C, Bellomo F, Adami G, Apostoli P, De Palma G, Bovenzi M, Campanini M, Filon FL. Cobalt Oxide Nanoparticles: Behavior towards Intact and Impaired Human Skin and Keratinocytes Toxicity. Int J Environ Res Public Health. 2015 Jul 17; 12 (7):8263-80.

Allegato IV

Crosera M, Adami G, Mauro M, Bovenzi M, Baracchini E, Larese Filon F. In vitro dermal penetration of nickel nanoparticles. Chemosphere 145 (2016) 301e306.

Allegato V

Mauro M, Crosera M, Bianco C, Bellomo F, Bovenzi M, Adami G, Larese Filon F. In vitro permeability of silver nanoparticles through porcine oromucosal membrane. Colloids Surf. B Biointerfaces. 2015 Aug 1; 132:10-6.

Allegato VI

Mauro M, Crosera M, Bovenzi M, Adami G, Larese Filon F. In vitro Silver Nanoparticles permeation trough Meningeal membrane – pilot study. To be submitted to International Journal of Nanomedicine

Allegato VII

Larese Filon F, Mauro M, Adami G, Bovenzi M, Crosera M. Nanoparticles skin absorption: New aspects for a safety profile evaluation. Regul Toxicol Pharmacol. 2015 Jul;72(2):310-22.

RIASSUNTO

L'utilizzo di nanomateriali, ovvero una nuova classe di sostanze composte da particelle ultrafini con dimensioni comprese fra 1 e 100 nm (American Society for Testing Materials - ASTM), è in costante aumento a livello globale. La particolarità di tali sostanze è rappresentata da un alto rapporto tra la superficie e il volume delle particelle, che determina caratteristiche chimico-fisiche completamente differenti rispetto alle omologhe macrosostanze di riferimento. Tali caratteristiche sono tali da imporre una loro classificazione come nuovi agenti chimici (Royal Society & Royal Academy of Engineering report 2004). Gli impieghi attuali dei nanomateriali risultano in continua evoluzione, spaziando in diversi ambiti, dall'industria farmaceutica e cosmetica, all'industria tessile, elettronica, aerospaziale ed informatica. Diversi sono anche gli impieghi in campo biomedico; tra questi la diagnostica e la farmacoterapia. È quindi prevedibile che in futuro una quota sempre maggiore di lavoratori e consumatori risulteranno esposti a tali sostanze.

Allo stato attuale non vi è una completa conoscenza degli effetti tossicologici ed ambientali di queste sostanze, pertanto, al fine di un loro utilizzo in totale sicurezza, risulta necessario capirne meglio l'impatto sulla salute, le vie di penetrazione nel corpo umano e il rischio per i lavoratori conseguente al loro utilizzo o lavorazione.

La cute rappresenta la prima barriera nei confronti delle sostanze tossiche che possono entrare in contatto con l'organismo umano. Successivamente agli anni '60, quando si riteneva che la cute rappresentasse una barriera totalmente impermeabile, è stato dimostrato come essa presenti differenti gradi di permeabilità nei confronti di alcuni xenobiotici, dipendente dalle caratteristiche delle sostanze in esame, dal sito anatomico di penetrazione, dal grado di integrità della barriera stessa e dall'eventuale presenza di patologie della cute.

La mucosa del cavo orale funge da primo filtro nei confronti delle sostanze che entrano in contatto con il tratto digestivo e può venir coinvolta in contaminazioni di superficie

determinate da esposizioni occupazionali e/o ambientali. È noto che, rispetto alla cute, presenti una permeabilità all'acqua quattro volte maggiore, e, per tale motivo, è stata studiata come via di somministrazione di farmaci, ma, ad oggi, pochi sono gli studi che ne hanno valutato le caratteristiche di permeazione nei confronti delle nanoparticelle (NPs). Una terza importante barriera biologica è quella che ricopre il sistema nervoso centrale, essa è rappresentata da tre foglietti di tessuto connettivo, che assieme costituiscono le meningi. Questi tre foglietti rivestono completamente l'encefalo permettendone un isolamento, tradizionalmente ritenuto completo, nei confronti degli xenobiotici. L'unica via di assorbimento diretto, in questo contesto, è rappresentata dalla via intranasale. Essa permette un passaggio diretto di sostanze dall'epitelio olfattivo all'encefalo, eludendo la selettiva barriera emato-encefalica.

Negli ultimi anni la letteratura scientifica si è arricchita di studi che hanno indagato le caratteristiche di assorbimento di farmaci attraverso questa via, ma pochissimi sono gli studi che hanno indagato la possibile penetrazione di nanoparticelle attraverso questa via, e nessuno, in particolar modo, ha indagato le caratteristiche di permeazione delle meningi.

L'attività di ricerca svolta nell'ambito del presente dottorato ha avuto per finalità l'indagine delle caratteristiche di permeabilità e di assorbimento della cute, della mucosa del cavo orale e delle meningi nei confronti di alcune nanoparticelle, scelte fra quelle più rappresentative in relazione alla diffusione d'utilizzo a livello globale. I risultati degli esperimenti condotti hanno dimostrato, in vitro, che l'esposizione cutanea a Pt, Rh, Co_3O_4 e Ni NPs determinano permeazione in tracce dei medesimi metalli attraverso la cute, mentre per le TiO_2 NPs tale permeazione non è stata dimostrata. È stato riscontrato, inoltre, che la mucosa del cavo orale e le meningi sono permeabili nei confronti dell'Ag in forma nanoparticellare.

Parole chiave: Nanoparticelle, permeazione cutanea, mucosa orale, meningi, *in vitro*, Franz Cells.

ABSTRACT

The use of nanomaterials, which is a new class of compounds composed of ultrafine particles with dimensions between 1 and 100 nm (American Society for Testing Materials - ASTM), is globally steadily increasing. The peculiarity of such substances is represented by a high ratio between the surface and the volume of the particles, which determines chemical and physical characteristics completely different compared to the homologous bulk materials. These characteristics are such as to require classification as new chemicals (Royal Society & Royal Academy of Engineering report 2004). Existing uses of nanomaterials are evolving, ranging in various fields, from the pharmaceutical, cosmetic and textile industry, electronics, aerospace and information technology. Several are also the applications in the biomedical field, including diagnostics and pharmacotherapy. It is therefore expected that in the future, an increasing proportion of workers and consumers will be exposed to these substances.

Nowadays there is a lack in the full understanding of the environmental and toxicological effects of these substances, therefore, in order to use them in a safe way, it is necessary to better understand the impact on health, the way of entry into the human body and the risk for workers following their use or processing.

The skin is the first barrier against toxic substances that may come into contact with the human body. After the ‘60, when it was believed that the skin represented a totally waterproof barrier, it has been proven that it present different degrees of permeability towards some xenobiotic, depending on the characteristics of the tested substances, the anatomical site of penetration, the degree of barrier integrity and the possible presence of skin disorders.

The oral mucosa acts as a first filter against the substances that come into contact with the digestive tract and may be involved in surface contamination caused by occupational and/or environmental exposure. It is known that, compared to the skin, it present a permeability to

water 4 times greater, and, for this reason, it has been studied as a way for drug administration, but, to date, there are few studies that evaluated the characteristics of permeation against nanoparticles (NPs). A third important biological barrier is the one which ensheath the central nervous system, which is represented by three sheets of connective tissue, that together form the meninges. These three sheets cover completely the brain allowing isolation, which is traditionally believed to be complete towards xenobiotics. The only way of direct absorption, in this context, is represented by the intranasal pathway, allowing a direct passage from the olfactory epithelium to the brain, bypassing the selective blood-brain barrier. In recent years, the scientific literature has been enriched by studies that have investigated the absorption characteristics of drugs by this route, but very few studies investigated the possible penetration of nanoparticles through this path, and no one in particular, has investigated the permeation characteristics of the meninges.

The research carried out during this PhD has had for objective the investigation of the permeability characteristics and absorption of the skin, the oral mucosa and the meninges against some NPs, chosen among the most representative in relation the spread of globally use.

The results of the experiments conducted have shown, in vitro, that dermal exposures to Pt, Rh, Ni and Co_3O_4 NPs determine traces of permeation of such metals through the skin, while the permeation for TiO_2 NPs was not demonstrated. It has been found, moreover, that the oral mucosa and the meninges are permeable towards Ag NPs.

Keywords: Nanoparticles, skin permeation, oral mucosa, meninges, in vitro Franz Cells.

1. SCOPI DELLA RICERCA

Il progetto di ricerca aveva per finalità l'indagine delle caratteristiche di permeazione in vitro di tre membrane biologiche (la cute, la mucosa del cavo orale e le meningi) nei confronti di nanoparticelle metalliche. Le nanoparticelle testate sono state scelte in base a quelle maggiormente diffuse ed utilizzate in ambiente occupazionale e in prodotti di consumo; tra queste le nanoparticelle di argento (AgNPs), biossido di titanio (TiO_2), nichel (NiNPs), platino e rodio (PtNPs, RhNPs) ed ossido di cobalto (Co_3O_4). La stima di un potenziale assorbimento percutaneo, transmucoso e transmeningeo risulta importante nell'ottica di una valutazione completa dei rischi derivanti da esposizione a sostanze tossiche, a complemento delle conoscenze riguardanti le vie classiche di esposizione, quali quella inalatoria e digestiva. In quest'ottica in molti Paesi i test in vitro vengono comunemente inclusi nei criteri per poter formulare la *skin notation* ai composti chimici (Drexler, 1998), ed è comune l'utilizzo dei test di permeazione per definire le caratteristiche di diffusione e la biodisponibilità di xenobiotici presenti in ambito occupazionale, cosmetico e farmaceutico.

L'apparato sperimentale utilizzato è stato quello delle celle di diffusione di Franz (Franz 1975), descritto dettagliatamente in seguito. Per gli studi inerenti la cute è stato applicato un protocollo standardizzato e sviluppato dal programma europeo EDETOX 2000 (Evaluations and predictions of DErmal absorption of TOXic chemicals) in grado di valutare la presenza di NPs a livello cutaneo ed il loro passaggio attraverso la cute, mentre per le altre due membrane biologiche il protocollo è stato parzialmente modificato in particolar modo per i tempi di esposizione, verosimilmente inferiori, a carico di queste membrane biologiche.

2. INTRODUZIONE

2.1 Nanoparticelle ed assorbimento attraverso membrane biologiche (Allegato IV)

La comunità scientifica è discorde in merito ad un potenziale assorbimento di NPs attraverso le membrane biologiche. Le potenziali vie di penetrazione descritte, simili per quanto concerne la cute, la mucosa del cavo orale ed per le meningi, sono rappresentate dalla via intercellulare, usualmente più importante, e da quella intracellulare. La penetrazione può inoltre avvenire attraverso gli annessi cutanei, quali i follicoli piliferi, le ghiandole sudoripare e sebacee per quanto riguarda la cute (Scheuplein 1967, Lademann 2009), mentre per le meningi la via intracellulare comprende sia il passaggio attraverso le cellule dell'epitelio olfattivo sia attraverso i neuroni del nervo olfattorio, rappresentando, di fatto, un trasporto trans-sinaptico. La complessità nell'analisi dell'assorbimento di NPs risiede nel fatto che i fattori che devono essere presi in considerazione riguardano sia le caratteristiche intrinseche delle NPs sia le loro capacità di interazione con i fluidi biologici. Fra le caratteristiche intrinseche una delle più significative è rappresentata dal diametro nanoparticellare, poiché rappresenta il primo discriminante nella capacità, da parte delle NPs, di poter essere endocitate all'intero delle cellule o di poter attraversare le tight junctions della via paracellulare. A questa caratteristica vanno tuttavia associate la carica di superficie, la capacità di dissoluzione nei fluidi biologici, e quindi di rilasciare ioni, la tendenza a formare aggregati, anche con le proteine. Ognuno di questi aspetti varia a seconda della NP studiata e dalle caratteristiche di integrità della membrana biologica in esame. È noto infatti che una membrana danneggiata presenta una discontinuità di barriera potenzialmente pericolosa. Questa condizione si può facilmente verificare sulla cute e sulla mucosa del cavo orale a seguito di insulti meccanici, fisici, chimici, o biologici, mentre a carico delle meningi generalmente a causa di patologie sistemiche, quali ad esempio ipertensione o meningo-encefaliti, in grado di danneggiare i normali meccanismi di barriera.

È quindi importante analizzare in maniera dettagliata la struttura anatomica di queste tre membrane e le differenze fra esse, di modo da comprenderne le differenze e le peculiarità.

2.2 Struttura anatomica e funzioni della cute

La cute è l'organo più esteso del corpo umano; svolge svariate funzioni, fra le quali la più rilevante è quella di barriera anatomica contro potenziali patogeni ed eventuali agenti nocivi, costituendo, di fatto, la prima linea di difesa dell'organismo contro le aggressioni esterne; ha un ruolo importante nel mantenimento dell'omeostasi fisiologica, prevenendo la disidratazione attraverso la regolazione della perspirazione e attraverso la termoregolazione, che permette di mantenere un' idonea temperatura corporea. La cute è anche in grado di sintetizzare molecole (ad esempio la vitamina D) e di metabolizzare composti già assorbiti facilitando l'eliminazione di prodotti di scarto. Nella cute sono anche presenti molte ghiandole sebacee e sudoripare. Le prime secernono sebo, una mistura di lipidi con funzione antibatterica, mentre le seconde producono una secrezione contenente ferormoni. Anatomicamente, la cute è costituita da due strati principali, uno più superficiale, stratificato ed avascolare, chiamato epidermide di spessore complessivo di circa 0,05- 0,1 mm, ed uno sottostante, denominato derma, di spessore 0,3-3 mm, costituito prevalentemente da collagene e contenente i vasi sanguigni e linfatici.

2.2.1 L'epidermide

L'epidermide è costituita per il 95% da cheratinociti, che formano un epitelio pavimentoso pluristratificato cheratinizzato (che subisce una proliferazione ed una differenziazione continua e programmata) e per la rimanente percentuale dai melanociti, dalle cellule di Langherans e dalle cellule di Merkel. Dallo strato più profondo a quello più superficiale

distinguiamo: lo strato basale, lo strato spinoso, lo strato granuloso, lo strato lucido e lo strato corneo (Figura 1.)

Lo strato basale è costituito da un monostrato di cellule cilindriche o cubiche, adese fra loro e alle sovrastanti cellule dello strato spinoso tramite desmosomi ed alla membrana basale sottostante tramite emidesmosomi. I desmosomi sono delle giunzioni proteiche fra cellule, che ancorano fra loro i filamenti intermedi dei citoscheletri cellulari. Gli emidesmosomi invece sono costituiti da placche proteiche che ancorano i filamenti intermedi delle cellule alla matrice extracellulare della lamina basale.

Le cellule dello strato basale assolvono alla principale funzione di produzione dei componenti della lamina basale, e funzionano anche cellule staminali, dalla cui proliferazione e differenziazione derivano i cheratinociti degli strati superiori. Nelle prime fasi del loro ciclo queste cellule sono anche in grado di sintetizzare cheratina, che poi viene assemblata per costituire i tonofilamenti.

Altre cellule presenti in questo strato, seppur in minore quantità, sono le cellule di Merkel, particolari tipi di meccanocettori, ed i melanociti, deputati alla protezione della cute dai raggi UV tramite la produzione e secrezione di melanina.

Lo strato spinoso è situato subito al di sopra dello strato basale ed è costituito da un pluristrato di cellule poliedriche di forma irregolare. Le cellule adiacenti sono connesse tramite “tight junctions”, mentre la connessione con il sottostante strato basale è garantito dai desmosomi. In questo strato i cheratinociti cominciano a maturare e ad assemblare al loro interno i tonofilamenti. Quando migrando raggiungono la porzione superiore dello strato dove iniziano a produrre degli elementi caratteristici, i granuli di cheratoialina ed i corpi lamellari da cui cominciano ad assemblare i tonofilamenti.

Lo strato granuloso è costituito da cellule appiattite, contenenti i granuli precursori della filaggrina, sostanza responsabile dell’aggregazione dei filamenti di cheratina nei corneociti

dello strato corneo. Dalla fusione di questi granuli con la membrana cellulare deriva la dispersione del loro contenuto nello spazio intercellulare, contenente anche la componente lipidica intercellulare dello strato corneo.

In alcune aree del corpo**,** sottoposte a particolari sollecitazioni meccaniche, quali il palmo della mano e la pianta dei piedi, esiste anche un ulteriore sottile strato, chiamato strato lucido e fondamentalmente costituito da cellule cheratinizzate che contengono un fluido viscoso simile alla cheratina, chiamata eleidina.

Lo strato corneo è lo strato più superficiale ed è formato da corneociti poligonali di aspetto lamellare, embricati fra loro in pile multicellulari, privi di nucleo e con citoplasma ripieno di filaggrina e di fibre cheratiniche, rivestiti all'esterno da un involucro rigido. Ogni cellula è incorporata in una matrice lipidica extracellulare prodotta dai granuli lamellari, ed assieme rappresentano la così detta struttura "mattoni e malta" ("brick and mortar structure") dove i corneociti non vitali costituiscono i mattoni e i lipidi intercellulari rappresentano la malta (Elias PM 1983, Elias PM 2010). Questo strato rappresenta la principale barriera anatomica responsabile della modulazione dell'assorbimento di sostanze chimiche, farmaci e particelle all'interno della cute (Monteiro-Riviere 2006, 2010), e può variare in spessore a seconda della regione cutanea ed in funzione della specie (Monetiro-Riviere 1990).

2.2.2 Il derma

Il derma è costituito da un denso tessuto connettivo costituito da collagene, elastina e fibre reticolari nella quale sono immersi una fitta rete di capillari, vasi linfatici e terminazioni nervose. La funzione principale è quella di nutrire e supportare l'epidermide, e di permettere l'assorbimento e lo scambio di metaboliti fra la cute ed il sangue. È suddiviso in due strati, uno più superficiale, definito derma papillare, che contiene collagene di tipo I e III e fibre

elastiche organizzate in modo irregolare, vasi sanguigni, linfatici e terminazioni nervose, è uno strato sottostante, definito derma reticolare, decisamente più spesso e costituito da fibre collagene di tipo I, fibre elastiche e poche cellule (Monteiro-Riviere, 2006). Le cellule maggiormente rappresentate nel derma sono i fibroblasti, seguiti dalle mast cells e dai macrofagi ed adipociti.

2.2.3. L'ipoderma

Sotto il derma è presente uno strato di tessuto adiposo chiamato sottocutaneo, che connette la cute ai tessuti sottostanti, ha funzione isolante per l'organismo. È costituito da tessuto connettivo contenente fibre collagene ed elastina, nella quale sono immersi gli adipociti.

2.2.4. Appendici cutanee

Sono rappresentate dai follicoli piliferi, dalle ghiandole sebacee associate, dai muscoli erettori dei peli e dalle ghiandole sudoripare. In particolare dai follicoli piliferi vengono prodotte le strutture cheratinizzate che comunemente chiamiamo peli, e che si portano verso l'ambiente esterno dall'invaginazione dell'epidermide da cui derivano. Le invaginazioni possono raggiugere lo strato del derma o a volte anche quello più profondo dell'ipoderma, dove risultano ancorate tramite tessuto connettivo ai muscoli erettori dei peli, che, in seguito a contrazione determinano l'erezione del pelo e favoriscono lo svuotamento del sebo prodotto dalle ghiandole sebacee all'interno del canale del follicolo pilifero. I follicoli piliferi possono contribuire in modo significativo all'assorbimento transcutaneo (Monteiro-Riviere, 2004), per quanto l'iniziale permeazione al loro interno richieda comunque l'attraversamento dello strato corneo.

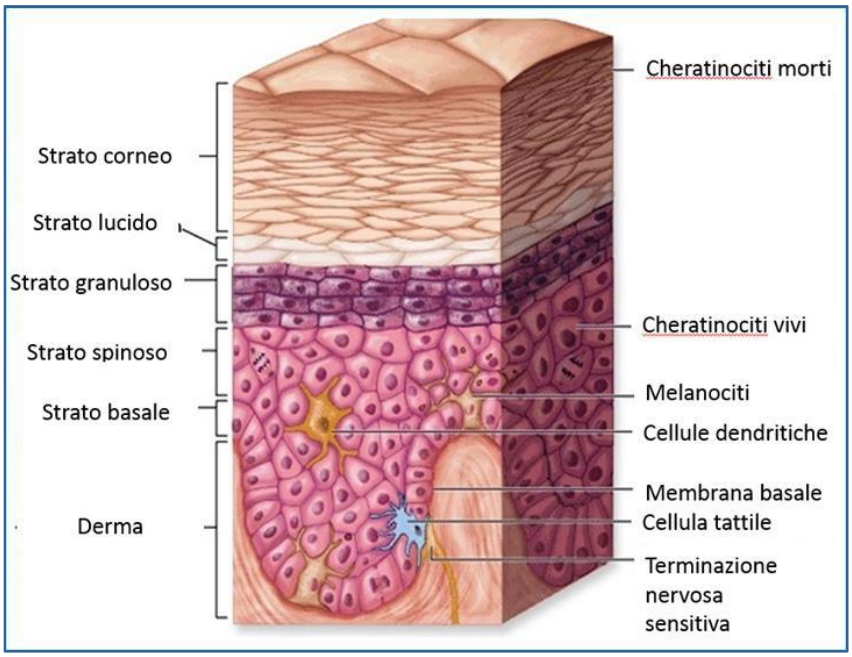

Fig. 1 Rappresentazione schematica della cute, tratto da Anthony L. Mescher: Junqueira's Basic Histology, Text and Atlas, Mc Graw Hill, 14^ ed., capitolo 18

2.3 Struttura anatomica della mucosa orale

La mucosa del cavo orale ha uno spessore medio di circa 500-800 μm ed assolve alla duplice funzione di prima barriera del tratto digestivo nei confronti degli xenobiotici e di selettiva e diretta via di assorbimento per i farmaci e per le sostanze che sono in grado di oltrepassala. Ha una struttura istologica che permette una maggiore permeabilità rispetto alla cute nei confronti di alcuni composti e permette la possibilità di un assorbimento diretto nel torrente circolatorio evitando l'effetto di primo passaggio attraverso il fegato.

In termini generali la struttura della mucosa orale è organizzata, similmente a quella cutanea, in un epitelio pavimentoso stratificato, cheratinizzato o non cheratinizzato, che poggia su compartimento connettivale, chiamato lamina propria. Al di sopra dell'epitelio si trova uno strato di muco di spessore fra i 70-100 μm, che funge da filtro nei confronti di sostanze

esterne ed è costituito principalmente da una mucina ad elevato peso molecolare, chiamata MG1, che deriva dalla saliva e si lega alla superficie dell'epitelio buccale.

L'epitelio orale è costituito per il 90% da cheratinociti, che si dispongono su più strati, che, dall'interno verso l'esterno si susseguono nel modo seguente: basale, spinoso, granuloso e cheratinizzato, ove presente. Nel processo di maturazione passano da una forma cubico-cilindrica a quella appiattita. Il rimanente 10% delle cellule è costituito da melanociti ed una bassa densità di cellule di Langerhans, cellule di Merkel e cellule del sistema immunitario (principalmente linfociti e macrofagi) (Squier and Kremer, 2001, http://www.addc.it/mucose.html).

Questo epitelio possiede un'alta percentuale di cellule germinative in costante replicazione, che garantisce un elevato turnover delle cellule epiteliali, stimato di circa 6 volte superiore a quello della cute.

È stato dimostrato che il principale ostacolo per la penetrazione dei farmaci è rappresentato dal terzo superiore dell'epitelio in quanto, spostandosi dallo strato basale a quelli più superficiali, la dimensione delle cellule aumenta e la loro forma diventa piatta. Dipendentemente da specifici requisiti funzionali richiesti, l'epitelio può variare leggermente all'interno delle diverse zone del cavo orale. Esistono, infatti, tre principali tipi di mucosa: di rivestimento, masticatoria e specializzata (Andersen and Mackenzie, 1986).

La mucosa orale di rivestimento si trova a livello del palato molle, della superficie ventrale della lingua, del pavimento della cavità orale e dei processi alveolari. È costituita da epitelio cheratinizzato non corneificato che poggia sulla sottostante lamina propria di tessuto connettivo lasso con abbondanti fibre elastiche. Questa organizzazione garantisce la flessibilità necessaria all'articolazione delle parole ed alla deglutizione.

La mucosa masticatoria si trova in corrispondenza delle zone maggiormente soggette ad insulti meccanici, quali le gengive ed il palato duro. È costituita da epitelio cheratinizzato corneificato e connettivo fibroso denso ed è priva della sottomucosa. Infine, la mucosa

specializzata riveste i due terzi anteriori del dorso della lingua ed è caratterizzata da epitelio cheratinizzato corneificato e non corneificato che ospita le papille linguali (Squier and Kremer, 2001).

La permeabilità della mucosa orale differisce significativamente nelle diverse regioni orali, a seconda del tipo di epitelio, del tipo e della quantità di lipidi intercellulari e della natura chimica delle sostanze applicate. Le regioni rivestite da epitelio non cheratinizzato contengono glicoceramidi ed hanno una permeabilità notevolmente superiore rispetto alle regioni con epitelio cheratinizzato, quali palato duro e gengiva, che contengono prevalentemente lipidi neutri.

Fra l'epitelio orale e la lamina propria si interpone la membrana basale, una struttura che fornisce supporto meccanico all'epitelio sovrastante e costituisce una barriera selettiva, che permette lo scambio di nutrienti e cataboliti fra epitelio e tessuto connettivo. Questa membrana è composta da tre diversi strati: lamina lucida, lamina densa e lamina reticolare e la sua integrità è di primaria importanza per garantire la connessione fra l'epitelio e la lamina propria e per il controllo della crescita e della differenziazione delle cellule epiteliali (Adams, 1976).

La lamina propria è costituita da due porzioni, una papillare, più superficiale, e una reticolare più profonda, costituite entrambe da tessuto connettivo, che nella parte reticolare diviene più compatto grazie ad una maggiore quantità di componente fibrillare disposta in modo intrecciato (Dalle Donne et al, 2011). Nelle regioni molto mobili del cavo orale, quali il palato molle e il pavimento della bocca, la lamina propria è connessa al muscolo sottostante da tessuto connettivo sottomucoso lasso. Al contrario, nelle aree dove la mucosa orale riveste l'osso, quali il palato duro ed i processi alveolo-dentari, la lamina propria è ancorata al periostio per mezzo di una sottomucosa fibrosa relativamente densa. Nella sottomucosa della cavità orale sono distribuiti gli adenomeri di numerose piccole ghiandole salivari accessorie (Wheater, 2014)

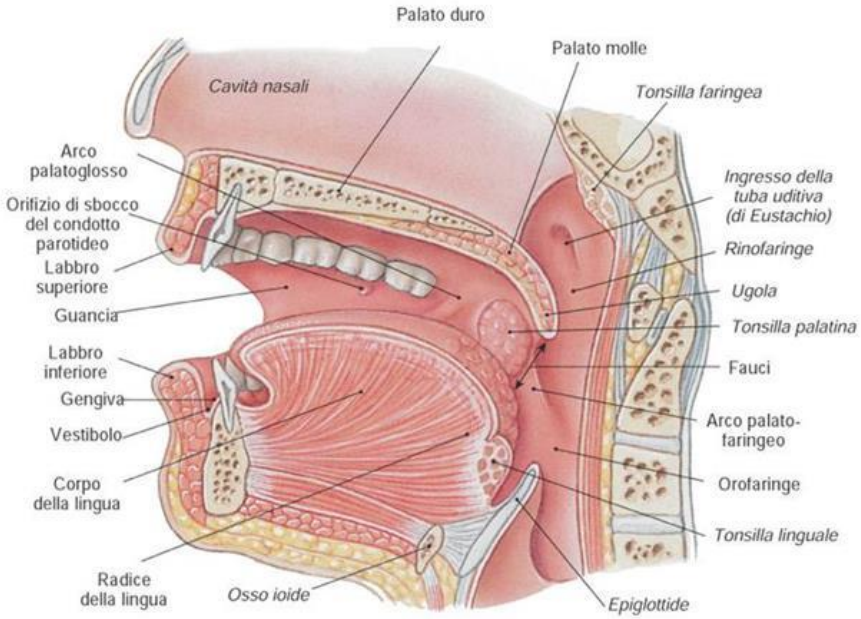

Fig. 2 Anatomia della cavità orale. Da Martini FH, Timmons MJ, Tallitsch RB. Anatomia Umana; Edises.

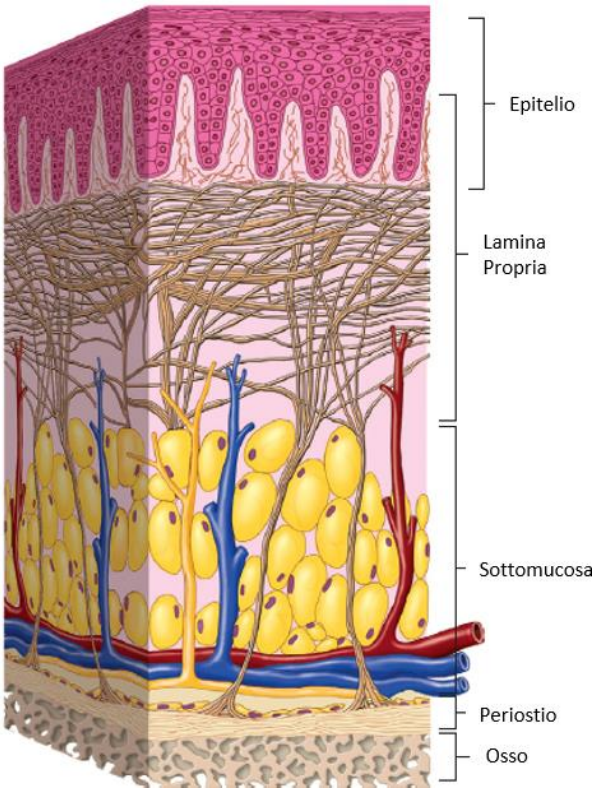

Fig. 3 Rappresentazione schematica della mucosa del cavo orale, tratto da Antonio Nanci: Ten Cate's Oral Histology, Development, Structure and Functions. Elsevier 8th ed.

2.4 Struttura anatomica delle meningi nella porzione di rivestimento del bulbo olfattorio

Le meningi sono costituite da 3 foglietti di tessuto connettivo che avvolgono completamente il sistema nervoso centrale (SNC) al fine di proteggerlo da eventuali insulti esterni.

A partire dalla superficie encefalica distinguiamo dunque la pia madre, l'aracnoide e la dura madre. Quest'ultima si fonde con il periostio del tavolato interno del cranio aderendo saldamente ad esso, mentre le altre due membrane (chiamate assieme leptomeningi), costituite da un tessuto più delicato, provvedono ad avvolgere completamente l'encefalo in tutte le sue pieghe e circonvoluzioni (Nieuwenhuys R, Voogd J, van Huijzen C. "Il sistema nervoso centrale", Springer-Verlag Italia, 2010, pag 97). Il bulbo olfattorio (Fig. 4), posto nella porzione inferiore e mediale della scatola cranica, rappresenta un'eccezione nel contesto delle strutture encefaliche, poiché seppur rivestito dalle meningi, da esso trae origine il nervo olfattorio, che rappresenta, assieme al nervo trigemino, l'unico collegamento diretto tra l'ambiente esterno ed il cervello (Vyas 2005). I rami del nervo olfattorio partendo dal bulbo raggiungono la cavità nasale attraversando le aperture della lamina cribrosa dell'etmoide e della dura madre che la riveste. Attraversando la scatola cranica, per penetrare nella cavità nasale, i rami del nervo olfattorio vengono infatti avvolti da prolungamenti della dura madre, che discendono nel naso attraverso i suddetti fori. (G. Valentin, 1844).

Conseguentemente a tale caratteristica la via di somministrazione intranasale di farmaci e altre molecole di vario genere ha destato notevole interesse nel corso degli ultimi decenni per il suo possibile uso nel trattamento di disturbi cognitivi, neurodegenerativi ed anche per l'assunzione, meno nobile, di sostanze d'abuso (Kao 2000, Hanson 2008, Meredith 2015).

A livello microscopico la dura madre è costituita da uno strato esterno di fibroblasti e fibre collagene e da uno strato interno, dello spessore di circa 8 μm, costituito da cellule che sono strettamente accostate con l'aracnoide sottostante e con il collagene extracellulare della porzione media soprastante, senza un significativo spazio extracellulare. L'aracnoide è formata da uno strato barriera esterno, dove le cellule sono unite da tight junctions, e uno strato interno, che si fonde con la pia madre. Lo spazio subaracnoideo è costituito dall'unione degli spazi intracellulari di aracnoide e pia madre ed è attraversato a tutto spessore dalle trabecole che lo delimitano sui versanti durale e neurale. I capillari esterni allo strato barriera dell'aracnoide sono fenestrati, mentre quelli che decorrono all'interno dello stesso e dell'encefalo sono privi di queste fenestrature (Nieuwenhuys, 2010) (Fig. 5).

Da un punto di vista istologico, quindi, le strutture che garantiscono la sostanziale impermeabilità delle meningi sono le tight junctions (giunzioni serrate) tra le cellule, dove gli strati esterni delle membrane plasmatiche di due cellule adiacenti sono fusi. Queste barriere si riscontrano a livello dello strato (barriera) esterno dell'aracnoide e sull'endotelio dei capillari presenti nell'aracnoide e nella pia madre.

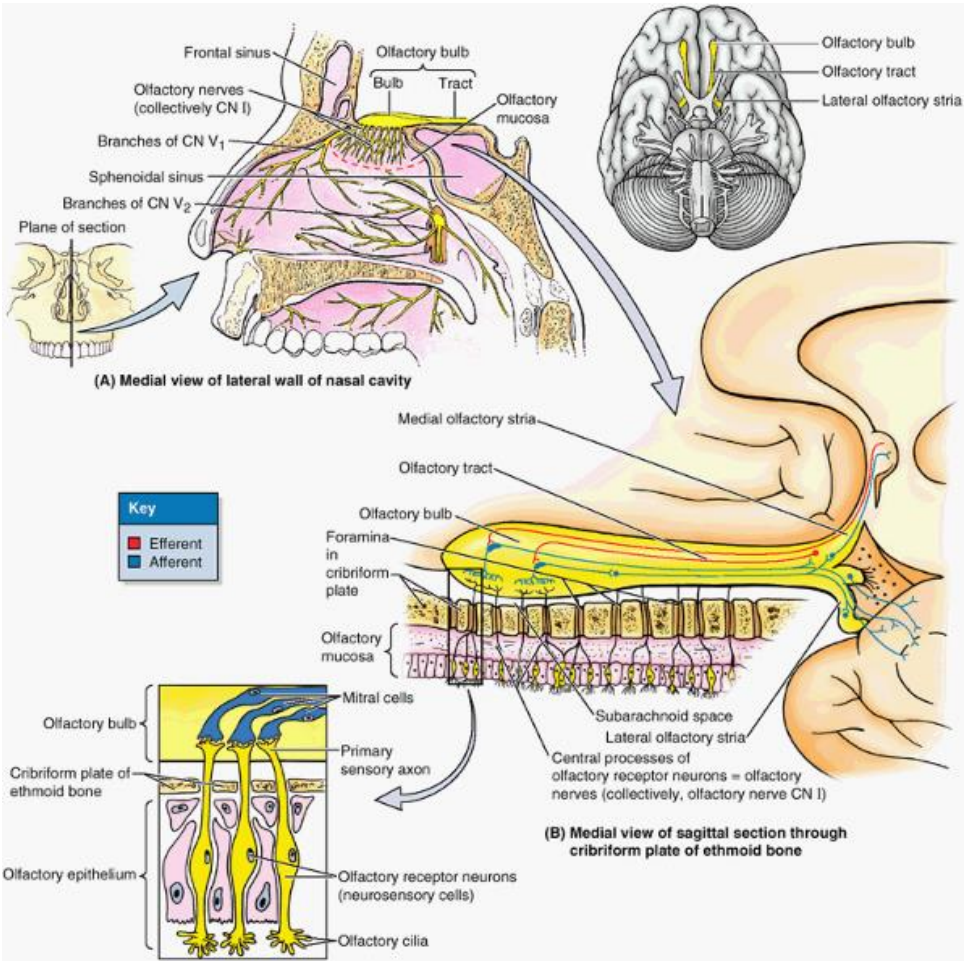

Fig. 4 bulbo olfattorio, sue aree di proiezione nel parenchima cerebrale e distribuzione dei filuzzi olfattori attraverso la lamina cribrosa dell'etmoide. Tratto da Keith L. Moore, Arthur F. Dalley. Clinically oriented anatomy. Lippincott Williams & Wilkins, 1999, pag. 1089

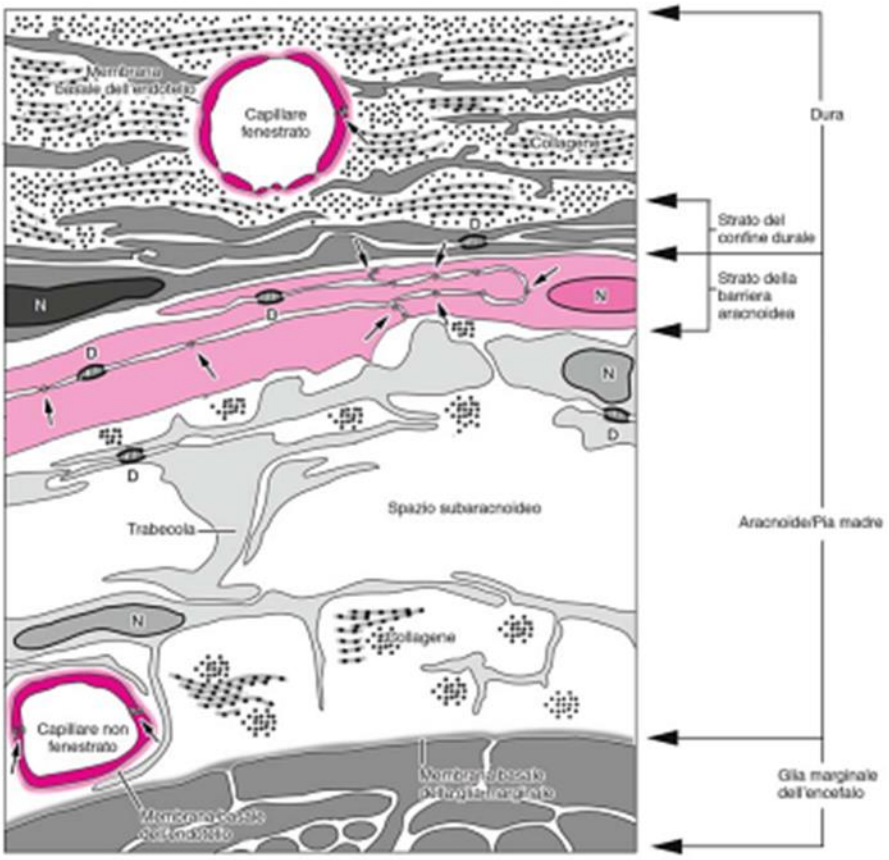

Fig. 5 Schema che illustra l'ultrastruttura delle meningi a livello cranico. La dura risulta costituita da uno strato esterno di fibroblasti e fibre collagene e uno strato di cellule del margine durale. In condizioni fisiologiche lo spazio subdurale è assente. L'aracnoide è costituita da uno strato barriera esterno, dove le cellule sono unite da tight junctions (frecce piccole), ed uno strato interno, che si fonde con la pia madre. Lo spazio subaracnoideo è attraversato a tutto spessore dalle trabecole che congiungono gli strati cellulari del versante durale e neurale. I capillari esterni allo strato barriera dell'aracnoide sono fenestrati, mentre i capillari che decorrono all'interno dello stesso e nell'encefalo sono privi di queste fenestrazioni.Immagine ricostruita sulla base dello schema pubblicato da Nabeshima e coll. D = desmosoma, N= nucleo

3. MATERIALI E METODI

3.1 Celle di diffusione di Franz

Il sistema in vitro più utilizzato per lo studio della permeazione passiva attraverso la cute è costituito dalle celle di diffusione di Franz. Questo apparato è costituito da due comparti, uno donatore, superiore, ed uno ricevente, inferiore, fra i quali viene posta la cute o la membrana biologica da studiare (Fig.6). Dopo aver fissato il tessuto in modo che non vi siano perdite di soluzioni durante i test, la sostanza da testare viene posta nel compartimento superiore, a contatto con la porzione epiteliale della membrana, mentre il compartimento ricevente viene riempito di soluzione fisiologica, mantenuta in agitazione a temperatura costante. Il comparto ricevente è dotato di un tubicino di campionamento attraverso cui possono essere effettuati i prelievi della fase ricevente ai tempi prefissati e di una camicia esterna collegata al sistema di termostatazione (Fig.7). I lembi di tessuto vengono posizionati fra le due camere e nella cella donatrice vengono disperse le NP metalliche in sudore sintetico o soluzione fisiologica ed applicate come fase donatrice per un intervallo di tempo predefinito. Come fase ricevente viene utilizzata soluzione fisiologica. Per la valutazione della quantità di metallo permeata vengono prelevate ad intervalli stabiliti delle aliquote della fase ricevente, prontamente sostituite con soluzione fisiologica fresca e successivamente analizzate. Al termine degli esperimenti vengono recuperate la fase donatrice, quella ricevente ed il tessuto biologico utilizzato, per effettuarvi le successive analisi. La temperatura nel sistema è stata mantenuta a 32°C per gli esperimenti sulla cute, mentre a 37°C per gli esperimenti sulla mucosa orale e sulle meningi, al fine di riprodurre le normali condizioni fisiologiche. L'intervallo temporale di esposizione delle membrane è variabile a seconda del tipo di membrana studiata. In particolar modo gli esperimenti sulla cute sono stati condotti per un periodo di 24 ore, quelli sulla mucosa orale per 4 ore e quelli sulle meningi per 2 ore, alla luce di un tempo di esposizione verosimilmente differente a carico delle tre membrane in uno scenario reale.

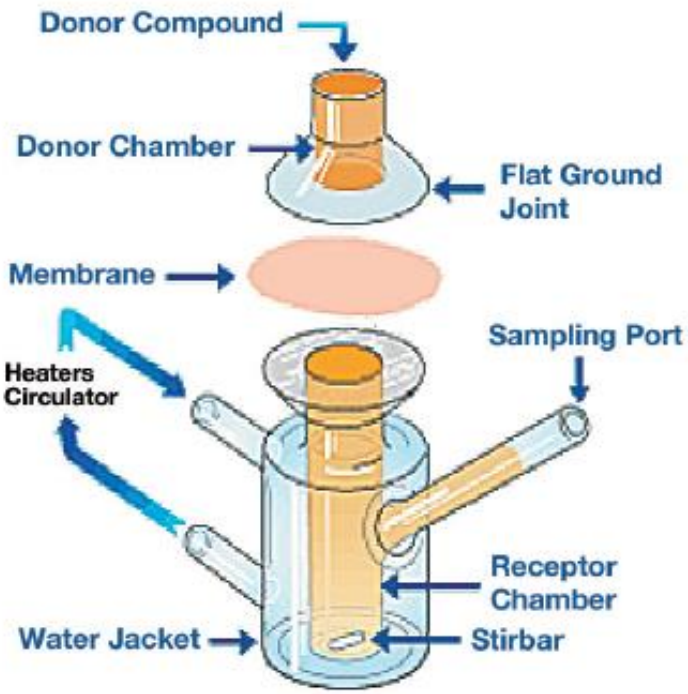

Fig. 6 Rappresentazione schematica di una celle di diffusione di Franz usata negli esperimenti di permeazione cutanea.

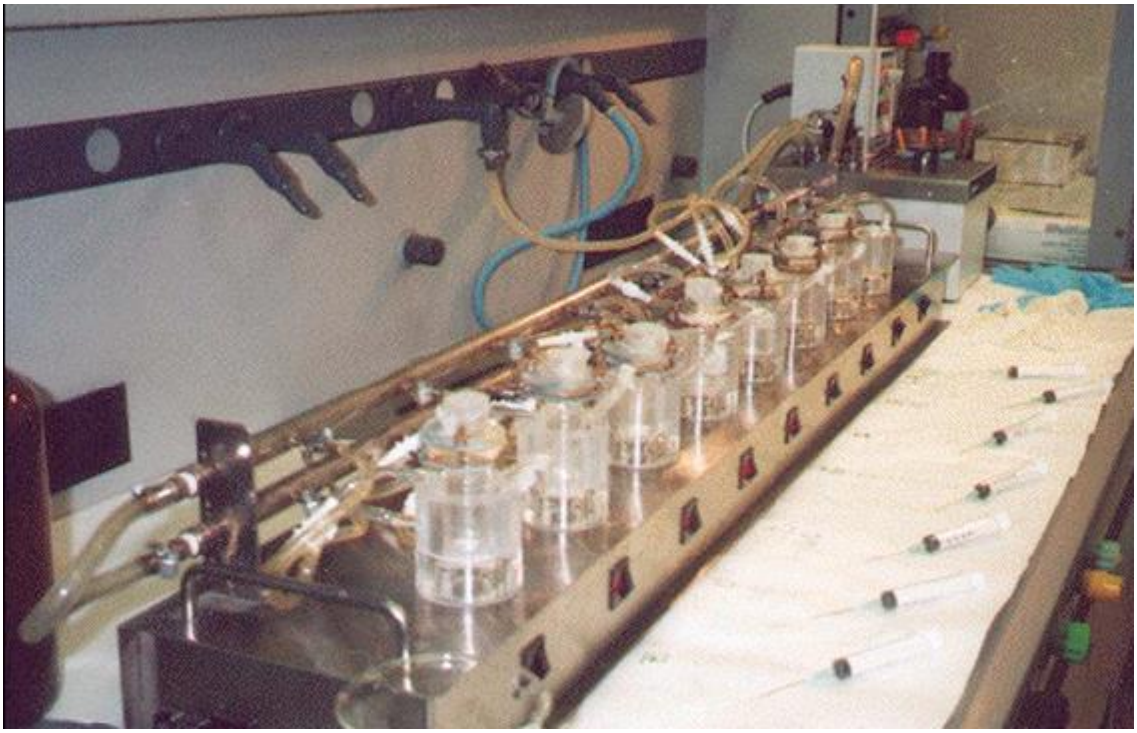

Fig.7 La consolle di lavoro e sistema di termostatazione delle celle di Franz.

La determinazione del contenuto di NPs all'interno delle fasi donatrici, delle fasi riceventi e dei diversi tessuti viene indagato successivamente tramite diverse tecniche di indagine, quale ad esempio la Microscopia Elettronica a Trasmissione (TEM), eventualmente accoppiata a tecniche spettrofotometriche.

La quantità totale di metallo contenuto nelle membrane è stato invece analizzata dopo mineralizzazione del tessuto biologico con acidi forti. Le analisi quantitative del metallo presente nella membrana e nelle soluzioni donatrice e ricevente sono state condotte con tecniche spettrofotometriche.

Nella fase di rielaborazione dei dati ottenuti dalle analisi il passaggio della sostanza attraverso la membrana indagata viene espresso in termini di flusso, calcolato nella parte lineare del profilo di permeazione, di lag time, ovvero il tempo necessario affinché il flusso raggiunga un valore massimo costante (Franz, 1975; Rougier, 1990; Bronaugh and Franz, 1986) e di coefficiente di permeabilità Kp (cm h^{-1}) che si ottiene dividendo il flusso per la dose applicata (figura 8).

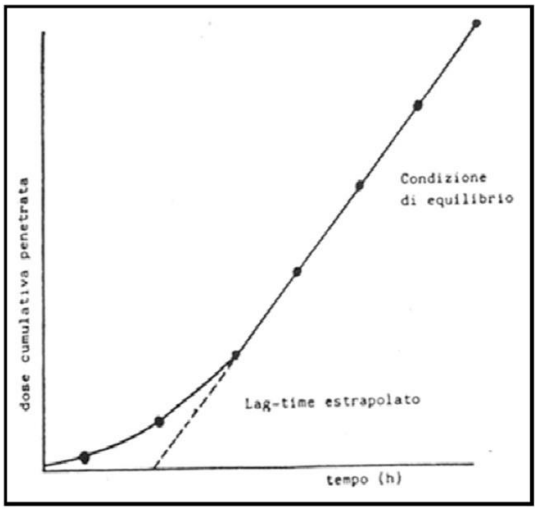

Figura 8. Esempio di una curva cumulativa di permeazione in funzione del tempo: la pendenza della parte rettilinea rappresenta il flusso, mentre l'intercetta con l'asse delle ascisse fornisce il valore di lag time.

3.2 Procedura sperimentale generale

3.2.1 Preparazione delle membrane biologiche

Preparazione della cute:

La cute utilizzata negli esperimenti di permeazione deriva da scarti di interventi chirurgici di addominoplastica gentilmente forniti dal reparto di Chirurgia Plastica degli Ospedali Riuniti di Trieste. L'età dei pazienti era compresa fra i 40 ed i 65 anni. Dopo l'escissione i lembi dai lembi di cute viene rimosso il grasso sottocutaneo e vengono congelati ad una temperatura di -25°C all'interno di sacchetti di plastica per un periodo massimo di 4 mesi. Questo metodo non ne altera le proprietà strutturali, infatti è stato dimostrato che le proprietà di permeazione non variano fra cute fresca e campioni congelati della stessa cute (Franz, 1975). Al momento del loro utilizzo la cute viene fatta scongelare per un periodo di circa 30 minuti in soluzione fisiologica ed a temperatura ambiente, i lembi vengono quindi tagliati in riquadri di circa 4 cm di lato e viene rimosso l'eventuale grasso residuo. Lo spessore finale dei campioni è di circa 1 mm (misurata tramite calibro ventesimale). I campioni di cute che devono subire un danneggiamento superficiale vengono abrasi tramite un protocollo standardizzato (Bronaugh e Steward, 1985). Quest'ultimo prevede che venga strisciato sulla cute integra un ago di siringa, 20 volte in una direzione e 20 nella direzione perpendicolare. Nei test di permeazione i lembi di cute, integra e lesa, vengono fissati fra i due comparti di una cella, con lo strato corneo rivolto verso la soluzione donatrice e quello dermico verso la soluzione ricevente. Per ogni esperimento viene utilizzata cute proveniente da diversi donatori, in modo da minimizzare l'effetto della variabilità dovuta alle caratteristiche intrinseche del tessuto. La soluzione fisiologica usata come fase ricevente negli esperimenti viene preparata sciogliendo 2,38 g di Na_2HPO_4, 0,19 g di KH_2PO_4 and 9 g di NaCl in 1 l di acqua milliQ con un pH finale di 7,35. Il sudore sintetico usato per disperdere le polveri metalliche è una soluzione allo 0,5% di

NaCl, 0,1% di urea e 0,1% di acido lattico. Il pH viene portato al valore finale con ammoniaca.

Preparazione della mucosa orale

Le membrane derivano da mucosa orale suina, in particolar modo le regioni sublinguale e parodontale. I prelievi vengono effettuati immediatamente dopo l'uccisione dei maiali (di un anno d'età) presso un macello sito in località Prosecco, Trieste e successivamente crioconservate a -25°C per un periodo massimo di 1 settimana. Il giorno degli esperimenti le mucose vengono lasciate a bagno in soluzione fisiologica a temperatura ambiente per circa 30 minuti prima di iniziare gli i test, di modo da non alterarne le proprietà di permeabilità (Caon e Simoes, 2011). Il tessuto connettivo sottostante viene rimosso con una lama, viene raggiunto uno spessore finale uniforme di circa 1 mm. Ogni lembo di mucosa utilizzato viene quindi fissato fra comparto donatore e comparto ricevente in modo tale che l'epitelio sia in contatto con la soluzione donatrice ed il tessuto connettivo con la soluzione ricevente. L'integrità delle mucose viene testata prima e dopo ogni esperimento tramite il protocollo suggerito da Lestari (2009).

Preparazione delle meningi:

Le meningi per gli esperimenti in vitro sono state prelevate da maiali, immediatamente dopo l'uccisione degli stessi (un anno d'età) presso un macello sito in località Prosecco, Trieste. Le meningi sono state conservati a 4°C durante il breve trasporto e successivamente crioconservate a -25°C per un periodo massimo di 1 settimana. Il giorno degli esperimenti i tessuti vengono rimossi dal freezer e lasciati a bagno in soluzione fisiologica a temperatura ambiente per circa 30 minuti. L'integrità delle membrane viene testata prima e dopo ogni

esperimento riempiendo la camera donatrice con acqua milliQ e monitorizzando la presenza della soluzione nella camera ricevente per un periodo di 30 minuti (Lestari 2009).

3.2.2 Integrità delle membrane biologiche

L'integrità delle membrane viene testata prima e dopo ogni esperimento mediante misure di conducibilità (o resistenza: R = 1/C) elettrica utilizzando un conduttimetro (Metrohm, 660, Metrohm AG Oberdorfstr. 68 CH-9100 Herisau) operante a 300 Hz collegato a due elettrodi in acciaio inox (Fasano et al., 2002). Una volta montata la cella e fissata la membrana biologica si attende un periodo di 30 minuti necessario per l'instaurarsi dell'equilibrio termico e a questo punto vengono effettuate le misure di conducibilità tramite due elettrodi immersi nella soluzione ricevente. I dati di conducibilità, ottenuti in S, vengono convertiti in Kcm^{-2}. I campioni delle membrane che hanno una resistenza inferiore a 3,95 ± 0,27 Kcm^{-2} sono ritenuti danneggiati e vengono scartati (Davies et al, 2004).

3.2.3 Test di permeazione

Prima e dopo ogni esperimento le celle di Franz vengono lavate con acido nitrico diluito (6% v/v) e risciacquate con acqua milliQ. Il compartimento inferiore di ogni cella viene riempito completamente con soluzione fisiologica e lasciato riscaldare per circa 30 minuti, fino al raggiungimento della temperatura desiderata (32°C per la cute e 37°C per la mucosa orale e le meningi). La membrana da studiare viene posizionata con lo strato corneo (nel caso della cute) epidermico (nel caso della mucosa orale) o durale (nel caso delle meningi) a contatto con la soluzione donatrice, facendo attenzione che non si formino bolle all'interfaccia fra la membrana e la soluzione ricevente (riduzione della superficie di contatto) e fissando quindi le due camere tramite delle pinze di polietilene, di modo che non si verifichino perdite delle varie fasi.

Una volta riempita la camera donatrice con una quantità di sospensione tale da ricoprire completamente la membrana, le aperture della cella (quella superiore ed il tubo laterale), vengono chiuse con tappi in plastica o parafilm per evitare fenomeni di evaporazione delle soluzioni (Franz, 1975).

Il tempo di esposizione è stato fissato a 24 ore per test sulla cute, a 4 ore per quelli sulla mucosa orale e a 2 ore per quelli sulle meningi, come precedentemente spiegato.

Ad ogni campionamento vengono prelevati 1,5 ml di soluzione ricevente da ogni cella attraverso il tubo laterale utilizzando una siringa in polietilene da 2,5 ml, il liquido prelevato viene prontamente sostituito con soluzione fisiologica fresca. Ogni aliquota prelevata viene posta in provette da 1,5 ml e conservata in congelatore alla temperatura di -25°C fino al momento delle successive analisi. Al termine di ogni esperimento le fasi donatrici, le fasi riceventi e le membrane biologiche vengono congelate.

3.2.4 Mineralizzazione delle membrane dopo l'esposizione

Le membrane vengono scongelate a temperatura ambiente per 2 ore, successivamente tagliate, pesate e poste in becher con 10 ml di HNO_3 al 69 % v/v per la mineralizzazione (le quantità di pelle in generale sono comprese tra 0,6 e 1,2 g). La soluzione così ottenuta viene portata alla temperatura di 150°C per un periodo di 10 ore. Dopo 2 ore viene aggiunta, goccia a goccia, H_2O_2 al 30% v/v fino ad un totale di 2 ml; si procede quindi ad una diluizione dei campioni con acqua milliQ fino al raggiungimento di un volume pari a 10 ml. Si prosegue con le analisi.

3.2.5 Misure analitiche strumentali

Per le analisi delle concentrazioni delle NPs studiate nel corso degli esperimenti sono state utilizzate le seguenti tecniche analitiche strumentali:

- Spettroscopia di Assorbimento Atomico Elettro-Termica con Fornetto di Grafite (GF-AAS);
- Spettroscopia di Emissione Atomica con sorgente al Plasma Induttivamente Accoppiato (ICP-AES);
- Spettrometria di Massa con sorgente al Plasma Induttivamente Accoppiato (ICP-MS).

La scelta della tecnica analitica più opportuna è stata definita volta per volta in funzione delle concentrazioni attese nelle varie soluzioni da analizzare e dei limiti di rilevabilità degli strumenti per i vari elementi studiati.

3.2.5.1 Spettroscopia di Assorbimento Atomico Elettro-Termica con Fornetto di Grafite

Lo strumento utilizzato per le analisi delle soluzioni riceventi negli esperimenti con NPs di Pt, Rh, e nella cute mineralizzata esposta a Pt e Rh è uno spettrometro Thermo M series GF95Z (UK) dotato di fornetto di grafite e di autocampionatore FS95, sito presso il Dipartimento di Scienze Chimiche, Laboratorio di Chimica Analitica Ambientale e Strumentale, Università di Trieste. Lo strumento utilizzato per le analisi condotte sulle soluzioni riceventi negli esperimenti con le TiO_2NPs è un Varian Duo instrument (GTA 120, AA 240 Z), sito presso il Dipartimento di Specialità Medico Chirurgiche, Scienze Radiologiche, Sanità Pubblica, Università di Brescia.

3.2.5.2 Spettroscopia di Emissione Atomica con sorgente al Plasma Induttivamente Accoppiato

Lo strumento utilizzato per le analisi delle fasi donatrici e della cute esposta a TiO_2NPs, Co_3O_4NPs, NiNPs e delle fasi donatrici e della mucosa orale e delle meningi esposte ad AgNPs, è uno Spettrometro ottico al Plasma assiale Spectroflame Modula-E (SPECTRO, Germany), sito presso il Dipartimento di Scienze Chimiche, Laboratorio di Chimica Analitica

Ambientale e Strumentale, Università di Trieste. Lo strumento utilizzato per le analisi delle fasi donatrici nell'esperimento

3.2.5.3 Spettrometria di Massa con sorgente al Plasma Induttivamente Accoppiato

Lo strumento utilizzato per le analisi delle fasi riceventi delle celle in cui la mucosa orale e meningi sono state esposte ad AgNPs, delle fasi riceventi e della cute delle celle esposte a Co_3O_4NPs è uno spettrometro ICP-MS Agilent 7500ce (USA) equipaggiato con una cella di collisione per l'abbattimento delle interferenze, presso il Dipartimento di Traumatologia, Ortopedia e Medicina del Lavoro, Laboratorio di Tossicologia Industriale, Università di Torino. Lo strumento utilizzato per le analisi delle fasi riceventi e della cute delle celle esposte a Co_3O_4NPs è uno ICP-MS spettrometro ELAN DRC II, (Perkin Elmer, Waltham, USA), presso il Dipartimento di Specialità Medico Chirurgiche, Scienze Radiologiche, Sanità Pubblica, Università di Brescia.

3.2.5.4 Dynamic Light Scattering e potenziale Zeta

ll Dynamic Light Scattering (DLS) è una tecnica non invasiva che fornisce il profilo di distribuzione di grandezza di sospensioni contenenti nanoparticelle. Nelle misure DLS il campione viene illuminato da un raggio laser, e le variazioni d'intensità della luce diffusa vengono misurate in funzione del tempo. Le variazioni d'intensità misurate sono determinate dal movimento browniano delle particelle all'origine dello scattering, la cui velocità è inversamente proporzionale alle dimensioni delle NPs. Grazie ad un auto correlatore, la velocità delle variazioni d'intensità viene misurata, e il coefficiente di diffusione delle particelle calcolato dalla funzione della correlazione. L'equazione di Stokes Einstein consente poi di convertire il coefficiente di diffusione in diametro idrodinamico. La misura del potenziale zeta serve per predire la stabilità delle dispersioni. Le nanoparticelle disperse in soluzione presentano una carica superficiale, causata da fenomeni di ionizzazione o

assorbimento di specie cariche. Le particelle caricate sono circondate in soluzione da diversi strati ionici, la cui composizione risulta diversa da quella del materiale in forma tradizionale. Quando si muovono in soluzione le NPs si spostano insieme ad un doppio strato ionico. Il potenziale Zeta è il potenziale al livello di questo doppio strato e consente di predire la stabilità delle NPs. Valori elevati di potenziale zeta (i.e. <-30mV e >+30mV) fanno si che le NPs rimangano lontane l'una dall'altra, respingendosi abbastanza per eliminare la possibilità di aggregazione.

Lo strumento utilizzato per le analisi DLS negli studi condotti sulle nanoparticelle di ossido di Titanio e ossido di Cobalto è un 90 Plus PALS instrument (Brookhaven Instruments Corporation, Holtsville, NY, USA), sito presso L'Istituto IMEM-CNR, Parco Area delle Scienze, Parma; quello utilizzato per le analisi sulle nanoparticelle di Argento è un ZetasizerNano Z (Malvern Instruments Ltd.), sito presso l'Helmholz Zentrum München Deutches Forschungszentrum für Gesundheit und Umvelt (GmbH), Neuherberg; le analisi DLS sulle nanoparticelle di Platino e Rhodio sono state condotte da MICROMERITICS Analytical Service.

3.2.5.5 Microscopio Elettronico a Scansione accoppiato all'analisi elementare a raggi X (SEM-EDX)

Il SEM permette di ottenere una caratterizzazione morfologica del campione analizzato ad elevati ingrandimenti (oltre 100000 x) con una risoluzione fino a circa 5 nm. Il principio della tecnica si basa sull'interazione fra un fascio di elettroni accelerati ed il campione che si vuole osservare: il fascio incidente viene scansionato sulla superficie desiderata del campione, in modo sequenziale e con passo periodico. A seguito dell'interazione (urto), dal campione vengono emessi gli elettroni secondari, che vengono registrati dal rivelatore e convertiti in segnali elettrici, ovvero, in un'immagine in bianco e nero, simile ad una fotografia. Quando si accoppia a questa tecnica quella dell'analisi elementare (EDX - Energy Dispersive X-ray

analysis) si può effettuare anche una caratterizzazione chimica degli elementi presenti nel campione, utilizzando quantità minime di prodotto (μg). La spettroscopia EDX sfrutta l'emissione di raggi X prodotti a seguito della collisione del fascio elettronico incidente con la superficie del campione. La sorgente di elettroni è costituita da un filamento di tungsteno, che viene portato oltre i 1000°C per riscaldamento elettrico. Il fascio elettronico, generato per effetto termoionico, viene dapprima accelerato da una differenza di potenziale di 0,3-30 kV; passa poi attraverso un collimatore elettromagnetico per essere deflesso e, quindi, viene finemente indirizzato verso il piatto su cui è alloggiato il campione in esame. Gli elettroni incidenti pertanto, a loro volta, provocano l'emissione degli elettroni più interni degli atomi del campione: il successivo rilassamento e ritorno alla configurazione fondamentale, induce l'emissione di un fotone con energia predefinita e specifica per ogni elemento.

Lo strumento utilizzato per le analisi SEM-EDX delle nanoparticelle di Argento è uno SEM (Hitachi, TM 3000) fornito di Energy Dispersive X-ray Spectroscope (EDX SwiftEd 3000), sito presso Laboratorio di Tossicologia Industriale, Università di Torino.

4. STUDI CONDOTTI

4.1 Permeazione transcutanea di Nanoparticelle di Platino (PtNPs) e Rhodio (RhNPs) attraverso cute intera, integra e lesa:

Introduzione e scopo dello studio:

Gli elementi del gruppo del platino (platino, rodio, palladio, nel complesso denominati *"Platinum Group Elements"* - PGE) nei secoli scorsi hanno rappresentato una importante fonte di esposizione occupazionale nelle raffinerie e nelle industrie di produzione di catalizzatori, dove venivano raggiunte elevate concentrazioni di sali di PGE, e contestualmente vi era un elevato riscontro di reazioni allergiche IgE-mediate nei lavoratori. È noto, infatti, che i sali di questi metalli, ed in particolare di platino e palladio, possiedono un alto potere sensibilizzante, tale da scatenare fenomeni allergici quali asma, rinocongiuntivite, dermatite ed orticaria nei i lavoratori esposti (Santucci et al. 2000; Cristaudo et al. 2005). Studi condotti su animali hanno dato risultati discordanti, evidenziando in un caso assenza di metallo nel siero e nelle urine di animali trattati con solfato di platino a livello dermico (Taubler 1977) e presenza dello stesso in animali esposti a cloro platinato di ammonio (Roshchin et al 1984). Ad oggi queste esposizioni sono fortunatamente rare ed infrequenti, ma questi elementi si ritrovano in aria ambiente principalmente a seguito delle emissioni degli autoveicoli (Moldovan et al. 2002), che determinano una loro messa in circolo come particolato atmosferico prevalentemente in forma micro e nanoparticellare. Da un punto di vista igienistico si ritiene che l'esposizione totale a PGE attraverso l'inalazione quotidiana di PM10 possa raggiungere approssimativamente i 0.062 ng/m^3 per il platino (Schierl 2000) e i 0.004 ng/m^3 per il rodio (Bocca et al. 2006).

L'interazione di questi elementi con l'organismo umano desta preoccupazione, poiché i tradizionali filtri ed i sistemi barriera dell'organismo umano potrebbero essere deficitari nei confronti di queste particelle, che, in virtù delle loro piccole dimensioni (< 100 nm) assumono

nuove proprietà biochimiche che permettono loro di esercitare effetti biologici differenti rispetto ai macromateriali di riferimento.

Lo scopo del presente studio è stato quello di valutare un possibile assorbimento cutaneo di PlNPs e RhNPs, attraverso campioni di cute intera, integra e danneggiata in un sistema di diffuzione passiva in vitro. Non erano presenti studi in letteratura su questo argomento.

Materiali e metodi

Sono state allestite 4 celle con campioni di cute intatta e 4 celle con cute lesa (Bronaugh and Stewart, 1985). Come soluzione ricevente è stata utilizzata soluzione fisiologica le PtNPs e RhNPs, stabilizzate con polivinilpirrolidone, sono state disperse in sudore sintetico a PH 4.5, fino ad ottenere una concentrazione di 2.0 g/L, ed applicate come soluzione donatrice sulla superficie epidermica della cute per 24 h. I due metalli sono stati testati separatamente. Per ogni esperimento sono state aggiunte due celle di Franz come bianchi. Queste celle sono state trattate come le altre ad eccezione del fatto che nella camera donatrice non sono state introdotte NPs. Alla 24^ ora la soluzione ricevente ed i campioni di cute sono state rimosse. I dati ottenuti sono stati analizzati con Excel per Windows, versione 2007, e il Software Stata, versione 11.0 (StataCorp LP, College Station, TX, USA). Tutti I dati sono stati riportati come media ± deviazione standard (SD). La differenza fra campioni indipendenti è stata testata tramite test di Mann-Whitney. È stato considerato come limite di significatività statistica un valore di $p < 0.05$

Risultati

Le analisi condotte con il Microscopio Elettronico a Trasmissione (TEM) hanno rivelato che le PtNPs e RhNPs avevano dimensioni pari a 5.8 ± 0.9 nm e 5.3 ± 1.9, rispettivamente. Dopo 24 ore di esposizione a PtNPs, la concentrazione di metallo riscontrata nelle soluzioni riceventi era al di sotto del limite di rilevabilità in entrambi gli esperimenti con la cute integra

e lesa. La concentrazione di platino, valutata complessivamente, era doppia nella cute danneggiata se comparata con la cute integra, con un valore medio e deviazione standard di 1.74 ± 1.24 μg cm^{-2} e 0.80 ± 0.20 μg cm^{-2} rispettivamente. Il contenuto di platino nella cute integra (media e deviazione standard) decresceva significativamente dall'epidermide (0.75 ± 0.21 μg cm^{-2}) al derma (0.05 ± 0.00 μg cm^{-2}) ($p<0.049$), mentre nella cute danneggiata questa differenza non era significativa. Nella cute danneggiata la concentrazione di platino era riscontrabile in concentrazione maggiore in ogni strato se confrontato con la cute integra, raggiungendo tuttavia la significatività statistica solamente nel confronto fra i due strati dermici (0.43 ± 0.28 μg cm^{-2} and 0.05 ± 0.00 μg cm^{-2}, rispettivamente) ($p < 0.049$). La quantità di rodio nella cute a tutto spessore è stata valutata alla fine dell'esperimento e la concentrazione del metallo era più di 17 volte maggiore nella cute danneggiata se confrontata con la cute integra, con un valore medio e deviazione standard di 7.41 μg cm^{-2} ± 5.55 e 0.43 μg cm^{-2} ± 0.08 rispettivamente. Dopo il periodo di 24 ore di applicazione delle RhNPs nella soluzione donatrice è stato calcolato un flusso di permeazione pari a 0.04 ± 0.04 μg cm^{-2} h^{-1} e un lag time di 7.9 ± 1.1 h (media e deviazione standard) attraverso la cute danneggiata, mentre attraverso la cute integra non è stata dimostrata alcuna permeazione.

Discussione e conclusioni:

Lo studio condotto ha dimostrato, per la prima volta, che Rodio e Platino, applicati in forma nanoparticellare, possono penetrare la barriera cutanea. Piccole percentuali di Rodio, ma non di Platino, sono state riscontrate anche nelle soluzioni riceventi delle celle con cute danneggiata, dimostrando che per il primo di questi due metalli è stato possibile anche un fenomeno di permeazione attraverso la membrana cutanea a tutto spessore. L'assenza di Platino nelle soluzioni riceventi potrebbe essere spiegato dalla trascurabile quantità di ioni Pt che è stata rivelata dai test di dissoluzione del filtrato della soluzione donatrice oppure da un fenomeno di forte interazione fra il metallo e i componenti della cute (cellule, e matrice

extracellulare), avvallato dal riscontro di concentrazioni maggiori del metallo a livello dello strato dermico. Questo risultato è coerente con altri studi di permeazione su cute danneggiata, che mostrano un'aumentata deposizione di nano particelle a livello intradermico quando l'epidermide è abrasa con microaghi (Wei Z. 2010) o ablazione a radiofrequenze (Birchall J. 2006). Un comportamento simile è stato riscontrato nel profilo di permeazione della polvere di cromo (Larese et al. 2008), a causa del forte legame con le proteine della cute. Questi dati mostrano proprietà di dissoluzione delle PtNPs simili a quelle delle nanoparticelle di oro (AuNPs) ma differenti rispetto ad altri metalli quali argento, nickel o cobalto (Larese et al. 2009a, 2009b, 2013), nei quali il rilascio di ioni influenza la permeazione transcutanea. Questo è in linea con la differente ossidabilità dei metalli di base rispetto ai metalli nobili quali il Pt, Au o Rh.

Da un punto di vista tossicologico il potenziale danno derivante dall'assorbimento di questi metalli dipende dalla complessazione chimica che subiscono. Le evidenze epidemiologiche suggeriscono che la capacità sensibilizzante del platino è ristretta alle forme alogenate, ed in particolar modo alle forme sostituite con il cloro (Linett and Hughes 1999; WHO 1991, Marget 2000), inoltre l'intensità della risposta allergica, che nelle forme più severe viene descritta da una sindrome chiamata "*Platinosi*" (Brubaker et al 1975) sembra aumentare concordemente al numero degli atomi di cloro.

Le forme metalliche di Platino e Rodio (stato di ossidazione: 0), state testate nel presente studio e che sono per la maggior parte prodotte attualmente delle emissioni degli autoveicoli, sono tradizionalmente considerate biologicamente inerti e non allergeniche. Le evidenze epidemiologiche sembrano inoltre indicare che le concentrazioni atmosferiche attuali non sono sufficienti a causare un aumento delle reazioni allergiche nella popolazione generale (Merget and Rosner 2001).

Un recente lavoro di Colombo e collaboratori (2008) ha dimostrato, tuttavia, in uno studio in vitro che riproduceva il sistema polmonare, che questi metalli con stato di ossidazione 0 se entrano in contatto con fluidi biologici a PH acido (PH = 4.5) ed in presenza di ioni cloro (Fuchs and Rose 1974) (Zereini et al 1997) possono dare origine a specie clorurate del metallo. Si può ipotizzare il verificarsi di una condizione simile a livello cutaneo in condizioni di esercizio fisico intenso, che riduce il PH della cute (Dyer et al. 1998), o a seguito di utilizzo di disinfettanti cutanei a base di cloro, comunemente usati come agenti antisettici. Se si assume questa ipotesi anche 'assorbimento di platino in forma metallica potrebbe evidenzia un possibile rischio per la salute.

I risultati prodotti evidenziano quindi la necessità di una prevenzione della contaminazione cutanea da parte di queste nanoparticelle, poiché anche piccole abrasioni cutanee possono significativamente aumentare l'assorbimento di queste sostanze attraverso la cute, che potrebbero portare a conseguenze che non sono state ancora indagate completamente.

Per la bibliografia completa si faccia riferimento all'Allegato I

4.2 Permeazione transcutanea di Nanoparticelle di biossido di Titanio

Introduzione e Scopo dello studio:

Le nanoparticelle di biossido di Titanio (TiO_2NPs) sono ampiamente utilizzate in prodotti industriali e di consumo in virtù delle loro azione catalitica, che a queste dimensioni (< 100 nm) è più efficiente rispetto all'omologa sostanza in forma di fine particolato. Questa caratteristica è attribuibile al loro elevato rapporto superficie/volume (Shi et al. 2013). Il TiO_2 è fra le prime 5 NPs utilizzate a livello globale (Shukla et al. 2001), essendo presente in una vasta gamma di prodotti di consumo quali cosmetici, paste dentifrice (Kaida, 2003), lozioni solari (Wolf et al, 2003), trattamenti locali per l'acne volgare, la dermatite atopica, lesioni iperpigmentate della cute ed altre patologie non dermatologiche (Wiesenthal A., 2011). La sua formulazione nano è preferita nell'industria cosmetica poiché evita la colorazione bianca della cute a seguito della sua applicazione. Molti Autori hanno studiato la possibile penetrazione di TiO_2 NPs all'interno della cute, usando sia campioni di NPs nude sia NPs rivestite (Dussert, A.S. et al. 1997, Durand L. et al 2009, Pflücker, F. et al. 1999, Peira E. et al. 2014, Adachi K. et al 2010, Monteiro-Riviere N.A, 2011, Kiss B, 2015), ed i risultati hanno dimostrato che il TiO_2 non penetra la cute e i sottostanti tessuti, ma rimane in superficie impregnado i primi layers dello strato corneo. Per quanto riguarda studi di citotossicità, molti studi in vitro hanno dimostrato una riduzione della vitalità cellulare sui cheratinociti (Shi et al. 2013, Kiss B. et al. 2015, Jaeger A. et al. 2012, Chan J. et al 2011, Simon M. et al. 2011, Xue C. et al. 2010), ma studi in vivo su animali non hanno confermato questo effetto (Shi et al. 2013). È improbabile NPs di ossidi di metallo possano penetrare la cute umana integra in condizioni normali, ma un'alterazione dello strato corneo può aumentarne la penetrazione (Larese Filon F. et al. 2015, Senzui, M. 2010). Non ci sono dati disponibili sull'assorbimento cutaneo di TiO_2NPs con l'utilizzo di un protocollo di abrasione cutanea. È importante verificare questo punto poiché il danneggiamento superficiale dello0 strato corneo è comune in molti settori lavorativi, quali

quello della sanità, dell'edilizia fra i "*wet workers*" (Bauer A. et al. 2010). Lo scopo del presente studio è stato quello di verificare in vitro l'assorbimento cutaneo di TiO_2NPs su campioni di cute integra e danneggiata, usando il protocollo definito dal progetto EDETOX (Williams F.M., 2014) e valutare la loro potenziale tossicità dopo breve e lunga esposizione (24-48 h e 7 giorni) su cheratinociti.

Materiali e Metodi:

Sono stati condotti due separati esperimenti di permeazione in vitro su cute umana, usando le celle di diffusione di Franz. Nel primo esperimento è stata utilizzata cute intatta (Exp. 1) e nel secondo (Exp. 2) cute abrasa. Sono state utilizzate rispettivamente 6 celle nel primo esperimento e 5 celle nel secondo. Ogni esperimento è stato condotto per 24 ore. Come soluzione donatrice è stata utilizzata una sospensione contenente TiO_2NPs alla concentrazione di 606 $\mu g/cm^{-2}$ dispersa in sudore sintetico, mentre come fase ricevente è stata utilizzata soluzione fisiologica. Per ogni esperimento sono state aggiunte due celle di Franz come bianchi, dove la soluzione donatrice utilizzata era costituita solo da sudore sintetico. Ogni esperimento è stato ripetuto 2 volte.

Risultati

Le analisi al TEM hanno rivelato che le TiO_2NPs avevano una regolare forma sferica e tendevano ad una lieve aggregazione. La distribuzione di grandezza aveva un valore medio di 38 nm. Il valore del raggio idrodinamico in acqua (RH) era centrato sul valore di 154 nm, mentre aumentava considerevolmente quando veniva valutato in sudore sintetico, raggiungendo il valore di 727 nm al tempo 0 e 1254 nm dopo 24 ore. Questo fenomeno era chiaramente in accordo con il valore di potenziale Z misurato. I valori della carica di superficie suggerivano che le TiO_2NPs erano più stabili in acqua, grazie alla maggiore stabilizzazione elettrostatica. Dopo 24 ore di esposizione, la concentrazione media di Ti nella

soluzione ricevente era inferiore al livello di rilevamento (LOD) di 5 mcg/L sia nelle celle con cute intatta sia in quelle con cute danneggiata.

La quantità media di Ti nella cute intatta, dopo 24 ore di esposizione, era di 0,47 ± 0,33 mg/ cm^2 nello strato epidermico, mentre nel derma la concentrazione era inferiore LOD. La cute danneggiata, valutata nel sua interezza, ha mostrato valori di concentrazione simili (0,53 ± 0,26 μg/cm ^{2}).

Discussione e conclusioni:

Non è stata dimostrata permeazione delle TiO_2NPs attraverso la cute integra e lesa dopo 24 ore di esposizione. Questo risultato può essere spiegato dalla grande stabilità e dalla bassa capacità di ionizzazione delle NPs testate. Nella cute integra le TiO_2NPs sono state riscontrate nello strato epidermico ma non nel derma, e la concentrazione del metallo riscontrata all'interno della cute era similare in entrambi i test, il che ci permette di affermare che lesioni della cute non dovrebbero aumentare la penetrazione di queste NPs. I nostri risultati sono in linea con quelli derivanti da molti altri studi (Larese Filon F et al. 2015). Un altro aspetto importante da considerare è la grande dimensione delle particelle e la loro tendenza a formare aggregati, che riducono ulteriormente la capacità di assorbimento da parte della cute (Larese Filon F et al. 2015).

L'assenza di penetrazione attraverso l'epidermide è anche la ragione principale che spiega l'assenza di un effetto promotore di queste NPs nei confronti della carcinogenesi cutanea (Sagawa Y. et al. 2012, Xu J. et al. 2011). Tuttavia, altri studi come quello condotto da Tan e collaboratori (Tan M. et al. 1996) hanno evidenziato che i livelli di TiO2NPs nell'epidermide e nel derma di soggetti che avevano applicato una protezione solare contenente l'8% di TiO_2NPs era superiore ai livelli riscontrati nei controlli, valutato mediante tecnica del tape stripping. Questa differenza non era statisticamente significativa data la piccola dimensione

campionaria. Bannat e Müller-Goymann (2000)), hanno rilevato che le TiO_2NPs possono essere in grado di penetrare la superficie attraverso follicoli dei capelli o pori, dopo applicazione di una emulsione olio in acqua con 5% TiO_2NPs, ma non forniscono dati sul destino di tali particelle. Wu e collaboratori (2009) hanno valutato la penetrazione e la possibile tossicità di TiO_2NPs dopo esposizione demica di animanli in vitro (orecchie di suini) e in vivo (orecchie di maiale domestico e topi BALB/c glabri): non hanno riscontrato penetrazione dello strato corneo sulle escissioni di orecchie di maiale dopo 24 ore di esposizione. Tuttavia dopo 30 giorni di applicazione topica sull'orecchio di maiale, in vivo (24 mg di 5% TiO_2 su una superficie di 3 cm^2) hanno riscontrato penetrazione TiO_2 nello strato profondo dell'epidermide. Dopo 60 giorni di esposizione cutanea (400 mg/cm^2) su topi glabri è stato riscontrato TiO_2 in diversi tessuti ed aveva indotto svariate lesioni patologiche in diversi organi importanti, ma queste conclusioni sono state messe in discussione da altri autori (Jonaitis T. et al 2012). Adachi e collaboratori (Adachi K et al. 2013) hanno applicato sulla cute del dorso di topi glabri un'emulsione contenente il 10% wt% di TiO_2NPs per 56 giorni, ed hanno riscontrato che le particelle si trovavano solo al livello dello strato corneo dell'epidermide e dell'epitelio follicolare. Essi non hanno trovato alcuna prova di penetrazione TiO_2 in aree vitali. Inoltre questi Autori non hanno trovato Titanio in organi interni utilizzando la spettroscopia di massa a plasma accoppiato induttivamente. La maggiore concentrazione Titanio è stata trovata solo in campioni di tessuto polmonare, ed è stata determinata, probabilmente, dall' inalazione di TiO_2NPs.

Il nostro studio conferma la bassa penetrazione nella cute delle TiO_2NPs e l'assenza di una potenziale permeazione anche utilizzando un protocollo di abrasione della cute. Le TiO_2NPs tendono ad aggregare in condizioni fisiologiche, raggiungendo dimensioni maggiori che non sono compatibili con l'assorbimento cutaneo (Larese Filon F et al. 2015) anche utilizzando un protocollo di danneggiamento della cute. Inoltre queste NPs non possono rilasciare ioni

metallici in condizioni fisiologiche, pertanto il Titanio rimane negli strati superiori dello strato corneo o nei follicoli piliferi. Il nostro studio ha dimostrato che le TiO_2NPs non sono in grado di permeare la cute intatta nè danneggiata. Tuttavia il nostro studio presenta alcune limitazioni. La prima limitazione è legata al disegno in-vitro del nostro studio che può verificare solo la diffusione passiva attraverso la cute, mentre in condizioni in vivo potrebbe avvenire anche una penetrazione attiva. Il secondo limite è il metodo analitico disponibile per il rilevamento di Titanio: la spettrofotometria di assorbimento atomico (GF-AAS) con fornetto di grafite utilizzata ha un limite di rilevazione di 5 mcg/L, che è abbastanza elevato rispetto ad altre tecniche analitiche, come la spettrometria di massa con plasma induttivamente accoppiato (ICP-MS), che non può essere usato a causa della potenziale formazione di interferenze spettrali poliatomiche generate dai gas di plasma, argon, componenti della matrice e residui dal campione (Newman M., 2009). Recentemente l'ICP-MS in modalità a singola particella è stata adottata con successo per l'analisi di NPs nei campioni di acqua (Newman M., 2009) suggerendo che questa tecnica potrebbe essere utilizzata in campioni pre-trattati con acido nitrico. Tuttavia questa tecnica ha per titanio un limite di rilevazione superiore alla GF-AAS (5 mg/g) e Krystek e collaboratori (Krystek P. et al. 2014) hanno dimostrato che può essere utilizzata solo per i campioni con concentrazioni di Titanio> 4 µg/g di tessuto per ottenere risultati riproducibili. Questi aspetti analitici sono fondamentali quando si studia il contenuto di metalli in campioni biologici.

In conclusione i risultati del nostro studio non hanno riscontrato permeazione di TiO_2NP né attraverso la cute intatta né danneggiata. Sono state riscontrate NP nello strato epidermico, ma non nello strato dermico, e la concentrazione nella cute era simile in entrambe le prove, quindi le lesioni cutanee non sembrano modificare la permeazione di queste NPs. Questi risultati possono essere spiegati dalla grande stabilità e dalla scarsa capacità di queste particelle di ionizzare e sono in accordo a diversi studi in letteratura. Pur con le limitazioni sopra espresse i

nostri risultati conducono, nel complesso, a formulare un profilo di assorbimento percutaneo rassicurante per le TiO_2NPs. Sono tuttavia necessari ulteriori studi in vivo per la valutazione della sicurezza di queste NPs in condizioni di esposizione solare reale e su cute con lesioni attiniche da esposizione a raggi UV.

Per la bibliografia completa si faccia riferimento all'Allegato II

4.3 Permeazione transcutanea di Nanoparticelle di ossido di Cobalto attraverso cute integra e danneggiata

Introduzione e scopo dello studio:

Le nanoparticelle di Co_3O_4 (Co_3O_4NPs) sono fra le più importanti NPs di ossidi di metalli di transizione, poiché, in virtù delle loro peculiari caratteristiche magnetiche il loro utilizzo è stato proposto in applicazioni interessanti in campo biomedico, come ad esempio adiuvanti per vaccini (Cho W.S., 2012), come agenti di contrasto in risonanza magnetica (Karimi Z. et al. 2013), nel trattamento di alcune forme tumorali e come sistema di drug-delivery (Papis E. et al, 2009), ed in applicazioni industriali, dove trovano impiego, ad esempio, all'interno di catalizzatori e sensori per i gas, in dispositivi elettrocromici ed in pannelli per l'assorbimento di energia solare (Wei-Yang L. et al. 2005, Ren-Jang W. et al. 2003, Rahman M.M. et al.2012, Lou X.W. et al 2008, Shu-Lei C. et al 2008, Makhlouf, S.A. et al. 2002, Ando M. et al. 2004). Le Co_3O_4NPs sono classificate come nocive per gli esseri umani e pericolosi per l'ambiente, ma i dati sperimentali sono carenti. È noto che il cobalto è anche un sensibilizzante della cute (Rui F. et al 2013), ed un precedente studio del nostro gruppo dimostrato che l'esposizione cutanea a CoNPs del diametro medio di 80 nm può determinare permeazione della cute da parte di questo metallo (Larese Filon F. et al, 2013). Alcuni studi in letteratura hanno dimostrato, inoltre, che le Co_3O_4NPs sono in grado di indurre danno di membrana e genotossicità in cellule HepG2 attraverso la produzione di ROS e stress ossidativo (Alarifi S. et al. 2013). Non ci sono dati in letteratura riguardanti la capacità di permeazione di queste NPs attraverso la cute, pertanto lo scopo dello studio è stato quello di valutare il loro potenziale assorbimento percutaneo, poiché il numero di consumatori e lavoratori potenzialmente esposti a queste NPs può aumentare nei prossimi anni.

Materiali e metodi:

Sono stati condotti due esperimenti indipendenti di permeazione in vitro della durata di 24 ore ciascuno: in un esperimento è stata utilizzata cute integra (Exp. 1.) ed in uno cute danneggiata (Exp. 2,). In entrambi gli esperimenti sono state utilizzate 6 celle di Franz, esposte ad una sospensione di Co_3O_4NPs alla concentrazione di 1000 mg/L in soluzione fisiologica. Sei celle sono state trattate solo con soluzione fisiologica ed utilizzate come controllo (bianchi). La presenza di NPs nella cute è stata studiata con il TEM. La caratterizzazione delle NPs è stata ottenuta con le tecniche di Dynamic Light Scattering (DLS) e del potenziale Z. Per indagare la capacità di ionizzazione di queste NPs nei fluidi biologici sono stati condotti dei test di dissoluzione in sudore sintetico, la soluzione è stata ultrafiltrata (Amicon 10kD) ed analizzata tramite ICP-AES per analizzare la quantità di cobalto contenuta. I dati ottenuti sono stati analizzati con Excel per Windows, versione 2007, e il Software Stata, versione 11.0 (StataCorp LP, College Station, TX, USA). Tutti I dati sono stati riportati come media ± deviazione standard (SD). La differenza fra campioni indipendenti è stata testata tramite test di Mann-Whitney. È stato considerato come limite di significatività statistica un valore di $p < 0.05$

Risultati:

I risultati ottenuti dalla caratterizzazione delle Co_3O_4NPs hanno dimostrato che queste NP possedevano una superficie irregolare e non sferica, ed avevano tendenza a formare agglomerati di alcuni decine di NP. La distribuzione delle dimensioni delle NP era stretta e centrata intorno a un valore medio di 17 ± 0,2 nm. Non sono state trovate differenze nell'aggregazione delle soluzioni donatrici a 0 e 24 h. Il valore del raggio idrodinamico (RH) osservato in acqua era attorno ad un valore di 318 nm, mentre è aumentato notevolmente quando valutato in sudore sintetico, raggiungendo un valore superiore a 800 nm, che è rimasto abbastanza stabile durante tutto il tempo dell'esperimento (824 a 882 nm a t_0 e t_{24}). Questo

fenomeno era chiaramente in accordo con i valori di potenziale Z misurati. I valori di carica superficiale suggerivano una maggiore stabilità delle Co_3O_4NPs in acqua, in virtù della maggiore stabilizzazione elettrostatica. I risultati ottenuti dalla ultrafiltrazione della sospensione di NP hanno mostrato che la concentrazione di cobalto era sempre inferiore allo 0,1% della dispersione originale di NP.

Negli esperimenti condotti su cute intatta e nei controlli, la concentrazione di cobalto nelle fasi riceventi aveva valori simili, la concentrazione di cobalto non aumentava nel tempo e quindi non è stato riscontrato un flusso di permeazione. Nell'esperimento 2, in cui è stata utilizzata cute danneggiata, vi è stata invece permeazione del metallo, con i valori di flusso pari a 2,1 ± 2,0 $ng/cm^{-2}/h^{-1}$ e di lag time pari a 4,3 ± 2,1 h (media e deviazione standard). La quantità di cobalto permeata attraverso la pelle nelle 24 ore era significativamente maggiore quando è stato utilizzato il protocollo di danneggiamento della cute (57 ± 38 ng/cm^{-2}), mentre non sono state riscontrate differenze significative sulla cute intatta fra i controlli (0,92 ± 0,03 ng/cm^{-2}) e le celle esposte a Co_3O_4NPs (1,08 ± 0,20 ng/cm^{-2}). Le analisi ICP-AES della cute hanno rivelato una maggiore quantità di cobalto nell'epidermide (15,43 ± 3,01 mcg/cm^{-2}) rispetto al derma (1,42 ± 0,21 mcg/cm^{-2}) nella cute intatta (exp. 1 $p < 0,05$). La cute danneggiata aveva un contenuto di Co inferiore rispetto alla cute intatta (12,31 ± 6,18 mcg/cm^{-2} vs 16,85 ± 10,98 mcg/cm^{-2}, rispettivamente), senza raggiungere la significatività statistica, suggerendo che co può essere "immagazzinata" all'interno della pelle.

Discussione e conclusioni:

Questo studio ha valutato, per la prima volta in letteratura, l'assorbimento cutaneo di Co_3O_4NPs usando cute umana in un sistema di permeazione in vitro. I risultati hanno evidenziato che queste NPs sono in grado di attraversare la cute solamente quando questa barriera è danneggiata, mentre non è stato dimostrato alcun assorbimento attraverso la cute integra. Nella soluzione donatrice non è stato riscontrato alcun rilascio di ioni da parte di

queste NPs, elemento molto importante da valutare quando si studiano NPs metalliche. È noto infatti, che le NPs metalliche possono permeare la cute se hanno dimensioni molto ridotte (pari a 4 nm per i Quantum Dots, Chu M. et al. 2007), ma, più comunemente, il metallo di cui sono costituite può attraversare la barriera cutanea sotto forma di ioni rilasciati dalla superficie delle NPs (Larese Filon F. et al. 2007), che risulta enorme se confrontato con l'area di superficie degli omologhi materiali in forma tradizionale (Crosera M. et al 2009). Per gli ossidi metallici tuttavia, che risultano più stabili e meno solubili rispetto al metallo in forma non ossidata, questo rilascio è trascurabile (Barceloux D.G. et al. 1999, Collier C.G. et al 1992). Secondo alcuni Autori le nanoparticelle di ossido di cobalto sono meno tossiche rispetto agli ioni cobalto (Chattopadhyay S. et al. 2015), seppur ad un livello citologico, anche esse possono rilasciare ioni con un meccanismo del tipo "cavallo di troia" (Ortega R. et al. 2014), e causare una rapida induzione di specie reattive dell'ossigeno (ROS). La produzione di ROS da parte delle nanoparticelle sembrerebbe essere maggiore rispetto a quella determinata dagli ioni cobalto (Alarifi S. et el. 2013, Alinovi R. et al 2015, Limbach L.K. et al. 2007, Lundborg M. et al. 1992).

Abbiamo effettuato un confronto fra i risultati ottenuti nel presente studio e quelli derivanti da uno studio precedente, dove sono state impiegate nanoparticelle di Cobalto, ma che possedevano dimensioni maggiori (Larese Filon F. et al 2013). Il contenuto di metallo nella cute danneggiata era simile quando sono state utilizzate le Co_3O_4NPs (89,6% rispetto all'esperimento con CoNPs), mentre il contenuto nelle soluzioni riceventi ed il flusso transcutaneo erano significativamente minori (5,6% e 5%, rispettivamente).

Da questo punto di vista, considerando anche le dimensioni più piccole delle Co_3O_4NPs, è possibile affermare che esse sono più sicure delle CoNPs per quanto riguarda la permeazione della cute. Solo le CoNPs possono permeare attravero la cute intatta, determinando la presenza del metallo nelle fasi riceventi, mentre non vi è permeazione delle Co_3O_4NPs. Questa

differenza può essere spiegate dalla capacità delle prime di rilasciare ioni cobalto (Sabbioni E. et al 2014) e dalla sostanziale stabilità invece delle seconde in soluzione fisiologica, con conseguante incapacità di ionizzare (Barceloux D.G. et al. 1999, Collier C.G. et al 1992). Questo è stato dimostrato anche nel presente studio tramite l'analisi della concentrazione di ioni nella soluzione ultrafiltrata derivante dalla fase donatrice.

Si può concludere, quindi, che quando la cute è danneggiata o affetta da patologie che ne alterino le proprietà di barriera è fattibile un assorbimento di ossidi di metallo. Questo suggerisce la necessità di una maggiore protezione della cute nei consumatori e nei lavoratori portatori di patologie cutanee ed esposti a metalli ed anche ad ossidi di metallo, poiché un'alterazione della barriera cutanea è comune nei lavoratori e in soggetti con dermatite atopica (Bauer A. et al, 2010). Le NPs testate non potevano invece permeare la cute intatta, confermando che quando il rilasciare ioni non è possibile la permeazione non è così facile, diversamente da quanto accade con le CoNPs, che ionizzano facilmente.

Per la bibliografia completa si faccia riferimento all'Allegato III

4.4 Permeazione trancutanea di Nanoparticelle di Nichel

Introduzione e scopo dello studio

L'esposizione cutanea a Nichel (Ni) rappresenta una delle cause più comunemente riconosciute di dermatite da contatto, e nel modo colpisce circa 1,2 milioni di persone ogni anno. Le nanoparticelle di nichel (NiNPs) possiedono caratteristiche specifiche differenti rispetto al metallo in forma tradizionale, come ad esempio un forte potere magnetico, un basso punto di fusione, ed un'elevata area di superficie. Per tali motivazioni sono sempre più impiegate in svariate applicazioni industriali ed anche biomediche quali, ad esempio, nella produzione di nastri magnetici, in alcune fasi della catalisi chimica, in dispositivi per la rilevazione di gas ed anche come adiuvanti all'interno dei vaccini. Pertanto sempre più lavoratori e consumatori saranno esposti a queste NPs. È stato riportato un caso in letteratura in cui un lavoratore ha sviluppato sensibilizzazione al Ni a seguito della manipolazione ripetuta di una polvere di NiNPs senza essere stato equipaggiato con particolari protezioni individuali. Il presente studio ha avuto come scopo la valutazione della possibile permeazione cutanea da parte di queste nanoparticellle.

Materiali e metodi

Sono stati condotti due esperimenti indipendenti con l'utilizzo di cute intatta (Exp.1) e danneggiata (Exp.2). Ogni esperimento è stato effettuato allestendo 8 celle di diffusione di Franz. Come fase donatrice è stata utilizzata una sospensione di NiNPs alla concentrazione sovramassimale di 1g/L. Per ogni esperimento sono state aggiunte due celle come controllo, in cui la soluzione donatrice era costituita solo da sudore sintetico.

Risultati

Le nanoparticelle testate, valutate tramite TEM, avevano dimensioni medie pari a 77,7 ± 24,1 nm ed avevano tendenza a formare aggregati di maggiori dimensioni (range micrometrico) in sudore sintetico, che ne determinavano una precipitazione sulla superficie cutanea in pochi

minuti. La concentrazione delle nanoparticelle nella sospensione donatrice, pari a 1.0 g/L^{-1}, è stata confermata tramite analisi ICP-AES. La concentrazione di nichel nella soluzione donatrice ultrafiltrata, all'inizio del test, ha mostrato che il 12.6 ± 2.1% era in forma ionizzata, dato che non si è modificato significativamente nel corso dell'esperimento. Il nichel è permeato attraverso entrambi i tipi di cute, integra e danneggiata, con concentrazioni fino a due ordini di grandezza nelle soluzioni riceventi delle celle con cute danneggiata (0.032 ± 0.010 $\mu g/cm^{-2}$, e 5.2 ± 2.0 $\mu g/cm^{-2}$ a 24 ore, rispettivamente. p= 0,02). La concentrazione totale del nichel all'interno della cute era pari a 9,67 ± 2,70 $\mu g/cm^{-2}$ nella cute intatta e 29,2 ± 11,2 $\mu g/cm^{-2}$ nella cute lesa, espresse come media e deviazione standard. Le abrasioni della cute hanno determinato un raddoppio della concentrazione del metallo nell'epidermide (8.86 ± 2.66 $\mu g/cm^{-2}$ cute intatta e 18.4 ± 9.2 $\mu g/cm^{-2}$ cute danneggiata, p=0.006) ed ad un aumento di circa 10 volte nel derma (0.81 ± 0.27 $\mu g/cm^{-2}$ cute intatta e 10.8 ± 4.3 $\mu g/cm^{-2}$, cute danneggiata, p=0.006). La concentrazione di Nichel diminuiva significativamente (p = 0,01) dall'epidermide al derma, in entrambi i tipi di cute testati. Il flusso attraverso la cute danneggiata è di due ordini di grandezza superiore rispetto a quello attraverso la cute intatta (0,30 ± 0,12 $\mu g\ cm^{-2}/h^{-1}$ e 1,7 ± 0,6 $ng\ cm^{-2}/h^{-1}$, rispettivamente) (p = 0.006), mentre i valori di lag times sono simili (6.0 ± 1.4 h e 6,6 ± 0,8, rispettivamente).

Discussione e conclusioni:

Le applicazioni delle nanotecnologie stanno inondando il mercato con una serie di prodotti contenenti nanoparticelle ingenierizzate ed in prospettiva le future applicazioni sembrano poter essere ancora maggiori. Le nanoparticelle metalliche, inoltre, rappresentano un importante sottogruppo di questi nuovi materiali, poiché assumono proprietà chimico-fisiche differenti su scala nanometrica. Da un punto di vista tossicologico, tuttavia, le informazioni attualmente disponibili non sono esaustive per quanto concerne il loro potenziale di rischio per la salute umana. È noto che il nichel è un forte sensibilizzante e può causare dermatite

allergica da contatto, ma non è nota la sua capacità di permeazione della cute quando è utilizzato in forma nanoparticellare.

In questo studio è stato testato l'assorbimento transcutaneo di una polvere commerciale di nanonichel applicata su cute umana, intatta ed abrasa, tramite modello ex-vivo. I risultati hanno confermato che il nanonichel penetra e permea la cute, in concentrazioni significativamente maggiori quando la barriera cutanea è danneggiata. Confrontando questi risultati con quelli derivanti da uno studio precedente in cui abbiamo utilizzato una polvere di nichel con dimensione media 2,2-3,0 µ ed analogo protocollo sperimentale, si nota come le concentrazioni di metallo riscontrate nelle soluzioni riceventi siano dello stesso ordine di grandezza. Il quantitativo di nichel utilizzato nella fase donatrice era notevolmente inferiore nel caso della polvere di nanonichel, ma la percentuale di ionizzazione del metallo in questa polvere era notevolmente superiore (12,6% per NiNPs e 0,002% per Ni polvere fine). Questo dato è probabilmente dovuto all'alto rapporto superficie/volume delle nanoparticelle rispetto al metallo in forma tradizionale. Poiché le NiNPs avevano dimensione media di 80 nm e hanno tendenza ad aggregare in soluzione acquosa, è ipotizzabile che la maggior parte della permeazione transcutanea sia determinata dagli ioni rilasciati in sudore sintetico. Questa ipotesi è supportata anche dal basso numero di NiNPs visualizzate tramite l'indagine al TEM. I risultati di questo studio confermano inoltre la capacità della cute di ritenere ioni nichel. Se, infatti i valori di permeazione della cute intatta erano circa tre volte maggiori rispetto a quelli dei controlli, la concentrazione del metallo nella cute intatta (epidermide e derma) era circa 20 volte superiore rispetto ai controlli, e circa 40 volte superiore se si considera solo lo strato epidermico. Quindi la cute, ed in particolare l'epidermide, può fungere da reservoir di ioni nichel, che potrebbero essere rilasciati nel tempo (Fullerton e Hoelgaard, 1988).

In conclusione, i risultati di questo studio sollevano alcune preoccupazioni in relazione alla gestione di questi nanomateriali, perché è dimostarto che anche un contatto con modeste quantità di NiNPs sono in grado di determinare un assorbimento rilevante di nichel, maggiore

rispetto al metallo in forma tradizionale, e in grado di determinare sensibilizzazione e sintomatologia allergica nelle persone esposte. È necessario, pertanto, l'utilizzo di misure preventive, collettive ed individuali, quando si producono e maneggiano tali sostanze.

Per la bibliografia completa si faccia riferimento all'Allegato IV

4.5 Permeazione transmucosa di Nanoparticelle di Argento

Introduzione e scopo dello studio:

Le nanoparticelle di argento (AgNPs) sono diffusamente utilizzate negli imballaggi per la conservazione degli alimenti, nei dentifrici, negli spazzolini da denti, nei biberon, nei sistemi di purificazione dell'acqua (Kim et al. 2010, Hadrup et al. 2012). Tali utilizzi comportano il loro contatto con la mucosa orale, le cui proprietà di penetrazione non sono ancora completamente conosciute. L'argento è utilizzato per le sue note proprietà antibatteriche e il suo buon profilo di sicurezza (Wijnhoven et al. 2009) ma è altresì nota, dai dati presenti in letteratura, l'intossicazione da argento (Argiria) in persone che hanno introdotto questo metallo attraverso la via orale (Chang et al. 2006; Johnston et al. 2010) o attraverso la via transcutanea utilizzando garze medicate contenenti AgNPs su una superficie di cute ustionata superiore al 30% della superficie corporea totale (Trop et al. 2006).

La mucosa orale agisce tradizionalmente come prima barriera nei confronti degli xenobiotici nel tratto digestivo, ma è stata anche indagata come possibile via di *drug delivery* per formulazioni medicali (Harris D. and Robinson J.R. 1992). Essa possiede, infatti, una struttura istologica che permette una maggiore permeabilità di alcuni composti farmacologici rispetto a quanto avviene a livello cutaneo ed inoltre può evitare l'effetto di primo passaggio attraverso il fegato, diversamente da quanto accade attraverso la via intestinale tradizionale (Wertz P.W. and Squier C.A. 1991).

Lo spessore medio della mucosa orale è approssimativamente di 500-800 μm e le caratteristiche di permeabilità differiscono nelle diverse regioni del cavo orale, in relazione al tipo di epitelio, al tipo ed alla quantità di lipidi intercellulari ed alla natura chimica delle sostanze che vengono applicate. È stato dimostrato che la barriera più importante per la penetrazione delle sostanze esterne è rappresentata dal terzo superiore dell'epitelio (Gandhi R.

e Robinson J. 1988), poiché le dimensioni delle cellule crescono e la loro forma si appiattisce passando dallo strato basale a quello superficiale.

Da quando la nanotecnologia si è diffusa ed è aumentato l'uso di elementi in forma nanoparticellare in molti settori della vita quotidiana, solamente pochi studi hanno valutato la possibile differenza nei profili di permeazione fra nanoparticelle e omologhe sostanze in forma macromolecolare attraverso la membrana mucosa, inoltre non è chiaro se le nanoparticelle possono essere rischiose per la salute e la sicurezza umana o se, al contrario, possano essere sfruttate come nano-carriers per migliorare la somministrazione di farmaci (Teubl 2012, Roblegg 2011).

Gli studi presenti in letteratura hanno indagato la penetrazione di NPs di polistirene, con risultati controversi. Olmsted e colleghi (2001) hanno dimostrato che nanoparticelle neutre del diametro di 59 nm vengono completamente immobilizzate a livello del muco della cervice, mentre secondo Teubl e collaboratori (2012) nanoparticelle delle dimensioni di 25 nm, 50 nm and 200 nm possono oltrepassare il film di muco e penetrare nella mucosa buccale in modo direttamente proporzionale alle loro dimensioni, contrariamente a quanto si potrebbe ipotizzare.

Poiché le caratteristiche di penetrazione attraverso la mucosa orale non sono ancora del tutto note abbiamo progettato uno studio al fine di verificare la capacità delle AgNPs di oltrepassare tale barriera e di essere così disponibili per l'assorbimento sistemico. Abbiamo scelto di utilizzare la mucosa buccale perché si ritiene che sia quella maggiormente implicata nell'assorbimento a livello del cavo orale e le AgNPs poiché, grazie alle note proprietà antibatteriche, sono comunemente utilizzate in molti devices che possono entrare in contatto con la mucosa orale.

Materiali e metodi

Sono stati condotti degli esperimenti di permeazione transmucosa in vitro. Sono state create due differenti soluzioni donatrici ed applicate separatamente sulla superficie esterna della mucosa di due gruppi di 4 celle ciascuno. La prima era una sospensione di AgNPs alla concentrazione di 500 mg/L (Esp. 1), mentre la seconda era una soluzione ottenuta dall'ultrafiltrazione della prima (filtri Amicon Ultra-4, 10KDa MWCO) e contenente solo ioni Ag (Esp.2). Le AgNPs utilizzate (core di argento: 25%, rivestimento in polivinirropirolidone: 75%) avevano dimensioni pari a 19 ± 5 nm (media e deviazione standard). Gli esperimenti sono stati condotti per un totale di 4 ore (Robbleg, Frolig 2012). Ogni esperimento è stato ripetuto due volte per un totale di 8 celle, con 64 analisi del contenuto di argento nelle celle riceventi e 7 analisi delle membrane mucose. Alcuni campioni di mucosa sono stati anche fissato in glutaraldeide al 10%, per le analisi al microscopio elettronico a scansione (SEM-EDX). Le NPs utilizzate sono state caratterizzate tramite microscopio elettronico a trasmissione TEM, tecnica DLS e del potenziale Z. L'analisi dei dati è stata condotta tramite Excel per Windows 2007 ed il Software Stata, versione 11.0 (StataCorp LP, College Station, TX, USA). Tutti i dati sono stati riportati come media ± deviazione standard (DS). La differenza fra campioni indipendenti è stata testata con test di Mann-Whitney. Come limite di significatività statistica si è scelto un valore di $p < 0.05$.

Risultati

Le analisi al TEM hanno rivelato che le AgNPs usate nella soluzione donatrice erano della dimensione pari a 19 ± 5 nm e uniformi in dimensione e forma (numero di nanoparticelle analizzate = 100) ed alla concentrazione utilizzata non sono stati visualizzati aggregati. L'analisi quantitativa delle aliquote ultrafiltrate ha rivelato che il 5% della soluzione donatrice si poteva considerare ionizzata (o quantomeno in una forma capace di attraversale i filtri di 10 KDa): questo significa che come fase donatrice nell'esperimento 2 è stata utilizzata una dose pari a 3.8 $\mu g\ cm^{-2}$. L'analisi delle dimensioni delle nanoparticelle ottenuta tramite analisi DLS

mostrava una curva di distribuzione abbastanza stretta, elemento che depone per una buona omogeneità delle NPs utilizzate. Il diametro medio delle NPs risultava pari a 57.10 nm, con una dispersione, indicata come indice di polidispersione (PdI= polidispersity index), pari a 0.28. Tale dato, definito come diametro idrodinamico, ed apparentemente discrepante rispetto a quello ottenuto con l'analisi TEM, tiene in considerazione anche lo spessore del rivestimento delle nanoparticelle in polivinilpirrolidone, e risulta pertanto maggiore. È stato dimostrato un flusso di permeazione attraverso la mucosa ed il trend delle concentrazioni di argento nelle fasi riceventi era crescente in funzione del tempo, con valori finali similari nelle celle esposte ad AgNPs e alla soluzione ultrafiltrata (12.2 ± 7.4 ng cm^{-2} h^{-1} e 11.8 ± 11.1 ng cm^{-2} h^{-1}, rispettiavemente). Anche i valori dei flussi di permeazione ed i lag times, sono risultati similari alla quarta ora di esperimento nelle celle esposte ad AgNPs e alla soluzione ultrafiltrata (flussi: 6.8 ± 4.5 ng cm^{-2} h^{-1} e 5.2 ± 4.3 ng cm^{-2} h^{-1} rispettivamente, lag times: 1.9 ± 0.7 h e 1.7 ± 0.7 h). La concentrazione di argento nella mucosa ha mostrato valori similari in entrambi gli esperimenti (1.6 ± 2.0 µg/cm^2 nella mucosa esposta ad AgNPs e 1.2 ± 0.8 µg/cm^2 alla soluzione ultrafiltrata). Le indagini SEM-EDX non hanno mostrato tracce di cluster di AgNPs nei tessuti. L'analisi SEM ha rivelato la presenza di zone elettrondense al di sopra del tessuto mucoso esposto ad AgNPs, ma l'analisi specifica delle zone elettrondense ha dimostrato l'assenza di argento o particelle di cloruro di argento.

Discussione e conclusioni:

La mucosa orale è stata largamente indagata come possibile via di assorbimento sistemico per farmaci, ma pochi sono gli studi che hanno approfondito il suo ruolo nei confronti dell'assorbimento di sostanze in forma nanoparticellare. Se da un lato la mucosa orale agisce come prima barriera nei confronti di xenobiotici e patogeni, dall'altro si pone come porta d'ingresso alla circolazione sistemica per le sostanze che riescono a penetrarla. Pochi studi sono stati condotti per misurare la permeabilità della mucosa nei confronti delle nano

particelle, e la maggior parte di questi si è concentrato sull'analisi di nanoparticelle di polistirene, giungendo a risultati discordanti.

Olmsted e colleghi hanno dimostrato che microsfere di polistirene (del diametro di 59-1000 nm) sono completamente immobilizzate nello strato di muco della cervice uterina e non possono penetrare la mucosa, mentre Holpuch e collaboratori hanno dimostrato che nanoparticelle di polistirene delle dimensioni di 210 nm possono oltrepassare l'epitelio integro della mucosa umana e possono essere riscontrate a livello del tessuto connettivo sottostante, dimostrando quindi la capacità delle NPs di penetrare la membrana basale. Robblegg e colleghi hanno investigato il comportamento delle NPs attraverso la membrana mucosa orale effettuando una serie di esperimenti con NP di diverse dimensioni e con diversa carica superficiale e utilizzando membrane mucose a diversa temperatura. Questo gruppo ha dimostrato che NPs di polistirene (PP) a carica neutra delle dimensioni di 25, 50 e 200 nm possono tutte attraversare la mucosa, sorprendentemente in modo direttamente proporzionale alle loro dimensioni. NPs a carica positiva, delle dimensioni di 200 nm possono anch'esse attraversare la membrana mucosa, mentre NPs delle stesse dimensioni ma cariche negativamente aggregano e vengono immobilizzate nello strato mucoso e solamente quelle di grandezza pari a 20 nm possono passare. Inoltre è stato dimostrato che anche la concentrazione di NPs gioca un ruolo nell'uptake orale, poiché aumentando la loro concentrazione (50-100-200 µg/ml) l'assorbimento decresce, dato probabilmente attribuibile alla formazione di aggregati. Questo studio aveva lo scopo di indagare le capacità di permeazione di AgNPs attraverso la mucosa orale suina mediante l'utilizzo delle celle di diffusione statica di Franz. I risultati hanno evidenziato, per la prima volta, che le AgNPs possono favorire l'assorbimento di argento attraverso la mucosa del cavo orale in una quantità analoga a quella ottenuta utilizzando argento in forma ionizzata. Si può pertanto affermare che la maggior quantità di argento assorbito è determinata dalla forma ionizzata del metallo. Un'ulteriore supporto a questa ipotesi è fornito dai risultati delle indagini al SEM, che non

identificano la presenza di cluster di AgNPs nel tessuto, mentre dalle analisi quantitative viene garantita la presenza del metallo nel tessuto mineralizzato. Si sottolinea che il nostro studio ha indagato esclusivamente l'assorbimento di AgNPs attraverso la mucosa orale integra, ma nella vita quotidiana ci sono circostanze comuni che possono condurre ad un'alterazione della sua integrità, quali ad esempio la presenza di reflusso gastroesofageo, di infezioni e di abrasioni accidentali che nel complesso potrebbero comportare un incremento dell'uptake mucoso.

Per la bibliografia completa si faccia riferimento all'Allegato I

4.6 Studio pilota sulla permeazione transmeningea di nanoparticelle di Argento

Introduzione e scopo dello studio:

Le nanoparticelle di Argento (AgNPs) sono comunemente utilizzate in molti spray antibatterici per la disinfezione di una vasta gamma di superfici, in ambito professionale ed extraprofessionale. Il loro utilizzo in forma nebulizzata è stato anche proposto come rimedio per i disturbi respiratori, il che significa che molti pazienti possono essere esposti a una considerevole quantità di AgNPs per inalazione (http://thesilveredge.com/nebulize-colloidal-silver.shtml). L'argento è un metallo generalmente ben tollerato e non tossico per l'uomo, ma esistono isolate segnalazioni di disturbi neurologici, renali ed epatici a seguito del suo assorbimento in grandi quantità (Brandt D. et al. 2005; Stepien K.M. et al 2009). Kim e colleghi hanno studiato alcuni spray commerciali contenenti AgNPs ed hanno riscontrato dei livelli di esposizione superiori al livello di esposizione esente da rischio (Kim 2015). L'esposizione per inalazione pone quindi sia il problema, ben noto, di una possibile traslocazione delle NPs attraverso la barriera alveolo-capillare a livello polmonare, sia un possibile problema, meno conosciuto, legato all'assorbimento diretto a livello del sistema nervoso centrale (SNC) attraverso la via intranasale, capace di aggirare la serrata barriera emato-encefalica (BBB). Si ritiene che il SNC sia un organo altamente protetto dalla penetrazione di xenobiotici, grazie alla presenza di strutture di barriera, ma esiste, tuttavia, un collegamento diretto tra l'ambiente esterno e le porzioni anteriori del SNC, garantito dal nervo olfattorio. Quest'ultimo fuoriesce dalla scatola cranica attraverso le aperture della lamina cribrosa dell'etmoide e della dura madre che la riveste, portandosi in direzione della cavità nasale. In questo tragitto i rami del nervo olfattorio sono avvolti da prolungamenti della dura madre, che discendono nel naso attraverso i suddetti fori. (Trattato di Neurologia, G. Valentin, Professore di Anatomia e Fisiologia dell'Università di Berna, tradotto dal tedesco da A.G. Jourdan, prima traduzione italiana a cura di M.G. Dott. Levi Medico. Venezia. Nel premiato stab. Di G. Antonelli Ed. 1844).

Questa via di penetrazione è stata estesamente studiata negli ultimi decenni per la somministrazione di farmaci utilizzati in patologie del SNC quali i disturbi cognitivi, patologie neurodegenerative, psichiatriche ed anche per alcuni disturbi funzionali (Meredith 2015, Kao nel 2000, Hanson 2008, Pardridge 2005; Illum 2004, Patel et al 2010). Alcuni studi hanno dimostrato che, quando i farmaci venivano somministrati in forma nanoparticellare, tutti i comparti del sistema nervoso centrale (liquido cerebro-spinale, bulbo olfattivo, tratto olfattivo, cervello e cervelletto,) ricevevano da 1,6 a 3,3 volte la concentrazione del farmaco rispetto alla sua somministrazione in forma tradizionale (Oberdorster 2009). Questa via di penetrazione, ad oggi, risulta poco studiata per quanto concerne un potenziale assorbimento di NPs metalliche, e rappresenta una questione di interesse in quanto potrebbe rendere il sistema nervoso centrale vulnerabile agli effetti neurotossici di xenobiotici presenti in un ambiente inquinato e/o in scenari professionali (Tĭalve & Henriksson, 1999; Arvidson, 1994; Dorman et al. 2002). Lo studio condotto ha avuto come scopo la valutazione della potenziale permeabilità delle membrane meningee nei confronti delle più comuni NPs ingenierizzate, ovvero le AgNPs.

Materiali e metodi

Sono state utilizzate due differenti soluzioni donatrici, che sono state applicate separatamente sulla superficie esterna delle meningi. La prima era una sospensione di AgNPs alla concentrazione di 500 mg/L (Esp. 1), mentre la seconda era una soluzione ottenuta dall'ultrafiltrazione della prima (filtri Amicon Ultra-4, 10KDa MWCO) e contenente solo ioni Ag (Esp.2). Le AgNPs avevano dimensioni pari a 19 ± 5 nm (media e deviazione standard). L'esperimento è stato condotto per un totale di 2 ore. L'esperimento 1 è stato ripetuto due volte per un totale di 6 celle, con 42 analisi del contenuto di argento nelle celle riceventi e 6 analisi delle membrane mucose. Il test 2 è stato ripetuto 2 volte, per un totale di 2 celle, 14 analisi del contenuto di argento nelle celle riceventi e 2 analisi delle membrane meningee.

Risultati:

È stato dimostrato un flusso di permeazione attraverso le meningi. Il trend delle concentrazioni di argento nelle fasi riceventi è risultato crescente in funzione del tempo, con valori finali similari nelle celle esposte ad AgNPs e alla soluzione ultrafiltrata (0.042 ± 0.042 µg cm-2 h-1 e 0.044 ± 0.035 µg cm-2 h-1, rispettivamente, $p > 0.005$). Anche i valori dei flussi di permeazione e le concentrazioni di argento nelle meningi sono risultati similari alla seconda ora di esperimento nelle celle esposte ad AgNPs e alla soluzione ultrafiltrata (flussi: 0.76 ± 0.9 ng cm-2 h-1 e 0.72 ± 0.1 ng cm-2 h-1 rispettivamente, mucose: 0.27 ± 0.05 µg/cm2 nella mucosa esposta ad AgNPs e 0.29 ± 0.06 µg/cm2 alla soluzione ultrafiltrata, $p > 0.005$).

Discussione e conclusioni:

Le AgNPs sono comunemente utilizzate in spray, nebbie antisettiche ed anche in forma nebulizzata per la cura di problematiche respiratorie. È possibile pertanto un loro contatto con le mucose delle prime vie aeree e con la mucosa olfattoria. Lo studio pilota condotto si proponeva di valutare il passaggio di AgNPs attraverso le meningi, membrame che avvolgono il SNC ed i filuzzi olfattori nel tragitto che va dal bulbo olfattorio alla mucosa della cavità nasale (Nieuwenhuys R 2010, Lennart Heimer, Vishram Singh, G. Valentin, 1844). I risultati hanno dimostrato che è possibile un assorbimento, seppur minimo, di questo metallo. Abbiamo testato due soluzioni, una contenente AgNPs delle dimensioni di 19 nm e l'altra contenente una soluzione identica alla prima ma ultrafiltrata, nella quale cioè le NPs sono state rimosse ed è rimasto solo l'argento disciolto, rilasciato dalle stesse. Poiché le concentrazioni riscontrate transmembrana erano simili in entrambi gli esperimenti, riteniamo probabile che la permeazione sia in gran parte attribuibile alla porzione ionizzata del metallo. Ciò è in linea con i risultati di altri studi condotti dal nostro gruppo su altre membrane biologiche, quali la cute e la mucosa orale (Larese Filon 2009, Mauro 2015).

È necessario considerare, tuttavia, che questi dati derivano da uno studio in vitro, e quindi possono sottovalutare il fenomeno poiché non prendono in considerazione qualsiasi tipo di

assorbimento attivo. Studi condotti in vivo su animali, infatti, hanno mostrato che una traslocazione di NP dalla mucosa olfattiva al bulbo olfattivo è possibile per la maggior parte delle NPs esaminate, come quelle di argento (De Lorenzo 1970), carbonio (Oberdorser 2004, Zhang et al, 2006), grafite (Oberdorser 2004), manganese (Elder 2006), oro (Yu et al, 2007) e biossido di titanio (Wang et al. 2008 a, b). Nella maggior parte dei casi, gli autori propendono per un lento assorbimento attraverso la via intraneuronale attraverso i filuzzi olfattivi, poiché la dimensione delle NPs testate, che avevano dimensioni comprese tra i 30 ed i 70 nm, erano troppo grandi per passare attraverso le tight junctions della membrana basale della mucosa olfattiva. D'altra parte i risultati di uno studio condotto iniettando nanoparticelle di oro radioattivo a livello di mucosa olfattoria (Czerniawska 1970), hanno dimostrato che i valori maggiori di radioattività sono stati riscontrati a livello del liquido cerebrospinale (CSF) che circonda il bulbo olfattivo ed il corpo calloso. Gli autori hanno interpretato questo risultato come una possibile prova di un collegamento perineurale diretto tra la mucosa olfattiva e il CSF (Orosz et al. 1957). In quest'ultimo caso è stato descritto altrove in letteratura che la via di traslocazione è molto più rapida (Illum, 2000).

Anche se il nostro studio non è stato progettato per distinguere tra i diversi percorsi della via intranasale, riteniamo che una penetrazione attraverso le tight junctions delle AgNPs testate (19 nm) sia improbabile. Il riscontro di concentrazioni di metallo transmembrana è tuttavia un dato interessante se si considera la struttura anatomica dei filuzzi olfattori. Piccoli gruppi di questi neuroni, infatti, vengono avvolti da una unica e comune cellula di Schwann, che crea alcune cavità extracellulari tra un neurone e l'altro, chiamati "Mesassoni". Queste cavità funzionano come un potenziale reservoir di ioni (Mistry 2009 De Lorenzo 1960), che quindi possono passare tra il fluido extracellulare e l'assoplasma, determinando un potenziale assorbimento ritardato di tali sostanze.

Sebbene l'argento sia comunemente considerato un metallo generalmente ben tollerato e non tossico per gli esseri umani, recenti evidenze hanno dimostrato che può avere effetti

neurotossici, sia in vivo che in vitro (Xu L 2015 a, b, Oh JH 2015). Natàlia Garcia-Reyero e collaboratori (2015) hanno dimostrato in vivo che nel SNC dei pesci l'esposizione a $AgNO_3$ e AgNPs determina effetti di stress ossidativo, alterazione nella produzione di neurotrasmettitori ed affezioni neurologiche. Skalska J e collaboratori (2015) hanno dimostrato in vivo che l'esposizione di ratti adulti ad Ag in forma ionica e nanoparticellare (10nm) porta a degenerazione sinaptica, con gravità maggiore quando vengono usate NPs. La regione del cervello più colpita sembra essere l'ippocampo, le cui alterazioni possono condurre a deterioramento cognitivo (Skalska J et al 2015, Bagheri-Abassi F 2015).

In conclusione, i risultati del nostro studio forniscono, per la prima volta, la prova che le meningi sono permeabili nei confronti dell'argento quando questo viene applicato in forma nanoparticellare. Seppur con i limiti determinati dalla dimensione campionaria dello studio questo dato ci permette di dire che questa membrana biologica non è completamente impermeabile agli agenti esterni, pertanto la via intranasale richiede ulteriori sforzi investigativi volti a chiarirne le caratteristiche di permeabilità nei confronti di altre NPs. Ogni NPs metallica, infatti, possiede differenti caratteristiche chimico-fisiche, che variano in funzione delle dimensioni, della chimica di superficie e dei possibili rivestimenti esterni. Pertanto la loro interazione con le meningi richiede di essere valutata caso per caso.

Per la bibliografia completa si faccia riferimento all'Allegato VI

5. CONCLUSIONI

In conclusione i risultati degli esperimenti condotti nel corso del presente dottorato hanno dimostrato che le nanoparticelle di nichel (78 nm cica) sono in grado di determinare permeazione del metallo sia attraverso la cute integra, sia attraverso la cute danneggiata, con un significativo aumento delle concentrazioni transcutanee quando la barriera cutanea presenta alterazioni. Le nanoparticelle di rodio e platino (6 nm circa), ossido di cobalto (17 nm circa) e biossido di titanio (40 nm circa), invece, non penetrano la barriera cutanea quando essa è intatta, mentre, solamente quelle di rodio e di ossido di cobalto sono in grado di determinare permeazione del metallo in tracce nelle soluzioni riceventi quando la cute è danneggiata. In generale si può affermare che gli ossidi di metallo testati risultano più stabili in soluzione rispetto ai metalli con stato di ossidazione 0. Questo è determinato dal fatto che una loro dissoluzione nei fluidi biologici è scarsa o assente e, conseguentemente, il rilascio di ioni nelle soluzioni donatrici è pressoché pari a zero. Il biossido di titanio, infatti, non è in grado di passare attraverso la barriera cutanea in alcuno dei casi testati (cute integra e cute lesa), mentre l'ossido di cobalto permea solo in tracce attraverso la cute danneggiata (concentrazioni nel range dei ng/cm^{-2}), diversamente dai risultati di uno studio precedente in cui sono state testate nanoparticelle di cobalto (Larese Filon F. et al 2013). I risultati in quel caso avevano determinato una concentrazione di metallo di circa 17 volte superiore rispetto a quelle del cobalto ossido attraverso la cute danneggiata ed erano anche in grado di determinare permeazione del metallo attraverso la cute intatta.

Da un punto di vista tossicologico questo dato è valevole anche per altri ossidi di metallo, come confermato anche da una nostra recente revisione dei dati presenti in letteratura (Larese et al. 2015) e garantisce una maggior sicurezza per lavoratori e consumatori esposti a tali nanoparticelle.

Per quanto riguarda le nanoparticelle metalliche in forma non ossida, invece, sono interessanti i dati derivanti dal nanonichel. Se si confrontano i risultati dello studio condotto con le

nanoparticelle di nichel nel presente progetto di dottorato con quelli di un precedente lavoro del nostro gruppo (Larese et al., 2009), in cui è stata testata una polvere fine di nichel (range micrometrico) si nota che, anche se il quantitativo di nichel utilizzato nella fase donatrice era notevolmente inferiore nel caso del nanonichel, la percentuale di ionizzazione del metallo in soluzione era notevolmente superiore rispetto a quello della polvere fine (12,6% per NiNPs e 0,002% per Ni polvere fine). Questo conferma che, per le nanoparticelle di metallo, la capacità di dissoluzione in fluidi biologici è uno dei principali determinanti ai fini della permeazione, e che nell'intervallo di dimensioni nanometriche l'alto rapporto superficie/volume delle particelle permette una maggiore ionizzazione.

I risultati derivanti dagli studi condotti utilizzando nanoparticelle di argento (20 nm circa) applicate sulla mucosa del cavo orale e sulle meningi hanno sostanzialmente dimostrato che la permeazione di questo metallo attraverso queste membrane è possibile. Le concentrazioni riscontrate nelle fasi riceventi erano simili sia quando è stata utilizzata come fase donatrice una sospensione di nano particelle di argento sia quando è stata utilizzata la soluzione ultrafiltrata derivante dalla sospensione, il che ci permette di concludere che la massima parte della permeazione del metallo è avvenuta in virtù della quota di metallo disciolta e/o ionizzata. Un'ulteriore supporto a questa ipotesi è fornito dai risultati delle indagini al SEM, che non hanno identificano la presenza di cluster di AgNPs nella mucosa, mentre le analisi quantitative hanno garantito la presenza del metallo nel tessuto mineralizzato.

Nel caso della mucosa del cavo orale e delle meningi le membrane sono state indagate solo in forma integra, ma in condizioni reali è possibile un loro danneggiamento a seguito di reflusso gastroesofageo, infezioni o abrasioni accidentali, per quanto riguarda la mucosa orale, e affezioni sistemiche quali ipertensione arteriosa, patologie neurodegenerative, infiammatorie o infettive, nel caso delle meningi.

Queste ultime considerazioni evidenziano la necessità di ulteriori studi sperimentali volti alla comprensione delle caratteristiche di permeazione di queste membrane quando la loro struttura è danneggiata ed anche nei confronti di altre nanoparticelle che possono essere comunemente riscontrate in ambiente occupazionale.

6. BIBLIOGRAFIA

Adams D (1976). Keratinization of the oral epithelium. Annals of The Royal College of Surgeons of England 58, 351-358.

Andersen LKT, Mackenzie I (1986). Oral mucous membrane. In Human oral embryology and histology. Copenhagen: Munksgaard

Bronaugh RL and Franz T J (1986) Vehicle effects on percutaneous absorption : in vivo and in vitro comparisons with human skin. Br. J. Dermatol. 115: 1-11.
Bronaugh RL, Stewart RF (1985) Methods for in vitro percutaneous absorption studies V: Permeation through damaged skin.J Pharm Sci. 74(10):1062-6.

Caon T, Simoes CM (2011) Effect of freezing and type of mucosa on ex vivo drug permeability parameters. AAPS Pharm Sci Tech 12(2): 587-592

Dalle Donne I, Gagliano N, Bertolini B, Bonfanti P, Colombo A, Rossi AR, Stefanini S, Milzani A (2011). Istologia ed elementi di anatomia microscopica. EdiSES

Davies DJ, Ward RJ, Heylings JR (2004). Multi-species assessment of electrical resistance as a skin integrity marker for in vivo percutaneous absorption studies. Toxicol. In vitro 18:351-358.

Drexler H (1998) Assignment of skin notation for MAK values and its legal consequences in Germany. Int. Arch. Occup. Environ. Health 71, 503-505.

EDETOX, 2000. Evaluations and Predictions of Dermal Absorption of Toxic Chemicals, EU Framework V: Quality of Life, Environment and Health Key Action Funding (Project Number: QLKA-2000-00196).

Elias PM (1983). Epidermal lipids, barrier function and desquamation. J. Invest. Dermatol. 80 (Suppl.), 44S–49S.

Elias PM, Williams ML, Crumrine D, Schmuth M (2010) Inherited disorders of corneocyte proteins. Curr Probl Dermatol. 39:98-131.

Franz TJ (1975) On the relevance of *in vitro* data. J. Invest. Dermatol. 93: 633-640.

G. Valentin (1844) Trattato di Neurologia, prima traduzione italiana a cura di M.G. Dott. Levi Medico. Venezia. G. Antonelli Ed., pag. 220-228

Hanson LR, Frey WH 2nd. (2008). Intranasal delivery bypasses the blood-brain barrier to target therapeutic agents to the central nervous system and treat neurodegenerative disease. BMC Neurosci. 9 Suppl 3:S5.

Kao HD, Traboulsi A, Itoh S, Dittert L, Hussain A (2000) Enhancement of the systemic and CNS specific delivery of l-Dopa by the nasal administration of its water soluble prodrugs. Pharm. Res. 17, 978–984.

Knorr F, Lademann J, Patzelt A, Sterry W, Blume-Peytavi U, Vogt A (2009) Follicular transport route – research progress and future perspectives. Eur. J. Pharm. Biopharm. 71, 173–180.

Lestari ML, Nicolazzo JA, Finnin BC (2009) A novel flow through diffusion cell for assessing drug transport across the buccal mucosa in vitro. J Pharm Sci. 98(12):4577-88.

Meredith ME, Salameh TS, Banks WA (2015) Intranasal Delivery of Proteins and Peptides in the Treatment of Neurodegenerative Diseases. 17(4):780-7.

Monteiro-Riviere NA, Bristol DG, Manning TO, Rogers RA, Riviere JE (1990). Interspecies and interregional analysis of the comparative histologic thickness and laser Doppler blood flow measurements at five cutaneous sites in nine species.J Invest Dermatol. Nov;95(5):582-6.

Monteiro-Riviere NA (2004) Anatomical factors affecting barrier function. In: Dermatotoxicology. Eds. H. Zhai and H.I. Maibach, CRC Press. pp. 43-70.

Monteiro-Riviere NA (2006) Structure and function of skin. In: Dermal Absorption Models in Toxicology and Pharmacology. Ed. J.E. Riviere, Taylor and Francis. pp. 1-19.

Monteiro-Riviere, NA (2010) Structure and function of skin. In: Monteiro-Riviere, N.A. (Ed.), Toxicology of the Skin – Target Organ Series, Informa Healthcare, vol. 29. New York, NY, pp. 1–18 (Chapter 1).

Nieuwenhuys R, Voogd J, van Huijzen C (2010) “Il sistema nervoso centrale”, Springer-Verlag Italia, pag 97

Nieuwenhuys, Voogd, van Huijzen (2010) Il sistema nervoso centrale. Springer, 2° edizione italiana a cura di Michele Papa, pag 97 e 124.

Rougier A, Rallis M, Krien P, Lotte C (1990). In vivo percitaneous absorption: a key role for stratum corneum/ vehicle partitioning. Arch. Dermatol. Res. 282: 498 - 505.

Scheuplein RJ (1967) Mechanisms of percutaneous absorption, II. Transient diffusion and the relative importance of various routes of skin penetration. J. Invest. Dermatol. 48: 79-88.

Squier CA, Kremer M (2001) Biology of oral mucosa and esophagus. J Natl Cancer Inst Monogr.;(29):7-15.

Vyas TK, Shahiwala A, Marathe S, Misra A (2005) Intranasal drug delivery for brain targeting. Curr Drug Deliv. 2(2):165-75.

Wheater (2014) Istologia e anatomia microscopica Barbara Young, John W. Heath, Phillip Woodford, 6° ed. cap 13

ALLEGATI

ALLEGATO I

PERMEATION OF PLATINUM AND RHODIUM NANOPARTICLES THROUGH INTACT AND DAMAGED HUMAN SKIN.

Mauro M, Crosera M, Bianco C, Adami G, Montini T, Fornasiero P, Jaganjac M, Bovenzi M, Filon FL.

Pubblicato in: Journal of Nanoparticles Research (2015) 17:253

Abstract

Keywords: platinum, rhodium, nanoparticles, sensitizer, intact and damaged skin.

1. Introduction

During the past centuries PGEs (Platinum Group Elements) exposure has been mainly an occupational hazard. Workers who were employed in refineries and in catalyst production - where high concentrations of PGEs salts were observed - showed a high incidence of allergic IgE-mediated reactions. Platinum salts have been strongly associated with an increased incidence of asthma, rhinoconjuntivitis, dermatitis and urticaria among exposed workers (Santucci et al. 2000; Cristaudo et al. 2005), while few data regarding rhodium sensitizing potential were collected (Cristaudo et al. 2005).

Nowadays these kinds of exposures are uncommon, thanks to improved working conditions; nevertheless, concern on human health is growing because of environmental spreading of PGEs in the particulate, which is mainly emitted by vehicles during operations (Moldovan et al. 2002).

Among PGEs, platinum concentration ranks highest in the environment. Estimates say (Barbante et al. 2001) that Pt emission worldwide can reach up to 0.5-1.4 ton/year by means of automobile exhaust only, and the total potential PGE intake - through daily inhalation of PM10 - is thought to be approximately 0.062 ng/m^3 for platinum (Schierl 2000) and 0.004 ng/m^3 for rhodium (Bocca et al. 2006).

The dimensions of PGEs emissions from vehicle catalysts are usually present either in the form of large agglomerates but also in the form of nanometer size particles, potentially more dangerous. These can be present in airborne particulate matter (PM), roadside dust, soil, sludge and water, eventually causing a bioaccumulation of toxic substances in living organisms (Ravindra et al. 2004). Rhodium nanoparticles (RhNPs) and platinum nanoparticles (PtNPs), released from PGEs emissions, can interact with human body and can be absorbed as nanoparticles or as ions released in physiological solutions or synthetic sweat in the skin. Nanoparticles can release more ions than bulk material due to their high surface/small size.

From a biological point of view nanoparticles (NPs) may gain new properties and exert different biological effects due to their low dimension (less than 100 nm). The skin usually acts as a barrier to xenobiotics, but the recent evidence of its micro and nanoporous structure (Baroli 2010) raises a question on its role towards NP size elements.

Another relevant aspect to take into consideration in toxicological studies is that different types of platinum compounds show different toxicity potential. Some compounds are classified as cytotoxic, mutagenic and carcinogenic on microorganisms at very low concentrations (WHO 1991; Bunger et al. 1996; Gebel et al. 1997) while charged PGEs compounds, and mostly platinum chlorides (WHO 1991; Marget 2000), are associated with allergic lung and skin reactions.

The metallic form of platinum and rhodium is traditionally considered biologically inert and non-allergenic, but experimental data are uneven.

While some recent studies have focused on platinum's antioxidant potential (Kajita et al. 2007; Yoshihisa et al. 2010; Onizawa et al. 2009), others evaluated the effects of the substance on the respiratory tract and on skin tissue.

Colombo et al. (2008) demonstrated *in vitro* that PGE-chloride species can be formed from vehicle exhaust catalysts (VECs) and road dust in simulated lung fluids when acidic conditions (ph=4.5) and chloride ions are present (Fuchs and Rose 1974; Zereini et al. 1997). Pt was determined to be the PGE element with the highest bioavailability rate, due to its environmental concentration, and it is well known that even a small amount of such Pt-chloride species could exert toxic and allergenic effects on human beings, representing a potential health risk.

Konieczny et al. (2013) investigated the effects of PVP-coated PtNPs on epidermal keratinocytes, evaluating the cytotoxicity, genotoxicity, morphology, metabolic activity, and changes in the activation of signaling pathways. In this study, PtNPs of two sizes were used: 5.8 nm and 57 nm. Authors found that PtNPs trigger toxic effects on primary keratinocytes, decreasing cell metabolism, but these changes have no effects on cell viability or migration. Moreover, smaller NPs exhibited more deleterious effect on DNA stability and higher caspases activation than the big ones.

Health effects of metal Rh have not been investigated yet, but currently it seems not to play a biological role, to the best of our knowledge.

As regards Pt and Rh skin absorption, few data are available. In vivo experimental studies on animals showed conflicting results. Taubler demonstrated in 1977 that, after repeated dermal application of platinum sulphate on guinea pigs and rabbits, no traces of metal were detected in urine and serum of the animals, while Roshchin and colleagues (1984) found traces of Pt in blood, urine and internal organs of animals treated with a dermal application of ammonium chloroplatinate. Recently Franken et al. (2014) demonstrated that Pt and Rh salts can permeate the skin in in-vitro system. In occupational health, as well as in environmental

safety, percutaneous absorption is a key issue in evaluating the risk of human exposure to toxic agents.

Due to the increasing exposure to PtNPs and RhNPs in traffic polluted areas, we performed in vitro experiments to assess the diffusion characteristics of these nanoparticles through the skin, since no absorption studies are available on this topic. In this study, experiments were performed using the Franz cell method, adapting the experience and the protocols employed during the European project EDETOX (Evaluations and predictions of DErmal absorption of TOXic chemicals), a three-years research program (2001-2004) funded by European Union (EDETOX, 2000) and already used to testing the skin permeation of other metal nanoparticles such as silver, gold and cobalt (Larese et al., 2009; 2011; 2013).

2. Materials and methods

2.1 Chemicals

All chemicals were analytical grade. Urea, disodium hydrogen phosphate, potassium dihydrogen phosphate, hydrogen peroxide (30% v/v) were purchased from Carlo Erba (Milan, Italy); lactic acid (90%) from Acros Organics (Geel, Belgium); sodium chloride, sodium hexachloroplatinate, rhodium chloride trihydrate, polyvinylipyrrolidone (K30, average Mw 40,000), ammonium hydroxide (25% w/v), nitric acid (>69% v/v), sodium hydroxide and methanol from Sigma Aldrich (Milan, Italy).

Water reagent grade was produced with a Millipore purification pack system (milliQ water). The physiological solution used as receptor fluid was prepared by dissolving 2.38 g of Na_2HPO_4, 0.19 g of KH_2PO_4 and 9 g of NaCl into 1 L of milliQ water (final pH 7.35). The synthetic sweat solution used as donor fluid consisted in 0.5% sodium chloride, 0.1% urea and 0.1% lactic acid in milliQ water; pH 4.5 was adjusted with ammonia.

2.2 Platinum and rhodium nanoparticles synthesis and characterization

PtNPs and RhNPs, stabilized with polyvinylpyrrolidone (PVP), were synthesized by reduction of Na_2PtCl_6 and $RhCl_3{\cdot}3H_2O$ respectively, adapting the method described for palladium NPs by Peng Choo et al. (2002). Briefly, the reduction was performed refluxing for 3 hours a methanol-water solution containing Na_2PtCl_6 or $RhCl_3{\cdot}3H_2O$, NaOH and the PVP. The molar ratio monomer vinylpyrrolidone: metal was 20:1. For the synthesis of Pt NPs, 235.4 mg of Na_2PtCl_6 and 1.14g of PVP were dissolved in 30mL of H_2O, followed by the addition of 60 □L of NaOH 0.1M and 30 mL of MeOH. For the synthesis of Rh NPs, 257.9 mg of

$RhCl_3 \cdot 3H_2O$ and 2.17 g of PVP were dissolved in 30mL of H_2O, followed by the addition of 60 □L of NaOH 0.1M and 30 mL of MeOH. After refluxing for 3h, the suspensions were evaporated at reduced pressure until drying to remove MeOH and the products were dissolved in 50 mL of H_2O to reach a nominal metal concentration of 2g/L. The pH of the final solutions was adjusted to 5.5 by addition of HCl 0.1 M (~ 63 mL). The reactions for the synthesis of the metal NPs are quantitative (yields 100%), as demonstrated by the ICP-AES analysis of the solutions recovered by the ultrafiltration tests (see below).

At the time of the experiments, the NPs suspensions have been purified by ultrafiltration with Centrifugal Filters Amicon® Ultra-4, MWCO 10kDa (Millipore) in order to remove methanol, salts and eventual unreduced metal ions. After the ultrafiltration, the starting volume has been restored with milliQ water and diluted 1-3 with synthetic sweat to prepare the final donor solution used in the experiments.

NPs shape and size have been determined by means of Transmission Electron Microscopy (TEM) and by Dynamic Light Scatterig (DLS) on the starting suspensions and on the same diluted with synthetic sweat. In order to verify the stability of the donor phases, DLS analysis was repeated after 24 hours from the dilution.

Total metal concentrations were analyzed by Inductively Coupled Plasma-Atomic Emission Spectroscopy (ICP-AES).

2.3 Preparation of skin membranes

Human abdominal full thickness skin was obtained as surgical waste. Prior to freezing, subcutaneous fat was removed and hair shaved. All the pieces of full thickness skin were stored in freezer at -25°C for a period up to, but not exceeding, 4 months. It has been shown that this method of storage does not damage the skin since no difference in permeability was observed between fresh and frozen segments of the same skin in a separate series of experiments (Franz, 1975). Skin integrity was tested before and after each experiment using electrical conductibility by means of a conductometer (Metrohm, 660, Metrohm AG Oberdorfstr. 68 CH-9100 Herisau) operating at 300Hz connected to two stainless steel electrodes (Fasano et al., 2002). The conductibility data, obtained in μS, were converted in $K\Omega cm^{-2}$. Cells with a resistance lower than 3.95±0.27 $K\Omega cm^{-2}$, were considered to be damaged as suggested by Davies et al. (2004).

2.4 In vitro diffusion system

Percutaneous absorption studies were performed using static diffusion cells following the Franz method (1975). The receptor compartment has a mean volume of 14.0 mL and was maintained at 32°C by means of circulation of termostated water in the jacket surrounding the cell. This temperature value has been chosen in order to reproduce the hand's physiological temperature at normal conditions. The concentration of the salt in the receptor fluid is approximately the same that can be found in the blood. The solution in each cell was continuously stirred using a Teflon coated magnetic stirrer. Each piece of skin was clamped between the donor and the receptor compartment; the mean exposed skin area was 3.29 cm^2 and the average membranes thickness was 1mm. For each experiment was used the skin of 2 different donors, from each of which 4 Franz cells (3 exposed and 1 blank) were set up, for a total of 8 independent cells, in each experiment. Donors were men and women with a range of age from 55 to 70 years.

The experiments were performed as follows:

Experiment 1

At time 0, the exposure chambers of 6 Franz diffusion cells were filled with 3.0 mL of the freshly prepared donor solution providing an amount of 0.60 mg cm^{-2} of PtNPs in order to ensure an infinite dose. At selected intervals (4, 8, 12, 20 and 24 h) 1.5 mL of the dermal bathing solution was removed and collected for the analyses. Each receptor sample was immediately replaced with an equal volume of fresh made physiological solution. At 24 h, the dermal bathing solution and the donor solution were removed and stored in the freezer for the following analyses, while skin samples were treated as following described. The protocol used was the same of other previous studies (Larese et al., 2009a, 2011, 2013).

Experiment 2

Exp. 1 was repeated using an abraded skin protocol as suggested by Bronaugh and Stewart (1985): The skin was abraded by drawing the point of a 19-gauge hypodermic needle across the surface (20 marks in one direction and 20 perpendicular).

Experiment 3

Exp. 1 was repeated using 1.0 mL of RhNPs solution at 2000 mg L^{-1} diluted 1-3 with synthetic sweat as donor phase.

Experiment 4

Exp. 3 was repeated using the abraded skin protocol described above.

Blanks: For each experiment, two Franz cells were added as blank. The blank Franz cells were treated as the other cells with the exception that the exposure chamber was filled only with synthetic sweat.

As the equipment used was static, there is no relationship between the cells tested, hence each of them represents an independent evaluation. Every NPs treated cell was analyzed 5 times for metal content in receiving phases, 2 times for metal content in donor phases, and 2 times for metal content into the skin, for a total of 72 analyses for each experiment.

2.5 Skin digestion

After the experiment the skin pieces were removed from the diffusion Franz cells. Intact skin samples have been separated into epidermis and dermis by heat shock immersing them in water at 60°C for 1 min and stored in freezer at -25°C while damaged skin samples have been frozen without separation.

At the time of the analysis, the skin membranes were dried for 2 h at room temperature, then cut into sections, weight and put into beakers with 10 mL of HNO_3 69% v/v and 2 mL H_2O_2 of for digestion (amounts of skin were between 0.5 and 0.8 g). They were agitated for 24 h at room temperature and then heated at the boiling point until the remaining solutions were of 2 mL in volume. The solutions were diluted to a volume of 10 mL with milliQ water for the following analysis.

2.6 Quantitative analysis

An electro-thermal atomic absorption spectrometry (GF-AAS) with Zeeman background correction was used to measure the platinum and rhodium concentrations in the receiving phases and in the solutions obtained from skin mineralization. The instrument used for analysis was a Thermo M series AA spectrometer equipped with a GF95Z Zeeman Furnace and a FS95 Furnace Autosampler (Thermo Electron Corporation, Cambridge, UK). Pt detection limit at the analytical wavelength of 266.0 nm was 10 $\mu g\ L^{-1}$. Rh detection limit at the analytical wavelength of 343.5 nm was 5 $\mu g\ L^{-1}$. A five-point standard curve (in the range of 10-100 $\mu g\ L^{-1}$) was used for the analytical measurements. The correlation coefficient of the standard curve was at least 0.9995 (r). The samples were analyzed measuring against standard solutions for instrumental calibration. The precision of the measurements as relative standard deviation (RSD%) for the analysis was always less than 5%.

2.7 Data analysis

Data analysis was performed with Excel for Windows, release 2007 and Stata Software, version 11.0 (StataCorp LP, College Station, TX, USA). All data were reported as mean ± standard deviation (SD). The difference among independent data was assessed by means of

the Mann-Whitney test. A p value of <0.05 was considered as the limit of statistical significance.

3. Results

The concentrations of 2.0 g/L of the NPs suspensions were confirmed by the ICP-AES analysis, while the metal concentrations in the ultrafiltered solutions were always less than 1 mg L^{-1} (0.05% of the starting suspensions). These data clearly indicate that Na_2PtCl_6 and $RhCl_3 \cdot 3H_2O$ were fully reduced during the preparation of the NPs suspension.

Representative TEM images of PtNPs and RhNPs, diluted in water and in synthetic sweat, are presented in figure 1 and 2, respectively. The mean sizes of the metal cores were 5.8 ± 0.9 nm for PtNPs and 5.3 ± 1.9 for RhNPs (NPs measured =100). No significant differences have been observed changing the dilution media.

Size distributions obtained by DLS are presented in figure 3a and 3b. In the case of PtNPs, the size distributions are narrow and only marginally affected by the use of synthetic sweat, with maxima ranging from 17 to 25 nm. In the case of RhNPs, broader distributions have been observed and the use of synthetic sweat resulted in a significant decrease of the mean diameter, from 565 nm in water to 120 nm in synthetic sweat. Notably, for both the metals, no significant modification of the size distribution has been observed after 24 hours in synthetic sweat. The apparent mismatch between TEM and DLS sizes is the result of various facts, as previously reported (Blosi et al., 2011). Firstly, the laser scattering technique measures the hydrodynamic diameter inclusive of PVP and coordinated molecules. Furthermore, polymer-protected metal NPs can form agglomerates consisting of various metal cores wrapped up in the same polymer chain. The mean hydrodynamic diameters of these agglomerates, revealed by DLS, are therefore larger than the mean sizes of the primary NPs, revealed by TEM. The intensity of the interaction between the protecting polymer and the surface of the metal NPs affects the mismatch between the two measurements (Blosi et al., 2014) and can play a crucial role in defining the behavior of the agglomerates into media with a high ionic strength, such as the synthetic sweat.

After twenty-four hours of exposure to PtNPs, the amount of metal found in the receiving solutions was under the Limit of detection (LOD) in both experiments with intact and damaged skin, while after the same period of exposure to RhNPS, a flux permeation of 0.04 ± 0.04 μg cm^{-2} h^{-1} and a lag time of 7.9 ± 1.1 h (mean and standard deviation) were calculated through damaged skin, while no permeation profile was detectable through intact skin (Fig. 4).

When assessed as a whole, the total platinum concentration was double in damaged skin compared with intact skin, with a mean value and standard deviation of 1.74 ± 1.24 μg cm^{-2} and 0.80 ± 0.20 μg cm^{-2} respectively, $p<0.02$. The presence of rhodium into the full thickness skin was assessed too, and data revealed that the concentration was more than 17 times higher in damaged skin compared to intact skin, with a mean value and standard deviation of 7.41 μg cm^{-2}± 5.55 and 0.43 μg cm^{-2} ± 0.08 respectively ($p<0.001$).

The platinum content in intact skin was double compared with rhodium (0.80 ± 0.20 μg cm^{-2} and 0.43 ± 0.08 μg cm^{-2}, respectively, expressed as mean and standard deviation) and both metal concentrations decreased significantly from the epidermis (0.75 ± 0.21 μg cm^{-2} and 0.39 ± 0.08 μg cm^{-2}, respectively) to the dermis (0.047 ± 0.004 μg cm^{-2} and 0.03 ± 0.04 μg cm^{-2}, respectively) ($p<0.049$) (Fig.5).

Comparing the whole metal content in full thickness damaged skin, Rh concentration is more than 4 times higher than Pt, as showed in fig.6. When assessed as a whole, the total platinum concentration was double in damaged skin compared with intact skin, with a mean value and standard deviation of 1.74 ± 1.24 μg cm^{-2} and 0.80 ± 0.20 μg cm^{-2} respectively, $p=0.02$.

The platinum content in intact skin (mean and standard deviation) decreased significantly from the epidermis (0.75 ± 0.21 μg cm^{-2}) to the dermis (0.047 ± 0.004 μg cm^{-2}) ($p=0.049$) (Fig.4).

RhNPs were applied for 24h in the donor solutions and after this period a flux permeation of 0.04 ± 0.04 μg cm^{-2} h^{-1} and a lag time of 7.9 ± 1.1 h (mean and standard deviation) were calculated through damaged skin, while no permeation profile was detectable through intact skin (Fig. 5).

The presence of Rh into the full thickness skin was assessed at the end of the experiment. The concentration of the metal was more than 17 times higher in damaged skin compared to intact skin, with a mean value and standard deviation of 7.41 μg cm^{-2}± 5.55 and 0.43 μg cm^{-2} ± 0.08 respectively ($p<0.001$). Rh content in intact skin (mean and standard deviation) decreased significantly from the epidermis (0.39 ± 0.08 μg cm^{-2}) to the dermis (0.03 ± 0.04 μg cm^{-2}) too ($p=0.02$) (Fig.6).

When a comparison of the metal content in full thickness damaged skin is made, Rh concentration is more than 4 times higher compared to Pt, as showed in fig.7.

4. Discussion

The present study investigated skin absorption of very small PtNPs and RhNPs, using full thickness human skin (epidermis and dermis) both with intact and damaged skin barrier, in an

in vitro diffusion cell system. These results suggest that Pt, administrated in nano-sized form, can penetrate intact and damaged skin but no traces of metal were found in receiving solutions (no permeation), while Rh can permeate in a little amount through damaged but not through intact skin after 24 hours.

Considering the distribution of metals in the skin layers, the concentration of Pt and Rh in the outermost layer (epidermis) was always higher than the correspondent concentration in the dermis. Moreover damaged skin presented always higher amount of metals compared to intact skin (double for Pt and 17 fold higher for Rh).

These results are consistent with other damaged-skin permeation studies, which showed an enhance in the intradermal delivery of nanoparticles when epidermis is abraded with microneedles (Zhang W. et al. 2010) or by radio frequency (Birchall J. et al. 2006).

Skin lesions increased the amount of Pt that remains in the skin but do not led to a detection of the metal in the receiving phase: this was probably due to a strong interaction between NPs and skin components (cells and extracellular matrix) that could stop the Pt migration. A similar behavior has been demonstrated in the permeation profile of chromium powder (Larese et al. 2008) due to the strong interaction with skin proteins, which is possible for skin sensitizers.

Rh can permeate the skin reaching the receiving phase in experiments performed with damaged skin: this different behavior can be related to the smaller medium size of RhNPs respect to PtNPs (as visualized by TEM) or just to lower binding property of Rh to skin proteins.

Metal NPs can penetrate the skin as NPs or as dissolute ions: in the first scenario NPs can be stored in hair follicles and from there can reach epidermis and dermis (Rancan et al. 2012); in the second scenario NPs can dissolute releasing ions, which can penetrate the skin as salts. In our study the dissolution tests revealed a negligible amount of Pt and Rh ions in the filtered donor phase in physiological conditions. This behavior is similar to the one of gold NPs, but different from other metals such as silver, nickel or cobalt (Larese et al. 2009a, 2009b, 2013), in which ions release influence skin permeation. This is in line with the different oxidability of base metals compared to noble metals such as Pt, Au or Rh.

PtNPs ad RhNPs applied on the skin can exert local effects (sensitization i.e.) and only in a disrupted stratum corneum Rh can permeate the skin. Our findings can be compared to absorption profiles of Pt and Rh salts, recently published by Franken et al. (2014). The application of salts causes the permeation of both metals through the skin with higher amount for Pt (flux 0.2 ± 0.02 ng/cm^2/h as mean and Standard error of the mean) compared to Rh

(flux 0.05 ± 0.01 ng/cm^2/h). These results are consistent with other experiments performed comparing skin permeation using Cr in metal form (Cr) and its salts (Larese et al. 2009), since it is well known that skin permeation is lower using Cr (0). Moreover flux of Rh detected in our study in damaged skin was 80 times higher than the one obtained by Franken et al. (2014) reaching 40 ± 40 ng/cm^2/h (as mean and standard deviation) while metal's skin content are lower in intact skin and higher in damaged skin experiments compared to results obtained with salts (Franken et al. 2014). Considering that both experiments were run using an infinite dose (in donor phase) we can suggest that the exposure to PtNPs and RhNPs can cause Pt and Rh skin penetration with possible local effects and that only in a damaged skin system Rh can permeate the skin in higher amount compared to salts exposure. The fact that PtNPs can't permeate the skin can be explained by a possible strong binding to skin proteins as demonstrated for chromium (Larese et al. 2009).

Skin absorption of Pt and Rh salts is known (Taubler J. 1977; Roshchin AV. 1984; Franken et al, 2014) while data are lacking for PtNPs and RhNPs, which can be present in the environment due to emissions from vehicle exhaust catalysts (VECs) and road dusts (Merget and Rosner 2001; Colombo et al. 2008; Forte et al. 2008) as well as in industries, where these NPs are produced to be used in catalysis processes (Iavicoli er al. 2012).

In past centuries allergic reactions were observed in refineries workers (Hunter et al.1945; Orbaek 1982; Niezborala and Garnier 1996) exposed to high concentrations of Pt and included lung and skin symptoms as sneezing, wheezing, breathlessness, cough, tightness of chest, eczematous and urticarial skin lesions and sign of mucous membrane inflammation (Health and Safety Executive 1990), which overall constitute a syndrome called "*Platinosis"* (Brubaker et al. 1975).

Nowadays these occupational exposures are fortunately uncommon and there is epidemiological evidence that the sensitizing capability of Pt compounds is restricted to the halogenated ones, the most effective of which comprises chlorides (Linett and Hughes 1999; WHO 1991; Marget 2000) and the allergic response seems to increase with the increasing number of chlorine atoms. Metallic form of platinum and rhodium (state of oxidation: 0), which are mostly emitted by VECs, are traditionally considered biologically inert and non allergenic, and there is some evidence that the current environmental concentrations are not high enough to cause a general outbreak of allergic reaction in the population (Merget and Rosner 2001). Nevertheless it is known that NPs can exert different biological activities than bulk material due to their small size.

In existing environmental conditions a small but not negligible exposure to platinum comes from VECs, which can be inhaled and can deposit on human epidermis. When PtNPs stand in acid condition, such as the one upon the skin layer, them could dissolve and release ions in higher amount compared to bulk materials, due to the small size/high surface ratio of NPs. Pt penetration into the skin can cause allergic reaction locally, but can also induce systemic reaction with an increased risk to develop respiratory allergic diseases such as rhinitis and asthma. No data are available on this aspect and more studies are needed.

Few data are available about health effects of rhodium. While epidemiological studies substantially demonstrate its low allergenic potential, in vitro studies point out toxicological hazards.

Positive *skin prick test* (SPT) to rhodium have been frequently interpreted as a cross-reactivity reactions in platinum salt allergic workers of precious metals refineries (Murdoch and Pepys 1987; Nakayama and Ichikawa 1997) and catalyst productions (Cristaudo et al. 2005). In a study conducted on 720 eczematous patients sensitized to metals (Santucci et al. 2000) rhodium patch tests resulted positive only in 2 cases.

Nevertheless allergic contact dermatitis caused by rhodium salts has been recently demonstrated in subjects working in jewellery trade (Goossens et al. 2011) and one case of immediate-type asthma and rhinitis due to rhodium salts has been demonstrated in a electroplating plant worker (Merget et al. 2010).

Iavicoli et al. (2012) demonstrated i*n vitro* cell cycle arrest and DNA damage on fibroblasts treated with rhodium and iridium salts, with an earlier effect in rhodium treated cells. Since rhodium carboxylates is capable to unpair DNA bases and inhibit DNA synthesis, magnetic nanoparticles coated with rhodium (II) citrate have been proposed recently as target-specific drug delivery system in breast cancer therapy. Carneiro et al. (2011), investigating this topic in an *in vitro* experiment, pointed out a higher metal toxicity on breast normal cell line than on breast carcinoma cell line for concentrations > 200 μM of RhNPs.

In view of the above results and since a skin penetration of Pt and Rh administrated in nano-sized and stabilized form was demonstrated in the present study, an interaction between these elements on skin surface is possible, leading potentially to consequences that have not been investigated yet. Further studies are needed to better understand the toxicological potential of PtNPs and RhNPs on skin, especially once they are present in more complex matrixes such as vehicle exhaust catalysts or road dust.

Figures and Graphs

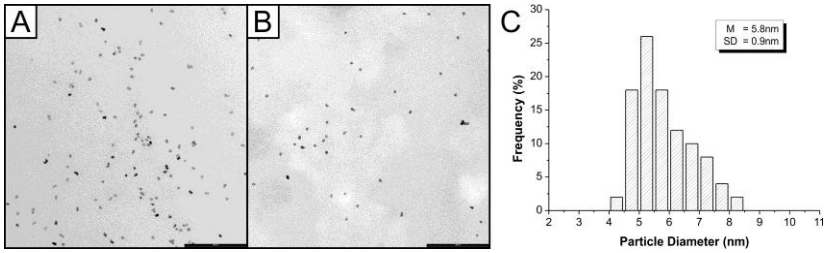

Figure 1 Representative TEM images of PtNPs suspension in water (A) and in synthetic sweat (B) (bar 100 nm) and size distribution of the metallic core (C)

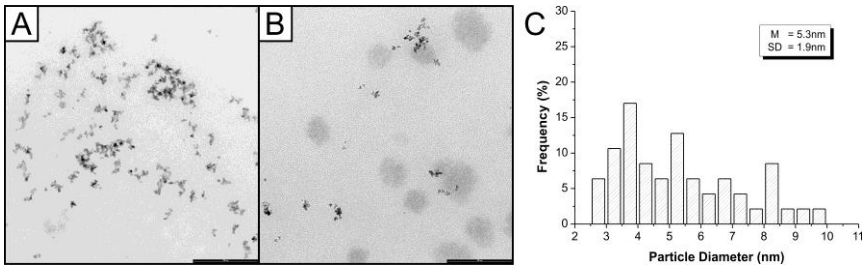

Figure 2 Representative TEM images of RhNPs suspension in water (A) and in synthetic sweat (B) (bar 100 nm) and size distribution of the metallic core (C)

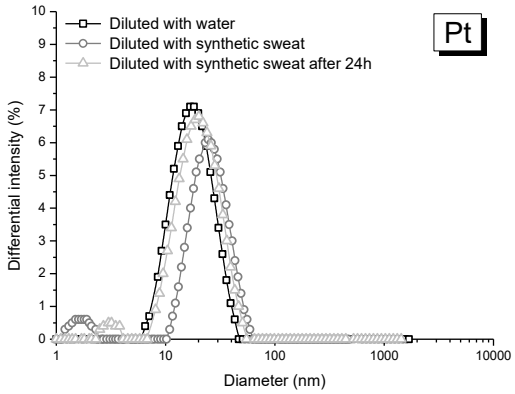

Figure 3a DLS particle size distribution for PtNPs in different environments

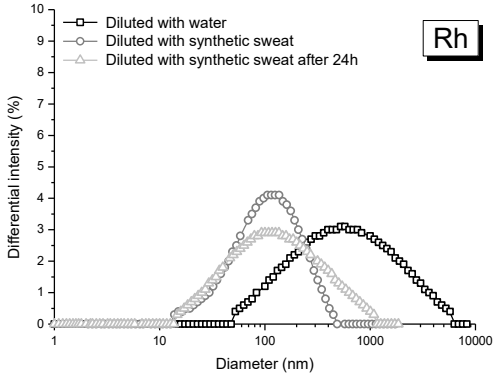

Figure 3b DLS particle size distribution for RhNPs in different environments

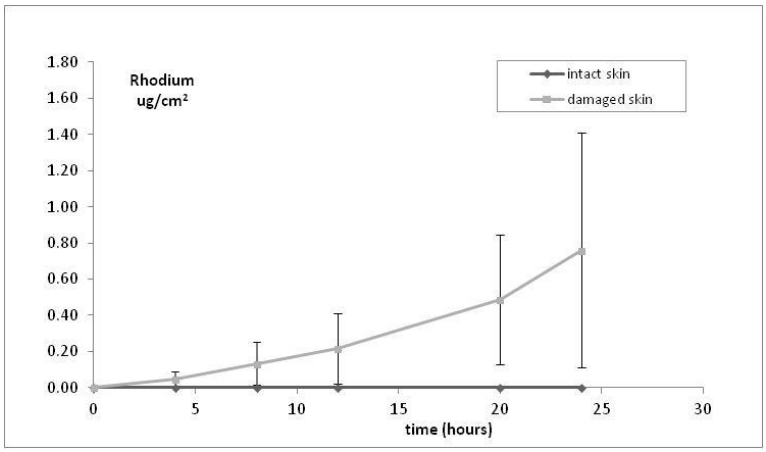

Figure 4 Permeation profile of RhNPs after skin application of 1.0 mL of RhNPs solution at 2000 mg L^{-1} diluted 1:3 with synthetic sweat, through 6 intact and 6 damaged skin samples (means and standard deviations)

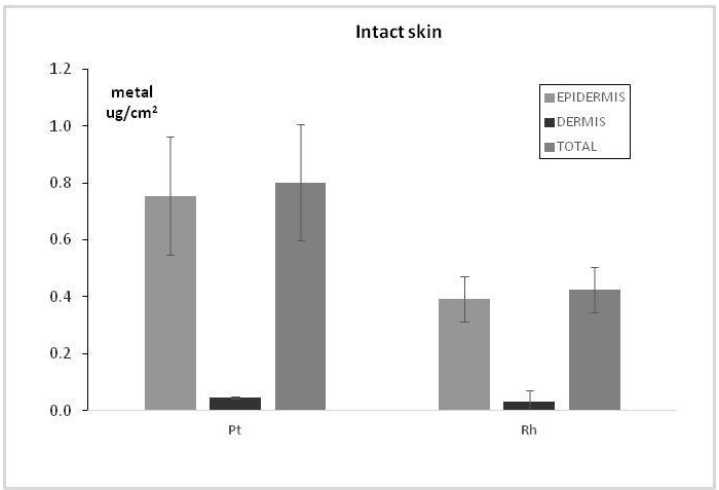

Figure 5 Mean values and standard deviations of platinum and rhodium concentrations (μg/cm^2) inside intact skin presented as: epidermal layer, dermal layer, and both of them evaluated together (total). Results derived from 6 intact and 2 control skin samples for each metal tested.

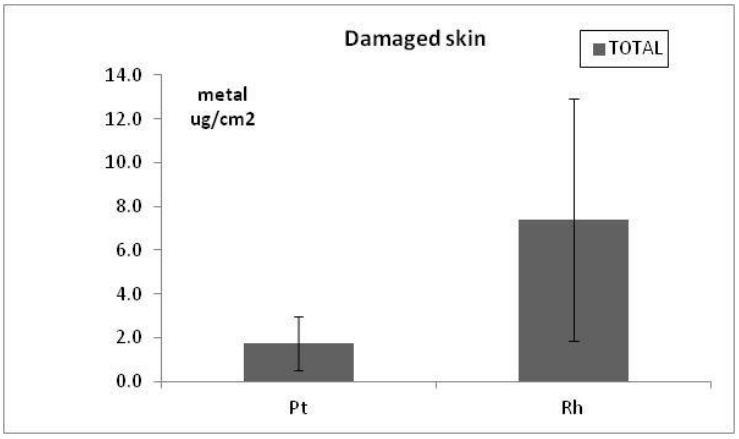

Figure 6 Mean values and standard deviations of platinum and rhodium concentrations (μg/cm^2) inside full tickness damaged skin. Results derived from 6 damaged and 2 control condition skin samples for each metal tested.

Acknowledgements

The authors acknowledge the financial support of FRA 2009 and 2012 from University of Trieste and of Cost Action Skinbad BM 0903. MICROMERITICS Analytical Service is kindly acknowledged for DLS analysis.

Conflict of Interest statement

The authors declare that they have no conflict of interest.

References

Barbante C, Veysseyre A, Ferrari C, van de Velde K, Morel C, Capodaglio G, Cescon P, Scarponi G, Boutron C (2001) Greenland snow evidence of large scale atmospheric contamination for platinum, palladium and rhodium. Environmental Science Technology 35: 835-839.

Baroli B (2010) Penetration of nanoparticles and nanomaterials in the skin: fiction or reality? J Pharm Sci. 99: 21-50.

Baroli B, Ennas MG, Loffredo F, Isola M, Pinna R, Lòpez-Quintela MA (2007) Penetration of Metallic Nanoparticles in Human Full-Thickness Skin. Journal of Investigative Dermatology 127: 1701-1712.

Barry BW (2001) Novel mechanisms and devices to enable successful transdermal drug delivery. Eur. J Pharm. Sci. 14: 101-114.

Birchall J, Coulman S, Anstey A, Gateley C, Sweetland H, Gershonowitz A, Neville L, Levin G (2006) Cutaneous gene expression of plasmid DNA in excised human skin following delivery via microchannels created by radio frequency ablation. Int J Pharm. 312 (1-2): 15-23.

Blosi M, Albonetti S, Dondi M, Martelli C, Baldi G (2011) Microwave-assisted polyol synthesis of Cu nanoparticles J. Nanopart. Res. 13:127–138

Blosi M, Albonetti S, Ortelli S, Costa AL, Ortolani L, Dondi M (2014) Green and easily scalable microwave synthesis of noble metal nanosols (Au, Ag, Cu, Pd) usable as catalysts. New J.Chem. 38: 1401-1409.

Bocca B, Caimi S, Smichowski P, Gómez D, Caroli S (2006) Monitoring Pt and Rh in urban aerosols from Buenos Aires, Argentina. Science of Total Environment 358 (1-3): 255-264.

Bronaugh RL, Steward RF (1985) Methods for in vitro percutaneous absorption studies V: permeation through damaged skin. J. Pharm. Sci. 74: 1062–1066.

Brubaker PE, Moran JP, Bridbord K, Hueter FG (1975) Noble metals: a toxicological appraisal of potential new environmental contaminants. Environmental Health Perspectives 10: 39-56.

Bünger J, Stork J, Stalder K (1996) Cyto and genotoxic effects of coordination complexes of platinum, palladium and rhodium in vitro. International Archives of Occupational and Environmental Health 69 (1): 33-38.

Carneiro ML, Nunes ES, Peixoto RC, Oliveira RG, Lourenço LH, da Silva IC, Simioni AR, Tedesco AC, de Souza AR, Lacava ZG, Báo SN (2011) Free Rhodium (II) citrate and rhodium (II) citrate magnetic carriers as potential strategies for breast cancer therapy. Journal of Nanobiotechnology, doi: 10.1186/1477-3155-9-11. p 1-17.

Colombo C, Monhemius AJ, Plant JA (2008) The estimation of the bioavailabilities of platinum, palladium and rhodium in vehicle exhaust catalysts and road dusts using a physiologically based extraction test. Science of the total environment 389 (1): 46-51.

Colombo C, Monhemius AJ, Plant JA (2008) Platinum, palladium and rhodium release from vehicle exhaust catalysts and road dust exposed to simulated lung fluids. Ecotoxicology and Environmental Safety 71 (3): 722-730.

Cristaudo A, Sera F, Severino V, De Rocco M, Di Lella E, Picardo M (2005) Occupational hypersensitivity to metal salts, including platinum, in the secondary industry. Allergy 60 (2): 159-164.

Davies DJ, Ward RJ, Heylings JR (2004) Multi-species assessment of electrical resistance as a skin integrity marker for in vitro percutaneous absorption studies. Toxicol. In vitro 18 (3): 351–358.

EDETOX Evaluations and predictions of dermal absorption of toxic chemicals. 2001-2004 QLK4-CT-2000-00196 www.edetox.ncl.ac.uk

Fasano WJ, Manning LA, Green JW (2002) Rapid assessment of rat and human epidermal membranes for in vitro dermal regulatory testing: correlation of electrical resistance with tritiated water permeability. Toxicol. In vitro 16 (6): 731–740.

Forte G, Petrucci F, Bocca B (2008) Metal allergens of growing significance: epidemiology, immunotoxicology, strategies for testing and prevention. Inflammation & Allergy Drug Targets 7 (3): 145-62.

Franken A, Eloff FC, Du Plessis J Badenhorst J, Jordaan Am Du Plessis L (2014) In vitro permeation of platinum and rhodium through Caucasian skin. Toxicol. in vitro 28 (8): 1396-1401.

Franz TJ (1975). Percutaneous absorption. On the relevance of in vitro data. J Invest Dermatol. 93: 633–640.

Fuchs WA, Rose AW (1974) Geochemical behavior of platinum and palladium in the weathering cycle in the Stillwater Complex, Montana. Econ. Geol. 69: 332-346.

Gebel T, Lantzsch H, Plessow K, Dunkelberg H (1997) Genotoxicity of platinum and palladium compounds in human and bacterial cells. Mutat Res. 389 (2-3): 183-190.

Goossens A, Cattaert N, Nemery B, Boey L, De Graef E (2011) Occupational contact dermatitis caused by rhodium solutions. Contact dermatitis 64 (3): 158-161.

Health and Safety Executive (1990) «Occupational exposure limits.» Guidance note EH 40910. London: Her Majestry's Stationary Office.

Hunter D, Milton R, Perry KMA (1945) Asthma caused by the complex salts of platinum. British journal of industrial medicine 2 (2): 92-98.

Iavicoli I, Cufino V, Corbi M, Goracci M, Caredda E, Cittadini A, Bergamaschi A, Sgambato A (2012) Rhodium and iridium salts inhibit proliferation and induce DNA damage in rat fibroblasts in vitro. Toxicology in vitro. 26 (6): 963-969.

Kajita M, Hikosaka K, Iitsuka M, Kanayama A, Toshima N, Miyamoto Y (2007) Platinum nanoparticle is a useful scavenger of superoxide anion and hydrogen peroxide. Free Radical Research 41 (6): 615-626.

Konieczny P, Goralczyk AG, Szmyd R, Skalniak L, Koziel J, Larese Filon F, Crosera M, Cierniak A, Zuba-Surma EK, Borowczyk J, Laczna E, Drukala J, Pyza E, Semik D, Woznicka O, Klein A, Jura J (2013) Effects triggered by platinum nanoparticles on primary keratinocytes. Int J Nanomedicine. 8: 3963–3975.

Larese Filon F, D'Agostin F, Crosera M, Adami G, Bovenzi M, Maina G (2008) In vitro percutaneous absorption of chromium powder and the effect of skin cleanser. Toxicology in vitro 22 (6): 1562-1567.

Larese Filon F, D'Agostin F, Crosera M, Adami G, Renzi N, Bovenzi M, Maina G (2009a) Human skin penetration of silver nanoparticles through intact and damaged skin. Toxicology 255 (1-2): 33-37.

Larese Filon F, D'Agostin F, Crosera M, Adami G, Bovenzi M, Maina G, (2009b). In vitro absorption of metal powders through intact and damaged skin. Toxicology in vitro 23 (4): 574-579.

Larese Filon F, Crosera M, Adami G, Bovenzi M, Rossi F, Maina G (2011) Human skin penetration of gold nanoparticles through intact and damaged skin. Nanotoxicology 5 (4): 493-501.

Larese Filon F, Crosera M, Timeus E, Adami G, Bovenzi M, Ponti J, Maina G (2013) Human skin penetration of cobalt nanoparticles through intact and damaged skin. Toxicology in Vitro 27 (1): 121-127.

Linett PJ, Hughes EG (1999) 20 years of medical surveillance on exposure to allergenic and non allergenic platinum compounds: the importance of chemical speciation. Occupational and Environmental Medicine 56 (3): 191-196.

Merget R (2000) Occupational platinum salt allergy. Diagnosis, prognosis, prevention and therapy, in Anthropogenic Platinum-Group Element Emissions. Their impact on man and environment. Zereini F and Alt F (Eds.). Springer- Verlag, Berlin 32.

Merget R, Rosner G (2001) Evaluation of the health risk of platinum group metals emitted from automotive catalytic converters. The science of the Total Environment 270 (1-3): 165-173.

Merget R, Sander I, van Kampen V, Raulf-Heimsoth M, Ulmer HM, Kulzer R, Bruening T (2010) Occupational immediate-type asthma and rhinitis due to rhodium salts. American Journal of Industrial Medicine 53 (1): 42-46.

Moldovan M, Palacios MA, Gòmez MM, Morrison G, Rauch S, McLeod C, Ma R, Caroli S, Alimonti A, Petrucci F, Bocca B, Schramel P, Zischka M, Pettersson C, Wass U, Luna M, Saenz JC, Santamaría J (2002) Environmental risk of particulate and soluble platinum group elements released from gasoline and diesel engine catalytic converters. Science of Total Environment 296 (1-3): 199-208.

Monteiro-Riviere NA, Inman AO (2006) Challenges for assessing carbon nanomaterial toxicity to the skin. Carbon. 44 (6): 1070-1078.

Murdoch RD, Pepys J (1987) Platinum group metal sensitivity: reactivity to platinum group metal salts in platinum halide salt-sensitive workers. Ann. Allergy 59 (6): 464-469.

Nakayama H, Ichikawa T (1997) Occupational contact urticaria syndrome due to rhodium and platinum. In: Amin S, Maibach HI, Lahti S (ed) Contact urticaria syndrome, New York, pp 233-240

NANODERM (2007) Quality of Skin as a Barrier to ultra-fine Particles. Final Report (Project Number: QLK4-CT-2002-02678).

Niezborala M, Garnier R (1996) Allergy to complex platinum salts: a historical prospective cohort study. Occupational and Environmental Medicine 53 (4): 252-257.

Onizawa S, Aoshiba K, Kajita M, Miyamoto Y, Nagai A (2009) Platinum nanoparticle antioxidants inhibit pulmonary inflammation in mice exposed to cigarette smoke. Pulmunary Pharmacology and Therapeutics 22 (4): 340-349.

Orbaek P (1982) Allergy to the complex salts of platinum. A review of the literature and three case reports. Scandinavian Journal of work and environmental health 8 (2): 141-145.

Peng Choo H, Yong Liew K, Liu H (2002) Factors affecting the size of polymer stabilized Pd nanoparticles. J. Mater. Chem. 12: 934-937.

Rancan F, Gao Q, Graf C, Troppens S, Hadam S, Vogt A (2012). Skin penetration and cellular uptake of amorphous silica nanoparticles with variable size, surface functionalization and colloidal stability. ACS Nano 8: 6829-6842

Ravindra K, Bencs L, Van Grieken R (2004) Platinum group elements in the environment and their health risk. The Science of the Total Environment 318 (1-3):1-43.

Roshchin AV, Veselov VG, Panova AI (1984) lndustrial toxicology of metals of the platinum group. J. Hyg. Epidemiol. Microbiol. Immunol. 28: 17-24.

Sadrieh N, Wokovich AM, Gopee NV, Zheng J, Haines D, Parmiter D, Siitonen PH, Cozart CR, Patri AK, McNeil SE, Howard PC, Doub WH, Buhse LF (2010) Lack of significant dermal penetration of titanium dioxide from sunscreen formulations containing nano- and submicron-size TiO2 particles. Toxicological Science 115 (1): 156-166.

Samberg ME, Oldenburg SJ, Monterio-Riviere NA (2010) Evaluation of Silver Nanoparticle Toxicity in Skin in Vivo and Keratinocytes in Vitro. Environmental Health Perspectives 118 (3): 407-413.

Santucci B, Valenzano C, de Rocco M, Cristaudo A (2000) Platinum in the environment: frequency of reactions to platinum-group elements in patients with dermatitis and urticaria. Contact Dermatitis 43 (6): 333-338.

Sato K, Feibleman C, Dobson RL (1970) The electrolyte composition of pharmacologically and thermally stimulated sweat: a comparative study. J Invest Dermatol. 55(6): 433-8.

Schierl R (2000) Environmental monitoring of platinum in air and urine. Microchemical Journal 67: 245-248.

Sonavane G, Tomoda K, Sano A, Ohshima H, Terada H, Makino K (2008) In vitro permeation of gold nanoparticles through rat skin and rat intestine: Effect of particle size. Colloids Surf. B Biointerfaces 65: 1–10.

Taubler J (1977) Allergic response to platinum and palladium complexes. Determination of no-effect level. US Environmental Protection Agency, North Carolina, EPA-600/1-77-039,NTIS Accession Number PB 271 659, pp. 81

WHO (1991) Environmental Health Criteria 125- Platinum. Geneva: International Programme on Chemical Safety.

Yoshihisa Y, Honda A, Zhao QL, Makino T, Abe R, Matsui K, Shimizu H, Miyamoto Y, Kondo T, Shimizu T (2010) Protective effects of platinum nanoparticles against UV-light induced epidermal inflammation. Experimental Dermatology. 19 (11): 1000-1006.

Zereini F, Skerstrupp B, Alt F, Helmers E, Urban H (1997) Geochemical behavior of platinum group elements (PGE) in particulate emissions by automobile exhaust catalysts: experimental results and environmental investigations. The Science of the Total Environment 206: 137-146.

Zhang W, Gao J, Zhu Q, Zhang M, Ding X, Wang X, Hou X, Fan W, Ding B, Wu X, Wang X, Gao S (2010) Penetration and distribution of PLGA nanoparticles in the human skin treated with microneedles. International Journal of Pharmaceutics 402: 205–212.

ALLEGATO II

TITANIUM DIOXIDE NANOPARTICLE PENETRATION INTO THE SKIN AND EFFECTS ON HACAT CELLS.

Crosera M, Prodi A, Mauro M, Pelin M, Florio C, Bellomo F, Adami G, Apostoli P, De Palma G, Bovenzi M, Campanini M, Filon.

Pubblicato in: International Journal of Environmental Research and Public Health. 2015 Aug 7; 12(8):9282-97.

Abstract:

TiO_2NPs suspensions (concentration 1.0 g/L) in synthetic sweat solution were applied on Franz cells for 24 hours using intact and needle-abraded human skin. Titanium content into skin and receiving phases was determined. Cytotoxicity (MTT, AlamarBlue® and propidium iodide, PI, uptake assays) was evaluated on HaCat keratinocytes after 24, 48 hours and 7 days exposure.

After 24 hours of exposure, no titanium was detectable in receiving solutions for both intact and damaged skin. Titanium was found into epidermal layer after 24 hours of exposure (0.47 ± 0.33 μg/cm^2) while in the dermal layer concentration was below the limit of detection. Damaged skin, in its whole, has shown a similar concentration (0.53±0.26 μg/cm^2). Cytotoxicity studies on HaCaT cells demonstrated that TiO_2NPs induced cytotoxic effects only at very high concentrations, reducing cell viability after 7 days exposure with EC_{50}s of $8.8x10^{-4}$M (MTT assay), $3.8x10^{-5}$M (AlamarBlue® assay) and $7.6x10^{-4}$M (PI uptake, index of a necrotic cell death).

Our study demonstrated that TiO_2NPs can't permeate intact and damaged skin and can be found only in stratum corneum and epidermis. Moreover, the low cytotoxic effect observed on human HaCaT keratinocytes suggests that these nano-compounds have potential toxic effect at the skin level only after long-term exposure.

Keywords: titanium dioxide, nanoparticles (NPs), in vitro, human skin absorption, cytotoxicity

1. Introduction

TiO_2 nanoparticles (NPs) are being widely used in industrial and consumer products due to their strong catalytic activity, compared to their fine-particle counterpart. This characteristic has been attributed to their larger surface area per unit mass, given their smaller size [1].

TiO_2 is in the top five NPs used in a wide array of consumer products [2], including cosmetics, toothpaste [3], sunscreens [4], and skin treatments for acne vulgaris, condyloma acuminata, atopic dermatitis, hyper-pigmented skin lesions and other non-dermatologic diseases [5]. TiO_2 is the most widely used nanomaterial in dermal consumer products [6]. It is also used in paints, foods, pigments, etc. [7]. TiO_2 appears as a white powder and its nanoparticle formulation is preferred in cosmetics industry because avoids white coloration of the skin, after application.

Chronic toxicity studies on TiO_2 focuses on the respiratory system but more effort should be put into studying chronic exposure for topically applied consumer goods, especially with the increase in consumer use of sunscreens that contain TiO_2NPs [1].

TiO_2NPs present in cosmetics have the potential to penetrate through the stratum corneum into viable skin layers via intercellular channels, hair follicles and sweat glands [8]. Several authors have studied the possible penetration of TiO_2NPs into the skin, using both naked and coated titania samples [9-13], finding that TiO_2 doesn't penetrates the skin and the underlying living tissue, remaining on the skin surface or only impregnating the first layers of stratum corneum. Monterio-Riviere et al. [14] showed minimal penetration after UVB exposure in vitro and in vivo skin. Kiss et al. in 2010 [15] investigated the in vivo penetration of TiO_2 on human skin transplanted to immunodeficent mice. They demonstrated in vivo that TiO_2NPs do not penetrated to the intact epidermal membrane, but exposed directly to cell culture in vitro exert significant effects on cell viability. Cytotoxicity of TiO_2NPs was demonstrated in keratinocytes, using different tests and exposures, with or without UV-exposure [1, 16-19] but many in vivo experiments on animals did not confirm this effect [1]. More recently Adachi et al. [20] and Wu et al. [21] found sign of irritant dermatitis with focal parakeratosis in the stratum corneum and epidermal spongiosis applying uncoated TiO_2NPs for long time. Wu et al. [21] found that these NPs can penetrate into the deep layer of the viable epidermis in pig ears after 30 days of exposure and into hairless skin mouse inducing pathological changes in major organs after 60 days. However, these results were contested by Jonaitis et al. [22] that reported methodological deficiencies. Also Sadrieh et al. [23] found TiO_2 in dermis after 22 days of application of sunscreen creams containing TiO_2NPs in mini pigs but they suspected a contamination.

It is unlikely that metal oxide nanoparticles penetrate the intact human skin under normal conditions, given the tough layer of stratum corneum, but the impairment of the stratum corneum could increase skin penetration of nanoparticles [8, 24]. Previous data in vitro on pig skin treated with tape stripping to remove stratum corneum [11] did not demonstrated TiO_2NPs skin absorption. However no data are available on TiO_2NPs absorption using a needle abraded skin protocol. It is important to verify if, also in a damaged skin condition, TiO_2NPs fails to cross the skin barrier, as an impairment of stratum corneum is very common in workers (i.e. wet workers, construction workers, healthcare workers) [25].

To increase the knowledge on this topic we studied in vitro skin absorption of TiO_2NPs on intact and damaged human skin with the protocol defined in the European project EDETOX [26] and used to study other kind of NPs [27-29]. To complete our study we tested TiO_2NPs used in skin penetration tests to evaluate their toxicity on short and long term exposures (24-48 hours and 7 days) on keratinocytes.

2. Experimental Section

2.1 Chemicals

All chemicals were analytical grade. Urea, sodium chloride, sodium hydrogen phosphate, potassium dihydrogenphosphate, were purchased from Carlo Erba (Milan, Italy); lactic acid (90% v/v) was bought from Acros Organics (Geel, Belgium); nitric acid (69.5% v/v), hydrogen peroxide (30% v/v), hydrofluoric acid (48 % w/v) and ammonium hydroxide (25% w/v) from Sigma Aldrich (Milan, Italy). Water reagent grade was produced with a Millipore purification pack system (Milli-Q water). The physiological solution used as the receptor

phase was prepared by dissolving 2.38 g of Na_2HP0_4, 0.19 g of KH_2P0_4 and 9 g of NaCl into 1 L of Milli-Q water (final pH 7.35). The synthetic sweat solution used as donor fluid consisted in 0.5% sodium chloride, 0.1% urea and 0.1% lactic acid in Milli-Q water; pH 4.5 was adjusted with ammonia.

The commercially available TiO_2 nanopowder (CAS 13463-67-7, provided by Sigma Aldrich – Milan, Italy) was used.

2.2 Nanoparticles characterization

The TiO_2 have been visualized by Transmission Electron Microscopy (TEM) once they were dispersed in synthetic sweat and at the end of the experiments (after the 24 h exposure time) to visualize the dimensions of the NPs and the aggregation state of the donor phase.

Since the behavior and the aggregation state of the NPs in different mediums depends strongly on the surface charge of the NPs and the ionic strength of the suspension, a further characterization using both Dynamic Light Scattering and Z-potential techniques has been carried out. Brookhaven Corp has performed the measurements using the 90Plus PALS instrument. In Alinovi et al. 2015 [30] is reported the complete characterization.

Finally, in order to evaluate the ions release from the NPs once they were put in synthetic sweat, 4 ml of the donor phase have been ultrafiltered using the Amicon Ultra-4 centrifugal filters (10K MWCO). The ultrafiltration has been performed in centrifuge at 5000 rpm for 30 min in order to remove the NPs, but not eventual titanium ions, from the solution. The solution has been analyzed by ICP-AES to quantify the titanium concentration. The ultrafiltration has been repeated on three different aliquots at the beginning of the permeation experiments and on other three aliquots at the end of the 24-hour exposure time. The titanium concentration was always below the limit of detection.

2.3 Preparation of skin membranes

Human abdominal full thickness skin was obtained as surgical waste from patients aged 45-65 years. After the skin excision subcutaneous fat was removed with a scalpel blade and hair shaved from the epidermal layer, then skin samples were stored at -25°C for a period up to, but not exceeding, 4 months. It has been demonstrated that this procedure do not damage skin barriers properties. At the day of the experiment skin samples have been defrost in physiological solution at room temperature for a 30 minute period and then 4x4 cm^2 pieces were cut from each skin specimen and mounted separately on the diffusion cells. Damaged skin samples were obtained using a needle-abrasion technique described elsewhere [31]. Skin integrity was tested before and after each experiment using electrical conductibility by means of a conductometer (Metrohm, 660, Metrohm AG Oberdorfstr. 68 CH-9100 Herisau) operating at 300 Hz and connected to two stainless steel electrodes [32]. The conductibility data in µS were converted into $K\Omega/cm^2$. Cells with a resistance lower than 3.95 ± 0.27 $K\Omega/cm^2$ were considered to be damaged and rejected as suggested by Davies et al. [33].

2.4 In vitro diffusion system

Percutaneous absorption studies were performed using static diffusion cells following the Franz method [34]. The receptor compartment had a mean volume of 14.0 mL and was maintained at 32°C by means of circulation of thermostated water in the jacket surrounding the cell. This temperature value was chosen in order to reproduce the hand physiological temperature at normal conditions. The physiological solution used as the receptor phase was prepared by dissolving 2.38 g of Na_2HP0_4, 0.19 g of KH_2P0_4 and 9 g of NaCl into 1 L of Milli-Q water (final pH 7.35).

The concentration of the salt in the receptor fluid was approximately the same that can be found in the blood. The physiological solution used as receiving phase was continuously stirred using a Teflon coated magnetic stirrer. Each piece of skin was clamped between the donor and the receptor compartment; the mean exposed skin area was 3.29 cm^2 and the average membranes thickness was 1 mm. Two different experiments were conducted using intact (exp. 1) and damaged skin (exp 2) as described below:

2.5 Experiment 1

The donor phase has been prepared just before the experiment using a sonicated suspension of TiO_2NPs at a concentration of 1.0 g/L dispersed in synthetic sweat at pH 4.5, to reproduce in vivo condition. The TiO_2 concentration in the donor phase was confirmed by Inductively Coupled Plasma-Atomic Emission Spectroscopy (ICP-AES) analysis prior to the test.

At time 0, the exposure chambers of 6 Franz diffusion cells were mounted with intact skin samples and filled with 2.5 mL of the donor suspension (606 $\mu g/cm^2$) to ensure an infinite dose. The experiment was run for 24 hours, and during this period 1.5 ml of the dermal bathing solution was removed at selected intervals (4, 8, 16, 24 h) and analyzed. Each receptor sample was immediately replaced with an equal volume of fresh physiological solution. At 24 h the dermal bathing solution and the donor phase of each diffusion cell were recovered for the following analysis.

2.6 Experiment 2

Experiment 1 was repeated using an abraded skin protocol as suggested by Bronough and Steward [31]. Skin was abraded by drawing the tip of a 19-gauge hypodermic needle across the surface (20 marks in one direction and 20 perpendicular).

2.7 Blanks

For each experiment, two cells were added as blank. The blank cells were treated as the other cells with the exception that only synthetic sweat was used in the donor compartment.

2.8 Skin digestion after the experiment

After the experiment the skin pieces were washed three times with physiological solution to remove TiO_2NPs on the skin, then removed from the diffusion cells and treated as follows: skin samples from exp. 1 were separated into epidermis and dermis by heat shock immerging in water at 60°C for 1 min before freezing, while skin samples from exp. 2 were simply stored

in freezer at -25°C. At the time of the analysis, the skin membranes were dried for 2 h at room temperature, then cut into sections, weight and put into 100 mL disposable Digitubes^{TM} with 10 mL of HNO_3 and 2 mL of H_2O_2 for digestion. They were heated for 24 h at 90°C in a block heater (SPB 100-12, PerkinElmer), then added of 0.2 ml of HF and heated until the remaining solutions were of 2 mL in volume. The solutions were diluted to a volume of 10 mL with Milli-Q water for the analysis with ICP-AES.

2.9 Analytical measurements

The metal concentrations in the receiving phase skin were determined by Zeeman corrected graphite furnace atomic absorption spectrophotometry (GF-AAS) using a Varian Duo instrument (GTA 120, AA 240 Z). The calibration standards were prepared by standard solutions of single elements ranging from 0.5 to 1000 µg/l: titanium in H_2O atomic absorption standard solution (Sigma-Aldrich, Milwaukee, USA). The limit of detection (LOD) calculated as three standard deviations of the background signal obtained on ten blind samples at the operative wavelength of 364.3 nm was 5µg/l. The precision of the measurements as relative standard deviation (RSD%) for the analysis was always less than 5%.

Total titanium concentration in the donor phases and in the solutions resulting from the mineralization of the skin sample were performed by Inductively Coupled Plasma-Atomic Emission Spectrometry (ICP-AES) using a Spectroflame Modula E optical plasma interface (OPI) instrument (by SPECTRO, Germany). The analyses were conducted using a calibration curve obtained by dilution (range: 0–10 mg/l) of titanium standard solution for ICP-AES analyses (by Teknolab A/S, Norway). The limit of detection (LOD) at the operative wavelength of 334.941 was 0.02 mg/l. The precision of the measurements as relative standard deviation (RSD%) for the analysis was always less than 5%.

2.10 Cell tests

2.10.1 Cell culture

The immortalized human keratinocyte HaCaT [35] cell line was purchased from Cell Line Service (DKFZ, Eppelheim, Germany). Cells were cultured in high-glucose Dulbecco's Modified Eagle's medium (DMEM) supplemented with 2 mM L-Glutamine, 100 U/ml penicillin-100 µg/ml streptomycin and 10% fetal bovine serum (FBS) at 37°C in a 5% CO_2 atmosphere. Cells received fresh medium every 3 days and were subcultured every 7 days.

Stock solutions of TiO_2NPs (1 mg/ml ethanol) were diluted to the required concentrations ($1.5x10^{-7}$ – $1.0x10^{-3}$ M) in the cell culture medium and sonicated before use.

2.10.2 MTT assay

Cells ($5x10^3$ cells/well) were plated in 96-wells plates for 24 h and then exposed to TiO_2NPs ($1.5x10^{-7}$ – $1.0x10^{-3}$ M). After 24, 48 h and 7 days of exposure, a 10% MTT solution was added, and after 4 h the insoluble crystals were solubilized with DMSO [36]. Plates were read in a Microplate Autoreader (Bio-Tek Instruments) at 540/630 nm. Data are reported as % of control and are the mean ± SE of 4 independent experiments performed in triplicate.

2.10.3 AlamarBlue® Assay

Cells ($15x10^3$ cells/well) were cultured in 96-wells plates and, after 24h, exposed to TiO_2NPs ($1.5x10^{-7}$ – $1.0x10^{-3}$ M) for 24, 48h and 7 days. After 4 h of incubation with the AlamarBlue® reagent, fluorescence intensity was read by a FluoroCount Microplate Fluorometer (Packard, Germany) at an excitation wavelength of 530 nm and emission wavelength of 590 nm. Data are reported as % of control and are the mean ± SE of 4 independent experiments performed in triplicate.

2.10.4 Propidium Iodide uptake

Cells (1x105 cells/well) were seeded in 96-wells plates and after 24 h exposed to TiO2NPs (1.5x10-7 – 1.0x10-3 M) for 24, 48h and 7 days. Propidium iodide (PI) uptake was performed as previously described [37, 38]. Briefly, after treatment cells were rinsed with 200 μL of 3.0x10-6 M PI in PBS and fluorescence intensity was read by a Fluorocount microplate Fluorometer (Packard, Germany) with excitation length of 530 nm and emission length of 590 nm after 30 minutes. All samples were subsequently permeabilized with 1% Triton-X for 30 minutes to obtain total cell content for each sample and fluorescence read. Positive control was obtained permeabilizing untreated cells with 1% Triton-X. Data are reported as % of positive control (equal to 100% PI uptake) after normalization on total cell content and are the mean ± SE of 3 independent experiments performed in triplicate.

2.11 Statistical analysis

Ti concentration data ($\mu g/cm^3$) in the receptor solution were converted to the total amount that penetrated ($\mu g/cm^2$), with a correction for dilution due to sample removal.
Data analysis was performed with Excel 2007 for Windows, and Stata Software, version 11.0 (StataCorp LP, College Station, TX, USA). Skin absorption data were reported as mean ± standard deviation (SD). The difference among independent data was assessed by means of the Mann-Whitney test.

Cytotoxicity data were reported as mean ± standard error (SE) of at least three independent experiments performed in triplicate. The concentration giving the 50% of the maximal effect (EC_{50}) was calculated using the GraphPad software version 4.0 (Prism GraphPad, Inc.; San Diego, CA, USA). A $p<0.05$ was considered as significant.

3. Results and Discussion

3.1 Nanoparticles characterization

The characterization performed on TiO_2NPs specimen showed that the NP_S have a regular spherical shape and appear as slightly aggregated (Figure 1).

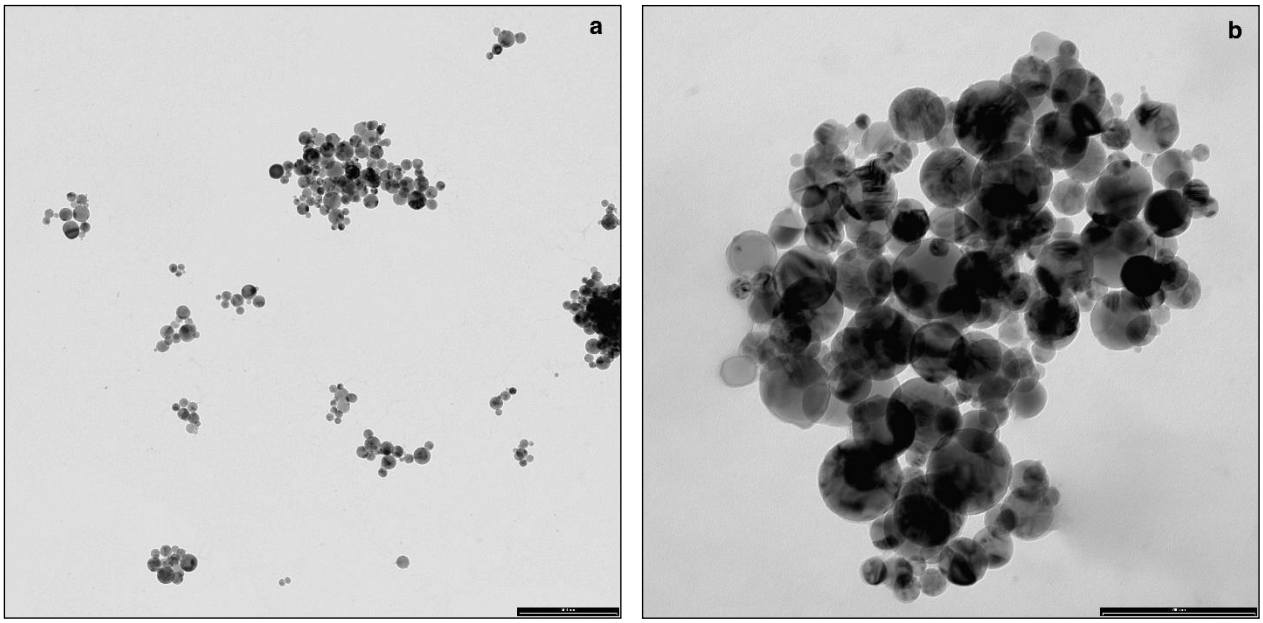

Fig. 1a,b: Representative TEM images of agglomerated TiO_2 NPs dispersed in synthetic sweat at the beginning of the experiments (bar: a = 500 nm, b = 200 nm)

The size distribution is centered on the value of 38 nm. The hydrodynamic radius value (RH) observed in water was centered on 154 nm, while it increased considerably when assessed in synthetic sweat, reaching a value of 727 nm (Figure 2) at time 0 and 1254 nm after 24 hours.

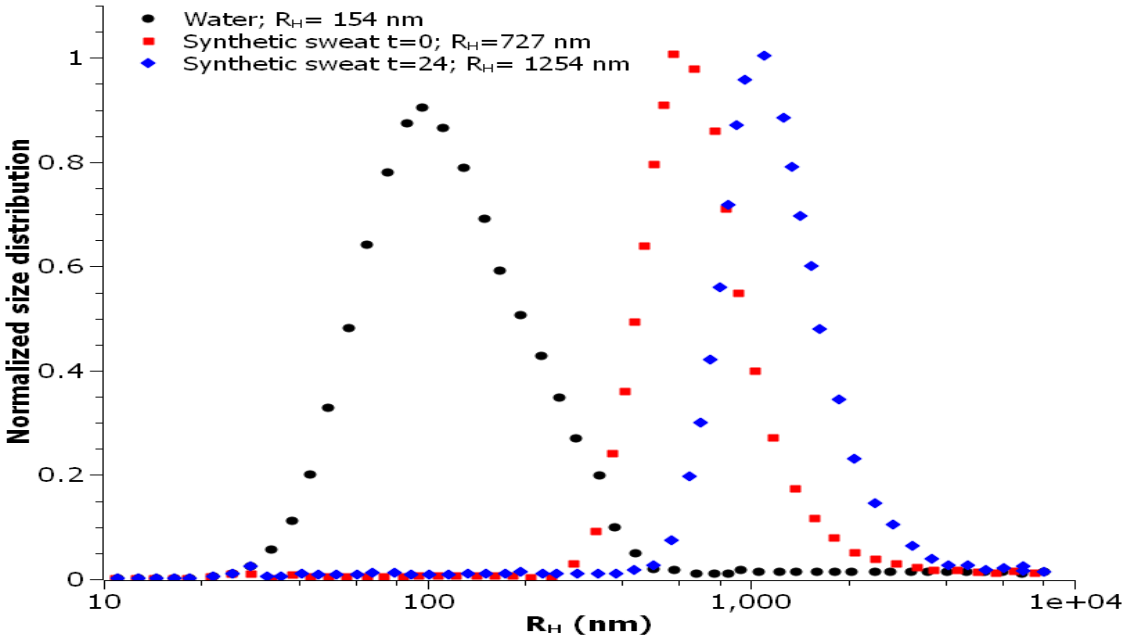

Fig. 2 Size distribution of TiO_2 NPs in water and synthetic sweat suspension, estimated by DLS.

This phenomenon was clearly in agreement with the measured Z-potential values, reported in Table I. The surface charge values suggested that TiO_2NPs were more stable in water, thanks to their higher electrostatic stabilization.

Table I. Comparison of Z-potential values in water and in synthetic sweat

Medium **Specimen**	**Water**	**Synthetic sweat** **t = 0**	**Synthetic sweat** **t = 24h**
TiO_2	Mean: -31.7 Std: 1.02 mV	mean: -36.8 Std: 3.8 mV	mean: -19.0 Std: 4.1 mV

3.2 Franz diffusion cells experiments

After 24 hours of exposure, the average concentration of Ti in the receiving solution was below the level of detection (LOD) of 5µg/L for both intact and damaged skin.

As shown in Figure 3, the average amount of Ti into intact skin, after 24 hours of exposure was 0.47 ± 0.33 µg/cm^2 in the epidermal layer, while in the dermal layer concentration was below LOD.

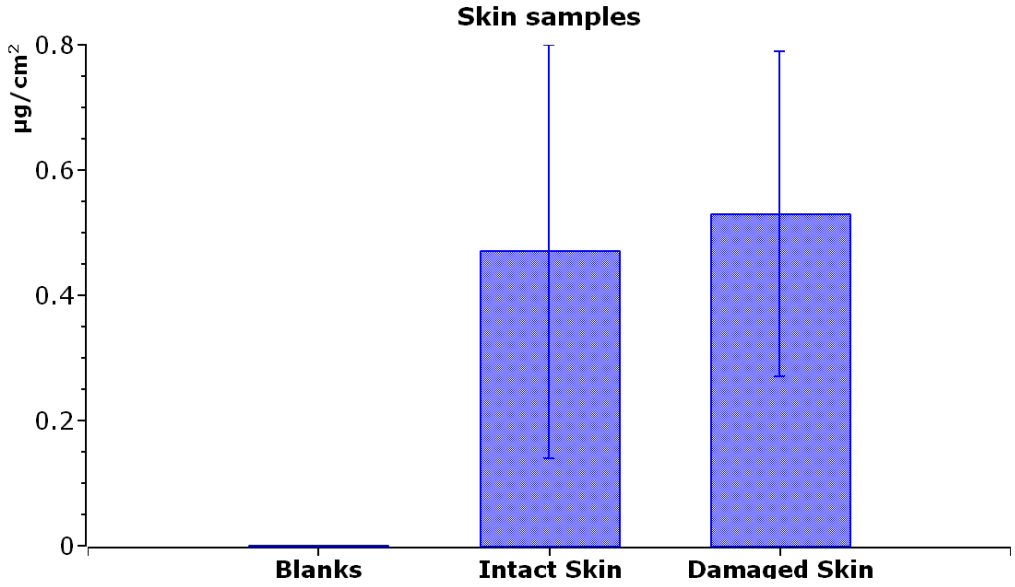

Figure 3. Titanium content (µg/cm^2) inside the skin (epidermis + derma) of blank cells (exposed to physiological solution), intact skin and damaged skin (exposed to TiO_2 NPs). Mean and standard deviation of 6 cells each.

Damaged skin, evaluated in its whole, has shown a similar concentration (0.53 ± 0.26 μg/cm^2) to intact skin titanium content.

3.3 Effect of TiO2NPs on cell viability

The cytotoxic effect induced by TiO_2NPs on HaCaT skin keratinocytes was evaluated using the MTT reduction assay and the AlamarBlue® assay. Figure 4A shows the concentration-response curves obtained after 24, 48 hours and 7 days exposure to TiO_2NPs ($1.5x10^{-7}$ – $1.0x10^{-3}$ M) obtained by the MTT assay. TiO_2NPs induced a very low cytotoxic effect that was significant ($p<0.05$) for concentrations higher than $1.1x10^{-4}$ M for all the exposure times considered. Intriguingly, cytotoxicity was independent on the time of exposure, since the effects observed after 24, 48 hours or 7 days were almost overlapping. After 7 days exposure, TiO_2NPs reduced cell viability with an EC_{50} equal to $8.8x10^{-4}$ M (95% confidence limits, CL = 6.2 - $12.4x10^{-4}$ M).

Figure 4B shows the effect of TiO_2NPs on cell viability evaluated by the AlamarBlue® assay. The cytotoxic effect was slightly higher with respect to that evaluated by the MTT assay. In particular, the TiO_2NPs-induced cytotoxic effect was significant ($p<0.05$) at concentrations higher than $1.2x10^{-5}$ M for all the exposure times considered. The highest effect was achieved after 7 days exposure, after which TiO_2NPs reduced cell viability with an EC_{50} equal to $3.8x10^{-5}$ M (95% CL = 2.6 - $5.3x10^{-5}$ M).

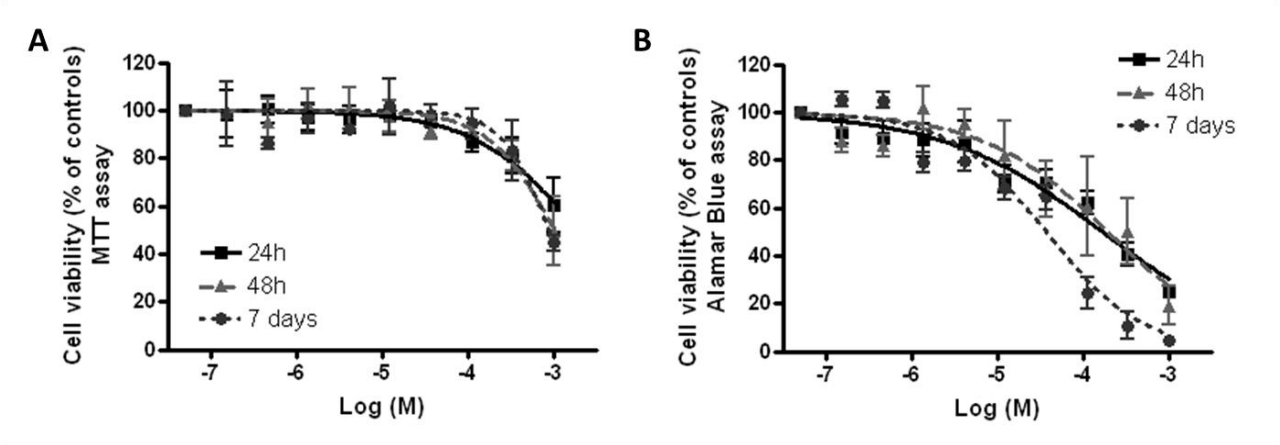

Figure 4: Cytotoxicity of TiO_2 NPS. Cell viability was measured by MTT assay (A) and AlamarBlue® assay (B) after 24 h, 48 h and 7 days exposure to TiO_2 NPS ($1.5x10^{-7}$ – $1.0x10^{-3}$ M) on HaCaT cells. Data are reported as % of untreated controls (equal to 100% cell viability) and are the mean ± SE of 4 independent experiments performed in triplicate.

3.4 Effect of TiO2NPs on membrane damage

The plasma membrane damage induced by TiO_2NPs was evaluated after 7 days NPs exposure by propidium iodide (PI) uptake. As shown in figure 5, TiO_2NPs induced a concentration-dependent PI uptake starting from $1.1x10^{-4}$ M, with an EC_{50} value equal to $7.6x10^{-4}$ M (95% CL = 6.2 - $9.4x10^{-4}$ M).

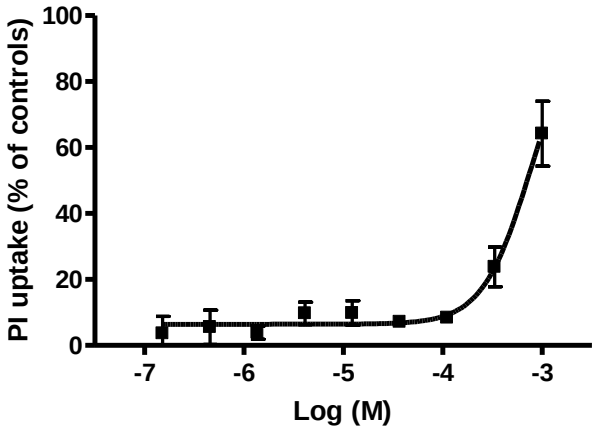

Figure 5. PI uptake in HaCaT cells exposed for 7 days to TiO_2 NPS ($1.5x10^{-7}$ – $1.0x10^{-3}$ M). Data are reported as mean ± SE of 3 independent experiments performed in triplicate.

3.5 Discussion

No Titanium permeation was demonstrated after 24 hours of exposure of the skin to TiO_2NPs both intact and damaged skin. Into the skin, titanium was detectable only in epidermis while no metal was found into the dermis. Our study confirmed what already reported by many Authors [8]. This can be explained by the great stability of the molecule and its negligible ionization in physiological condition, which lead to an accumulation on the surface of the skin. Another important aspect to be considered is the big size of the particles and their tendency to form aggregates that further reduce the skin absorption capability [8].

In our permeation experiment on intact human skin, we did not found TiO_2NPs within the dermal layer. Since the total amount of NPs was similar in intact and damaged skin, we can assume that lesions do not increase permeation (at least, with current limits of detection).

In most of actually available study results, after TiO_2NPs dermal exposure, TiO_2NPs are not significantly systematically available [1]. The lack of penetration trough the epidermis is also the main reason for the absence of skin carcinogenesis promoting effects [39, 40]. However, other studies such as Tan et al. [41], found that levels of TiO_2NPs in the epidermis and dermis of subjects who applied a sunscreen containing 8% TiO_2NPs was higher than the levels found in controls, via tape stripping technique. This difference was not statistically significant given the small sample size. Bannat and Müller-Goymann [42] (applying an oil-in-water emulsion with 5% TiO_2NPs), found that TiO_2NPs may be able to penetrate the surface through hair follicles or pores, but no details are given on the fate of such particles. Wu et al. [21] evaluated the penetration and potential toxicity of TiO_2NPs after in vitro (porcine ears) and in vivo (domestic pig ears, BALB/c hairless mice) animal dermal exposure: they did not found stratum corneum penetration 24h after exposure to isolated porcine skin. However after 30 days topical application on pig ear in vivo (24 mg of 5% TiO_2 on an area of 3 cm^2) they found penetration of TiO_2 in the deep layer of the epidermis. After 60 days dermal exposure (400 $\mu g/cm^2$) in hairless mice TiO_2 was found reaching different tissues and inducing diverse pathological lesions in several major organs, but these conclusions has been questioned by

other authors [22]. Adachi et al. [20] applied to the dorsal skin of hairless rats an emulsion containing 10% wt% TiO_2NPs for 56 days finding that the particles were only located to the stratum corneum layer of epidermis and follicular epithelium. They did not find any evidence of TiO_2 penetration into viable areas. Moreover these AA did not find titanium into internal organ using inductively coupled plasma mass spectroscopy. Increased Titanium concentration was found only into lung samples probably due to the inhalation of TiO_2NPs.

Our study confirms the low penetration into the skin of TiO_2NPs and the lack of permeation potential also using a damaged skin protocol. TiO_2NPs tend to aggregate in physiological condition reaching bigger sizes that are not compatible with skin absorption [8] also using a damaging skin protocol. Moreover these NPs can't release metallic ions in physiological condition so titanium remains in the upper layers of stratum corneum or into hair follicles.

To evaluate the toxic potential of TiO_2NPs at the skin level, a preliminary study was carried out on human HaCaT keratinocytes, an accepted *in vitro* model for the screening of cutaneous toxicity of compounds [43]. On HaCaT cells, TiO_2NPs induced a slight cytotoxic effect, reducing cell viability with EC_{50} values equal to $8.8x10^{-4}$ M (MTT assay) and $3.8x10^{-5}$ M (AlamarBlue® assay) after 7 days exposure. These results are in line with previous studies carried out on HaCaT cells reporting the ability of TiO_2NPs to induce oxidative stress and mitochondrial damage [19, 44-45]. However, our results suggest a low toxic potential of TiO_2NPs since the effects were significant starting from the concentration of $1.1x10^{-4}$ M (MTT assay). Intriguingly, at the same concentrations TiO_2NPs induced a significant uptake of PI. This observation suggests that the cytotoxic effect induced by TiO_2NPs is mediated by a membrane damage, which can be compatible with a necrotic cell death, or a late-apoptotic cell death as recently demonstrated [45]. However, since the effects were significant only at the higher concentrations tested and after long time exposure (i.e. 7 days), we can affirm that TiO_2NPs own a low cytotoxic potential, in line with a previous study reporting no effect on cell viability and morphology after short-term treatment and minor effects after a long-term treatment as long as 3 months [46]. This low cytotoxicity is in line with a previous study reporting that TiO_2NPs do not induce phototoxicity, acute cutaneous irritation, or skin sensitization [47], strengthening the low risk associated to these NPs.

Our study demonstrated that TiO_2NPs can't permeate intact and damaged skin and can exert a low cytotoxicity effect only at high dose and long exposure. Nevertheless our study has some limitations. The first limitation is related to the in-vitro design of our study that can verify only passive diffusion through the skin, while also active penetration could happen in in-vivo condition. The second limitation is the analytical method available for titanium detection: the Zeeman corrected graphite furnace atomic absorption spectrophotometry (GF-AAS) used has a limit of detection of 5μg/L, that is quite high compared to other analytical techniques, such us inductively coupled plasma mass spectroscopy (ICP-MS), that can't be used because of the potential formation of polyatomic spectral interferences generated by the plasma gas, argon, residual matrix components from the sample [48]. Recently ICP-MS in single particle modus has been successfully adopted for the analysis of NPs in water samples [48] suggested that this technique could be used pre-treating samples with nitric acid. Nevertheless this techniques has for titanium a limit of detection higher than GF-AAS (5 μg/g) and Krystek et

al. [48] demonstrated that can be used only for samples with titanium concentrations >4 μg/g tissue to obtain reproducible results. These analytical aspects are crucial when we are studying metal content into biological samples.

Further studies for the safety evaluation of TiO_2NPs in sunscreens are needed, simulating real-world exposure conditions (sunburned skin and UV exposure) on users to verify if a long-term exposure can cause local or systemic effects [48].

4. Conclusions

We did not found permeation of TiO_2NPs neither through intact nor damaged skin. We located NPs in the epidermal layer but not in the dermal layer, and skin concentration was similar in both tests: skin lesions do not appear to alter permeation of these NPs.

These results can be explained by the great stability and low ionizing capacity of these particles and are in accord to several studies in literature. On the whole, the absence of TiO_2NPs permeation both in intact and in damaged skin as well as the low cytotoxicity observed on human HaCaT keratinocytes suggested a low toxic potential of these nano-compounds at the skin level. Moreover further studies for the safety evaluation of TiO_2NPs in sunscreens are needed, simulating real-world conditions on sunburned skin and with UV exposure.

Acknowledgements

This study was supported by the Italian Ministry of Health Ricerca Finalizzata 2009 Grant: Integrated approach to evaluating the biological effects on lung, cardiovascular system and skin of occupational exposure to nanomaterials (NanO I-LuCaS). RF-2009-1472550.

Author Contributions

Matteo Crosera and Andrea Prodi did experiments, data evaluation and wrote the paper.
Marcella Mauro participated to the experiments and data evaluation
Marco Pelin, Chiara Florio and Francesca Bellomo did experiments with Hacat cells
Gianpiero Adami, Piero Apostoli and Giuseppe De Palma performed chemical analysis
Marco Campanini performed nanoparticles characterization
Francesca Larese Filon designed the study and corrected the paper

Conflicts of Interest

The authors declare no conflict of interest

References and Notes

1. Shi, H., Magaye, R., Castranova V. and Zhao, J. Titanium dioxide nanoparticles: a review of current toxicological data. Particle and fibre toxicology 10, 15-20 (2013).

2. Shukla, R., Sharma, V., Pandey, A., Singh, S., Sultana S. and Dhawan, A. ROS-mediated genotoxicity induced by titanium dioxide nanoparticles in human epidermal cells. Toxicol in vitro 25, 231-241 (2001).

3. Kaida, T., Kobayashi, K., Adachi, M. and Suzuki, F. Optical characteristics of titanium oxide interference film and the film laminated with oxides and their application for cosmetics. J Cosmet Sci 55, 219-220 (2004)

4. Wolf R, H. Matz, E. Orion e J. Lipozencic, Sunscreens-the ultimate cosmetic Acta Dermatovenerol Croat 11, 158-162, (2003).

5. Wiesenthal, A., Hunter, L., Wang, S., Wickliffe J. and Wilkerson, M. Nanoparticles: small and mighty. Int J Dermatol 50,. 247-254, (2011).

6. Robertson, T., Sanchez, W., and Roberts,, M. Are commercially available nanoparticles safe when applied to skin?. J Biomed Nanotechnol, 6, 452-468 (2010).

7. Lyyränen, A.J., Auvinen A., Vanhala E. and Hämeri K. Industrial worker exposure to airborne particles during the packing of pigment and nanoscale titanium dioxide. Inhal Toxicol 12, 839-849 (2012).

8. Larese Filon F, Mauro M, Adami G, Bovenzi M, Crosera M.Nanoparticles skin absorption: New aspects for a safety profile evaluation.Regul Toxicol Pharmacol 13;310-322 (2015).

9. Dussert AS1, Gooris E, Hemmerle J Characterization of the mineral content of a physical sunscreen emulsion and its distribution onto human stratum corneum. Int J Cosmet Sci.19, 119-29 (1997).

10. Durand L, Habran N, Henschel V, Amighi K. In vitro evaluation of the cutaneous penetration of sprayable sunscreen emulsions with high concentrations of UV filters. Int J Cosmet Sci 31,279-92 (2009).

11. Pflücker F, Hohenberg H, Hölzle E, Will T, Pfeiffer S, Wepf R, Diembeck W, Wenck H, Gers-Barlag H. The Outermost Stratum Corneum Layer is an Effective Barrier Against Dermal Uptake of Topically Applied Micronized Titanium Dioxide. Int J Cosmet Sci 21,399-411(1999).

12. Peira E, Turci F, Corazzari I, Chirio D, Battaglia L, Fubini B, Gallarate M. The influence of surface charge and photo-reactivity on skin-permeation enhancer property of nano-TiO_2 in ex vivo pig skin model under indoor light. Int J Pharm 5,90-9 (2014).

13. Adachi, K., Yamada, M., Yamamoto K., et al. In vivo effect of industrial titanium dioxide nanoparticles experimentally exposed to hairless rat skin. Nanotoxicology 4, 296-306 (2010).

14. Monteiro-Riviere NA, Wiench K, Landsiedel R, Schulte S, Inman AO, Riviere JE. Safety evaluation of sunscreen formulations containing titanium dioxide and zincoxide nanoparticles in UVB sunburned skin: an in vitro and in vivo study. Toxicol Sci. 123,264-80 (2011).

15. Kiss B1, Bíró T, Czifra G, Tóth BI, Kertész Z, Szikszai Z, Kiss AZ, Juhász I, Zouboulis CC, Hunyadi J. Investigation of micronized titanium dioxide penetration in human skin xenografts and its effect on cellular functions of human skin-derived cells. Exp Dermatol. 17,659-67(2008).

16. Jaeger A, Weiss DG, Jonas L, Kriehuber R. Oxidative stress-induced cytotoxic and genotoxic effects of nano-sized titanium dioxide particles in human HaCaT keratinocytes. Toxicology. 14,27-36 (2012).

17. Chan J, Ying T, Guang YF, Lin LX, Kai T, Fang ZY, Ting YX, Xing LF, Ji YY. In vitro toxicity evaluation of 25-nm anatase TiO2 nanoparticles in immortalized keratinocyte cells. Biol Trace Elem Res 144,183-96 (2011).

18. Simon M, Barberet P, Delville MH, Moretto P, Seznec H. Titanium dioxide nanoparticles induced intracellular calcium homeostasis modification in primary human keratinocytes. Towards an in vitro explanation of titanium dioxide nanoparticles toxicity. Nanotoxicology 5,125-39 (2011).

19. Xue C, Wu J, Lan F, Liu W, Yang X, Zeng F, Xu H. Nano titanium dioxide induces the generation of ROS and potential damage in HaCaT cells under UVA irradiation. J Nanosci Nanotechnol 10,8500-7 (2010).

20. Adachi K, Yamada N, Yoshida Y, Yamamoto O. Subchronic exposure of titanium dioxide nanoparticles to hairless rat skin. Exp Dermatol 22, 278-83 (2013).

21. Wu, J., Liu, W., Xue, C., Zhou, S., Lan, F., Bi, L., Xu, H., Yang, X. and Zeng, F. Toxicity and penetration of TiO2 nanoparticles in hairless mice and porcine skin after subchronic dermal exposure. Toxicol Lett 191, 1-8 (2009).

22. Jonaitis, T., Card, J. and Magnuson, B. Concerns regarding nano-sized titanium dioxide dermal penetration and toxicity study. Toxicology letters 192, 268-269 (2010).

23. Sadrieh N, Wokovich AM, Gopee NV, Zheng J, Haines D, Parmiter D, Siitonen PH, Cozart CR, Patri AK, McNeil SE, Howard PC, Doub WH, Buhse LF. Lack of significant dermal penetration of titanium dioxide from sunscreen formulations containing nano- and submicron-size TiO2 particles. Toxicol Sci 115, 156-66 (2010).

24. Senzui, M., Tamura, T., Miura, K., Ikarashi, H., Watanabe, Y. and Fujii, M. Study on penetration of titanium dioxide (TiO(2)) nanoparticles into intact and damaged skin in vitro. J Toxicol Sci 35, 107-113 (2010).

25. Bauer A, Schmitt J, Bennett C, et al. Interventions for preventing occupational irritant hand dermatitis. Cochrane Database Syst Rev 16,CD004414 (2010).

26. EDETOX Evaluations and predictions of dermal absorption of toxic chemicals. 2001-2004 QLK4-CT-2000-00196 www.edetox.ncl.ac.uk

27. Larese Filon F, D'Agostin F, Crosera M, et al. Human skin penetration of silver nanoparticles through intact and damaged skin. Toxicology 255, 33-37 (2009).

28. Larese Filon F, Crosera M, Adami G, et al. Human skin penetration of gold nanoparticles through intact and damaged skin. Nanotoxicology 5,493-501 (2011).

29. Larese Filon F, Crosera M, Timeus E, et al. Human skin penetration of cobalt nanoparticles through intact and damaged skin. Toxicol In Vitro 27,121-7 (2013).

30. Alinovi R, Goldoni M, Pinelli S, et al. Oxidative and pro-inflammatory effects of cobalt and titanium oxide nanoparticles on aortic and venous endothelial cells. Toxicol In Vitro 29,426-37 (2015).

31. Bronaugh, R. and Stewart, R. Methods for in vitro percutaneous absorption studies V: permeation trough damaged skin J Pharm Sci . 10, 1062-6 (1985).

32. Fasano, W., Manning, L., Green, J. Rapid assessment of rat and human epidermal membranes for in vitro dermal regulatory testing: correlation of electrical resistance with tritiated water permeability. Toxicol In Vitro 16,731–740 (2002).

33. Davies, D.J, Ward, R.J., Heylings, J.R. Multi-species assessment of electrical resistance as a skin integrity marker for in vivo percutaneous absorption studies. Toxicol. In Vitro 18,351–358 (2004).

34. Franz, T.J. On the relevance of in vitro data. J Invest Dermatol 93,633–640 (1965).

35. Boukamp, P., Petrussevska, R., Breitkreutz, D., Hornung, J., Markham, A. and Fusenig,N. Normal keratinization in a spontaneously immortalized aneuploid human keratinocyte cell line,» J Cell Biol 106,761-771 (1988).

36. Mosmann, T. Rapid colorimetric assay for cellular growth and survival: application to proliferation and cytotoxicity assays. J Immunol Methods 65, 55-63 (1983).

37. Pelin, M., Sosa, S., Della Loggia, R., Poli, M., Tubaro, A., Decorti, G., Florio, C. The cytotoxic effect of palytoxin on Caco-2 cells hinders their use for in vitro absorption studies. Food Chem Toxicol 50,206-211 (2012).

38. Pelin M, Sosa S, Pacor S, Tubaro A, Florio C. 2014. The marine toxin palytoxin induces necrotic death in HaCaT cells through a rapid mitochondrial damage. Toxicol Lett. 229(3):440-450.

39. Sagawa, Y., Futakuchi, M., Xu, J., Fukamachi, K., Sakai, Y., Ikarashi, Y., Nishimura, T., Suzui, M., Tsuda, H. and Morita, A. Lack of promoting effect of titanium dioxide particles on chemically-induced skin carcinogenesis in rats and mice. J Toxicol Sci 37,317-327 (2012).

40. Xu, J., Sagawa, Y., Futakuchi, M., Fukamachi, K., Alexander, D., Furukawa, F., Ikarashi, Y., Uchino, T., Nishimura, T. and Morita, A. Lack of promoting effect of titanium dioxide particles on ultraviolet B-initiated skin carcinogenesis in rats. Food Chem Toxicol 49, 1298-1302 (2011).

41. Tan, M., Commens, C., Burnett, L. and Snitch, P. A pilot study on the percutaneous absoprtion of microfine titanium dioxide from sunscreens. Australas J Dermatol 37, 185-187 (1996).

42. Bennat, C. and Müller-Goymann, C. Skin penetration and stabilization of formulations containing microfine titanium dioxide as physical UV filter. Int J Cosmet Sci 22, 271-283 (2000).

43. Gibbs S. 2009. In vitro irritation models and immune reactions. Skin Pharmacol Physiol. 22(2):103-113.

44. Gao X, Wang Y, Peng S, Yue B, Fan C, Chen W, Li X. 2015. Comparative toxicities of bismuth oxybromide and titanium dioxide exposure on human skin keratinocyte cells. Chemosphere. 135:83-93.

45. Jaeger A, Weiss DG, Jonas L, Kriehuber R. 2012. Oxidative stress-induced cytotoxic and genotoxic effects of nano-sized titanium dioxide particles in human HaCaT keratinocytes. Toxicology 296(1-3):27-36.

46. Kocbek P, Teskac K, Kreft ME, Kristl J. 2010. Toxicological aspects of long-term treatment of keratinocytes with ZnO and TiO2 nanoparticles. Small. 6(17):1908-1917.

47. Park YH, Jeong SH, Yi SM, Choi BH, Kim YR, Kim IK, Kim MK, Son SW. 2011. Analysis for the potential of polystyrene and TiO2 nanoparticles to induce skin irritation, phototoxicity, and sensitization. Toxicol In Vitro 25(8):1863-1869.

48. Newman, M., Stotland, M. and Ellis, J. The safety of nanosized particles in titanium dioxide- and zinc oxide-based sunscreens. J Am Acad Dermatol 61, 685-692 (2009).

ALLEGATO III

COBALT OXIDE NANOPARTICLES: BEHAVIOR TOWARDS INTACT AND IMPAIRED HUMAN SKIN AND KERATINOCYTES TOXICITY

Mauro M, Crosera M, Pelin M, Florio C, Bellomo F, Adami G, Apostoli P, De Palma G, Bovenzi M, Campanini M, Filon FL.

Pubblicato in: International Journal of Environmental Research and Public Health. 2015 Jul 17;12 (7):8263-80.

Abstract: Skin absorption and toxicity on keratinocytes of cobalt oxide nanoparticles (Co_3O_4NPs) have been investigated. Co_3O_4NPs are commonly used in industrial products and biomedicine. There is evidence that these nanoparticles can cause membrane damage and genotoxicity *in vitro*, but no data are available on their skin absorption and cytotoxicity on keratinocytes. Two independent 24 h *in vitro* experiments were performed using Franz diffusion cells, using intact (exp. 1) and needle-abraded human skin (exp. 2). Co_3O_4NPs at a concentration of 1000 mg/L in physiological solution were used as donor phase. Cobalt content was evaluated by Inductively Coupled – Mass Spectroscopy. Co permeation through the skin was demonstrated after 24 h only when damaged skin protocol was used (57 ± 38 ng·cm^{-2}), while no significant differences were shown between blank cells (0.92 ± 0.03 ng cm^{-2}) and those with intact skin (1.08 ± 0.20 ng·cm^{-2}). To further investigate Co_3O_4NPs toxicity, human-derived HaCaT keratinocytes were exposed to Co_3O_4NPs and cytotoxicity evaluated by MTT, Alamarblue® and propidium iodide (PI) uptake assays. The results indicate that a long exposure time (*i.e.*, seven days) was necessary to induce a concentration-dependent cell viability reduction (EC_{50} values: 1.3×10^{-4} M, 95% CL = $0.8–1.9 \times 10^{-4}$ M, MTT essay; 3.7×10^{-5} M, 95% CI = $2.2–6.1 \times 10^{-5}$ M, AlamarBlue® assay) that seems to be associated to necrotic events (EC_{50} value: 1.3×10^{-4} M, 95% CL = $0.9–1.9 \times 10^{-4}$ M, PI assay). This study demonstrated that Co_3O_4NPs can penetrate only damaged skin and is cytotoxic for HaCat cells after long term exposure.

Keywords: cobalt oxide; nanoparticles; *in vitro*; human skin absorption; keratinocytes toxicity

1. Introduction

The use of nanoparticles (NPs) has grown in the last decades in many fields of every day life, and imposes to the scientific community to take into account their toxicological potential. In fact, NPs may have an unpredictable impact on human health, since traditional toxicological knowledge, based on data derived from materials in their bulk form, is not applicable in the nano size range. One of the crucial aspect is NPs penetration into the body and skin can be a crucial route of entry due to skin contact and skin contamination that are very common in working conditions, where risk perception of the "skin route" is very low. Moreover, to protect workers from inhalation exposure, more NPs are produced as suspension decreasing inhalation risk but increasing potentially skin absorption.

Magnetic nanoparticles have been proposed in many biomedical applications, such as cancer diagnosis [1], radioactive vectors in cancer therapy [2], and as drug delivery systems [3]. CoO and Co_3O_4 are two important forms among the various cobalt oxides based on their distinctive structural features and properties [4] and it has been demonstrated that these transition metal oxides, when falling in the nanosized regime, have even more attractive

applications such as, e.g. heterogeneous catalysts, gas sensors, lithium ion batteries, electrochromic devices, solar energy absorbers, ceramic pigments and optical devices, *etc.* [5–11]. Actually, these NPs are used as contrast agents in magnetic resonance [12], as drug delivery system [13] and as adjuvants for use in human vaccination too, especially when both lymphocytes Th1 and Th2 responses are needed to clear pathogens [14]. On the other hand, some studies demonstrated the induction of membrane damage and genotoxicity in HepG2 cells through ROS and oxidative stress due to these NPs [15]. Cobalt oxide NPs are graded as harmful to humans and dangerous for the environment, but experimental data are lacking. Concerns arise because Cobalt is also a skin sensitizer [16] and a previous study of our group demonstrated that skin exposure to 80 nm CoNPs can lead to skin permeation of this metal [17]. There are no data on cobalt oxide nanoparticles behavior through skin barrier. There is the need to study if Co_3O_4NPs can release ions in physiological condition, if they can penetrate and permeate the skin and to understand whether skin permeation differs between metal and metal oxides NPs species.

The aim of this study was to evaluate Co_3O_4NPs human skin absorption, since consumers and workers exposure may increase in the next few years. We used the experience and the protocol employed during the European project EDETOX (Evaluations and predictions of DErmal absorption of TOXic chemicals), a three-year research program (2001–2004) funded by European Union [18] and already used to test the skin permeation of other metal nanoparticles such as silver, gold and cobalt [17,19,20].

2. Materials and Methods

2.1. Chemicals

All chemicals were analytical grade. Urea, sodium chloride, sodium hydrogenphosphate, potassium dihydrogenphosphate, were purchased from Carlo Erba (Milan, Italy); lactic acid (90% v/v) was bought from Acros Organics (Geel, Belgium); nitric acid (69.5% v/v), hydrogen peroxide (30% v/v), ammonium hydroxide (25% w/v) from Sigma Aldrich (Milan, Italy). Water reagent grade was produced with a Millipore purification pack system (milliQ water).

The commercially available cobalt (II,III) oxide (<50 nm) nanopowder was provided with physico-chemical characterization by Sigma (St. Louis, MO, USA).

2.2. Nanoparticles Characterization

The Co_3O_4NPs have been visualized by Transmission Electron Microscopy (TEM) using a 200 kV analytical JEM 2200-FS (JEOL Inc., Peabody, MA, USA, once they were dispersed in synthetic sweat and at the end of the experiments (after the 24 h exposure time) to visualize the dimensions of the NPs and the aggregation state of the donor phase.

In addition, since the behavior and the aggregation state of the NPs depends strongly on the surface charge of the NPs and the ionic strength of the suspension, further characterization using both Dynamic Light Scattering (DLS) and Z-potential techniques have been carried out.

The measurements have been performed using the 90 Plus PALS instrument, (Brookhaven Instruments Corporation, Holtsville, NY, USA.

2.3. Nanoparticles Dissolution

In order to evaluate the ions release from the NPs once they were put in synthetic sweat, 4 mL of the donor phase (described in *in vitro* diffusion system paragraph) have been ultrafiltered using the Amicon Ultra-4 centrifugal filters (10K MWCO) supplied by Millipore Corporation, Billerica, MA 01821 USA. The ultrafiltration has been performed in centrifuge at 5000 rpm for 30 min in order to remove the Co_3O_4NPs, but not cobalt ions, from the solution.
The solution has been analyzed by ICP – AES (Inductively Coupled Plasma-Atomic Emission Spectroscopy) to quantify the cobalt concentration. The ultrafiltration has been repeated on three different aliquots at the beginning of the permeation experiments, and on other three aliquots at the end of the 24-h and 7-day exposure times.

2.4. Preparation of Skin Membranes

Human abdominal full thickness skin was obtained as surgical waste from 2 patients aged 45–65 years after obtaining ethical committee approval. After the skin excision, subcutaneous fat was removed with a scalpel blade and hair was shaved from the epidermal layer, then skin samples were stored at −25 °C for a period up to, but not exceeding, 4 months. It has been demonstrated that this procedure does not damage skin barrier properties. At the day of the experiment skin samples have been defrost in physiological solution at room temperature for a 30 min period and then 4 × 4 cm^2 pieces were cut from each skin specimen and mounted separately on the diffusion cells. Thickness of the membranes were <1mm. Damaged skin samples were obtained using a needle-abrasion technique described elsewhere [21]. Skin integrity was tested before and after each experiment using electrical conductibility by means of a conductometer (Metrohm, 660, Metrohm AG Oberdorfstr. 68 CH-9100 Herisau) operating at 300 Hz and connected to two stainless steel electrodes [22]. The conductibility data in μS were converted into KΩ cm^{-2}. Cells with a resistance lower than 3.95 ± 0.27 KΩ·cm^{-2} were considered to be damaged and rejected, as suggested by Davies *et al.* [23].

2.5. In Vitro Diffusion System

Percutaneous absorption studies were performed using static diffusion cells following the Franz method [24]. The receptor compartment had a mean volume of 14.0 mL and was maintained at 32 °C by means of circulation of thermostated water in the jacket surrounding the cell. This temperature value was chosen in order to reproduce the hand physiological temperature at normal conditions. The physiological solution used as the receptor phase was prepared by dissolving 2.38 g of Na_2HP0_4, 0.19 g of KH_2P0_4 and 9 g of NaCl into 1 L of milliQ water (final pH 7.35). The synthetic sweat solution used as donor fluid consisted in

0.5% sodium chloride, 0.1% urea and 0.1% lactic acid in milliQ water; pH 4.5 was adjusted with ammonia.

The concentration of the salt in the receptor fluid was approximately the same that can be found in blood. The physiological solution used as receiving phase was continuously stirred using a Teflon coated magnetic stirrer (made in UK, distributed by VWR International, Milan, Italy). Each piece of skin was clamped between the donor and the receptor compartment; the mean exposed skin area was 3.29 cm^2 and the average membranes thickness was 1 mm. Two different experiments were conducted using intact (exp. 1) and damaged skin (exp. 2) as described below:

2.5.1. Experiment 1

The donor phase has been prepared just before the experiment using a sonicated suspension of Co_3O_4NPs at a concentration of 1000 mg/L dispersed in synthetic sweat at pH 4.5, to reproduce *in vivo* condition. The Co_3O_4 concentration in the donor phase was confirmed by Inductively Coupled Plasma – Atomic Emission Spectroscopy (ICP-AES) analysis prior to the test. At time 0, the exposure chambers of 6 Franz diffusion cells were mounted with intact skin samples and filled with 2.5 mL of the donor suspension (606 $\mu g \cdot cm^{-2}$) to ensure an infinite dose. The experiment was run for 24 h, and during this period 1.5 mL of the dermal bathing solution was removed at selected intervals (4, 8, 12, 16, 24 h) and analyzed. Each receptor sample was immediately replaced with an equal volume of fresh physiological solution. At 24 h the dermal bathing solution and the donor phase of each diffusion cell were recovered for the following analysis.

2.5.2. Experiment 2

Experiment 1 was repeated using an abraded skin protocol as suggested by Bronaugh and Steward [21] skin was abraded by drawing the point of a 19-gauge hypodermic needle across the surface (20 marks in one direction and 20 perpendiculars). As donor solution was used 2.5 mL of Co_3O_4NPs suspension (606 $\mu g \cdot cm^{-2}$), dispersed in synthetic sweat at pH 4.5 to ensure an infinite dose.

2.5.3. Blanks

For each experiment, two cells were added as blank. The blank cells were treated as the other cells with the exception that only synthetic sweat was used in the donor compartment.

2.5.4. Skin Digestion after the Experiment

After the experiment, the skin pieces were washed three times with physiological solution to remove Co_3O_4NPs on the skin, then removed from the diffusion cells and treated as follows: skin samples from exp. 1 were separated into epidermis and dermis by heat shock, immerging in water at 60 °C for 1 min before freezing, while skin samples from exp. 2 were simply stored in a freezer at −25 °C. At the time of the analysis, the skin membranes were dried for 2 h at

room temperature, then cut into sections, weighed and put into beakers with 10 mL of HNO3 69% v/v and 2 mL of H_2O_2 for digestion. They were agitated for 24 h at room temperature than heated at the boiling point until the remaining solutions were of 2 mL in volume. The solutions were diluted to a volume of 10 mL with milliQ water for the analysis with ICP-AES.

2.6. Analytical Measurements

The metal content in the receiving phase and into the skin was analyzed by Inductively Coupled Plasma – Mass Spectrometry (ICP-MS) using an ELAN DRC II, (Perkin Elmer, Waltham, USA) instrument equipped with dynamic cell reaction (DRC). The calibration curve was prepared by dilution of standard solution ranging from 0.5 to 1000 µg/L (cobalt in HNO_3 2% mono elemental standard solution, Carlo Erba Reagenti, Milano, Italy). The calibration curve and sample solutions were pumped in the spray chamber using a peristaltic pump. The blank samples were used to correct for any contamination in each batch. The concentration of cobalt was expressed as microgram per liter. The accuracy of the method was determined on the basis of the mean values obtained on certified reference materials NIST 1643e-1643d trace elements in water (National Institute of Standards and Technology). The coefficients of variation ranged from 4% to 8% among series and from 6% to 12% between series and the limit of detection, calculated as three standard deviations of the background signal obtained on 10 blind samples, were 0.005 µg/L. The laboratory participates in the inter-comparison program for toxicological analysis in biological materials for the determination of cobalt (G-EQUAS of the German Society of Occupational and Environmental Medicine).

Total cobalt concentration in the donor phases and in the solutions resulting from the mineralization of the skin sample were performed by Inductively Coupled Plasma – Atomic Emission Spectroscopy (ICP-AES) using a Spectroflame Modula E optical plasma interface (OPI) instrument (by SPECTRO, Germany). The analysis were conducted using a calibration curve obtained by dilution (range: 0–10 mg/L) of Spectrascan® cobalt standard solution for ICP-AES analyses (by Teknolab A/S, Norway). The limit of detection (LOD) at the operative wavelength of 228,616 nm was 0.05 mg/L. The precision of the measurements as relative standard deviation (RSD %) for the analysis was always less than 5%.

2.6.1. Cell Tests

Stock solutions of Co_3O_4 (1 mg/mL ethanol) were diluted to the required concentrations (1.5×10^{-7}–1.0×10^{-3} M, equivalent to 0.023–1500 µg/cm^2) using the cell culture medium and sonicated before using.

2.6.2. Cell Culture

Immortalized human keratinocyte cell line HaCaT [25] was purchased from Cell Line Service (DKFZ, Eppelheim, Germany). Cells were grown in Dulbecco's Modified Eagle's medium (DMEM) supplemented with 2 mM·L-Glutamine, 100 U/mL penicillin-100 µg/mL streptomycin and 10% fetal bovine serum (FBS). Cells were cultured in 75 cm^2 cell culture flasks at 37 °C in a 5% CO_2 atmosphere. All cell culture reagents were from Euroclone (Milan, Italy). Cells received fresh medium every 3 days and were subcultured every 7 days.

2.6.3. MTT Assay

Cells (5×10^3 cells/well) were plated in 96-wells plates for 24 h and then exposed to increasing concentrations of Co_3O_4NPs (1.5×10^{-7}–1.0×10^{-3} M, equivalent to 0.023–1500 µg/cm^2). After 24 h, 48 h and 7 days of exposure, cells were washed with PBS and a 10% MTT solution in complete medium was added a 10% MTT solution was added, and after 4 h the insoluble crystals were solubilized with DMSO [26]. To avoid artifacts in the optical density (OD) values, derived from the presence of particles, the solution was centrifuged for 2 minutes at 1300 rpm and transferred in a new plate. Plates were read in a Microplate Autoreader (Bio-Tek Instruments) at 540/630 nm. Data are reported as % of control and are the mean ± SE of 4 independent experiments performed in triplicate.

2.6.4. AlamarBlue® Assay

Cells (15 × 103 cells/well) were cultured in 96-wells plates. After 24 h, culture medium was removed and substituted with 200 µL of complete medium and cells exposed to different concentrations of Co_3O_4NPs (1.5×10^{-7}–1.0×10^{-3} M, equivalent to 0.023–1500 µg/cm^2). After 24 h, 48 h and 7 days, cells were washed to remove particles and a solution of 10% AlamarBlue® in complete medium (final volume 200 µL) was added to each samples. After 4 h of incubation with the reagent in a humidified 5% CO2 atmosphere, the solution was carefully transferred in a black plate. Fluorescence intensity was read by a Fluorocount microplate Fluorometer (Packard, Germany) at an excitation wavelength of 530 nm and emission wavelength of 590 nm. Data are reported as % of control and are the mean ± SE of 4 independent experiments performed in triplicate.

2.6.5. Propidium Iodide Uptake

Cells (5 × 103 cells/well) were seeded in 96-wells plates and after 24 h exposed to increasing concentrations of Co_3O_4NPs (1.5×10^{-7}–1.0×10^{-3} M, equivalent to 0.023–1500 µg/cm^2) for seven days. Propidium iodide (PI) uptake was performed as previously described [27,28]. Briefly, after treatment cells were washed 2 times with PBS and then rinsed with 200 µL of 3.0×10^{-6} M PI in PBS.
After 30 min, fluorescence intensity was read by a Fluorocount microplate Fluorometer (Packard, Germany) with excitation length of 530 nm and emission length of 590 nm.

Thereafter, all the samples were permeabilized with 1% Triton-X-100 for 30 minutes to obtain total cell content for each sample and fluorescence read. Positive control was obtained permeabilizing untreated cells with 1% Triton-X. Data are reported as % of positive control (equal to 100% PI uptake) after normalization on total cell content and are the mean ± SE of 3 independent experiments performed in triplicate.

2.7. Cell Fixation for TEM Analysis

HaCaT cells were seeded in cell culture dishes and when nearly to confluence, treated with 100 µM Co_3O_4NPs. After 24 h, cells were washed three times and fixed for 1 h in a solution of
2% glutaraldehyde (Serva, Heidelberg, Germany) in 0.1 M cacodylate buffer (pH 7.4). The fixed cells were washed twice (10 minutes each) with 0.1 M cacodylate buffer and then post-fixed with
1% osmium tetroxide for 1 h at 4 °C. Post-fixed samples were dehydrated with an ascending ethanol series ending with 100% ethanol and then embedded in Dow epoxy resin (DER332/732; Società Italiana Chimici, Rome, Italy). The last resin embedding was made under vacuum. Ultrathin sections were prepared with an Ultramicrotome Leica Ultracut UCT (Leica Microsystems, Milan, Italy) equipped with a diamond blade Drukker 3 mm (Emme3, Milan Italy). Ultra-thin sections were observed with a transmission electron microscope (EM208; Philips, Eindhoven, The Netherlands) and micrographs acquired with a Morada camera (Olympus Soft Imaging Solutions (OSIS), Munster, Germany). Double stain was not performed to avoid interference with NPs.

2.8. Statistical Analysis

Co concentration data ($\mu g \cdot cm^{-3}$) in the receptor solution were converted to the total amount that penetrated ($\mu g \cdot cm^{-2}$), with a correction for dilution due to sample removal.

Data analysis was performed with Excel for Windows, release 2007 and Stata Software, version 11.0 (StataCorp LP, College Station, TX, USA). Skin absorption data were reported as mean ± standard deviation (SD). The difference among independent data was assessed by means of the Mann-Whitney test.

Cytotoxicity data were reported as mean ± standard error (SE) of at least three independent experiments performed in triplicate. The concentration giving the 50% of the maximal effect (EC_{50}) was calculated using the GraphPad software version 4.0 (Prism GraphPad, Inc.; San Diego, CA, USA).

3. Results

3.1. Nanoparticles Characterization

TEM characterization of cobalt-oxide NPs (Co_3O_4) specimens showed that NPs were irregular and not spherical, with a tendency to form agglomerates of some decades of NPs (Figure 1a,b). The size distribution of NPs was narrow and centered around a mean value of 17 ± 0.2 nm [29]. No differences in aggregation were found in donor solution at 0 and 24 h The hydrodynamic radius value (R_H) observed in water was centered in 318 nm, while it changed considerably when assessed in synthetic sweat, reaching a value higher than 800 nm (Figure 2) and quite stable during all the time of the experiment (824 at t_0 and 882 nm at t_{24}). This phenomenon was clearly in agreement with the measured Z-potential values, reported in Table 1. The surface charge values suggested that Co_3O_4NPs were more stable in water, thanks to their higher electrostatic stabilization. Results derived from the ultrafiltration of the NPs suspension showed that the cobalt concentration was always less than 0.1% of the original NPs dispersion.

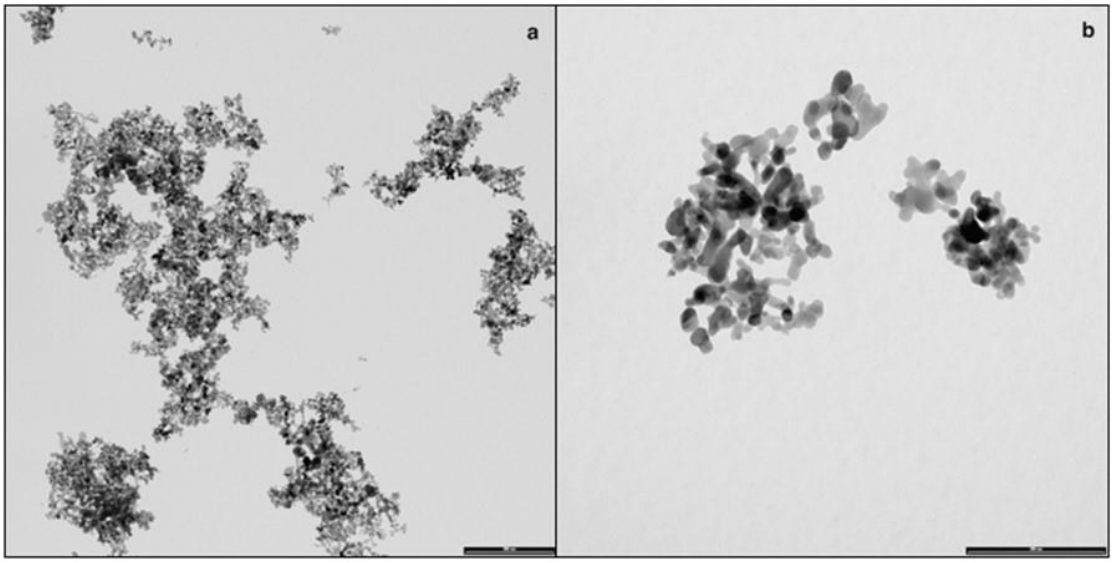

Figure 1. (**a**,**b**) Representative TEM images of agglomerated Co_3O_4NPs dispersed in synthetic sweat at the beginning of the experiments (bar: a = 500 nm, b = 200 nm).

Table 1. Comparison of Z-potential values in water and in synthetic sweat.

Medium Specimen	Water	Synthetic Sweat T = 0	Synthetic Sweat T = 24 h
Co_3O_4	Mean: –19.8 +/− 1.15 mV	Mean: –18.5 +/− 3.5 mV	Mean: –15.9 +/− 4.2 mV

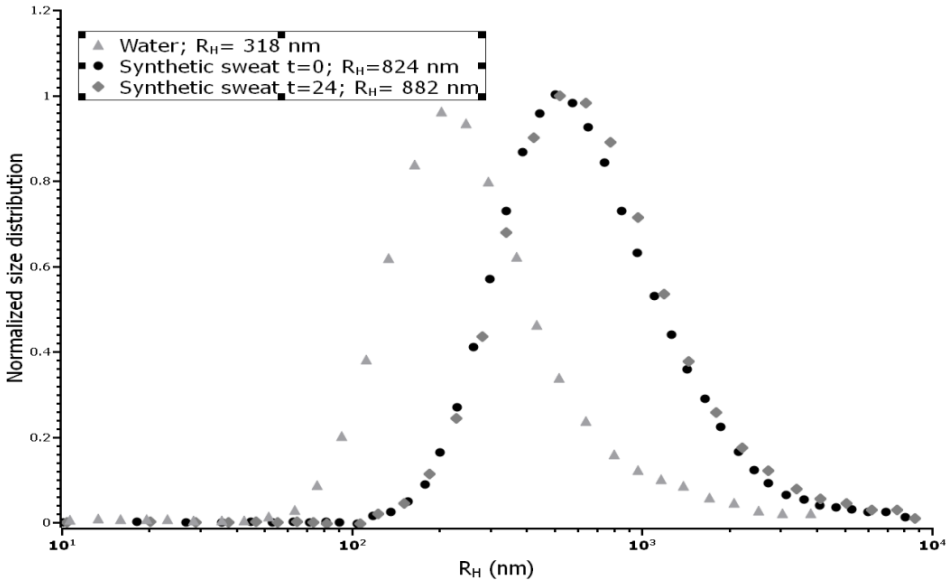

Figure 2. Size distribution of Co_3O_4NPs in water and in synthetic sweat suspension, estimated by DLS.

3.2. NPs Skin Permeation

In experiments with intact skin and in blanks, the concentration of cobalt in receiving phases was similar without an increase of the cobalt concentration during time and so a permeation flux was not achievable (Figure 3). In experiment 2, where damaged skin was used, a metal permeation was found, with flux values of 2.1 ± 2.0 ng·cm^{-2}·h^{-1} and a lag time of 4.3 ± 2.1 h (mean and standard deviation). The amount of cobalt permeated through skin in 24 h was significantly higher using the damaged skin protocol (57 ± 38 ng·cm^{-2}), while no significant differences were shown in intact skin between blank cells (0.92 ± 0.03 ng·cm^{-2}) and those exposed to Co_3O_4NPs (1.08 ± 0.20 ng·cm^{-2}).

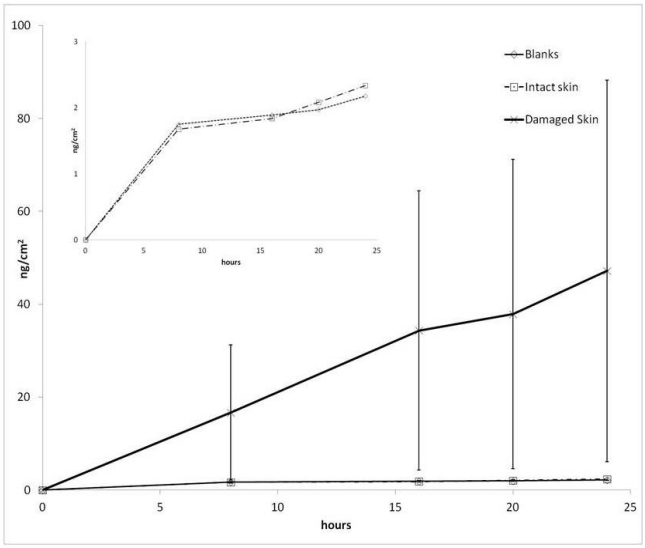

Figure 3. Cobalt permeation profile after skin application of Co_3O_4NPs on intact and damaged skin (main graph). Differences between intact skin, controls exposed to the ultra filtered solution, and blanks are reported in the small box (results expressed as means and standard deviation). Six replication for each experiment.

ICP-AES skin analysis revealed a higher amount of cobalt in epidermis (15.43 ± 3.01 μg·cm^{-2}) than in dermis (1.42 ± 0.21 μg·cm^{-2}) in intact skin (exp. 1 $p < 0.05$, Figure 4a). Damaged skin had lower Co content than intact skin (12.31 ± 6.18 μg cm^{-2} *vs* 16.85 ± 10.98 μg cm^{-2}, respectively), without reaching statistical significance (Figure 4b), suggesting that Co can be "stored" inside the skin.

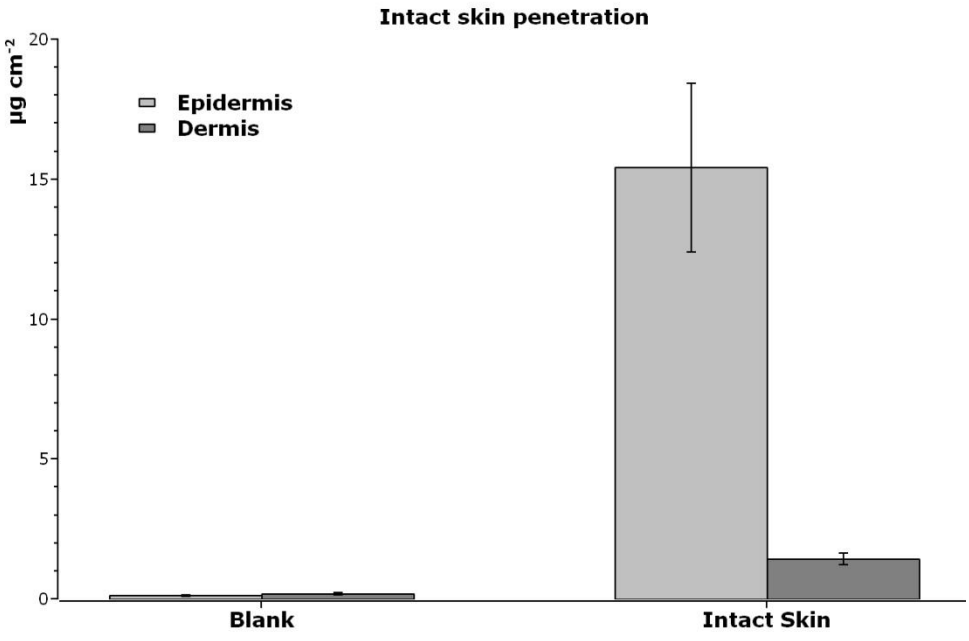

(**a**)

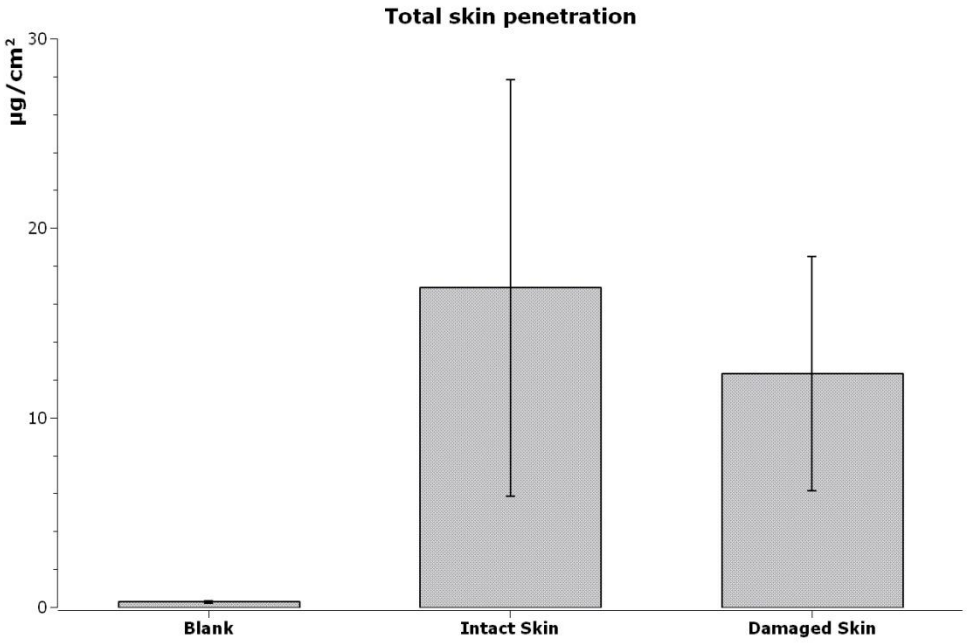

(**b**)

Figure 4. (**a**) Cobalt content (µg/cm^2) inside each layer of intact skin, exposed to Co_3O_4NPs and only to physiological solution (blank cells). Mean and standard deviation of sixcells each. (**b**) Cobalt content (µg·cm $^{-2}$) inside the skin (epidermis + derma) of blank cells (exposed to physiological solution), intact skin and damaged skin (exposed to Co_3O_4NPs). Mean and standard deviation of six cells each.

3.3. Effect of Co_3O_4NPs on Cell Viability

Cytotoxicity of Co_3O_4NPs was evaluated on HaCaT cells using two different viability tests: the MTT assay, which is mainly an index of mitochondrial activity, and the AlamarBlue® assay, which is an index of total cell viability. Cells were exposed to increasing concentrations of Co_3O_4NPs
(1.5×10^{-7}–1.0×10^{-3} M) for different times (24 h, 48 h and seven days). As shown in Figure 5, both cell viability assays, the MTT reduction assay (Figure 5A) and the AlamarBlue® assay (Figure 5B), indicate that at the highest concentration (1.0×10^{-3} M), Co_3O_4NPs significantly reduced cell viability by
47.1% ± 1.6% and 47.6% ± 7.3% (MTT and AlamarBlue® assays, respectively) after 24 h exposure and by 25.4% ± 3.9% and 37.3% ± 9.5% (MTT and AlamarBlue® assays, respectively) after 48 h exposure. However, only after seven days exposure a concentration-dependent effect was evidenced so that EC_{50} values could be calculated and were equal to 1.3×10^{-4} M (95% confidence intervals,
CI = 0.8–1.9×10^{-4} M, equal to 19.6 µg/cm^2, CI 12.0–28.6 µg/cm^2) and 3.7×10^{-5} M (95% CI =

2.2–6.1 × 10^{-5} M, equal to 5.57 μg/cm^2, CI 3.31–9.18 μg/cm^2), for the MTT and AlamarBlue® assays, respectively.

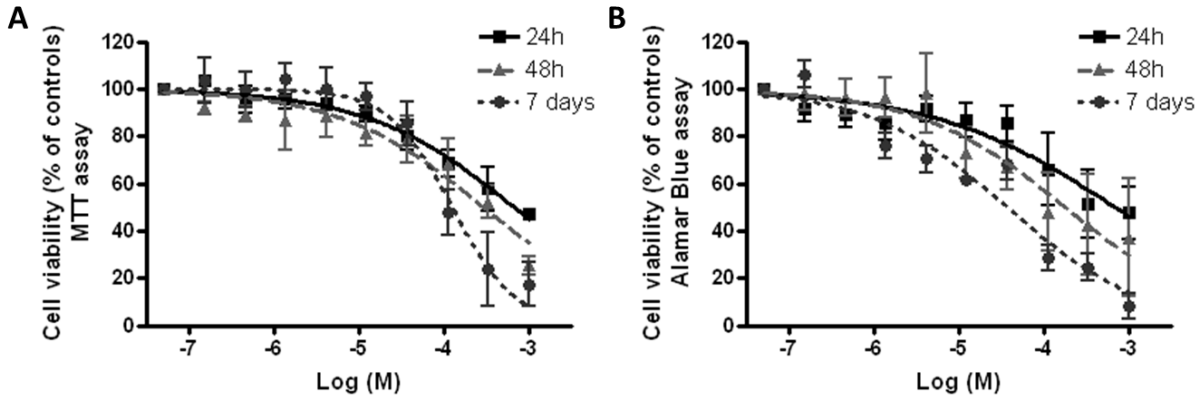

Figure 5. Cytotoxicity of Co_3O_4 NPS. Cell viability was measured by MTT assay (**A**) and Alamar Blue assay (**B**) after 24 h, 48 h and seven days exposure to Co_3O_4NPs
(1.5 × 10^{-7}–1.0 × 10^{-3} M, or 0.023–1500 μg/cm^2) on HaCaT cells. Data are reported as % of untreated controls (equal to 100% cell viability) and are the mean ± SE of four independent experiments performed in triplicate.

3.4. Effect of Co_3O_4NPs on Plasma Membrane Damage

To evaluate if cytotoxicity induced by Co_3O_4NPs was associated to plasma membrane damage, Propidium iodide (PI) uptake was evaluated. As shown in Figure 6, exposure to Co_3O_4NPs
(1.5 × 10^{-7}–1.0x10^{-3} M) for seven days induced a concentration-dependent increase of PI incorporation (99.3% ± 0.7%) that at the highest concentration (1.0 × 10^{-3} M) was comparable to that of the positive control, Triton-X-100 (100%). The calculated EC_{50} value was equal to 1.3 × 10^{-4}M (95% CL = 0.9–1.9 × 10^{-4} M, equal to 19.6 μg/cm^2, CI 13.6–28.6 μg/cm^2).

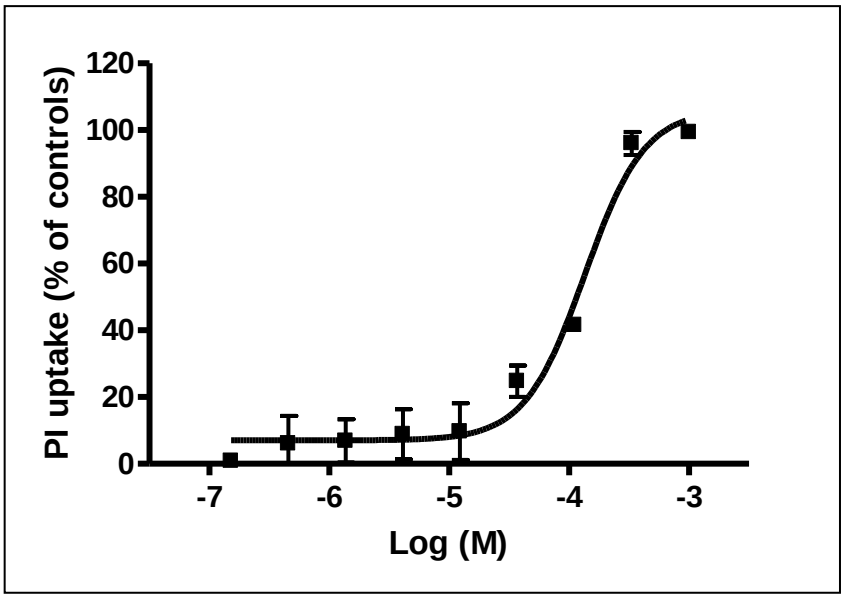

Figure 6. PI uptake in HaCaT cells exposed for seven days to Co_3O_4NPs (1.5×10^{-7}–1.0×10^{-3} M, or 0.023–1500 μg/cm^2). Data are reported as % of PI uptake with respect to positive control (Triton X-100, equal to 100% PI uptake) and are the mean ± SE of three independent experiments performed in triplicate.

3.5. Evaluation of Cellular Internalization of NPs Using Electron Microscopy Imaging

In Figure 7 it is possible to visualize electron-dense clusters of NPs aggregate inside the organelles. No NPs were detected inside the nucleus.

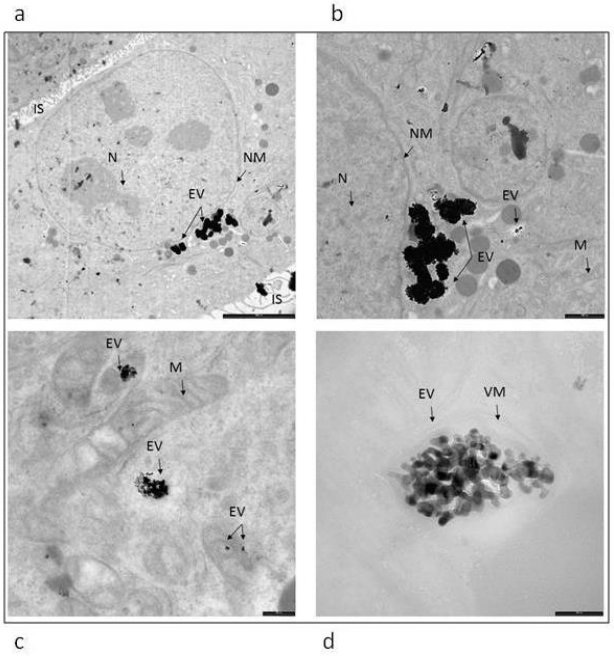

Figure 7. Ultrastructure of *in vitro* culturing keratinocytes exposed for 24 h to Co3O4NPs. ((**a**) bar 5um, (**b**) bar 200 nm, (**c**) bar 200 nm, (**d**) bar 100 nm). Electron-dense material of NPs aggregate is observed inside the organelles. EV: endocytic vesicles, IS: intercellular space, N: nucleus, NM: nuclear membrane, VM: vesicles membrane, M: mitochondria.

4. Discussion

For the first time, we studied skin absorption of cobalt-oxide NPs using an *in vitro* protocol on human skin. Our results add important information on knowledge on NPs interaction with human body and help us to understand the human risk related to NPs contamination. We demonstrated that cobalt oxide NPs can cross the skin, but only when this barrier is damaged. No absorption at all has been demonstrated through intact skin applying Co_3O_4NPs. No ions release was detected in donor solution.

It is known that metal NPs can penetrate (into the skin) and permeate (pass through the skin) as nanoparticles if they are very small (4 nm for Quantum dots [30]) or, more commonly, they can release a high percentage of ions, which eventually cross the skin barrier [20]. The dissolution of NPs is a relevant matter for material in nano-size range, since the high surface to volume ratio increases the risk of free metal ions release when compared to materials in traditional form [31].

For metal oxides, which are more stable and less-soluble than their metal counterpart [32], this release is negligible [33,34] and cobalt oxide NPs have been shown to be less toxic than cobalt ions [35] Nevertheless, at a cytological level, cobalt oxide NPs can release ions with a Trojan-horse type mechanism [32] and cause rapid induction of ROS [35], and with ROS levels higher than those induced by cobalt ions [15,29,36,37]. In angiogenic cells exposure to Co_3O_4NPs significantly reduced cell viability and increased pro-inflammatory cytokine gene expression [38].

To assess the penetration capability of the cobalt oxide NPs through the skin barrier, we compared the results of the present study with the ones obtained in a previous one, where metallic cobalt NPs have been tested using a similar protocol, but owned a larger size [17]. Table 2 shows that the metal content in damaged skin was similar when Co_3O_4NPs are used (89.6% respect to CoNPs exp), while metal concentration in receiving solution was significantly lower (5.6%) as well as flux through the skin (5%). From this point of view, considering also the smaller size of Co_3O_4NPs, it is possible to state that Co_3O_4NPs are safer than CoNPs, with regard to the permeation of the skin. When intact skin is used, only CoNPs can permeate the barrier and Co can be found in receiving phases, while no permeation at all was detectable after the application of Co_3O_4NPs. These differences can be explained by the fact that CoNPs can release cobalt ions [39], which can permeate easily the skin, while Co_3O_4NPs are very stable in physiological solution and cannot release ions [33,34], as demonstrated by scientific literature and confirmed in this study by the ultra filtration of the solution used as donor phases.

It can be concluded that when the skin barrier is damaged or affected by diseases that change barrier properties metal oxide absorption is feasible. This suggests the need for a better protection in people and workers with skin diseases exposed to metal and even to metal oxide NPs, as barrier disruption of the skin is common in workers and in atopic subjects [40]. Nevertheless, we demonstrated that our cobalt oxide nanoparticles could not permeate the normal skin, confirming that when metal NPs cannot release ions, the permeation is not so easy, as was demonstrated for CoNPs, which can release ions.

Comparison between cobalt oxide NPs, cobalt NPs and cobalt as bulk material [17] permits to understand better the potential that metal and metal oxide NPs present in relation to skin absorption. As CoNPs can permeate the skin in higher amount than bulk material, as previously demonstrated, our cobalt oxide NPs are stable and cobalt content in receiving phases is zero in intact skin and very low also in damaged skin.

Table 2. Co and Co_3O_4 concentration (μg/cm^2) into the skin and in receiving solution after 24 h exposure. To compare values with a previous study [26], we standardized results considering the different concentration of Co and Co_3O_4 in donor solution.

	Donor Suspension	**Co_3O_4NPs (Peak 17 nm) 606 μg·cm^{-2} (445 μg·cm^{-2} as Cobalt)**		**CoNPs (Peak 80 nm) [a] 1000 μg·cm^{-2}**		**Co_3O_4NPs Standardized Values 1000 μg·cm^{-2}**	
		Mean	**SD**	**Mean**	**SD**	**Mean**	**%**
Damaged Skin	Membrane (μg·cm^{-2})	4.78	0.90	12.0	3.8	10.75	89.6%
	Receiving Solution (ng·cm^{-2})	47	41	1870 *****	860	106	5.6%
	Flux (ng·cm^{-2}·h^{-1})	1.7	2.0	76 *****	49.3	3.82	5.0%

***** Mann-Whitney test $p < 0.01$.

Finally, the cytotoxic properties of Co_3O_4NPs were characterized on HaCaT cells, a human non-tumor keratinocyte cell line that is widely used as a simple model to assess cytotoxicity at the skin level [41]. Cytotoxicity was evaluated using a solution with NPs concentration similar to that used in permeation studies, performing two different assays: the MTT assay, that relies on the activity of mitochondrial dehydrogenases, and the AlamarBlue® assay, that involves also cytoplasmatic dehydrogenases [42,43]. In the HaCaT model, both methods evidenced with a similar pattern the ability of Co_3O_4NPs to reduce cell viability. However, an exposure time as long as seven days was required to induce a concentration-dependent cytotoxic effect, whereas at shorter exposure times (*i.e.*, 24 or 48 h) a significant cytotoxic effect was

observed only at the highest concentrations used. To better characterize Co_3O_4NPs-induced cytotoxicity, PI uptake was evaluated after seven days of exposure. Under this condition, Co_3O_4NPs caused a concentration-dependent PI incorporation, index of plasma membrane rupture. On the whole, these data demonstrated that Co_3O_4NPs are able to induce significant cytotoxic effects after a long time exposure (*i.e.*, seven days of exposure) and that this effect seems to be due to a damage at the plasma membrane level. These data, if confirmed on more complex models, could have a significant impact on the evaluation of the human risk associated to cutaneous exposure to these NPs.

5. Conclusions

Skin absorption of NPs is a matter of concern for workers and users that can be exposed to objects, powders and solution containing NPs. Our study demonstrated that Co_3O_4NPs cannot permeate through intact skin and that only a very low concentration of cobalt is detectable in receiving solutions when a damaged skin protocol is used. However, our results on cultured keratinocytes suggest that a long-term exposure to Co_3O_4NPs could induce cell damage and necrosis. We thus recommend the use of personal protective equipment to avoid contamination of the skin with NPs because the impaired skin barrier is common among workers and atopic subjects.

Acknowledgements

This study was supported by the Italian Ministry of Health Ricerca Finalizzata 2009 Grant: Integrated approach to evaluating the biological effects on Lung, Cardiovascular system and Skin of occupational exposure to nanomaterials (NanO I-LuCaS). RF-2009-1472550.

Author Contributions

Permeation experiments: Matteo Crosera, Marcella Mauro; cell toxicity experiments: Chiara Florio, Francesca Bellomo, Marco Pelin; chemical analysis: Matteo Crosera, Gianpiero Adami, Piero Apostoli, Giuseppe De Palma; NPs characterization: Marco Campanini; statystical analysis: Massimo Bovenzi; writing of the paper: Marcella Mauro, Francesca Larese Filon.

Conflicts of Interest

The authors declare no conflict of interest.

References

1. Chen, H.C.; Qiu, J.T.; Yang, F.L.; Liu, Y.C.; Chen, M.C.; Tsai, R.Y.; Yang, H.W.; Lin, C.Y.;
   Lin, C.C.; Wu, T.S.; *et al.* Magnetic-composite-modified polycrystalline silicon nanowire field-effect transistor for vascular endothelial growth factor detection and cancer diagnosis.
   Anal. Chem. **2014**, *86*, 9443–9450.
2. Radović, M.; Calatayud, M.P.; Goya, G.F.; Ibarra, M.R.; Antić, B.; Spasojević, V.; Nikolić, N.; Janković, D.; Mirković, M.; Vranješ-Đurić, S. Preparation and *in vivo* evaluation of multifunctional ^{90}Y-labeled magnetic nanoparticles designed for cancer therapy. *J. Biomed. Mater. Res. A.* **2015**, *103*, 126–134.
3. Da Silva, E.P.; Sitta, D.L.; Fragal, V.H.; Cellet, T.S.; Mauricio, M.R.; Garcia, F.P.; Nakamura, C.V.; Guilherme, M.R.; Rubira, A.F.; Kunita, M.H. Covalent $TiO_{(2)}$/pectin microspheres with $Fe_{(3)}O_{(4)}$ nanoparticles for magnetic field-modulated drug delivery. *Int. J. Biol. Macromol*. **2014**, *67*, 43–52.
4. Shi, R.; Chen, G.; Ma, W.; Zhang, D.; Qiu, G.; Liu, X. Shape-controlled synthesis and characterization of cobalt oxides hollow spheres and octahedra. *Dalton Trans*. **2012**, *41*, 5981–5987.
5. Wei-Yang, L.; Li-Na, X., Jun, C. Co_3O_4. Nanomaterials in Lithium-Ion Batteries and Gas Sensors. *Adv. Funct. Mater*. **2005**, *15*, 851–856.
6. Ren-Jang, W.; Cheng-Hung, H.; Chuin-Tih, Y.; Pi-Guey, S. Nanogold on powdered cobalt oxide for carbon monoxide sensor. *Sensor. Actuat. B-Chem*. **2003**, *96*, 596–601.
7. Rahman, M.M.; Khan, S.B.; Faisal, M.; Rub, M.A.; Al-Youbi, A.O.; Asiri, A.M. Electrochemical determination of olmesartan medoxomil using hydrothermally prepared nanoparticles composed SnO_2-Co_3O_4 nanocubes in tablet dosage forms. *Talanta* **2012**, *15*, 924–931.
8. Lou X.W.; Deng, D.; Lee, J.Y; Feng, J.; Archer, L.A. Self-supported formation of needlelike Co_3O_4 nanotubes and their application as lithium-ion battery electrodes. *Adv. Mater.* **2008**, *20*, 258–262.
9. Shu-Lei, C.; Jia-Zhao, W.; Hua-Kun, L.; Shi-Xue, D. Electrochemical deposition of porous Co_3O_4 nanostructured thin film for lithium-ion battery. *J. Power Sources* **2008**, *182*, 359–364.
10. Makhlouf, S.A. Magnetic properties of Co_3O_4 nanoparticles. *J. Magn. Magn. Mater.* **2002**, *246*, 184–190.
11. Ando, M.; Kadono, K.; Kamada, K.; Ohta, K. Third-order nonlinear optical responses of nanoparticulate Co_3O_4 films. *Thin Solid Films* **2004**, *446*, 271–276.
12. Karimi, Z.; Karimi, L.; Shokrollahi, H. Nano-magnetic particles used in biomedicine: Core and coating materials. *Mater. Sci. Eng. C-Mater*. **2013**, *33*, 2465–2475.

13. Papis, E.; Rossi, F.; Raspanti, M.; Dalle-Donne, I.; Colombo, G.; Milzani, A.; Bernardini, G.; Gornati, R. Engineered cobalt oxide nanoparticles readily enter cells. *Toxicol. Lett.* **2009**, *189*, 253–259.
14. Cho, W.S.; Dart, K.; Nowakowska, D.J.; Zheng, X.; Donaldson, K.; Howie, S.E. Adjuvanticity and toxicity of cobalt oxide nanoparticles as an alternative vaccine adjuvant. *Nanomedicine-UK* **2012**, *7*, 1495–1505.
15. Alarifi, S.; Ali, D.; Y A.O.; Ahamed, M.; Siddiqui, M.A.; Al-Khedhairy, A.A. Oxidative stress contributes to cobalt oxide nanoparticles-induced cytotoxicity and DNA damage in human hepatocarcinoma cells. *Int. J. Nanomed*. **2013**, *8*, 189–199.
16. Rui, F.; Bovenzi, M.; Prodi, A.; Belloni Fortina, A.; Romano, I.; Corradin, M.T.; Larese Filon, F. Nickel, chromium and cobalt sensitization in a patch test population in north-eastern Italy (1996–2010). *Contact Dermatitis* **2013**, *68*, 23–31.
17. Larese Filon, F.; Crosera, M.; Timeus, E.; Adami, G.; Bovenzi, M.; Ponti, J.; Maina, G. Human skin penetration of cobalt nanoparticles through intact and damaged skin. *Toxicol. In Vitro*. **2013**, *27*, 121–127.
18. Williams, F.M.; Cage, S.; Carmichael, P.; Corish, J.; Dick, I.; Fitzpatrick, D.; Golden, D.; Jakasa, I.; Kenyon, S.; Kezic, S.; *et al.* Evaluations and predictions of dermal absorption of toxic chemicals. In Proceedings of Occupational and Environmental Exposures of Skin to Chemicals, Stockholm, Švedska, 12–15 June 2005.
19. Larese Filon, F.; D'Agostin, F.; Crosera, M.; Adami, G.; Renzi, N.; Bovenzi, M.; Maina, G.; Human skin penetration of silver nanoparticles through intact and damaged skin. *Toxicology* **2009**, *255*, 33–37.
20. Larese Filon, F.; Crosera, M.; Adami, G.; Bovenzi, M.; Rossi, F.; Maina, G. Human skin penetration of gold nanoparticles through intact and damaged skin. *Nanotoxicology* **2011**, *5*, 493–501.
21. Bronaugh, R.; Steward, R. Methods for *in vitro* percutaneous absorption studies V: Permeation through damaged skin. *J. Pharm Sci.* **1985**, *15*, 1062–1066.
22. Fasano, W.; Manning, L.; Green, J. Rapid assessment of rat and human epidermal membranes for *in vitro* dermal regulatory testing: Correlation of electrical resistance with tritiated water permeability. *Toxicol. In Vitro* **2002**, *16*, 731–740.
23. Davies, D.J.; Ward, R.J.; Heylings, J.R. Multi-species assessment of electrical resistance as a skin integrity marker for *in vivo* percutaneous absorption studies. *Toxicol. In Vitro* **2004**, *18*, 351–358.
24. Franz,T.J. On the relevance of *in vitro* data. *J. Invest. Dermatol.* **1975**, *93*, 633–640.
25. Boukamp, P.; Petrussevska, R.T.; Breitkreutz, D.; Hornung, J.; Markham, A.; Fusenig, N.E. Normal keratinization in a spontaneously immortalized aneuploid human keratinocyte cell line. *J. Cell Biol.* **1988**, *106*, 761–771.

26. Mosmann, T. Rapid colorimetric assay for cellular growth and survival: Application to proliferation and cytotoxicity assays. *J. Immunol. Methods* **1983**, *65*, 55–63.
27. Pelin, M.; Sosa, S.; Della Loggia, R.; Poli, M.; Tubaro, A.; Decorti, G.; Florio, C. The cytotoxic effect of palytoxin on Caco-2 cells hinders their use for *in vitro* absorption studies. *Food Chem. Toxicol*. **2012**, *50*, 206–211.
28. Pelin, M.; Sosa, S.; Pacor, S.; Tubaro, A.; Florio, C. The marine toxin palytoxin induces necrotic death in HaCaT cells through a rapid mitochondrial damage. *Toxicol. Lett.* **2014**, *229*, 440–450.
29. Alinovi, R.; Goldoni, M.; Pinelli, S.; Campanini, M.; Aliatis, I.; Bersani, D.; Lottici, P.P.; Iavicoli, S.; Petyx, M.; Mozzoni, P.; Mutti, A. Oxidative and pro-inflammatory effects of cobalt and titanium oxide nanoparticles on aortic and venous endothelial cells. *Toxicol. In Vitro*. **2015**, *29*, 426–37.
30. Chu, M.; Wu, Q.; Wang, J.; Hou, S.; Miao, Y.; Peng, J.; Sun, Y. *In vitro* and *in vivo* transdermal delivery capacity of quantum dots through mouse skin. *Nanotechnology* **2007**, *18*, doi:10.1088/0957-4484/18/45/455103.
31. Crosera, M.; Bovenzi, M.; Maina, G.; Adami, G.; Zanette, C.; Florio, C.; Filon Larese, F. Nanoparticle dermal absorption and toxicity: A review of the literature. *Int. Arch. Occup. Environ. Health* **2009**, *82*, 1043–1055.
32. Ortega, R.; Bresson, C.; Darolles, C.; Gautier, C.; Roudeau, S.; Perrin, L.; Janin, M.; Floriani, M.; Aloin, V.; Carmona, A.; Malard, V. Low-solubility particles and a Trojan-horse type mechanism of toxicity: The case of cobalt oxide on human lung cells. *Part. Fibre Toxicol*. **2014**, *11*, doi:10.1186/1743–8977–11–14.
33. Barceloux, D.G; Barceloux, D. Cobalt. *J. Toxicol-Clin. Toxic.* **1999**, *37*, 201–206.
34. Collier, C.G.; Pearce, M.J.; Hodgson, A.; Ball, A. Factors affecting the *in vitro* dissolution of cobalt oxide. *Environ. Health Persp.* **1992**, *97*, 109–113.
35. Chattopadhyay, S.; Dash, S.K.; Tripathy, S.; Das, B.; Mandal, D; Pramanik, P.; Roy, S. Toxicity of cobalt oxide nanoparticles to normal cells; an *in vitro* and *in vivo* study. *Chem-Biol. Interact.* **2015**, *226*, 58–71.
36. Limbach, L.K.; Wick, P.; Manser, P.; Grass, R.N.; Bruinink, A.; Stark, W.J. Exposure of engineered nanoparticles to human lung epithelial cells: Influence of chemical composition and catalytic activity on oxidative stress. *Environ. Sci. Technol.* **2007**, *41*, 4158–4163.
37. Lundborg, M.; Falk, R.; Johansson, A.; Kreyling, W.; Camner, P. Phagolysosomal pH and dissolution of cobalt oxide particles by alveolar macrophages. *Environ. Health Persp.* **1992**, *97*, 153–157.
38. Spigoni, V.; Cito, M.; Alinovi, R.; Pinelli, S.; Passeri, G.; Zavaroni, I.; Goldoni, M.; Campanini M.; Aliatis, I.; Mutti, A.; Bonadonna, R.C.; Dei Cas, A. Effects of TiO_2 and Co_3O_4 Nanoparticles on Circulating Angiogenic Cells. *PLoS ONE* **2015**, *10*, doi:10.1371/journal.pone.0119310.

39. Sabbioni, E.; Fortaner, S.; Farina, M.; Del Torchio, R.; Petrarca, C.; Bernardini, G.; Mariani-Costantini R, Perconti, S.; Di Giampaolo, L.; Gornati, R.; Di Gioacchino, M. Interaction with culture medium components, cellular uptake and intracellular distribution of cobalt nanoparticles, microparticles and ions in Balb/3 T3 mouse fibroblasto. *Nanotoxicology* **2014**, *8*, 88–99.
40. Bauer, A.; Schmitt, J.; Bennett, C.; Coenraads, P.J.; Elsner, P.; English, J.; Williams, H.C. Interventions for preventing occupational irritant hand dermatitis. *Cochrane DB. Syst. Rev*. **2010**, *16*, doi:10.1002/14651858.
41. Gibbs, S. In vitro irritation models and immune reactions. *Skin Pharmacol. Phys*. **2009**, *22*, 103–113.
42. Rampersad, S.N. Multiple applications of Alamar Blue as an indicator of metabolic function and cellular health in cell viability bioassays. *Sensors* **2012**, *12*, 12347–12360.
43. Gonzalez, R.J.; Tarloff, J.B. Evaluation of hepatic subcellular fractions for Alamar blue and MTT reductase activity. *Toxicol. In Vitro*. **2001**, *15*, 257–259.

ALLEGATO IV

IN VITRO DERMAL PENETRATION OF NICKEL NANOPARTICLES

Crosera M, Adami G, Mauro M, Bovenzi M, Baracchini E, Larese Filon F.

Pubblicato in: Chemosphere 145 (2016) 301e306.

ABSTRACT

Nickel nanoparticles (NiNPs) represent a new type of occupational exposure because, due to the small size/high surface, they can release more Ni ions compared to bulk material. It has been reported a case of a worker who developed sensitization while handling nickel nanopowder without precautions. Therefore there is the need to assess whether the skin absorption of NiNPs is higher compared to bulk nickel.

Two independent in vitro experiments were performed using Franz diffusion cells. Eight cells for each experiment were fitted using intact and needle-abraded human skin. The donor phase was a suspension of NiNPs with mean size of 77.7 ± 24.1 nm in synthetic sweat.

Ni permeated both types of skin, reaching higher levels up to two orders of magnitude in the damaged skin compared to intact skin (5.2 ± 2.0 vs 0.032 ± 0.010 µg cm-2, p=0.006) at 24 hours. Total Ni amount into the skin was 29.2 ± 11.2 µg cm-2 in damaged skin and 9.67 ± 2.70 µg cm-2 in intact skin (mean and SD, p=0.006). Skin abrasions lead to doubling the Ni amount in the epidermis and to an increase of ten times in the dermis.

This study demonstrated that NiNPs applied on skin surface cause an increase of nickel content into the skin and a significant permeation flux through the skin, higher when a damaged skin protocol was used. Preventive measures are needed when NiNPs are produced and used due to their higher potential to enter in our body compared to bulk nickel.

Keywords: Nanoparticles; In vitro; Skin penetration; Damaged skin; Nickel.

1. INTRODUCTION

In industrialized countries, skin is at high risk of exposure to chemicals and other contaminants, which can be found in the environment and at a workplace. Contact allergy affects approximately 20% of the general population (Thyssen et al, 2009) and nickel (Ni) is recognized as one of the most common cause of contact dermatitis affecting millions of people worldwide (Rui et al., 2013, Schmidt and Goebeler, 2011).

A wide variety of metal objects, which come into repetitive contact with the skin, can release Ni ions that can diffuse through the skin and cause allergy (Flint, 1998). It is well demonstrated that, under physiologically conditions, nickel in metallic form may ionize and so permeate through the skin: cutaneous nickel exposure may result from wearing or handling jewels, coins, or utensils containing nickel (Lidén and Carter, 2001; Lidén et al., 2008, Midander et al., 2014, Thyssen et al., 2012). Also nickel powders, both metal and metal oxide, can release nickel ions once they have been immersed in artificial sweat (Midander et al., 2007; Mazinanian et al., 2013)

More extensive studies of nickel skin absorption have been undertaken. It was found that water solution of nickel salts can pass through the stratum corneum in in-vitro system (Tanojo et al., 2001), and nickel powder can penetrate in depth profiles of the stratum corneum after occlusion in in-vivo experiments (Hostynek, 2001). The presence of skin abrasions can increase nickel permeation when the skin is exposed to nickel powder in an in-vitro diffusion system (Larese Filon et al., 2009).

Actually, metal, metal oxide and metal alloy nanoparticles represent a group of promising materials useful in several areas as chemical and photochemical catalysis, magnetic materials, microelectronics, medical imaging, among others.

In particular, nickel nanoparticles (NiNPs) are emerging for many characteristics such as a high level of surface energy, high magnetism, low melting point, high surface area, and low burning point. For these characteristics their use has been proposed in high magnetic tapes, conducting pastes, chemical catalysis, adjuvant for enhancing immune responses to protein-based vaccines, microfilters, gas sensing equipment, combustion promotion, supercapacitor electrode material, and light absorbance (Alonso et al., 2010, Ansaldo et al., 2008, Patel et al., 2007, Wu et al., 2012).

Magaye and Zhao (2012) summarized the current knowledge on the genotoxicity and carcinogenicity potential of metallic nickel and nickel-based nanoparticles in in vitro and in vivo mammalian studies. The NiNPs, due to their small size/high surface, are able the enter human body in more efficient way that bulk nickel, moreover they can release more Ni ions, causing an increase of metal penetration. Recently a case of a 26-years-old female chemist, that developed nickel sensitization with respiratory and skin effects while handling nickel nanopowder with no protective measures, has been reported (Journeay and Goldman, 2014).

To investigate the potential nickel skin absorption after exposure to a commercially available nickel nanopowder, a series of in vitro permeation experiments with human skin has been carried out using the Franz static diffusion cell method (Franz, 1975). Experiments have been performed using intact as well as damaged skin to estimate the effect of skin lesions on skin absorption. The experience and the protocols employed during the European project EDETOX (Evaluations and predictions of DErmal absorption of TOXic chemicals), a three-year research program (2001-2004) funded by European Union (van de Sandt et al., 2004) and already used to testing the skin absorption of other metal nanoparticles such as gold, cobalt, platinum and rhodium nanoparticles (Larese et al., 2011, 2013, Mauro et al., 2015) was used.

2. MATERIALS AND METHODS

2.1. Chemicals

All chemicals were analytical graded. Magnesium nitrate, urea, sodium chloride, sodium hydrogenphosphate, potassium dihydrogenphosphate, were purchased from Carlo Erba (Milan, Italy); lactic acid (90% v/v) was bought from Acros Organics (Geel, Belgium); nitric acid (69.5% v/v), hydrogen peroxide (30% v/v), hydrochloric acid (36.5-38% v/v), ammonium hydroxide (25% w/v) from Sigma Aldrich (Milan, Italy). Ni nanopowder (CAS 7440-02-0) came from Sigma Aldrich (Milan, Italy), APS (Average Particle Size) <100 nm, purity ≥99.9% trace metals basis). Water reagent grade was produced with a Millipore purification pack system (milliQ water).

2.2. Preparation of the donor phase

The donor phase has been prepared just before the experiment: 100 mg of Ni nanopowder were dispersed by sonication for 10 minutes in 100 mL of synthetic sweat at pH 4.5. The synthetic sweat solution included 0.5% sodium chloride, 0.1% urea and 0.1% lactic acid in

milliQ water; pH 4.5 was adjusted with ammonia. The total nickel concentration (1.0 g L-1 of the donor solution has been confirmed by Inductively Coupled Plasma – Atomic Emission Spectroscopy (ICP-AES) analyses.

Once they have been dispersed in synthetic sweat and at the end of the experiments, NiNPs have been also visualized by means of Transmission Electron Microscopy (TEM).

At the time of the experiments, NiNPs have been removed from aqueous solution in three different aliquots (2 mL) of the freshly prepared solution by means of ultrafiltration in centrifuge at 5000 rpm for 30 min using the Amicon Ultra-4 centrifugal filters (10K MWCO) in order to evaluate the percentage of ionized metal in the donor phase. The filtered solutions have been collected and analysed for determining the concentrations by means of ICP-AES.

The ionization of the donor phase has been checked also after the 24-hour exposure, repeating the ultrafiltration procedure on the donor phases, once they have been removed from the cells at the end of the experiments.

2.3. Preparation of skin membranes

Human abdominal full thickness skin was obtained as surgical waste after the authorization of the local Ethical Committee and it was used for the absorption experiments immediately after the surgical operations. After the skin excision, subcutaneous fat was removed and hair shaved by a razor. From each skin specimen, 4x4 cm2 pieces were cut and mounted separately on the diffusion cells, that were previously washed a first time with freshly prepared Aqua Regia, a second time with diluted nitric acid and rinsed three times with milliQ water.

Skin integrity has been tested before and after the experiments using electrical conductibility by means of a conductometer (Metrohm, 660, Metrohm AG Oberdorfstr. 68 CH-9100 Herisau) operating at 300 Hz and connected to two stainless steel electrodes (Fasano et al. 2002). The conductibility data in μS were converted into KΩ cm-2. Cells with a resistance lower than 3.95 ± 0.27 KΩ cm-2 were considered to be damaged and rejected as suggested by Davies et al. (2004).

2.4. In vitro diffusion system

Percutaneous absorption studies were performed using static diffusion cells following the Franz method (Franz, 1975). The receptor compartment had a mean volume of 14.0 mL and

was maintained at 32°C by means of circulation of thermostated water in the jacket surrounding the cell. This temperature value was chosen in order to reproduce physiological temperature of the hand at normal conditions.

The physiological solution used as receptor fluid has been prepared by dissolving 2.38 g of Na2HP04, 0.19 g of KH2P04 and 9 g of NaCl into 1 L of milliQ water (final pH = 7.35). The concentration of the salts in the receptor fluid was approximately the same of the human blood. The receiving solution in each cell was continuously stirred using a Teflon coated magnetic stirrer.

Each piece of skin was clamped between the donor and the receptor chambers; the mean exposed skin area was 3.29 cm^2 and the average membranes thickness was 1.1 mm.

The experiments were carried out as follows:

Experiment 1: At time 0, the exposure chambers of 4 Franz diffusion cells were filled with 2.0 mL of the donor solution (0.6 mg cm-2) to ensure an infinite dose. The applied dose was the same of previous studies in order to better compare the results of the experiments as summarised in Larese et al. (2015). At selected intervals (4, 8, 16, 24 h) 1.5 ml of the dermal bathing solution has been removed and stored in freezer for the following analyses. Each receptor sample was immediately replaced with an equal volume of fresh physiological solution.

After 24 hours the donor phase of each diffusion cell has been removed and recovered for the following analysis; after the integrity test, also the receiving solutions and the skin pieces have been removed and stored in the freezer for the quantitative analyses.

The total nickel concentrations of the donor phases were confirmed after the experiments by means of Inductively Coupled Plasma-Atomic Emission Spectroscopy (ICP-AES).

Experiment 2: experiment 1 has been repeated using an abraded skin protocol as suggested by Bronaugh and Steward (1985) and adapted by Larese et al. (2006): skin pieces have been abraded by drawing the point of a 19-gauge hypodermic needle across the surface (20 marks in one direction and 20 perpendicular).

Blanks: for each experiment, two cells were added as blank. The blank cells were treated as the others with the exception that synthetic sweat, without NiNPs, has been introduced as donor phase.

Each experiment has been repeated two times, in order to use the skin of four different donors. As the equipment used was static, there is no relationship between the cells tested, hence each of them represents an independent evaluation, for a total of 8 cells with intact skin, 8 cells with damaged skin, and 8 blank cells.

Donors were healthy men and women with a range of age from 50 to 75.

2.5. Skin content evaluation

After the experiments the skin pieces were removed from the diffusion cells, accurately rinsed with milliQ water to remove residual NiNPs from the skin surface. The exposed area of each piece of skin has been cut with a chirurgical scissor, and finally has been separated into epidermis and dermis by heat shock immersing them in water at 60°C for 1 min.

All the skin fractions have been collected and stored individually in freezer at -25 °C. At the time of the analysis, the skin membranes have been dried for 2 hours at room temperature, then cut into sections and put into beakers with 10 mL of HNO3 69% v/v for digestion (amounts of skin were 0.96±0.20 g). They were agitated at room temperature over night and then heated at the boiling point (after 2 hours they were added, drop by drop, of 2 mL of H2O2 30% v/v) till the solution volumes were approximately of 2 mL. The solutions were diluted to a final volume of 10 mL with milliQ water for the ICP-AES analyses.

2.6. Quantitative analysis

The total nickel concentration measurements of the receiving phases were performed using Electro-Thermal Atomic Absorption Spectrometry (ETAAS) with Zeeman background correction. A Thermo M series AA spectrometer equipped with a GF95Z Zeeman Furnace and a FS95 Furnace Autosampler (Thermo Electron Corporation, Cambridge, UK) were used.

A 2% w/v solution of Mg(NO3)2 was used as modifying matrix. The samples were analysed measuring against standard solutions for instrumental calibration. Ni detection limit at the analytical wavelength of 232.0 nm was 0.2 µg L-1. The precision of the measurements as relative standard deviation (RSD%) for the analysis was always less than 5%.

The total nickel concentration in the donor phases and in the solutions resulting from the skin sample mineralization were performed by Inductively Coupled Plasma-Atomic Emission Spectrometry (ICP-AES) using a Spectroflame Modula E optical plasma interface (OPI) instrument (by SPECTRO, Germany). The analysis were conducted using a calibration curve

obtained by dilution (range: 0–10 mg L-1) of Spectrascan® Nickel standard solution for ICP-AES analyses (by Teknolab A/S, Norway). The limit of detection (LOD) at the operative wavelength of 231,604 was 0.020 mg L-1. The precision of the measurements as relative standard deviation (RSD%) for the analysis was always less than 5%.

2.7. Data analysis

Ni concentration data (µg cm-3) in the receptor solution were converted to the total amount that penetrated through the unit surface area (µg cm-2), with a correction for dilution due to sample removal during the sampling procedure, then plotted against time. The slope of this plot in the linear steady-state region gives the flux of Ni through the skin, simple division yielding the rate per cm2. Lag time was calculated as the intercept of the curve with X-axis.

Data analysis was performed using the statistical software STATA release 13 (Texas inc.). Data were reported as mean ± standard deviation (SD). The difference between independent data was assessed by means of the Mann-Whitney and Kruskal Wallis tests. A p value of 0.05 was considered as the limit of statistical significance.

2.8. Skin fixation protocol for TEM analysis

After removal, small sections (dimensions: 1 x 1 x 1 mm) were taken from selected skin samples and fixed for 3 h in a solution of 3% glutaraldheyde (Serva, Heildemberg, Germany) in 0.1M cacodylate buffer (pH 7.3). The fixed sections were washed twice (10 min each) with 0.1M cacodylate buffer and then post fixed with 1% osmium tetroxide for 1 h at 4 C. Post-fixed samples were dehydrated with an ascending ethanol series ending to 100% ethanol and then embedded in Down epoxy resin (DER332; Unione Chimica Europea, Milan, Italy) and DER732 (Serva). The last resin embedding was made under vacuum. Semi-fine and ultra-thin sections were prepared was prepared with an ultra-microtome Leica Ultracut UCT (Leica Microsystem, Milan, Italy) equipped with a diamond blade Drukker 3 mm (Emme3, Milan, Italy). Semi-fine sections were observed with an optical microscope Leitz Dialux 20 EB (Leica Microsystems, Milan, Italy) instead ultra-thin sections were double stained with lead citrate and uranyl acetate and observed with Transmission Electron Microscope (EM208; Philips, Heidhoven, The Netherlands) with an high definition acquisition system SIS Morada and a digital image acquisition system iTEM (FEI Italia, Milan, Italy).

3. RESULTS

The concentration of 1.0 g L-1 of the starting NiNPs dispersion has been confirmed by the ICP-AES analysis. Representative TEM images of NiNPs, diluted in synthetic sweat, before and after the experiments, and their size distribution, are presented in figures 1a,b, and 2, respectively. The mean size of the NPs was 77.7 ± 24.1 nm (number of NP measured =200), but they tended to form bigger aggregates reaching the micrometer range and they deposited on the skin surface in few minutes.

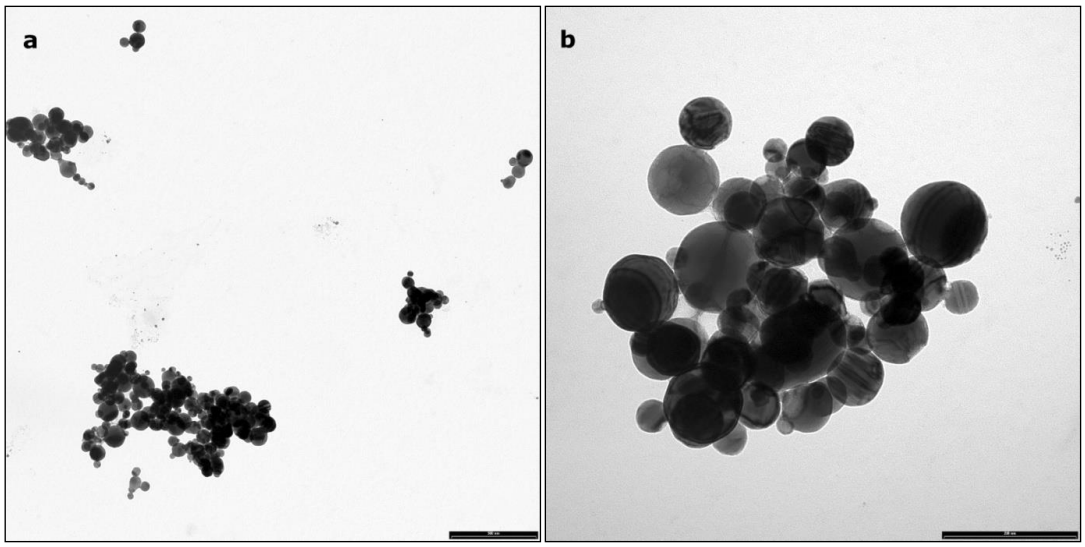

Figure 1: Representative TEM images of NiNPs aggregates in synthetic sweat (barr a=500 nm, b=200 nm).

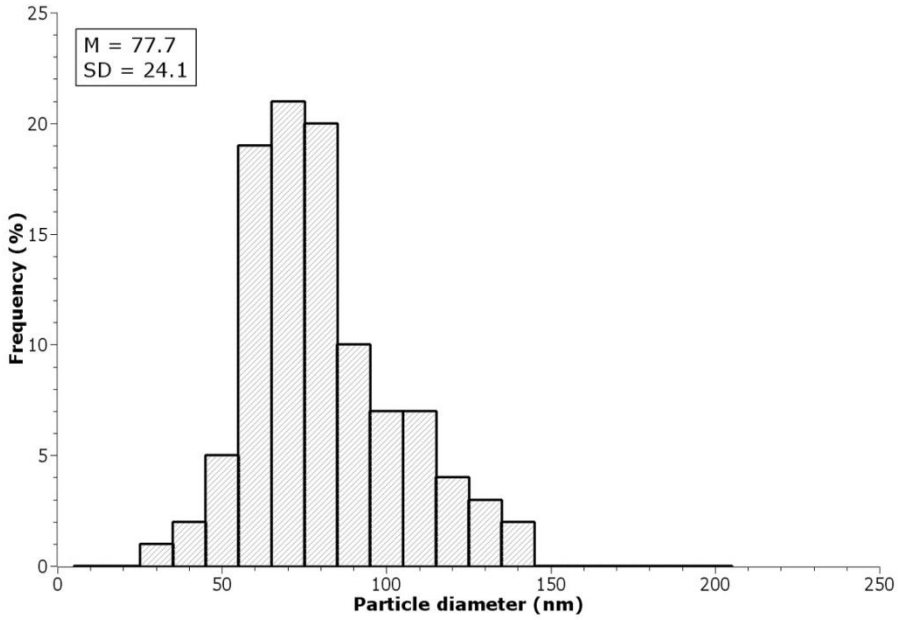

Figure 2: Size distribution of the NiNPs used in the experiments.

The nickel concentration in the ultrafiltered donor phase collected at the beginning of the test, after the removal of NiNPs, shown 12.6 ± 2.1% of ionized metal of the starting suspensions and did not significantly change at the end of the experiments.

Ni permeated the intact skin reaching 0.032 ± 0.010 µg cm-2 at 24 h (figure 3a) and this value is three times greater than that reach in the blank cells (0.010 ± 0.003 µg cm-2), p=0.02.

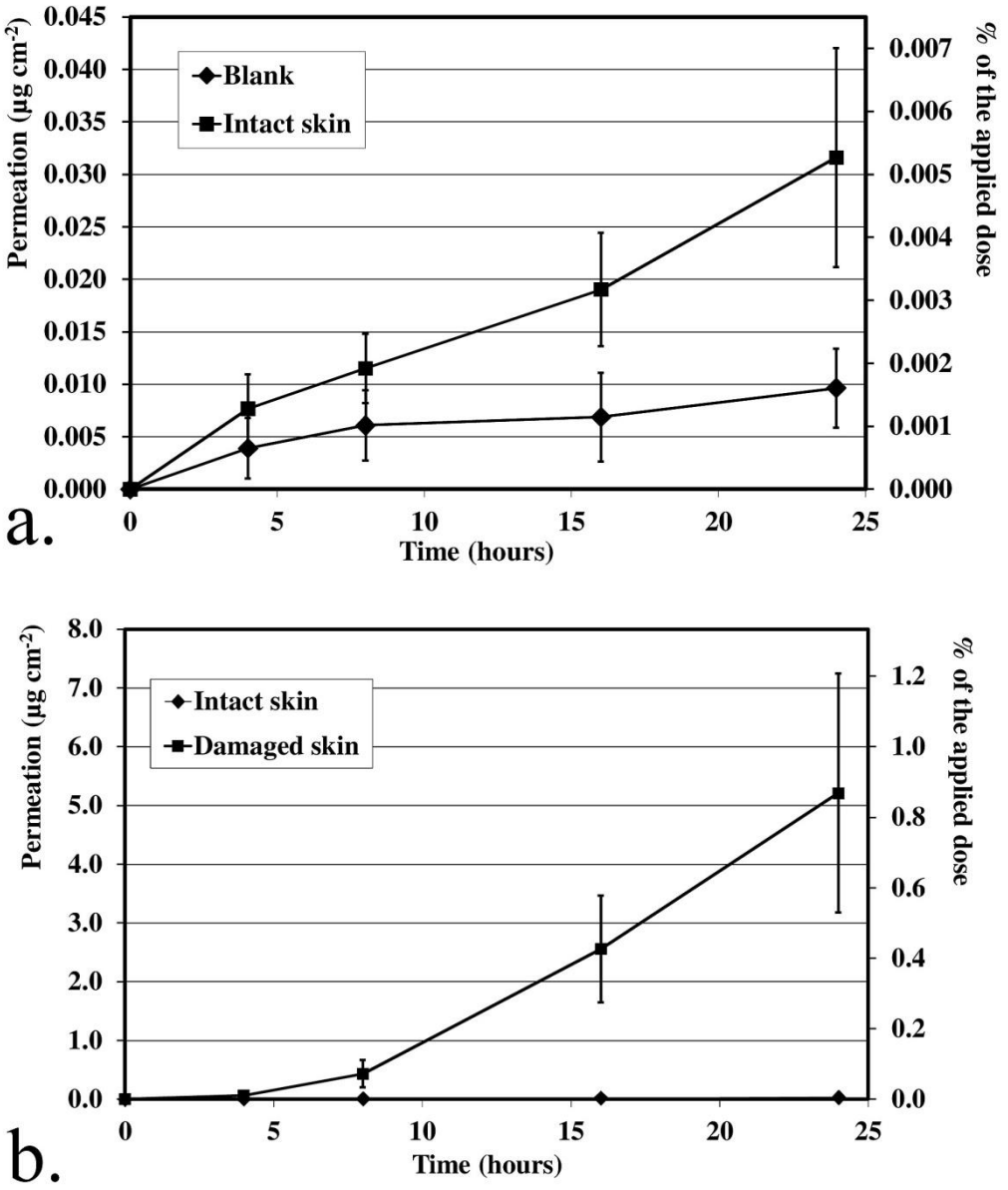

Figure 3: Permeation profiles of a) blanks and intact skin cells (means and standard deviations); b) damaged skin cells (means and standard deviations). Permeation profiles are expressed against the amount of nickel permeated as µg cm-2 (left y-axis) and as the percentage of the applied dose the permeated the skin (right y-axis).

In damaged skin the Ni absorption significantly (p=0.006) increased of around two orders of magnitude reaching 5.2 ± 2.0 µg cm-2 at the end of the exposure time (figure 3a). Ni amount found in the receiving solutions was always less than 1% of the NiNPs applied dose. (Fig. 3a,b) confirming that the experiments were conducted in an infinite dose scenario.

Flux through the skin increased of two orders of magnitude comparing intact (1.7 ± 0.6 ng cm-2 h-1) and damaged (0.30 ± 0.12 µg cm-2 h-1) skin (p=0.006), while a small difference was registered in the lag time values (6.0 ± 1.4 h and 6.6 ± 0.8, respectively).The total Ni amounts (expressed as µg cm-2) penetrated into the dermal layers (epidermis and dermis) for intact and damaged skin, compared to the blank cells values, are summarized in table 1. As shown in figure 4, the Ni amount decreased significantly (p=0.01) from the epidermis to the dermis both in intact and damaged skin and the skin abrasions lead to a doubling of the Ni amount recovered in the epidermis and to an increase of ten times in the dermis.

	Blank ($\mu g\ cm^{-2}$)	**Intact skin** ($\mu g\ cm^{-2}$)	**Damaged skin** ($\mu g\ cm^{-2}$)
Epidermis	0.24 ± 0.10	8.86 ± 2.66*	18.4 ± 9.2^°
Dermis	0.24 ± 0.05	0.81 ± 0.27*	10.8 ± 4.3^°
Total	0.49 ± 0.14	9.67 ± 2.70*	29.2 ± 11.2^*

Table 1: Nickel penetrated into the skin layers expressed as µg cm-2 (epidermis, dermis, total) in blanks, intact and damaged skin cells (mean ± standard deviation).

** p=0.02 intact skin vs blanks*

^ p=0.02 damaged skin vs blanks

° p=0.006 damaged vs intact skin

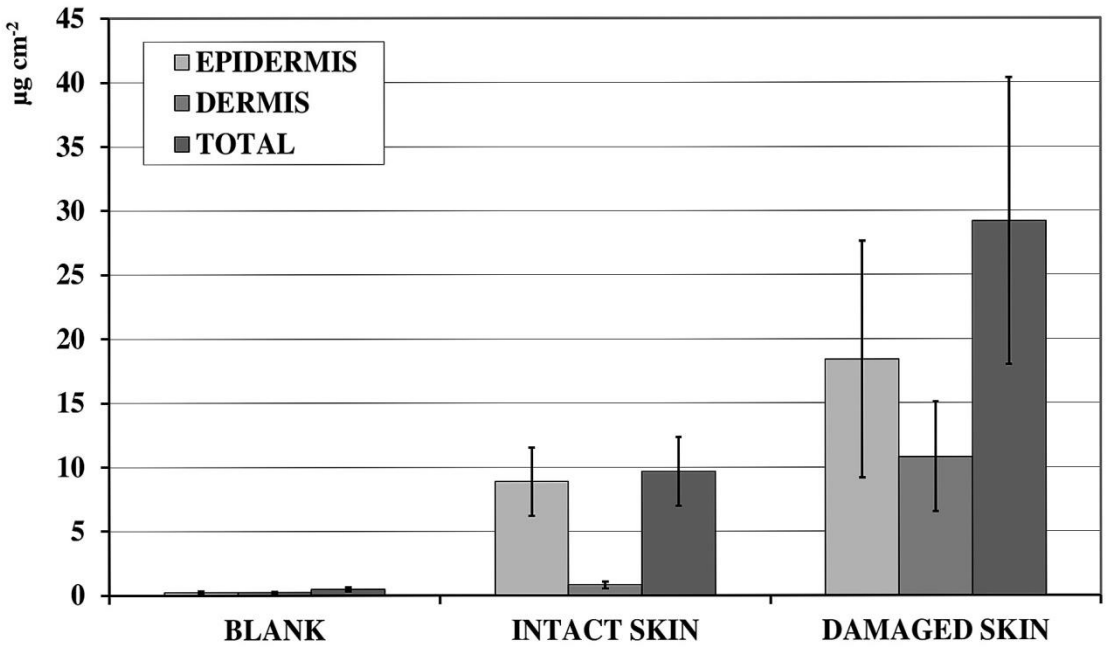

Figure 4: Mean values and standard deviations of nickel amounts (µg cm-2) in epidermis, dermis and total skin, in the three groups of cells (blank, intact and damaged skin).

Finally, TEM investigation on skin exposed samples (Fig. 5a) reveals sporadic formations compatible in size, shape and electron-density with NiNPs in the stratum corneum (Fig. 5b) and in the upper layers of the epidermis (Fig 5c). In the dermis and in the blank tissue samples no NPs have been found.

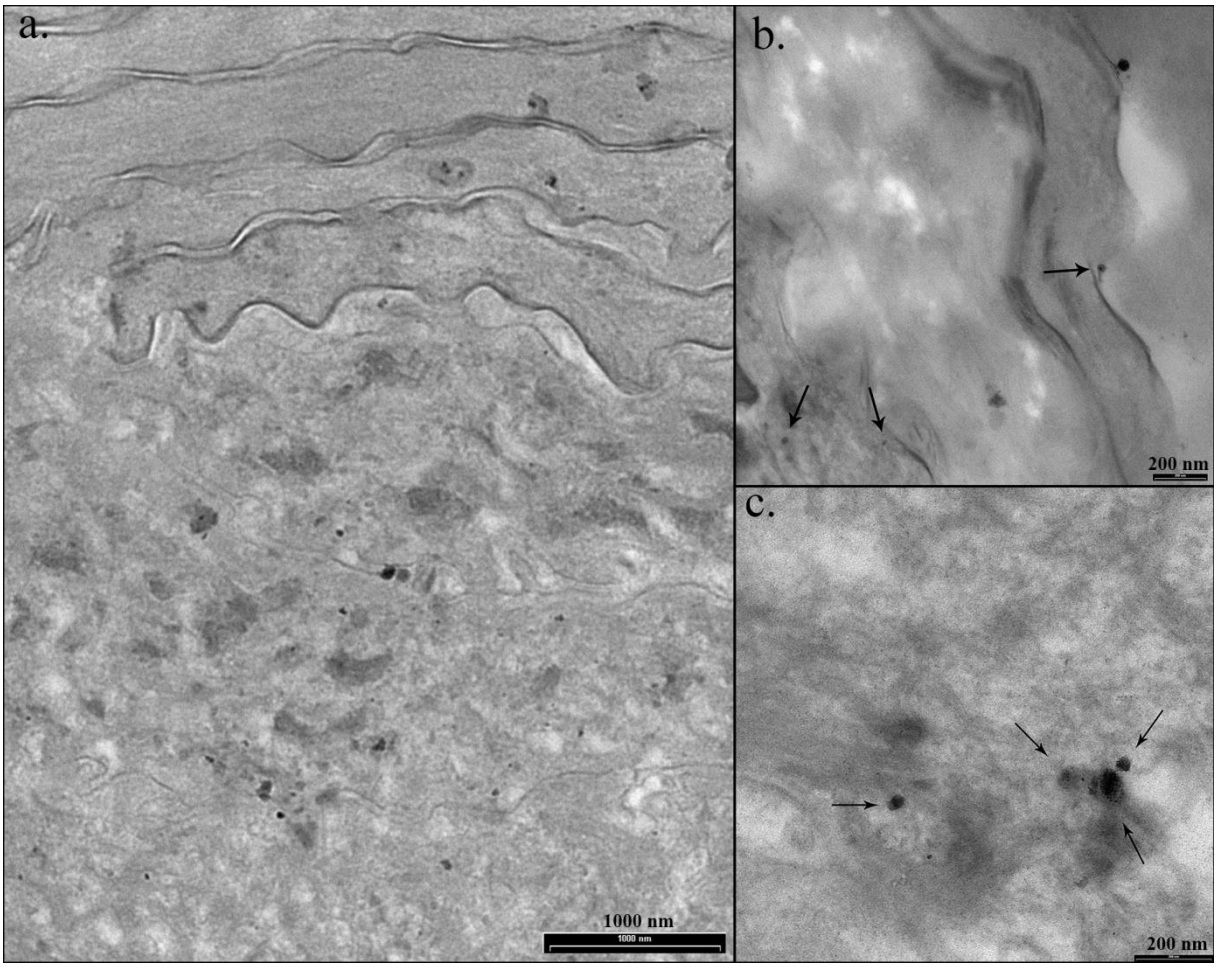

Figure 5: Representative TEM micrographs of NiNPs-treated skin samples (a) and of NPs in the stratum corneum (b) and in the epidermis (c). Barr: a = 1000 nm, b,c = 200 nm.

4. DISCUSSION

The applications of nanotechnologies are flooding the market with a number of products containing engineering nanoparticles and the possible applications in the near future seem to be much more greater. Metal NPs represent an important class of these new materials because of the different properties that metals assume at the nanoscale level. At the same time the toxicological evaluation processes are far from to be exhaustive and the exposure of workers and consumers to the new nanomaterials is still a matter of concern.

It is well known that the skin is a route of entry for metals ions after exposure to metal containing objects, metal salts and metal powders (Hostynek, 2003, Larese et al., 2009b), and this could be a cause of sensitization and allergic contact dermatitis (Thyssen and Menné, 2010). In this study the absorption of nickel through intact and damaged human skin after

exposure to a commercially available nickel nanopowder has been evaluated using an ex-vivo model. We confirmed that NiNPs applied on the skin surface caused penetration of nickel inside the skin and permeation through the skin, significantly higher when a damaged skin protocol has been used. Our results confirmed the ability of nickel to cross the skin barrier as demonstrated in a previous study in which the skin had been exposed to fine nickel powder with an average particle size (APS) of 2.2 – 3.0 µm (Larese et al., 2009). Comparison between the two experiments is reported in table n. 2.

	Nickel fine powder (Larese et al., 2009)	**Nickel nanopowder**
Average particle size	2.2 - 3 µm	77 nm
Total dose (mg cm^{-2})	23	0.6
Ion dose (mg cm^{-2})	0.02 - 0.06	0.06 - 0.09
Receiving Phases Blank (µg cm^{-2})	0.007 ± 0.003	0.010 ± 0.003
Receiving Phases Intact skin (µg cm^{-2})	0.032 ± 0.014	0.032 ± 0.010
Receiving Phases Damaged skin (µg cm^{-2})	3.81 ± 3.41	5.21 ± 2.03

Table 2: Comparison of nickel permeation data (M ± SD) after exposure to Ni nanopowder and Ni fine powder (from Larese et al., 2009).

With respect to the experiments with nickel fine powder in which a dose of 23 mg cm-2, in the present work a dose of 0.6 mg cm-2 has been applied: nevertheless the nickel permeation data at the end of the tests are of the same order of magnitude. It means that a dose forty times lower of nickel as nanopowder reached similar receiving solution concentrations than nickel fine powder. Considering the Ni ion concentrations of the donor phases of the two experiments (12.6% for NiNPs and 0.002% for Ni fine powder) it appears that comparable ion

doses have been applied (range of 0.02 - 0.06 mg cm-2 for Ni fine powder and of 0.06 - 0.09 mg cm-2 for NiNPs). This considerably higher ionisation is probably due to the higher surface/volume ratio of the nanoparticles respect to the same material in bulk form. Since naked NiNPs tend to form big aggregates in water dispersion and considering that 80 nm NPs seems too big to be absorbed through the skin (Larese et al 2015), it can be hypothesized that the permeation is most likely due to the ionized metal released from the nanopowder in synthetic sweat. This hypothesis is also confirmed by the low number of NPs visualized during TEM investigation, so the possibility that they are the result of artefacts due to the complex sample preparation cannot be excluded.

Moreover, considering the composition of the synthetic sweat, it might be expected the formation of small, hydrophilic complexes, such as chloride or lactate, that mainly pass through the aqueous environment of sweat duct respect to lipophilic intercellular route (Hostinek et al. (2001).

Furthermore, this study confirms the capability of the skin to accumulate nickel ions: in fact, in front of a permeation only three times greater in the intact skin compared to blank, the concentration in the skin is about twenty times greater (forty time if we consider the epidermis). Then the skin, and in particular the epidermis, can act as a reservoir of nickel which could be released over time (Fullerton and Hoelgaard, 1988) and an important role would be played by different factors such as the turnover time of the stratum corneum and the water-soluble forms of the metals in the sweat (Hostynek, 2003).From an exposure point of view, these results raise some concerns about the safety handling of these types of nanomaterials because also a contact with small amount of NiNPs, compared to bulk materials, could lead to a relevant absorption of nickel that can cause sensitization and symptoms in exposed people. Preventive measures are needed when NiNPs are produced and used, due to their higher potential to enter in our body compared to bulk nickel, as dictated by the EU Precautionary Principle (i.e. rapid response in the face of a possible danger to human where scientific data do not permit a complete evaluation of the risk).

5. REFERENCES

Alonso, F., Riente, P., Sirvent, J.A., Yus, M. (2010) Nickel nanoparticles in hydrogen-transfer reductions: Characterisation and nature of the catalyst, Applied Catalysis A: General, 378, 42–51.

Ansaldo, A., George, C., Parodi, M.T., Di Zitti, E., Roth, S., Ricci, D. (2008) Ex-situ synthesized nickel nanoparticles for multi-walled carbon nanotube growth on high aspect ratio substrates, Physica status solidi (b) 245, 1923 – 1926.

Bronaugh, R.L., Steward, R.F. (1985) Methods for in vitro percutaneous absorption studies V: permeation through damaged skin. J Pharm Sci 74:1062–1066

Davies, D.J., Ward, R.J., Heylings, J.R. (2004) Multi-species assessment of electrical resistance as a skin integrity marker for in vitro percutaneous absorption studies. Toxicol In Vitro 18(3):351–358

EDETOX., 2000. Evaluations and Predictions of Dermal Absorption of Toxic Chemicals, EU Framework V: Quality of Life, Environment and Health Key Action Funding (Project Number: QLKA-2000-00196).

Fasano, W.J., Manning, L.A., Green, J.W. (2002) Rapid assessment of rat and human epidermal membranes for in vitro dermal regulatory testing: correlation of electrical resistance with tritiated water permeability. Toxicology In Vitro 16:731–740

Flint, G.N. (1998) A metallurgical approach to metal contact dermatitis Contact Dermatitis, 39, 213-221.

Franz, T.J. 1975. Percutaneous absorption on the relevance of in vitro data. J Invest Dermatol. 64: 190-195.

Fullerton, A. and Hoelgaard, A. Binding of nickel to human epidermis in vitro. Brit. J. Dermatol 119, 675–682.

Hostynek, J.J., Dreher, F., Pelosi, A., Anigbogu, A., Maibach, H.I., 2001. Human stratum corneum penetration by nickel: in vivo study of depth distribution after occlusive application of the metal as powder. Acta Derm. Venereol. Suppl. 212, 5–10.

Hostynek, J.J. 2003 Factors determining percutaneous metal absorption. Food Chem. Toxicol. 41 (2003), pp. 327–345

Journeay, W.S. and Goldman, R.H. (2014) Occupational handling of nickel nanoparticles: a case report. American Journal of industrial medicine, 57(9), 1073-1076.

Lidén, C., Carter, S., 2001. Nickel release from coins. Contact Dermatitis 44, 160-165.

Lidén, C., Skare, L., Nise, G., Vahter, M. (2008) Deposition of nickel, chromium, and cobalt on the skin in some occupations – assessment by acid wipe sampling, Contact Dermatitis, 58, 347-354.

Larese Filon, F., Boeninger, M., Maina, G., Adami, G., Spinelli, P., Damian, A. (2006) Skin absorption of inorganic lead and the effects of skin cleansers. J. Occup. Environ. Med. 48, 692–699.

Larese Filon, F., D'Agostin, F., Crosera, M., Adami, G., Bovenzi, M., Maina G., (2009) In vitro absorption of metal powders through intact and damaged human skin. Toxicology in Vitro 23, 574-579.

Larese Filon, F., Crosera, M., Adami, G., Bovenzi, M., Rossi, F., Maina, G. (2011) Human skin penetration of gold nanoparticles through intact and damaged skin. Nanotoxicology 5(4):493–501.

Larese Filon, F., Crosera, M., Timeus, E., Adami, G., Bovenzi, M., Ponti, J., Maina G. (2013) Human skin penetration of cobalt nanoparticles through intact and damaged skin. Toxicol In Vitro 27(1):121–127.

Larese Filon, F., Mauro, M., Adami, G., Bovenzi, Crosera, M. (2015) Nanoparticles skin absorption: New aspects for a safety profile evaluation. Regulatory Toxicology and Pharmacology, 72, 310–322.

Magaye, R. and Zhao, J. (2012) Recent progress in studies of metallic nickel and nickel-based nanoparticles' genotoxicity and carcinogenicity. Environmental Toxicology and Pharmacology 34, 644–650.

Mauro, M., Crosera, M., Bianco, C., Adami, G., Montini, T., Fornasiero, P., Jaganjac, M., Bovenzi, M., Larese Filon, F. (2015) Permeation of platinum and rhodium nanoparticles through intact and damaged human skin. Journal of Nanoparticle Research, 17:253.

Mazinanian, N., Hedberg, Y., Wallinde, I.O. (2013) Nickel release and surface characteristics of fine powders of nickel metal and nickel oxide in media of relevance for inhalation and dermal contact, Regulatory Toxicology and Pharmacology 65, 135–146.

Midander K., Pan, J., Wallinder, I.O., Heim, K., Leygraf, C. (2007) Nickel release from nickel particles in artificial sweat. Contact Dermatitis, 56: 325–330.

Midander, K., Kettelarij, J., Julander, A., Lidén, C. (2014) Nickel release from white gold. Contact Dermatitis, 71, 108–128.

Patel, J.D., O'Carra, R., Jones, J., Woodward, J.G., Mumper, R.J. (2007) Preparation and characterization of nickel nanoparticles for binding to his-tag proteins and antigens, Pharmaceutical Research, 24, 343-352.

Rui, F., Bovenzi, M., Prodi, A., Belloni Fortina, A., Romano, I., Corradin, M.T., Larese Filon, F. (2013) Nickel, chromium and cobalt sensitization in a patch test population in north-eastern Italy (1996–2010) Contact Dermatitis, 68, 23–31.

Schmidt, M. and Goebeler, M. (2011) Nickel allergies: paying the Toll for innate immunity J Mol Med 89, 961–970.

Tanojo, H., Hostynek, J.J., Mountford, H., Maibach, H.I., 2001. In vitro permeation of nickel salts through human stratum corneum. Acta Derm-Venereol. Suppl. 212, 19–23.

Thyssen, J.P., Linneberg, a., Menné, T., Nielsen, N.H., Johansen J.D. (2009) Contact allergy to allergens of the TRUE-test (panels 1 and 2) has decreased modestly in the general population. British Journal of Dermatology, 161, 1124-1129.

Thyssen, J.P. and Menné, T (2010) Metal allergy – A review on exposure, penetration, genetics, prevalence, and clinical implications. Chemical Research in Toxicology, 23, 309-318.

Thyssen, J.P., Gawkrodger, D.J., White, I.R., Julander, A., Menné, T., Liden, C. (2012) Coin exposure may cause allergic nickel dermatitis: a review. Contact Dermatitis, 68, 3-14.

Sandt, J.J., Burgsteden, J.A., Cage, S., Carmichael, P.L., Dick, I., Kenyon, S., Korinth, G., Larese, F., Limasset, J.C., Maas, W.J., Montomoli, L., Nielsen, J.B., Payan, J.P., Robinson, E., Sartorelli, P., Schaller, K.H., Wilkinson, S.C., Williams, F.M. (2004) In vitro predictions of skin absorption of caffeine, testosterone, and benzoic acid: a multi-centre comparison study Regulatory Toxicology and Pharmacology, 39, 271-281.

Wu, X., Xing, W., Zhang, L., Zhuo, S., Zhou, J., Wang, G., Qiao, S. (2012) Nickel nanoparticles prepared by hydrazine hydrate reduction and their application in supercapacitor, Powder Technology, 224, 162–167.

ALLEGATO V

IN VITRO PERMEABILITY OF SILVER NANOPARTICLES THROUGH PORCINE OROMUCOSAL MEMBRANE

Mauro M, Crosera M, Bianco C, Bellomo F, Bovenzi M, Adami G, Larese Filon F.

Pubblicato in: Colloids Surf B Biointerfaces. 2015 Aug 1;132:10-6

Abstract

Silver nanoparticles (AgNPs) can come in contact with human oral mucosa due to their wide use in food industry and hygiene devices. We evaluate transmucosal absorption of 19 nm AgNPs using excised porcine buccal mucosa applied on Franz diffusion cells. Two donor solutions were used: one containing AgNPs (0.5 g/L) and one derived from the ultrafiltration of the former and containing only Ag in its soluble form. Experiments were carried out separately for 4 hours. Silver flux permeation was demonstrated through oral mucosa, showing similar values for AgNPs (6.8 ± 4.5ng cm^{-2} h^{-1}) and Ag ions (5.2 ± 4.3ng cm^{-2} h^{-1}). Our study demonstrates that silver can permeate the oromucosal barrier and that absorption is substantially due to Ag ions, since no permeation difference was found using the two solutions. Mucosal absorption has to be considered in further risk assessment studies.

Keywords: Silver nanoparticles, mucosal membrane, in vitro, Franz cells, permeation.

Graphical abstract

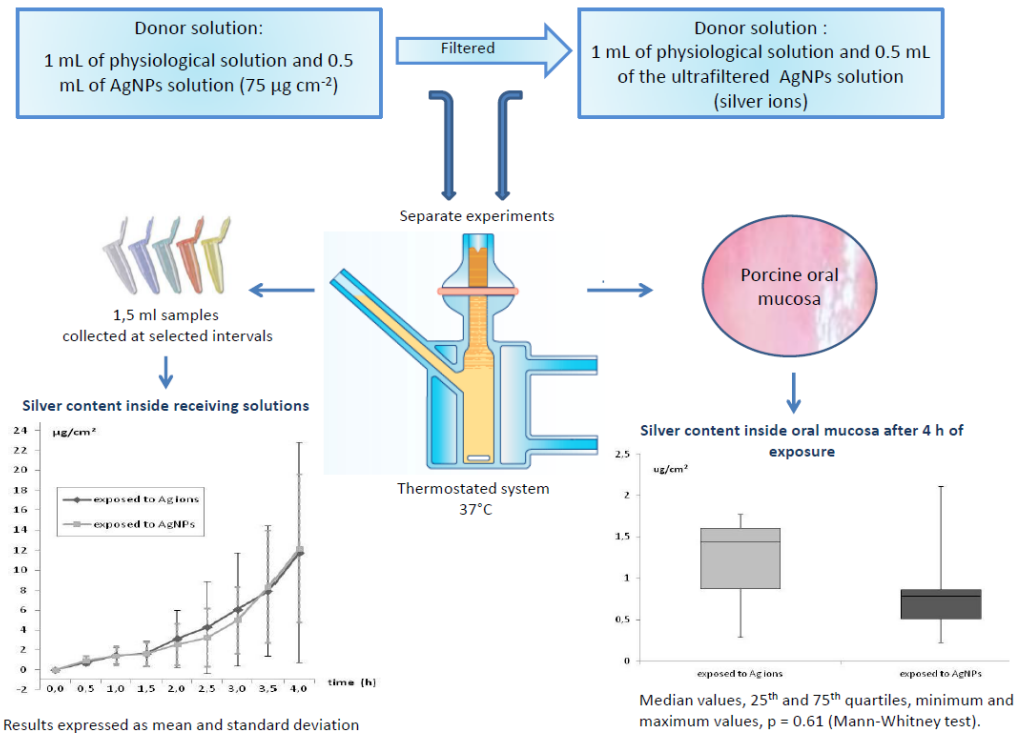

Results expressed as mean and standard deviation

Median values, 25th and 75th quartiles, minimum and maximum values, p = 0.61 (Mann-Whitney test).

1. Background:

Silver nanoparticles (AgNPs) are diffusely used in food packaging, containers, toothpaste and teeth brushes, nipples and nursing bottles, water purification devices etc. [1,2,3] These particles are therefore able to come in contact with oral mucosa, whose penetration properties are not completely known. Silver is used for its good antimicrobial properties and its safe profile,[4] but in literature silver intoxication (argyria) has been described through oral route, in people who drank it for deliberate uptake, [5, 6] or through skin route, when wound dressings containing Silver NPs are used on burns for more than 30% of the skin surface.[7] The Agency for Toxic Substances and Disease Registry (ATSDR) describes argyria as a "cosmetic problem", since it consist mostly in a not reversible bluish-gray discoloration of the skin.[8] Nevertheless there are isolated reports of more serious neurologic, renal and hepatic complications caused by the ingestion of colloidal silver.[9, 10]

Oral mucosa traditionally acts as first barrier to xenobiotics in the digestive tract, but it is also a possible drug delivery route for medical formulations, [11] since it can avoid liver metabolism if compared to the traditional intestinal route.[12]

Due to its histological structure oral mucosa shows a permeability 20 times higher to water[13] and 4 up to 4.000 times higher to different drugs compared to skin,[14] but very little is known about its behavior towards NPs penetration. It has been demonstrated that the main penetration barrier for drugs is the top third region of the epithelium, because the cells size grows, and the cells shape becomes flatter from the basal to the superficial layers. [15]

Since the spread of nanotechnologies has taken place in many fields of everyday life, there are many available products containing AgNPs but the knowledge on NPs permeation properties through mucosal membranes is still lacking.[16] Some authors demonstrated the capability of mucus layer to embed polystyrene NPs,[17] others demonstrated that them can cross this barrier and penetrate the buccal mucosa in a size dependent manner.[18] Nanosized pathogens too

(Norwalk virus, 38 nm diameter, and HPV, 55 nm diameter) can easily diffuse through the mucus layer that protect the gastric and nasal mucosa.[18, 19] On this basis mucosal vaccines have been developed in recent years and some of them are delivered through oral mucosa (as the vaccines against cholera, rotavirus and typhoid fever) while others through nasal mucosa by spray. [20, 21, 22] There is evidence that the administration of antigens at mucosal portals of entry inside lipid nanocapsules can induce a T-cellular immune responses up to 13-fold higher rather than the equivalent soluble formulation. [23]

Since NPs penetration through oral mucosa is not fully known, we performed experiments to investigate AgNPs permeation. We chose to test AgNPs due to their common use as antimicrobial agents in many devices that come in contact with oral cavity. We used porcine lining mucosa because it is the most similar to the human one[13] and is the oral region which is expected to contribute most to oromucosal absorption. In this study, experiments were performed using the Franz cell method, adapting the experience and the protocols employed during the European project EDETOX (Evaluations and predictions of DErmal absorption of TOXic chemicals)[24], a three-year research program (2001-2004) funded by European Union (EDETOX, 2000) and already used to testing skin permeation of other metal nanoparticles such as silver, gold and cobalt.[25, 26, 27]

2. Materials and methods

2.1 Chemicals:

All chemicals used were of analytical grade. Sodium chloride, sodium hydrogen phosphate, potassium dihydrogen phosphate, glutaraldehyde (50% v/v), nitric acid (69% v/v), hydrochloric acid (36.5-38% v/v) were purchased from Sigma Aldrich (Milan, Italy), ammonium hydroxide (25%) from J.T. Baker (Milan Italy). Water reagent grade was produced with a Millipore purification pack system (milliQ water).

The physiological solution used as receptor fluid was prepared by dissolving 2.38 g of Na_2HP0_4, 0.19 g of KH_2P0_4 and 9 g of NaCl into 1 L of milliQ water (final pH = 7.35)

2.2 Silver nanoparticles characterization

2.2.1 Donor phases preparation

AgNPs, stabilized with polyvinylpirrolidone (content of silver: 25% w/w, polymer 75%), were supplied by NanoAmor Materials Inc, (Houston, Texas, U.S.A.).

In order to better distinguish the permeation between AgNPs and silver ions, released from the NPs, two different donor phases were prepared just before the experiments.

The first donor phase, consisting of the AgNPs solution, was prepared using 200 mg (ratio metal:polymer=1:4) of AgNPs dispersed by sonication in 100 ml of physiological solution to obtain a concentration of 0.50 g/L (as metal content).

The nanoparticles suspension in water had a presence of 5% of silver in ionized form, determined using the ultrafiltration technique. The silver ions presence did not significantly change in four hours.

The second donor phase was prepared by the ultrafiltration of the first one to obtain only the water-soluble silver species present in the first donor phase at the moment of the experiment. Four ml of the AgNPs solution were ultrafiltered in centrifuge at 5000 rpm for 30 min by means of Amicon Ultra-4 centrifugal filters (10 KDa MWCO) in order to separate the AgNPs from the aqueous solution. The filtration has been repeated on five different aliquots in order to obtain an adequate solution volume to perform silver quantification analysis and permeation experiments. The five filtered aliquots were mixed for a total of 20 ml and used during the permeation experiments.

2.2.2 Ion release from AgNPs

In order to define the percentage of silver ions inside the AgNPs solution, the donor phases have been analyzed by means of Inductively Coupled Plasma –Atomic Emission Spectroscopy (ICP-AES).

2.2.3 Transmission electron microscope characterization

AgNPs dispersed in physiological solution were characterized to obtain nanoparticles size and morphology on a transmission electron microscope (EM208; Philips, Eindhoven, The Netherlands operating at 200 kV) with an high definition acquisition system based on a side-mounted TEM camera OSIS Morada and a iTEM software platform (Olympus Soft Imaging Solutions GmbH, Münster, Germany).

2.2.4 Dynamic light scattering measurements

The average values of the AgNPs size and polydispersity, defined as a relative width of the size distribution, were determined from dynamic light scattering (DLS) measurements, using a Zetasizer Nano Z (Malvern Instruments Ltd) analyzer applying a 633 nm laser oriented at 173° relative to the sample.

The software was optimized to report summary statistics based upon the intensity of light scattered. Four hundred µl sample volumes from nanosilver dispersion (dilution 1:5 in physiological solution) were loaded into low size disposable cuvette (supplied by manufacturer) and summary statistics were obtained using quadruplicate 3 min analysis (total analysis time=12min). Instrument performance was verified using a polymer reference standard known to be 60 nm.

2.2.5 Zeta potential measurement

Measurements were carried out using a ZetasizerNano ZS (Malvern). An aqueous suspension of silver nanoparticles was diluted 1:5 in a physiological solution. The zeta potential was calculated using Henry's equation.

2.3 Preparation of mucosal membranes

Due to its morphological and enzymatic similarities with the human mucosa[13] porcine oral mucosa was used for the in vitro experiments. The membranes were obtained immediately after pig's slaughter (age 1 year). During the transport to laboratory the tissue was stored at 4°C and then in freezer at -80°C for a period of time up to, but not exceeding, 1 week. On the day of the experiment, the tissue was removed from the freezer and thawed in physiological solution, at room temperature, for approximately 30 min before the permeation experiment. It has been shown that this method of storage does not affect the mucous barrier properties, since no change in the permeability has been described.[28]The underlying connective tissue was manually removed with a scalpel blade, and uniform thickness of approximately 0,6 mm was achieved with surgical scissors. Mucous membranes integrity was tested as suggested by Lestari. [29]

2.4 *In vitro diffusion system*

Mucosal permeation studies were performed using static Franz diffusion cells. The receiver compartments have a mean volume of 14.0 mL and were maintained at 37°C by means of circulation of thermostated water in the jacket surrounding the cells throughout the experiment. This temperature value has been chosen in order to reproduce physiological conditions. The concentration of the salt in the receiver fluids was approximately the same that can be found in the blood. The solution in each cell was continuously stirred using a Teflon coated magnetic stirrer.

Each excised sheet of mucosa was clamped between the donor and the receptor compartment in such a way that the epithelium faced the donor, and the connective tissue region faced the receiver compartment; the mean exposed area of the mucous membranes was 3.29 cm^2.

The experiments were performed as follows:

Exp. 1: At time 0, the exposure chambers of 4 Franz diffusion cells were filled with 1 mL of physiological solution and 0.5 mL of AgNPs suspension (75 μg cm^{-2}), in order to provide an infinite dose: the concentration in each cell has been confirmed at the end of the experiments by means of ICP-AES analysis.

At selected intervals (30, 60, 90, 120, 150, 180, 210, 240 min) 1 mL of the receiving bathing solution was removed and collected for the analysis, and immediately replaced with an equal volume of fresh made physiological solution. In order to avoid the precipitation of silver chloride (AgCl), 100 μl of NH_4OH 1N was added to each sample collected.

The experiment was carried out for 4 hours, as suggested in other studies.[16] At the end of the experiment the mucosa pieces were removed, washed abundantly with milliQ water, and subsequently stored in the freezer together with mucosal bathing solutions and the donor solutions for the following analysis

The experiment was repeated twice for a total of 8 cells.

Exp. 2: the exposure chambers of 4 Franz diffusion cells were filled with 1 mL of physiological solution and 0.5 mL of the Ag ultrafiltered solution. The other test conditions were the same of the experiment 1. The experiment was repeated twice for a total of 8 cells.

Blanks: for each experiment, two cells were added as blank. The blank cells were treated as the other cells with the exception that the exposure chambers were filled only with physiological solution.

2.5 Mucosa digestion after the experiment

All the mucosal exposed samples were collected and stored individually in freezer at -25° C for the following digestion and analysis. At the time of the analyzes, the skin membranes were

dried for 2 hours at room temperature, weight, and then cut into sections and put into glass tubes with 10 mL of HNO_3 69% v/v for digestion. The obtained solutions were heated at 80°C for 8 hours and then diluted to a final volume of 10 ml with milliQ water for the ICP-AES analysis.

2.6 Quantitative analysis

An Inductive Coupled Plasma Mass Spectrometer (ICP-MS 7500 CE Agilent instrument with integrated autosampler) was used to determinate the total silver concentration in the receiver phases.

A seven-point standard curve was used for ICP-MS measurements (0.01, 0.05, 0.1, 0.5, 1, 5 and 10 μg/L, ion mass 107 u.m.a.). The limit of detection of silver was 0.005 μg/L for ICP-MS and the precision of the measurements expressed as repeatability (RSD %) was always lower than 5%.

The total silver concentration in the donor phases and in the solutions resulting from the skin sample mineralization were performed by Inductively Coupled Plasma-Atomic Emission Spectrometry (ICP-AES) using a Spectroflame Modula E optical plasma interface (OPI) instrument (by SPECTRO, Germany). The analysis were conducted using a calibration curve obtained by dilution (range: 0–10 mg/L) of Silver ICP standard solution for ICP-AES analysis (Sigma-Aldrich, Italy). The limit of detection (LOD) at the operative wavelength of 328.068 was 0.010 mg/L. The precision of the measurements expressed as repeatability (RSD %) was always lower than 5%.

All standard solutions used for calibration curves had been prepared using physiological solution and 10% of ammonium hydroxide 1N in order to reproduce the matrix of the samples.

2.7 SEM-EDX analysis

One mucosal sample for each experiment (one blank, one exposed to AgNPs and one to ultrafiltered soluble silver) was fixed with glutaraldehyde 10% v/v, washed with ethanol-water at increasing concentration of ethanol and stored in ethanol 98% until SEM analysis.

Analysis were performed by means of a Scanning Electron Microscope (Hitachi, TM 3000) equipped with Energy Dispersive X-ray Spectroscope (EDX SwiftEd 3000) with a magnification of 30000x and an accelerating voltage of 15 kV. With this setting silver clusters with a diameter above 50 nm were easily detected.

2.8 Data analysis

Data analysis was performed with Excel for Windows, release 2007 and Stata Software, version 11.0 (StataCorp LP, College Station, TX, USA). All data were reported as mean or median as measures of central tendency and standard deviation (SD) or quartiles as measure of dispersion. The difference among independent data was assessed by means of the Mann-Whitney test. A p value of <0.05 was considered as the limit of statistical significance.

3. Results:

3.1 *characterization of AgNPs colloidal dispersion*

The colloidal dispersion of AgNPs in water showed Plasmon absorption at 405 nm. Transmission Electron Microscopy (TEM) measurements revealed that AgNPs used in donor solution were quite uniform in size and shape and as small as 19 ± 5 nm (number of measured nanoparticles: 100). At the concentration used in the permeation experiments no aggregates have been visualized (fig. 1).

The quantitative analysis of the filtered aliquots revealed that 5% of the donor solution was ionized and a dose of 3.8 μg cm^{-2} of silver was applied as donor phase in exp 2. Size distributions obtained by DLS are quite narrow, as presented in figure 2. The analysis

revealed a z-average size (d.nm) equal to 57.1 and a polidispersity index (PdI) of 0.28 (fig. 2), while Zeta potential was equal to – 11.4 ± 0.2 mV.

The apparent mismatch between TEM and DLS sizes is the result of various facts, as elsewhere reported[30]. Firstly, the laser scattering technique measures the hydrodynamic diameter inclusive of PVP and coordinated molecules. Furthermore, polymer-protected metal NPs can form agglomerates consisting of various metal cores wrapped up in the same polymer chain. The mean hydrodynamic diameters of these agglomerates, revealed by DLS, are therefore larger than the mean sizes of the primary NPs, revealed by TEM.

3.2 Ag permeation through mucous membrane

Passive silver flux permeation was demonstrated through oral mucosa. Figure 3 shows the time-dependent increasing trend of metal concentrations in receiving phases. The final values, expressed as mean and standard deviation, were 12.2 ± 7.4 µg/cm² and 11.8 ± 11.1 µg/cm² in cells exposed to AgNPs and to Ag ions (ultrafiltered solution), respectively. Flux permeation after 4 hours of application showed similar final values (6.8 ± 4.5 ng cm-2 h-1 and 5.2 ± 4.3 ng cm-2 h-1) and lag times (1.9 ± 0.7 h and 1.7 ± 0.7 h) using AgNPs and ultrafiltered solution, respectively (mean and standard deviation).

Silver content inside the mucosa showed similar values in both experiments too (median 0.8 µg/cm2 and 1.4 µg/cm2, 25th Pct 0.5 and 0.9, 75th Pct 0.1 and 0.2, in membranes exposed to AgNPs and to Ag ions (ultrafiltered solution), respectively) as showed in fig.4.

SEM-EDX investigations showed no traces of AgNPs clusters in the tissue. SEM analysis revealed the presence of electrondense zones upon the mucosal tissue exposed to Ag-NPs, but microanalysis on that points showed the absence of silver or silver chloride particles (fig. 5A-F).

4. Discussion

The oral mucosa is an attractive biological membrane, since it owns a dual role in the body: on one side it acts as the first barrier towards xenobiotics and human pathogens, and on the other it acts as the first gateway to systemic circulation towards substances which can permeate it. Many drugs have been studied in order to be absorbed through sublingual administration, but very few is known about permeation properties towards nanoparticles.

Previous studies have shown that the oral mucosa permeability depends mainly on the type of epithelium, the type and amount of intercellular lipids and the chemical nature of the substances applied. Regions coated with nonkeratinized epithelium, such as buccal mucosa and floor of mouth (lining mucosa), which we used in the study, contain glycosylceramides, and have a significantly higher permeability compared to regions with keratinized epithelium, such as hard palate and gengiva, which contain predominantly neutral lipids. 31

The first filter to external substances is the mucous layer 32 (average thickness of 70-100 μm), which consists mostly of a high molecular weight mucin, called MG1, which is a component of the saliva that binds to the surface of the buccal epithelium.33, 34 However it has been demonstrated that the main penetration barrier for drugs is the top third region of the epithelium, due to the growing size and shape of the cells that go up from the basal to the superficial layers.15

The xenobiotics that can cross the hindrance of this barrier reach the underneath connective tissue, called “lamina propria”, which provides support and nourishment to the mucosa through a network of blood vessels, capillaries and smooth muscles,11 and from here substances can spread throughout the body via systemic circulation.

AgNPs can come in contact with human mucosa because are present in many products such as toothpaste, alcohol free mouthwash35, nasal sprays, endotracheal tubes 36,37 and urinary

catheters,38,39 to prevent infections. Since the antimicrobial effect of silver depends on superficial contact, the high surface area to volume ratio offered by NPs allows a broader interaction with bacterial membrane and a wider contact with microorganisms.

Few studies have been conducted to investigate AgNPs behavior towards the mucosa of the digestive tract. Shahare and colleagues 40 showed that after an oral administration of 3-20 nm AgNPs to albino mice for 3 weeks, at a dose of 5, 10, 15 and 20 mg/kg body weight, all groups treated had a significant decrease in the body weight, confirming a toxic effect of the metal. Histological changes of the mucosa have been reported, such as a damage of the epithelial cell micovilli and the intestinal glands, which the authors hypothesized as the reason for the absorptive capacity reduction of intestinal epithelium and hence for the weight loss. Walczak and colleagues41 investigated the behavior of 60 nm AgNPs and of AgNO3 ions in an in vitro human digestion model. They found that after gastric digestion and in presence of proteins, the number of particles dropped significantly, due to the formation of clusters, and subsequently disintegrated back to single 60 nm AgNPs during intestinal digestion. Therefore results showed that under physiological conditions AgNPs can reach the intestinal wall in their initial size.

No other studies investigated AgNPs mucosal absorption but 2 studies demonstrated that polystyrene Nps can cross the pig mucosa: Holpuch and coworkers42 showed that 210 nm polystyrene NPs can cross intact human epithelium, derived from oral explants, and can be found in the underlying connective tissue. Teubl and colleagues18 investigated more systematically NPs behavior through oral mucous membrane, by performing experiments with different size and superficial charge of the NPs, and at different mucosal temperatures. They demonstrated that neutral 25 nm, 50 nm and 200 nm polystyrene nanoparticles (PP) can all cross the mucus layer and penetrate the buccal mucosa in a size dependent manner,

surprisingly higher for those with bigger size. This is in contrast to the generally accepted assumption that decreasing the particle diameter increases the absorption43, 44.

Our study investigated for the first time the behavior of silver NPs and its ultrafiltered solution towards oral mucosa, using 19 nm AgNPs applied in vitro on porcine oral explants. The aim was to distinguish the percentage of permeation, if any, due to NPs themselves from the percentage due to the ions issued. The findings suggest that an absorption through passive diffusion takes place, and it is mainly due to silver ions. This result is consistent with the ones obtained by other authors, 45 whom demonstrated that the dose-dependent toxic effects of AgNPs on animals (death, weight loss, cardiac enlargement, altered liver enzymes levels and immunological effects) were substantially mediated by silver ions released from AgNPs. Gaillet and coworkers support the same theory in a recent review.46

Indeed Silver, in whatever form, is not an essential mineral for humans, and so it can exert toxic effects. Systemic intoxication, called “argyria”, is fortunately a rare event, but a more common effect in human is the uptake reduction of some drugs, such as thyroxine, penicillamine and of some antibiotics,47.

For this reason the governmental agency Food and Drug Administration (FDA) issued numerous warning letters to e-commerce sites which promoted colloidal silver as antibiotic or drug for medical purposes.48, 49, 50

It could be interesting compare our results with those obtained by Bianco and coworkers,51 where AgNPs have been applied on full thickness human skin in similar experimental conditions. Interestingly the flux through oral mucosa is about 1 order of magnitude higher compared to skin, and the time required to reach a constant flux trough the membrane is definitely lower through the mucosa. This higher permeability is attributable to a slightly different histological structure of the mucosa compared to skin.

Our study adds important information to understand how nanoparticles can enter the body but nevertheless the protocol used presented some limitations related to: 1) the in-vitro condition, which can underestimate real world scenarios, since only passive diffusion can be studied using Franz-cells and 2) the use of porcine mucosa, which is a good model to study human's mucosa but there are no data, yet, which allow to bridge interspecies results.

5. Conclusions

Our study investigated the permeation of 19 nm silver nanoparticles (AgNPs) across excised porcine oral lining mucosa, using an in vitro diffusion cell system.

We demonstrated for the first time that AgNPs, can lead to silver absorption through oral mucosa, in a similar amount when AgNPs or silver soluble form is used, suggesting that the permeation of the mucosa is related mainly to ions diffusion. A further support to this hypothesis comes from the SEM-EDX results, since no evidence of AgNPs clusters has been revealed, while the quantification of total silver on the mineralized tissue ensures the presence of the metal.

Moreover the comparison with flux permeation values through the skin barrier, when similar experimental conditions were used, suggest that the permeability of silver through oral mucosa is one order of magnitude greater compared to skin, leading to a higher uptake in in-vivo conditions.

Even if the amount of silver found should be not hazardous for human health, these data suggest that oral cavity should be part of further risk assessment studies, since it acts as the first barrier for systemic uptake and can come in contact with different types of nanoparticles. Moreover this study investigated only the intact mucosa, but in everyday life there are common circumstances which may damage the mucosal integrity, such as gastroesophageal

reflux, infections or accidental abrasions, which all can lead to an increase in the oromucosal uptake.

Figures and Graphs

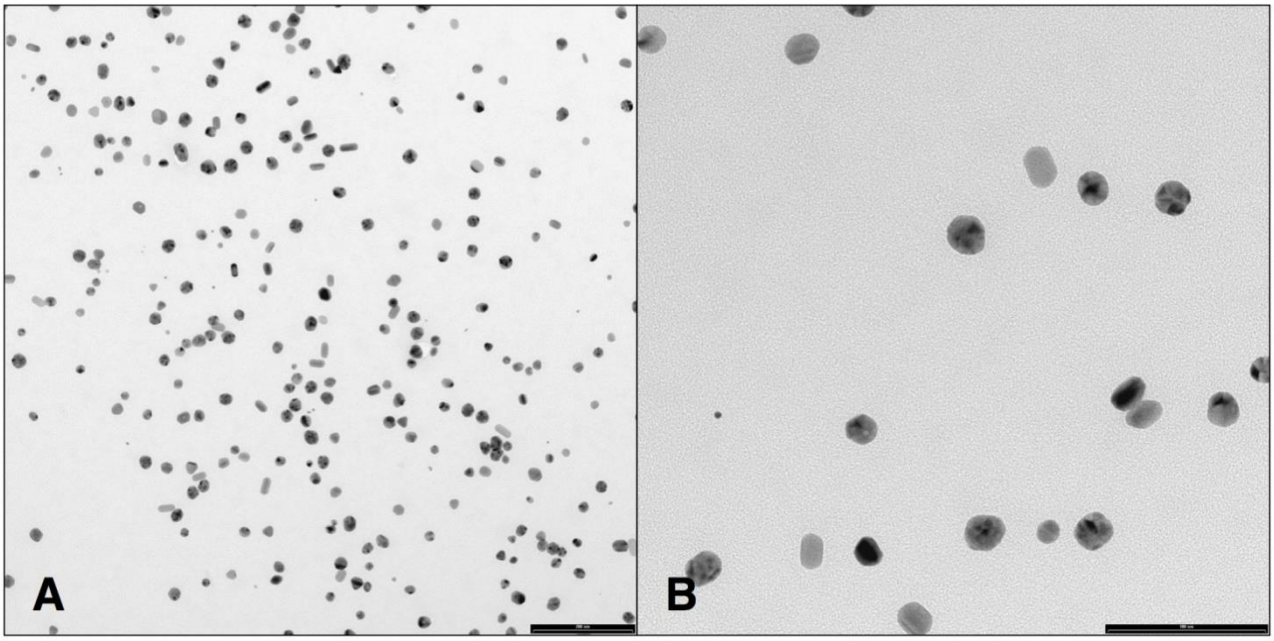

Fig 1. TEM images of the AgNPs dispersed in physiological solution: NPs appeared uniform in size and shape and as small as 19 ± 5 nm (A: bar = 200 nm; B: bar = 100 nm).

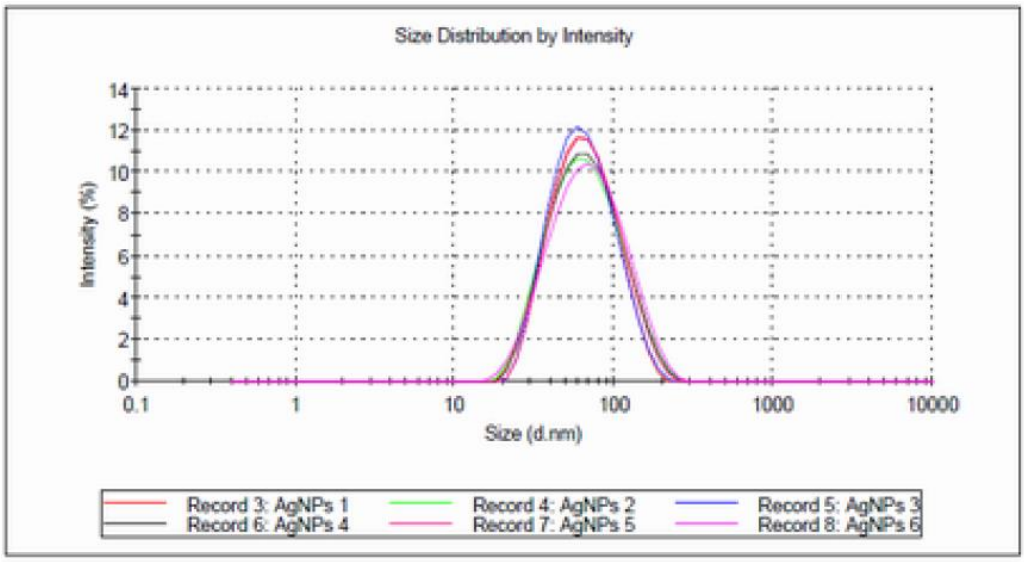

Fig 2. DLS analysis. The curve represent AgNPs size distribution by intensity. Thesummary statistics is based upon the intensity of light scattered of 6 different sam-ples derived from nanosilver dispersion.

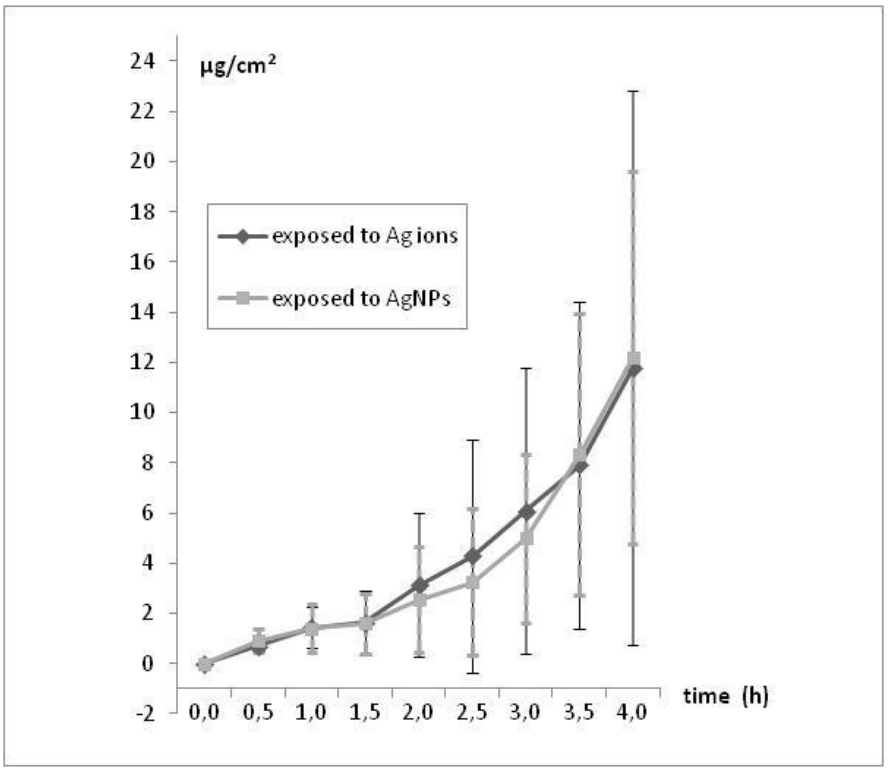

Fig. 3. Silver permeation profile in receiving phases of 8 cells exposed to AgNPs(square) and of 6 cells exposed to Ag ions (diamonds) expressed as mean andstandard deviation.

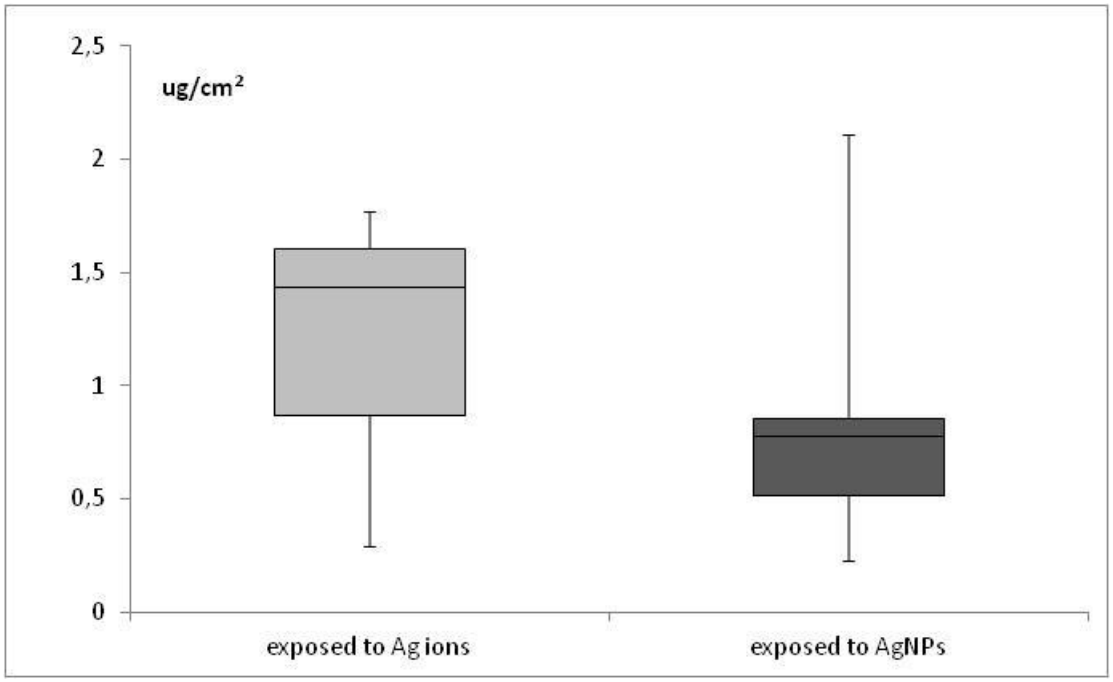

Fig. 4. Silver concentration in the mucosa of 7 cells exposed to AgNPs and 5 cellsexposed to Ag ions (median values, 25th and 75th quartiles, minimum and max-imum values, outsider value of 5.97 g/cm2in the mucosa exposed to AgNPs notshowed in the figure). p = 0.61 (Mann–Whitney test).

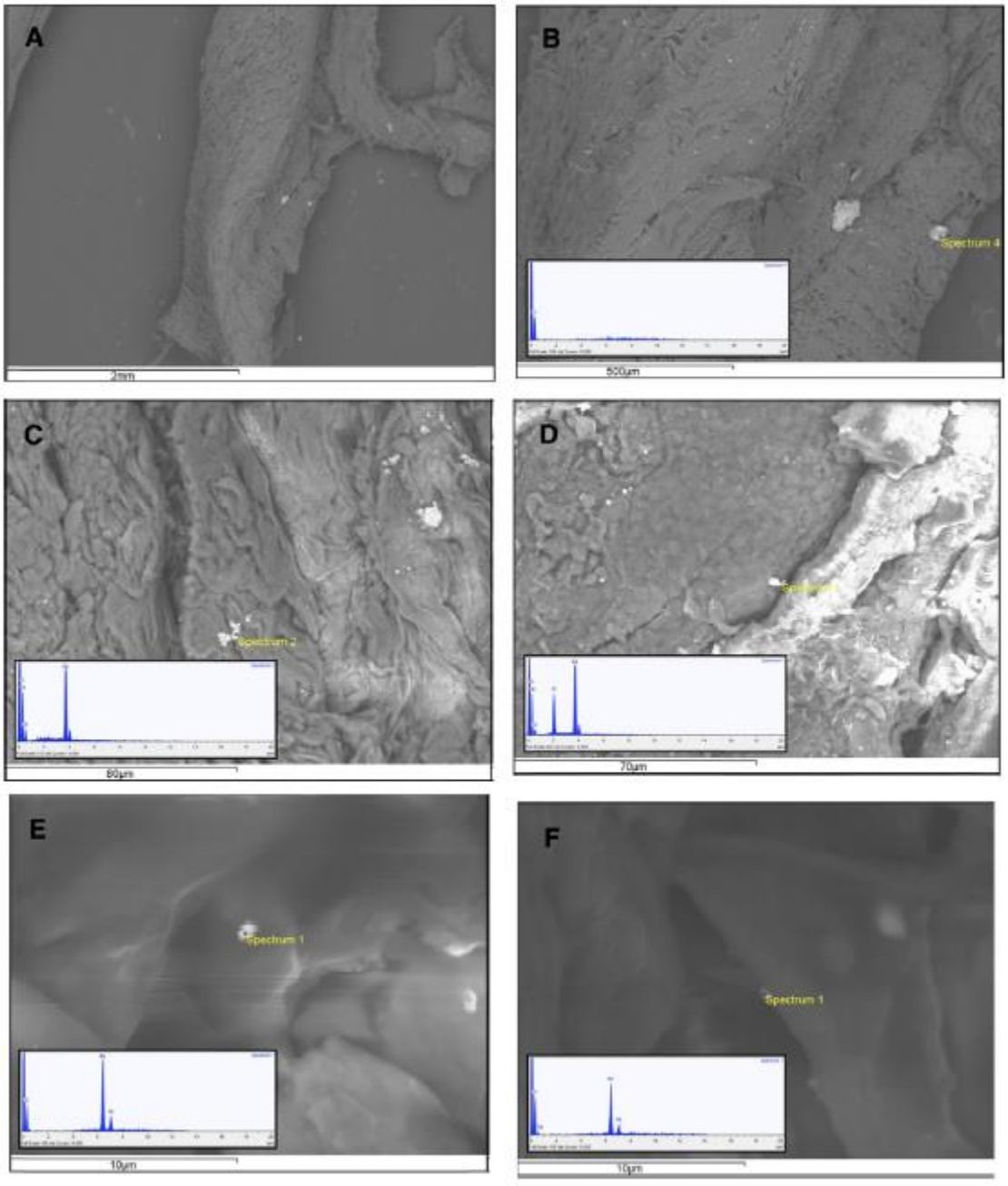

Fig. 5. SEM images at increasing magnifications of the mucosal tissue exposed to AgNPs with EDX microanalysis on the yellow spots (A: the entire sample–bar = 2 mm; B:bar = 500 μm, C: bar = 80 μm, D: bar = 70 μm; E, F: bar = 10 μm).

References:

1. Kim YS, Song MY, Park JD, Song KS, Ryu HR, Chung YH, Chang HK, Lee JH, Oh KH, Kelman BJ, Hwang IK, Yu IJ. Subchronic oral toxicity of silver nanoparticles. Part Fibre Toxicol.2010; 6;7:20. doi: 10.1186/1743-8977-7-20.

2. Hadrup N, Loeschner K, Bergström A, Wilcks A, Gao X, Vogel U, Frandsen HL, Larsen EH, Lam HR, Mortensen A. Subacute oral toxicity investigation of nanoparticulate and ionic silver in rats.2012; Arch Toxicol. 2012; 86 (4):543-51.

3. Collart D, Mehrabi S, Robinson L, Kepner B, Mintz EA. Efficacy of oligodynamic metals in the control of bacteria growth in humidifier water tanks and mist droplets. J Water Health. 2006; 4(2):149-56.

4. Bouwmeester H, Dekkers S, Noordam MY, Hagens WI, Bulder AS, de Heer C, ten Voorde SE, Wijnhoven SW, Marvin HJ, Sips AJ. Review of health safety aspects of nanotechnologies in food production. RegulToxicolPharmacol. 2009; 53(1):52-62.

5. Chang AL, Khosravi V, Egbert B. A case of argyria after colloidal silver ingestion. J CutanPathol. 2006; 33(12):809-11.

6. Johnston HJ, Hutchison G, Christensen FM, Peters S, Hankin S, Stone V. A review of the in vivo and in vitro toxicity of silver and gold particulates: particle attributes and biological mechanisms responsible for the observed toxicity. Crit Rev Toxicol. 2010; 40(4): 328-46

7. Trop M, Novak M, Rodl S, Hellbom B, Kroell W, Goessler W. Silver-coated dressing acticoat caused raised liver enzymes and argyria-like symptoms in burn patient. J Trauma. 2006; 60(3):648-52

8. "ToxFAQs™ for Silver". Agency for Toxic Substances and Disease Registry. Retrieved January 2013.

9. Brandt D, Park B, Hoang M, Jacobe HT.Argyria secondary to ingestion of homemade silver solution.J Am AcadDermatol. 2005;53 (2 Suppl 1):S105-7.

10. Stepien KM, Morris R, Brown S, Taylor A, Morgan L. Unintentional silver intoxication following self-medication: an unusual case of corticobasal degeneration.Ann ClinBiochem. 2009;46 (Pt 6):520-2

11. Harris D, Robinson JR. Drug delivery via the mucous membranes of the oral cavity. J Pharm Sci. 1992; 81(1):1-10.

12. Wertz PW, Squier CA. Cellular and molecular basis of barrier function in oral epithelium. Crit Rev Ther Drug Carrier Syst. 1991; 8 (3):237-69. Review.

13. Lesch CA, Squier CA, Cruchley A, Williams DM, Speight P. The permeability of human oral mucosa and skin to water. J Dent Res. 1989; 68(9):1345-9.

14. Fox CL Jr, Modak SM. Mechanism of silver sulfadiazine action on burn wound infections. Antimicrob Agents Chemother. 1974; 5(6):582-8.

15. Gandhi, R.E. and Robinson, J.R., Bioadhesion in drug delivery, Ind. J. Pharm. Sci. 1988; 50:145-152.

16. Roblegg E, Fröhlich E, Meindl C, Teubl B, Zaversky M, Zimmer A. Evaluation of a physiological in vitro system to study the transport of nanoparticles through the buccal mucosa. Nanotoxicology. 2012; 6(4):399-413.

17. Olmsted SS, Padgett JL, Yudin AI, Whaley KJ, Moench TR, Cone RA. Diffusion of macromolecules and virus-like particles in human cervical mucus. Biophys J. 2001; 81(4):1930-7.

18. Teubl BJ, Meindl C, Eitzlmayr A, Zimmer A, Fröhlich E, Roblegg E. In-vitro permeability of neutral polystyrene particles via buccal mucosa. Small. 2013; 9 (3):457-66.

19. Lai SK, Wang YY, Hida K, Cone R, Hanes J. Nanoparticles reveal that human cervicovaginal mucus is riddled with pores larger than viruses. ProcNatlAcadSci U S A. 2010; 107(2):598-603.

20. Treanor J, Nolan C, O'Brien D, Burt D, Lowell G, Linden J, Fries L. Intranasal administration of a proteosome-influenza vaccine is well-tolerated and induces serum and nasal secretion influenza antibodies in healthy human subjects. Vaccine. 2006; 24(3):254-62.

21. Smith JH, Brooks P, Johnson S, Tompkins SM, Custer KM, Haas DL, Mair R, Papania M, Tripp RA. Aerosol vaccination induces robust protective immunity to

homologous and heterologous influenza infection in mice. Vaccine. 2011; 29(14):2568-75.

22. Smith JH, Papania M, Knaus D, Brooks P, Haas DL, Mair R, Barry J, Tompkins SM, Tripp RA. Nebulized live-attenuated influenza vaccine provides protection in ferrets at a reduced dose. Vaccine. 2012; 30(19): 3026-33

23. Li AV, Moon JJ, Abraham W, Suh H, Elkhader J, Seidman MA, Yen M, Im EJ, Foley MH, Barouch DH, Irvine DJ. Generation of effector memory T cell-based mucosal and systemic immunity with pulmonary nanoparticle vaccination. SciTransl Med. 2013; 5(204) 204ra130

24. Edetox, 2000. Evaluations and Predictions of Dermal Absorption of Toxic Chemicals, EU Framework V: Quality of Life, Environment and Health Key Action Funding. (Project Number: QLKA-2000-00196).

25. Larese FF, D'Agostin F, Crosera M, Adami G, Renzi N, Bovenzi M, Maina G. Human skin penetration of silver nanoparticles through intact and damaged skin. Toxicology. 2009; 255(1-2):33-7

26. Filon FL, Crosera M, Adami G, Bovenzi M, Rossi F, Maina G. Human skin penetration of gold nanoparticles through intact and damaged skin. Nanotoxicology. 2011; 5(4):493-501.

27. LareseFilon F1, Crosera M, Timeus E, Adami G, Bovenzi M, Ponti J, Maina G. Human skin penetration of cobalt nanoparticles through intact and damaged skin. Toxicol In Vitro. 2013; 27(1):121-7.

28. Nicolazzo JA, Reed BL, Finnin BC. The effect of Various In Vitro Conditions on the Permeability Characteristics of the Buccal Mucosa. Journal of Pharmaceutical Sciences 2003; 92 (12): 2399-2410

29. Lestari ML, Nicolazzo JA, Finnin BC. A novel flow through diffusion cell for assessing drug transport across the buccal mucosa in vitro. J Pharm Sci. 2009; 98(12):4577-88.

30. Blosi M, Albonetti S, Dondi M, Martelli C, Baldi G.vMicrowave-assistedpolyolsynthesis of Cu nanoparticles. J.Nanopart. Res. 2011; 13:127–138

31. Squier CA, Wertz PW, Cox P. Thin-layer chromatographic analyses of lipids in different layers of porcine epidermis and oral epithelium. Arch Oral Biol. 1991; 36(9):647-53.

32. Huh CH, Bhutani MS, Farfán EB, Bolch WE. Individual variations in mucosa and total wall thickness in the stomach and rectum assessed via endoscopic ultrasound. Physiol Meas. 2003; 24(4):N15-22.

33. Bykov VL. [The tissue and cell defense mechanisms of the oral mucosa]. Morfologiia. 1996; 110(6):14-24.

34. Bykov VL. [The functional morphology of the epithelial barrier of the oral mucosa]. Stomatologiia (Mosk). 1997; 76 (3):12-7. Review.

35. Abadi MF, Mehrabian S, Asghari B, Namvar AE, Ezzatifar F, Lari AR. Silver nanoparticles as active ingredient used for alcohol-free mouthwash. GMS Hyg Infect Control. 2013; 8(1): Doc05. doi: 10.3205/dgkh000205.

36. Bouadma L, Wolff M, Lucet JC.Ventilator-associated pneumonia and its prevention.CurrOpin Infect Dis. 2012;25 (4):395-404.

37. Kollef MH, Afessa B, Anzueto A, Veremakis C, Kerr KM, Margolis BD, Craven DE, Roberts PR, Arroliga AC, Hubmayr RD, Restrepo MI, Auger WR, Schinner R; NASCENT Investigation Group.Silver-coated endotracheal tubes and incidence of ventilator-associated pneumonia: the NASCENT randomized trial.JAMA. 2008;300 (7):805-13.

38. Agarwala M, Barman T, Gogoi D, Choudhury B, Pal AR, Yadav RN.Highly effective antibiofilm coating of silver-polymer nanocomposite on polymeric medical devices deposited by one step plasma process. J Biomed Mater Res B ApplBiomater. 2014;102 (6):1223-35.

39. Chakravarti A, Gangodawila S, Long MJ, Morris NS, Blacklock AR, Stickler DJ.An electrified catheter to resist encrustation by Proteus mirabilis biofilm.J Urol. 2005;174(3):1129-32.

40. Shahare B, Yashpal M. Toxic effects of repeated oral exposure of silver nanoparticles on small intestine mucosa of mice.ToxicolMech Methods. 2013;23(3):161-7

41. Walczak AP1, Fokkink R, Peters R, Tromp P, Herrera Rivera ZE, Rietjens IM, Hendriksen PJ, Bouwmeester H. Behaviour of silver nanoparticles and silver ions in an in vitro human gastrointestinal digestion model. Nanotoxicology. 2013;7(7):1198-210

42. Holpuch AS, Hummel GJ, Tong M, Seghi GA, Pei P, Ma P, Mumper RJ, Mallery SR. Nanoparticles for local drug delivery to the oral mucosa: proof of principle studies. Pharm Res. 2010; 27(7):1224-36.

43. Hillyer JF, Albrecht RM J. Gastrointestinal persorption and tissue distribution of differently sized colloidal gold nanoparticles. Pharm Sci. 2001;90(12):1927-36.

44. Florence AT. Nanoparticle uptake by the oral route: Fulfilling its potential? Drug Discov Today Technol. 2005;2(1):75-81.

45. Hadrup N, Lam HR. Oral toxicity of silver ions, silver nanoparticles and colloidal silver-a review. RegulToxicolPharmacol. 2014; 68(1):1-7.

46. Gaillet S, Rouanet JM. Silver nanoparticles: Their potential toxic effects after oral exposure and underlying mechanisms - A review.Food ChemToxicol. 2014 Dec 30. pii: S0278-6915(14)00530-4. doi: 10.1016/j.fct.2014.12.019.

47. Pamela L. Drake, M.P.H., National Institute for Occupational Health and Safety; Edmund Pribitkin, M.D., Thomas Jefferson University; and Wendy Weber, N.D., Ph.D., M.P.H., NCCAM (July 2009). Colloidal Silver Products. U.S. Department of Health and Human Services.

48. "Colloidal Silver Not Approved". U.S. Food and Drug Administration. 2007-02-12. Retrieved 2008-09-22.

49. "FDA Warning Letter". U.S. Food and Drug Administration. 2001-03-13. Retrieved 2008-09-22.

50. "FDA Warning Letter". U.S. Food and Drug Administration. 2011. Retrieved 2013-04-11.

51. Bianco C, Adami G, Crosera M, Larese F, Casarin S, Castagnoli C, Stella M, Maina G. Silver percutaneous absorption after exposure to silver nanoparticles: a comparison study of three human skin graft samples used for clinical applications. Burns. 2014;40 (7):1390-6.

ALLEGATO VI

IN VITRO SILVER NANOPARTICLES PERMEATION TROUGH MENINGEAL MEMBRANE – PILOT STUDY

Mauro M, Crosera M, Bovenzi M, Adami G, Larese Filon F.

In fase di submission su: International Journal of Nanomedicine

1. Introduction:

Silver nanoparticles (AgNPs) are the main ingredient in many antibacterial sprays, which are commonly used on a wide variety of surfaces, in occupational settings and household activities. Even if their use should be regulated by European and American legislations (Federal Insecticide, Fungicide Rodenticide Act in the USA and Biocide act in the EU), many times their application is not controlled, moreover other parts of the world have no specific rules as regard their safety use. Kim and coworkers investigated some of these commercial products and found an excessive risk of inhalation exposure for some of the antibacterial spays tested, as the margin of exposure was higher than the no-risk concern level of 1000 (Kim 2015). Furthermore the use of spray containing AgNPs is even proposed and commercialized as remedy for respiratory disorders, such as asthma, which means that many patients may be exposed to considerable amounts of AgNPs through inhalation (http://thesilveredge.com/nebulize-colloidal-silver.shtml). Although Silver is a metal generally well tolerated and non-toxic for humans, there are isolated reports of neurological, kidney and liver disorders as a result of its absorption in large quantities (Brandt D et al. 2005; Stepien KM et al. 2009).

The inhalation exposure to NPs poses a well-known problem of its possible translocation trough the alveolar-capillary barrier in the respiratory system, which lead to a systemic uptake of xenobiotics, but there is also a less considered issue of a possible direct absorption via intranasal route, circumventing the very tight blood brain barrier (BBB).

The central nervous system (CNS) is an organ highly protected from penetration of xenobiotics given the presence of barrier structures, but a connection between the external environment and specific areas of the brain is achievable through the olfactory route, which goes from the nasal epithelium to the olfactory bulb.

For this feature the intranasal route has attracted considerable interest over the recent decades for drugs administration in the treatment of cognitive, neurodegenerative, psychiatric and functional disorders (Kao et al. 2000, Illum et al. 2004, Pardridge et al. 2005, Hanson et al. 2008, Patel et al, 2010, Meredith et al. 2015), and it has been demonstrated that all CNS compartments (cerebro-spinal fluid, olfactory bulb, olfactory tract, cerebrum and cerebellum) received 1.6 – 3.3 fold more of the drug when bound to NPs than when the drug is delivered in solution (Oberdorster 2009).

On the other hand this way of penetration raises a matter of concern since could leave the CNS vulnerable to neurotoxic effects of xenobiotics which may be encountered in polluted environment and in occupational sceneries (Arvidson et al. 1994, Tĭalve & Henriksson 1999, Dorman et al. 2002).

There have been described three main access routes from the nasal mucosa to the olfactory bulb (Lochhead and Thorne 2012, Mistry et al. 2009), which include an intracellular pathway, through olfactory nerve axons, a transcellular pathway, through sustentacolar cells of the olfactory epithelium and an extracellular pathway between neuronal and epithelial cells included in the mucosa.

The studies conducted on animals to investigate the olfactory route collectively show that NPs of different materials (gold, carbon and manganese NPs) (De Lorenzo 1970, Oberdorster 2004, Elder 2006) can be taken up by the olfactory and respiratory mucosa and gain access to the CNS (Oberdorster 2004). All these studies lean towards a greater likelihood of absorption through the intraneuronal pathway, since the NPs dimensions were too high to cross the tight junctions in the extracellular pathway.

We chose to investigate silver nanoparticles (AgNPs) absorption through meningeal membranes since these are the most common engineered nanoparticles in antiseptic spray on the market. Nothing is known as regards the permeability properties of meningeal membranes, which envelop the olfactory bundles inside the nasal mucosa and cover the inner part of the cranial surface, thus representing an anatomical barrier to NPs penetration both in the intracellular and in the extracellular pathway.

2. Material and methods

2.1. Chemicals

All chemicals used were of analytical grade. Sodium chloride, sodium hydrogen phosphate, potassium dihydrogen phosphate, glutaraldehyde (50% v/v), nitric acid (69% v/v), hydrochloric acid (36.5–38% v/v) were purchased from Sigma Aldrich (Milan, Italy), ammonium hydroxide (25%) from J.T. Baker (Milan Italy). Water reagent grade was produced with a Millipore purification pack sys-tem (milliQ water).The physiological solution used as receptor fluid was preparedby dissolving 2.38 g of Na_2HPO_4, 0.19 g of KH_2PO_4 and 9 g of NaCl into 1 L of milliQ water (final pH = 7.35).

2.2.1. Donor phases preparation

AgNPs, stabilized with polyvinylpirrolidone (content of silver: 25% w/w, polymer 75%), were supplied by NanoAmor Materials Inc.(Houston, TX, USA). In order to better distinguish the permeation between AgNPs and silver ions, released from the NPs, two different donor phases were prepared just before the experiments. The first donor phase, consisting of the AgNPs solution, was prepared using 200 mg (ratio metal : polymer = 1 : 4) of AgNPs dispersed by sonication in 100 ml of physiological solution to obtain a concentration of 0.50 g/L (as metal content).The nanoparticles suspension in water had a presence of 5% of silver in ionized form, determined using the ultrafiltration technique. The silver ions presence did not significantly change in 4 h. The second donor phase was prepared by the ultrafiltration of the first one to obtain only the water-soluble silver species present in the first donor phase at the moment of the experiment. Four milliliter of the AgNPs solution were ultrafiltered in centrifuge at 5000 rpm for 30 min by means of Amicon Ultra-4 centrifugal filters (10 KDa MWCO) in order to separate the AgNPs from the aqueous solution. The filtration has been repeated on five different aliquots in order to obtain an adequate solution volume to perform silver quantification analysis and permeation experiments. The five filtered aliquots were mixed for a total of 20 ml and used during the permeation experiments.

2.2.2. Ion release from AgNPs

In order to define the percentage of silver ions inside the AgNPs solution, the donor phases have been analyzed by means of Inductively Coupled Plasma–Atomic Emission Spectroscopy (ICP-AES).

2.2.3. Transmission electron microscope characterization

AgNPs dispersed in physiological solution were characterized to obtain nanoparticles size and morphology on a transmission electron microscope (EM208; Philips, Eindhoven, The Netherlands operating at 200 kV) with an high definition acquisition system based on a side-mounted TEM camera OSIS Morada and a iTEM soft-ware platform (Olympus Soft Imaging Solutions GmbH, Münster, Germany).

2.2.4. Dynamic light scattering measurements

The average values of the AgNPs size and polydispersity, defined as a relative width of the size distribution, were determined from dynamic light scattering (DLS) measurements, using a Zeta sizer Nano Z (Malvern Instruments Ltd.) analyzer applying a 633 nm laser oriented at

173◦relative to the sample. The software was optimized to report summary statistics based upon the intensity of light scattered. Four hundred microliter sample volumes from nano silver dispersion (dilution 1:5 in physiological solution) were loaded into low size disposable cuvette (supplied by manufacturer) and summary statistics were obtained using quadruplicate 3 min analysis (total analysis time = 12 min).Instrument performance was verified using a polymer reference standard known to be 60 nm.

2.2.5. Zeta potential measurement

Measurements were carried out using a ZetasizerNano ZS (Malvern). An aqueous suspension of silver nanoparticles was diluted 1:5 in a physiological solution. The zeta potential was calculated using Henry's equation.

2.3. Preparation of meningeal membranes

Thanks to the high percentage of genomic similarity, and so between the morpho-physiological features between pig and human (Kumar S et al. 2015, Amitrano et al. 2012) the pig model is commonly used in biomedical research studies and also in some cases of animal to human xenotransplantation. Porcine meninges were collected from a slaughterhouse in Trieste, IT. The membranes were excised from the animal skull immediately after the slaughter. The pigs were up to 1 year old. The head was sawed in half along the cranium caudal line, in order to achieve access to the ventral surface of the skull region. The meningeal surface adherent to the skull was detached from the underlying bone with surgical forceps. For each animal two pieces (∼5 cm diameter) of meninges (one from each side of the skull) were obtained. During the transport to laboratory the tissue was stored at 4◦C and then in freezer at −80◦C for a period of time up to, but not exceeding, 1 week. On the day of the experiments tissues were removed from the freezer and soaked in saline solution at room temperature for about 30 minutes before starting the permeation experiments. The integrity of the membranes was tested before and after each experiment by filling the chamber with water MilliQ donor and by monitoring the presence of the solution in the receiving chamber for a period of 30 minutes (Lestari 2009).

2.4. In vitro diffusion system

Meningeal permeation studies were performed using static Franz diffusion cells. The receiver compartments have a mean volume of 14.0 ml and were maintained at 37°C by means of circulation of thermostated water in the jacket surrounding the cells throughout the

experiment. This temperature value has been chosen in order to reproduce physiological conditions. The concentration of the salt in the receiver fluids was approximately the same that can be found in the blood. The solution in each cell was continuously stirred using a Teflon coated magnetic stirrer. Each excised sheet of meninge was clamped between the donor and the receptor compartment in such a way that the dura mater faced the donor compartment; the mean exposed area of the meningeal membranes was 3.29 cm^2. The experiment was performed as follows:

Exp. 1: At time 0, the exposure chambers of 3 Franz diffusion cells were filled with 1 ml of physiological solution and 0.5 ml of AgNPs suspension (75 g/cm2), in order to provide an infinite dose: the concentration in each cell has been confirmed at the end of the experiments by means of ICP-AES analysis. At selected intervals (20, 40, 60, 80, 100, 120, min) 1 ml of the receiving bathing solution was withdrawn and collected for the analysis, and immediately replaced with an equal volume of fresh made physiological solution. In order to avoid the precipitation of silver chloride (AgCl), 100 l of NH4OH 1 N was added to each sample collected. The experiment was carried out for 2 h. At the end of the experiment the meninges pieces were removed, washed abundantly with milliQ water, and subsequently stored in the freezer together with meningeal bathing solutions and the donor solutions for the following analysis.

Exp. 2: The exposure chambers of 2 Franz diffusion cells were filled with 1 ml of physiological solution and 0.5 ml of the Ag ultra-filtered solution. The other test conditions were the same of the experiment.

Blanks: For each experiment, two cells were added as blank. The blank cells were treated as the other cells with the exception that the exposure chambers were filled only with physiological solution.

2.5. Meningeal digestion after the experiment

All the meningeal exposed samples were collected and stored individually in freezer at −25°C for the following digestion and analysis. At the time of the analyzes, the membranes were dried for 2 h at room temperature, weight, and then cut into sections and put into glass tubes with 10 ml of $HNO_3$69% v/v for digestion. The obtained solutions were heated at 80°C for 8 h and then diluted to a final volume of 10 ml with milliQ water for the ICP-AES analysis.

2.6. Quantitative analysis

An Inductive Coupled Plasma Mass Spectrometer (ICP-MS 7500CE Agilent instrument with integrated autosampler) was used to determinate the total silver concentration in the receiver phases. A seven-point standard curve was used for ICP-MS measurements (0.01, 0.05, 0.1, 0.5, 1, 5 and 10 g/L, ion mass 107 u.m.a.).The limit of detection of silver was 0.005 g/L for ICP-MS and the precision of the measurements expressed as repeatability (RSD %)was always lower than 5%.The total silver concentration in the donor phases and in the solutions resulting from the skin sample mineralization were performed by Inductively Coupled Plasma-Atomic Emission Spectrometry (ICP-AES) using a Spectroflame Modula E optical plasma interface (OPI) instrument (by SPECTRO, Germany). The analysis was conducted using a calibration curve obtained by dilution (range: 0–10 mg/L) of silver ICP standard solution for ICP-AES analysis (Sigma–Aldrich, Italy). The limit of detection (LOD) at the operative wavelength of 328.068 was 0.010 mg/L. The precision of the measurements expressed as repeatability (RSD %) was always lower than 5%.All standard solutions used for calibration curves had been prepared using physiological solution and 10% of ammonium hydroxide 1 N in order to reproduce the matrix of the samples.

2.8. Data analysis

Data analysis was performed with Excel for Windows, release 2007 and Stata Software, version 11.0 (StataCorp LP, College Station, TX, USA). All data were reported as mean or median as measures of central tendency and standard deviation (SD) or quartiles as measure of dispersion. The difference among independent data was assessed by means of the Mann–Whitney test. A p value of <0.05 was considered as the limit of statistical significance.

3. Results

3.1. Characterization of AgNPs colloidal dispersion

The colloidal dispersion of AgNPs in water showed Plasmon absorption at 405 nm. Transmission electron microscopy (TEM) measurements revealed that AgNPs used in donor solution were quite uniform in size and shape and as small as 19 ± 5 nm (number of measured nanoparticles: 100). At the concentration used in the permeation experiments no aggregates have been visualized (Fig. 1).The quantitative analysis of the filtered aliquots revealed that 5%of the donor solution was ionized and a dose of 3.8 g/cm^2 of silver was applied as donor phase in exp. 2.

3.2. Ag permeation through meningeal membrane

A permeation of silver through the meninges has been demonstrated. In Figure 1 is shown the trend of concentrations of silver in the receivers phases, which is increasing as a function of time, with similar final values in cells exposed to AgNPs and to the ultrafiltered solution (0.042 ± 0.042 μg/cm^{-2}/h^{-1} and 0.045 ± 0.001 μg/cm^{-2}/h^{-1}, respectively, p> 0.005). Even the flux permeation and lag times values were similar at the second hour of experiment in cells exposed to AgNPs and in cells exposed to ultra-filtered solution (flow: 0.76 ± 0.9 ng/cm^{-2}/h^{-1} and 0.79 ± 0.0 ng/cm^{-2}/h^{-1}, respectively, lag times: 55.4 ± 13.6 min and 65.3 ± 7.1 min). The concentration of silver inside the meninges showed similar values too in both experiments (0,27 ± 0.05 g/cm^2 in the mucosa exposed to AgNPs and 0,29 ± 0:06 g/cm^2 to the ultrafiltered solution, p> 0.005), as shown in Figure 2.

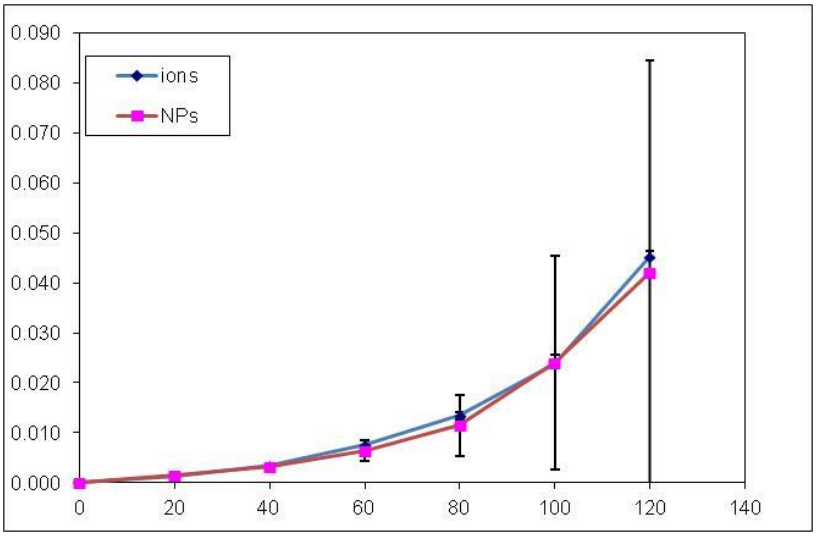

Fig 1. Silver in the receiving phases at any time tested. In cells exposed to AgNPs and to the ultrafiltered solution. Concentration expressed as μg/cm^{-2}/h^{-1}.

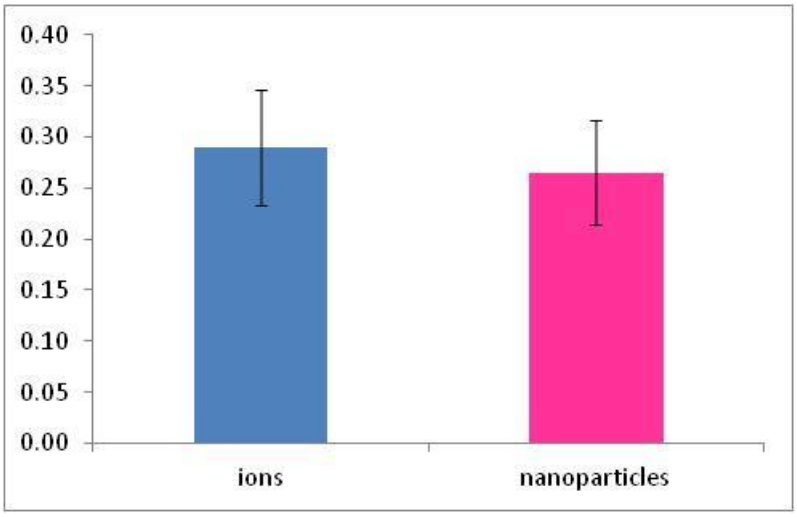

Figure 2. Concentration of silver inside the meningeal tissues, in cells exposed to AgNPs and in cells exposed to Ag ions. Data expressed as g/cm^2.

4. Discussion

The intranasal route, through the olfactory and trigeminal nerves, is commonly exploited for the administration of drugs when a quick and direct effect on the central nervous system is desirable (Pardridge 2005; Illum et al. 2004, Patel et al. 2010), while it has been less extensively investigated as potential absorption pathway for toxic substances in working scenarios. Some Authors demonstrated that after inhalation of metal fumes some substances such as manganese, cadmium and lead can be found inside the olfactory bulbs (Arvidson B 1994, Dorman DC 2002, Tjälve H and Henriksson J. 1999), but poorly is known as regard the behavior of engineered metal nanoparticles through this route. The use of these new materials is widespread and in keeps growing, due to the unique physico-chemical features that these materials gain at a nano-size range. It is well known that their high surface/volume ratio, indeed, can give rise to a greater chemical and biological interaction with biological matrixes.

Our study has investigated, in vitro, the passive permeation of AgNPs through the meninges, and the results shown that an absorption of this metal, even if minimal, is possible. We felt that it was interesting to investigate the meninges permeation characteristics, as it is commonly believed that this 3 membranes of connective tissue represent an excellent barrier against CNS penetration of xenobiotics, as them completely envelop the brain in all its folds and convolutions (Nieuwenhuys R 2010). In particular, with regard to the neuroanatomy of this specific region of the brain, the bundles of the olfactory nerve, which come out from the

lower face of the olfactory bulb and pass through the openings of the cribriform plate and the dura mater, are completely surrounded by tubular sheaths of meninges along the whole route up to the nasal olfactory mucosa (Lennart Heimer, Valentin G 1844).

We tested two solutions, one containing 19 nm Ag nanoparticles and the other containing a solution identical to the first one but ultrafiltered, which means that the nanoparticles have been removed and has remained only the dissolved silver released from NPs. Because the concentrations found transmembrane in both experiments were comparable, we believe likely that the permeation is largely attributable to the portion of the ionized metal. This is in line with the findings of other studies conducted by our group using other biological membranes, such as the skin and the oral mucosa (Larese Filon 2009, Mauro 2015).

It is necessary to consider, however, that these data derive from an in vitro study, and therefore may underrate the phenomenon as it is not taken into account any kind of active absorption. Studies conducted in vivo on animals, in fact, showed that a translocation of NPs from the olfactory mucosa to the olfactory bulb is possible for most of the nanoparticles investigated (De Lorenzo 1970-silver; Oberdorser 2004 - 36 nm graphite rods and C 30 nm NPs; Zhang, 2006 CO-polymer; Elder 2006 –Mn; Yu 2007-gold; Wang 2008 a, b - Rutile/155 nm Anatase TiO_2). In most cases, the authors leaned for a slow transport across the intraneuronal pathway within the olfactory bundles, because the size of the NPs tested, which ranged between 30-70 nm, were too large to pass through the tight junctions of the olfactory mucosa basement membrane. But in another study conducted using radioactive nanogold (Czerniawska 1970) the highest radioactivity level following injection into the nasal olfactory mucosa was found in the cerebrospinal fluid (CSF) surrounding the olfactory bulb and the corpus callosum cistern. The Authors interpreted this result as a possible proof of a direct perineural connection between the olfactory mucosa and the CSF (Orosz et al., 1957), which has been described as a very rapid translocation route from nose to brain (Illum, 2000).

Although our present study was not designed to differentiate between the different intranasal pathways, we believe that a penetration through the tight junctions of the 19 nm AgNPs is unlikely, but the finding of the Ag ions permeation through the meninges is still interesting considering the particular anatomical structure of the fila olfactoria. These neurons are isolated into fascicles, a group of which is wrapped by a single Schwann cell. This cell creates some extracellular space cavities between one neuron and the other, called Mesaxons, which work as a potential reservoir of ions (Mistry 2009, De Lorenzo 1960). This structure enables

ion exchange between the axoplasm and the extracellular fluid, leading to a potential delayed absorption of substances.

Although silver is commonly considered a metal generally well tolerated and non-toxic for humans, there is a growing evidence that both silver NPs ad dissolved silver are potential neurotoxicants and cause different effects in vivo and in vitro (Xu L 2015 a,b; Oh JH 2015). In a recent work Garcia-Reyero et al. (2015) demonstrated in vivo on fish that both $AgNO_3$ and AgNPs elicited effects in the brain of exposed animals related to oxidative stress, neurotransmitters and neurological diseases. This is confirmed also by Skalska J and coworkers (2015) who demonstrated that exposure of adult rats to both forms of silver (10nm silver nanoparticles and ionic silver) leads to ultrastructural changes in synapses, with a more severe synaptic degeneration caused by small AgNPs. The brain region more affected seems to be the hippocampus, so the observations may predict impairment of cognitive processes (Skalska J et al 2015, Bagheri-Abassi F et al. 2015).

In conclusion the results of our study provide, for the first time, an indication of the meninges permeation properties towards ions released from Ag nanoparticles, allowing us to say that this biological membrane is not completely impermeable to external agents. Even with the limitations determined by the sample size of the study, these results demonstrate that intranasal route requires further investigation, in order to clarify the characteristics of permeation through the membranes involved in this route of absorption and better protect workers and consumers who may be exposed to hazardous substances. In particular metal nanoparticles have different physicochemical characteristics, depending on their size, surface chemistry and coatings, to name a few, each of them can significantly alter NP biokinetics and their effects. So their interaction with biological barriers requires to be evaluated on a case-by-case basis. From all the aforementioned it is clear that it is necessary to spend more efforts to investigate NPs absorption through intranasal route.

References

Amitrano R, Tortora G (2012). Update: Laboratory Exercises in Anatomy and Physiology with Cat Dissections, Cengage Learning, p. 312.

Arvidson B (1994). A review of axonal transport of metals. Toxicology. 11;88 (1-3):1-14.

Bagheri-Abassi F, Alavi H, Mohammadipour A, Motejaded F, Ebrahimzadeh-Bideskan A (2015). The effect of silver nanoparticles on apoptosis and dark neuron production in rat hippocampus. Iran J Basic Med Sci. 18(7):644-8.

Brandt D et al. Argyria secondary to ingestion of homemade silver solution. J Am Acad Dermatol. 2005; 53 2 Suppl 1: S105-7;

Broadwell RD, Balin BJ. Endocytic and exocytic pathways of the neuronal secretory process and trans-synaptic transfer of wheat germ agglutininhorseradish peroxidase in vivo. J Comp Neurol. 1985; 242:632–50.

Czerniawska A. Experimental investigations on the penetration of 198Au from nasal mucous membrane into cerebrospinal fluid. Acta Otolaryng. 1970; 70:58–61. [PubMed: 5457201]

De Lorenzo AJ (1970). The olfactory neuron and the blood-brain barrier. In: Wolstenholme G, Knight J, editors. Taste and Smell in Vertebrates. Churchill, London: pp. 151–176

Dhuria SV, Hanson LR, Frey II WH. Intranasal delivery to the central nervous system: mechanisms and experimental considerations. J Pharm Sci. 2010; 99(4):1654–73.;

Dorman DC, Brenneman KA, McElveen AM, Lynch SE, Roberts KC, Wong BA (2002). Olfactory transport: a direct route of delivery of inhaled manganese phosphate to the rat brain. J Toxicol Environ Health; 65(20):1493-511.

Elder A, Gelein R, Silva V, Feikert T, Opanashuk L, Carter J, Potter R, Maynard A, Ito Y, Finkelstein J, Oberdörster G (2006). Translocation of inhaled ultrafine manganese oxide particles to the central nervous system. Environ Health Perspect. 114(8):1172-8.

Garcia-Reyero N, Kennedy AJ, Escalon BL, Habib T, Laird JG, Rawat A, Wiseman S, Hecker M, Denslow N, Steevens JA, Perkins EJ (2015). Differential effects and potential adverse outcomes of ionic silver and silver nanoparticles in vivo and in vitro. Environ Sci Technol. 48(8):4546-55. doi: 10.1021/es4042258. Epub 2014 Mar 31.

Hanson LR, Frey WH 2nd. (2008). Intranasal delivery bypasses the blood-brain barrier to target therapeutic agents to the central nervous system and treat neurodegenerative disease. BMC Neurosci. 9 Suppl 3:S5. Pardridge, 2005;

Illum L (2000). Transport of drugs from the nasal cavity to the central nervous system. Eur J Pharm Sci. 11(1):1-18.

Illum, L., 2004. Is nose-to-brain transport of drugs in man a reality? J. Pharm. Pharmacol. 56, 3–17.

Kao HD, Traboulsi A, Itoh S, Dittert L, Hussain A (2000) Enhancement of the systemic and CNS specific delivery of l-Dopa by the nasal administration of its water soluble prodrugs. Pharm. Res. 17, 978–984.

Kim E, Lee JH, Kim JK, Lee GH, Ahn K, Park JD, Yu IJ. Case Study on Risk Evaluation of Silver Nanoparticle Exposure from Antibacterial Sprays Containing Silver Nanoparticles. Journal of Nanomaterials Volume 2015, Article ID 346586, 8 pages http://dx.doi.org/10.1155/2015/346586

Kumar SR, Meredith G, Larson et al. Analyses of pig genomes Shops provide insight into porcine demography and evolution. Nature, vol. 1491 Nov. 15, 2012, p. 393-398, doi: 10.1038 / nature11622.

Larese FF, D'Agostin F, Crosera M, Adami G, Renzi N, Bovenzi M, Maina G (2008). Human skin penetration of silver nanoparticles through intact and damaged skin. Toxicology. 8;255(1-2):33-7.

Lennart Heimer. The human brain and spinal cord. Functional neuroanathomy and dissection guide. Springer Verlag. New York, Heidelberg, Berlin, p 288, Textbook of anatomy, head, neck and brain, second edition, Vishram Singh. Elsevier. Pag 332-333.

Lochhead JJ, Thorne RG (2012). Intranasal delivery of biologics to the central nervous system. Adv Drug Deliv Rev. 15;64(7):614-28.

Mauro M, Crosera M, Bianco C, Bellomo F, Bovenzi M, Adami G, Filon FL (2015). In vitro permeability of silver nanoparticles through porcine oromucosal membrane. Colloids Surf B Biointerfaces. 132:10-6.

Meredith ME, Salameh TS, Banks WA (2015) Intranasal Delivery of Proteins and Peptides in the Treatment of Neurodegenerative Diseases. 17(4):780-7.

Mistry A, Stolnik S, Illum L (2009). Nanoparticles for direct nose-to-brain delivery of drugs. Int J Pharm. 8;379(1):146-57.

Nieuwenhuys R, Voogd J, van Huijzen C. "The central nervous system", Springer-Verlag Italy, 2010, p 97.

Oberdörster G, Sharp Z, Atudorei V, Elder A, Gelein R, Kreyling W, Cox C (2004). Translocation of inhaled ultrafine particles to the brain. Inhal Toxicol. 16(6-7):437-45.

Oberdörster G, Elder A, Rinderknecht A (2009). Nanoparticles and the brain: cause for concern? J Nanosci Nanotechnol. 9(8):4996-5007.

Oh JH, Son MY, Choi MS, Kim S, Choi AY, Lee HA, Kim KS, Kim J, Song CW, Yoon S (2015). Integrative analysis of genes and miRNA alterations in human embryonic stem cells-derived neural cells after exposure to silver nanoparticles. Toxicol Appl Pharmacol. pii: S0041-008X(15)30131-9. doi: 10.1016/j.taap.2015.11.004. [Epub ahead of print]

Orosz A, Foldes I, Kosa C, Toth G (1957). Radioactive isotope studies of the connection between the lymph circulation of the nasal mucosa, the cranial cavity and cerebrospinal fluid. Acta Physiol Hung. 11(1):75-81.

Pardridge WM (2005).The blood-brain barrier and neurotherapeutics. NeuroRx. 2(1):1-2.

Patel D, Naik S, Chuttani K, Mathur R, Mishra AK, Misra A (2010) Intranasal delivery of cyclobenzaprine hydrochloride-loaded thiolated chitosan nanoparticles for pain relief. J Drug Target. 21(8):759-69.

Skalska J, Frontczak-Baniewicz M, Strużyńska L (2015). Synaptic degeneration in rat brain after prolonged oral exposure to silver nanoparticles. Neurotoxicology. 46:145-54. doi: 10.1016/j.neuro.2014.11.002.

Stepien KM et al., Unintentional silver intoxication following self-medication: an unusual case of corticobasal degeneration. Ann Clin Biochem. 2009; 46 (Pt 6):520-2)

Thorne RG, Emory CR, Ala TA, Frey II WH. Quantitative analysis of the olfactory pathway for drug delivery to the brain. Brain Res. 1995; 692(1–2):278–82

Thorne RG, Frey II WH. Delivery of neurotrophic factors to the central nervous system: pharmacokinetic considerations. Clin Pharmacokinet. 2001; 40(12):907–46

Tĭalve H and Henriksson J (1999). Uptake of metals in the brain via olfactory pathways. NeuroToxicity 20(2–3):181–196.

Valentin G (1844). Treaty of Neurology. First Italian translation by MG Dr. Levi Medical. Venice. G. Antonelli Ed. 1844, p. 220-228

Wang J, Chen C, Liu Y, Jiao F, Li W, Lao F, et al. Potential neurological lesion after nasal instillation of TiO2 nanoparticles in the anatase and rutile crystal phases. Toxicol. Letter. 2008b; 183(1-3):72–80.

Wang J, Liu Y, Jiao F, Lao F, Li W, Gu Y, et al. Time-dependent translocation and potential impairment on central nervous system by intranasally instilled TiO2 nanoparticles. Toxicology. 2008a; 254(1-2):82–90. [PubMed: 18929619]

Xu L 2015 (a) Silver nanoparticles induce tight junction disruption and astrocyte neurotoxicity in a rat blood-brain barrier primary triple coculture model

Xu L (b) , Shao A, Zhao Y, Wang Z, Zhang C, Sun Y, Deng J, Chou LL. Neurotoxicity of Silver Nanoparticles in Rat Brain After Intragastric Exposure. J Nanosci Nanotechnol. 2015 Jun;15(6):4215-23.

Yu LE, Yung L-YL, Ong C-N, Tan Y-L, Balasubramaniam KS, Hartono D, Shui G, Wenk MR, Ong W-Y. Translocation and effects of gold nanoparticles after inhalation exposure in rats. Nantoxicology. 2007; 1:235–242.

Zhang Q, Zha L, Zhang Y, Jiang W, Lu W, Shi Z, Jiang X, Fu S. The brain targeting efficiency following nasally applied MPEG-PLA nanoparticles in rats. J. Drug Targeting. 2006; 14:281–290.

ALLEGATO VII

NANOPARTICLES SKIN ABSORPTION: NEW ASPECTS FOR A SAFETY PROFILE EVALUATION

Larese Filon F, Mauro M, Adami G, Bovenzi M, Crosera M.

Pubblicato su: Regulatory Toxicology and Pharmacology, 2015 Jul;72(2):310-22.

Abstract

NanoParticles (NPs) skin absorption is a wide issue, which needs to be better understood. The attempt of this review is to summarize the scientific evidence concerning open questions, i.e.: the role of NPs intrinsic characteristics (size, shape, charge, surface properties), the penetration of NPs through the intact or impaired skin barrier, the penetration pathways which should be considered and the role of NPs interaction in physiological media. The outcomes suggest that one main difference should be made between metal and non-metal NPs. Both kinds have a secondary NPs size which is given after interaction in physiological media, and allows a size-dependent skin penetration: NPs ≤ 4 nm can penetrate and permeate intact skin, NPs size between 4-20 nm can potentially permeate intact and damaged skin, NPs size between 21-45 nm can penetrate and permeate only damaged skin, NPs size > 45 nm cannot penetrate nor permeate the skin. Other aspects play an important role, mostly for metal NPs, i.e. dissolution in physiological media, which can cause local and systemic effects, the sensitizing or toxic potential and the tendency to create aggregates. This paper suggests a decision tree to evaluate the potential risk for consumers and workers exposed to NPs.

1. Introduction

One of the main functions of the skin is to act as a barrier, allowing body protection from external substances, but it is also well known that many compounds are capable to penetrate and permeate this barrier and, in some cases, even cause local effects, such as irritation or sensitization phenomena, or also translocate into blood vessels reaching systemic circulation.

A lot of chemicals can come in contact with the skin, either in their bulk form or in a nanosize range (nanoparticles [NPs], 1-100 nm of diameter, British Standards Institution [BSI]), and there are already many applications of various NPs in dermatology, such as photoprotection, phototermal and photodynamic therapy, hair disorders treatment, and also in gene therapy, vaccination and nanodiagnostics [1].

The interaction of NPs with the skin is still a matter of investigation by researchers, since it has been demonstrated that some NPs can penetrate the outer stratum corneum layer of the skin, while others can permeate into the deeper dermal layer, reaching the systemic circulation.

The aim of our paper was to evaluate the available data on NPs skin penetration and permeation in order to suggest a decision tree that could assist researchers, workers and consumers in the risk evaluation, taking into consideration relevant aspects related to the skin contact with NPs.

Nowadays there is a wide debate in the scientific community to define which are the ways of NPs interaction with the skin and eventually cause health problems. Despite reviews summarized literature on this topic [1-6] there is still the need to have a useful guide which can support researchers and workers to predict a possible risk related to NPs skin exposure.

2. Skin functions

As one of the bigger organs of the human body, the skin fulfills many different functions: it acts as the first barrier to xenobiotics, it prevents dehydration and allows the metabolism of several compounds. Skin also plays an important role in the temperature regulation and in the immunological response. This latter function is ensured by Langerhans cells, which are able to process antigens and give rise to the inflammatory response to external insults.

Skin does also play a role in the biosynthesis of constitutive substances, such as keratin, collagen, melanin, lipids and carbohydrates; it allows neurosensory function by means of resident receptors for heat, touch and pain.

Skin holds sebaceous, apocrine and eccrine sweat glands. The first ones secrete sebum, which is a mixture of lipids that acts as antibacterial agent, while the second ones produce a secretion that contains scent used in the mark of the territory.

The skin barrier is composed of two layers: the epidermis and the dermis. The epidermis is made of a stratified squamous keratinized epithelium, which consists of two kinds of primary cells: the keratinocytes and the nonkeratinocytes. The former cells are stratified in different layers (stratum basale, stratum spinosum, stratum granulosum, stratum lucidum, and stratum corneum) while the second own protection functions (against UV-light damage) and immunological functions (melanocytes, Merkel cells and Langerhans cells). The outermost layer is the stratum corneum, which acts as the first barrier to external agents; it modulates chemicals, drugs and particles absorption into the deeper skin layers [7-8]. Its thickness can vary depending on the body regions (thicker in the palm and sole, thinner in scrotum and body flexures). Each cell of the stratum corneum has approximately a diameter of 30 μm and a thickness that ranges from 0.5 to 0.8μm [9].

The lipids within the stratum corneum derive from lamellar granules of the stratum spinosum [10], are arranged into lamellar sheets and consist of ceramides, cholesterol, fatty acids, and small amounts of cholesterol esters, as well as hydrolytic enzymes such as acid phosphates, proteases, lipases, and glycosidases. Each corneocyte is embedded in the lipid matrix produced by the lamellar granules in a brick and mortar structure proposed by various authors [11-12].

3. Skin absorption of chemicals

Chemicals may be absorbed through skin by different pathways [13-14], which are:

1. the intercellular route, with partitioning into the lipid matrix,
2. the intracellular route,
3. through sweat glands,
4. through hair follicles [15].

As regard the last one there is evidence that the hair follicle (HF) can act as a shunt increasing the penetration and absorption of topically applied substances [16-18] and NPs [19]. HF

canal can be considered as a significant reservoir for penetrated chemicals and NPs too, since substances stored there can continuously diffuse to the surrounding spaces, cross the capillary walls and even reach the blood system [20].

Skin exposure to irritant compounds may cause a disruption of the stratum corneum either by means of protein denaturation agents, such as detergents, or through lipids extraction from stratum corneum by means of solvent agents[21-22, 8], whose mechanisms increase both irritation effects and damage to the skin.

Skin diseases, such as irritant contact dermatitis, can increase the risk of haptens penetration, leading to a possible sensitization. It is also well known that permeability increases in atopic eczema, a disease characterized by an epidermal barrier dysfunction [23].

Moreover, other factors such as gender, differences in skin thickness, hair follicle density, blood flow, age, mechanical flexions [24-26], and systemic diseases, may all influence the skin barrier function [27-28].

4. Nanoparticles skin absorption

NPs skin absorption is an issue which the scientific community has been addressing, since the hazard of a transdermal flux of nanomaterials opens a debate on toxicological, therapeutic and drug delivery questions that have still to be defined [29-30].

One of the first topics that should be clarified is the mechanism of NPs penetration through the outermost rate-limiting barrier of the stratum corneum. Some authors hypothesized that NPs may be hold in the lipid matrix of the skin [26, 31] or in skin annexes [19] and subsequently can be slowly released into the deeper dermal layer. Concerning this theory, some characteristics such as NPs size, shape, charge, surface properties have to be further investigated to better understand which of them, and eventually in which degree, can affect skin penetration.

It is not satisfactory to sort NPs permeation properties only on the basis of intrinsic parameters, such as NPs dimension, composition or surface chemistry, since NPs characteristics may change completely when they interact with physiological media. Background factors, vehicle, density, temperature etc., may determine NPs aggregation and agglomeration, reaching non nano-size dimensions and perhaps changing surface charge.

Figure 1 shows the absorption pathways that should be considered in the evaluation of NPs skin permeation, while the following is a non-exhaustive list of NPs characteristics and for each of them the scientific evidence is reported:

4.1 NPs primary size:

Among the intrinsic parameters size, doubtless, is considered a critical factor. Recently Watkinson and colleagues [30], assuming that NPs behave like large molecules, tried to estimate their rate of penetration using a diffusion theory. They concluded that only NPs below 1 nm are able to permeate the intact skin. On the other hand many experimental data proved that even bigger size NPs can cross the skin barrier [32-33], even if smaller size NPs

can pass thought the skin more than the bigger ones. Sonavane and colleagues [34], reported a higher permeation through rat skin of AuNP with a diameter of 15 nm compared to the ones of 102 nm. Rancan and coworkers [19] showed that only silica NPs smaller than 42 nm can penetrate the skin through hair follicles and be internalized mostly by Langherans cells and even by keratinocytes in a damaged skin model. Bigger NPs did not reach hair follicles. In this study the authors did not find any effect of surface functionalization. Gopee and colleagues [35] demonstrated that quantum dots (QDs) of 37 nm can permeate only hairless mouse skin and Chu and colleagues [36] demonstrated that smaller QDs (4 nm) can penetrate also intact skin.

4.2 NPs in physiological media:

NPs penetration properties have to be evaluated in physiological solution or in synthetic sweat to reproduce what occurs in in-vivo conditions. The NPs characteristics (shape, size, surface charge, z potential) and the tendency to aggregate are crucial elements to define the interactions with human skin surface. It can be summarized that NPs tend to aggregate spontaneously alone or immediately after the contact with physiological media [19]. Bennet and colleagues [37] demonstrate that penetration of nanoparticles into and through the entire dermal profile of porcine skin in vitro is higher when a solution of TiO2NPs, previously disaggregated by photo induction, is used. If metal absorption occur, another prominent aspect is understand whether it is due to NPs permeation, to the permeation of their soluble fraction (e.g. metal ions) or if it is due to both mechanisms and which is the NPs/soluble fraction ratio.

4.3 Surface charge, Z potential

The surface charge can influence NPs permeation and penetration, but its role is not clear and has to be evaluated case by case. For some NPs, such as QD [38-39], there is evidence that surface charge as well as pH could influence NPs penetration.

Some authors [19, 40] found that positive charge on particle surface enhance their electrostatic interaction with the cell membrane and favors their internalization, while the diffusion of negative charged NPs seem to be slowed in the matrix by the electrostatic interactions with positively charged liposomal component [41-42].

4.4 Ions release (dissolution)

Ion release is a crucial point, because metal NPs can release a greater amount of ions compared to bulk material, due to their high surface/mass ratio. Furthermore some NPs can reach the hair follicles and from there work as a long lasting reservoir for ions release [15, 17]. A prolonged ions release could increase the risk of allergic contact dermatitis for NPs containing sensitizing metals, such as Nickel (Ni), Palladium (Pd) and Cobalt (Co).

4.5 Impurities

In the production process of NPs, impurities can be present (metals, toxic chemicals) and may have specific effects [43]. The presence of metals (Ni, Cr, Fe) into carbon nanotubes i.e. can influence their biological oxidative damage with effects influenced by the metal release into

the medium. That aspect can be less relevant when studying in vivo skin absorption but can play an important role on in-vitro cytotoxicity studies. Altunbek and colleagues demonstrated that after removal of organic impurities from ZnO NPs through H2O2 treatment an increase in the agglomeration of the NPs was observed [44].

4.6 Skin conditions

A damaged skin barrier allows a penetration and permeation of NPs or can increase their absorption. This is a relevant matter in working scenarios, because there is a wide percentage of workers with impaired skin function in many professions [45-47].

5. NPs local effects on the skin

5.1 Mechanical action

In 2007 Rouse reported that mechanical flexion (lasting up to 60 or 90 min) can increase skin penetration of small Fullerene NPs (3.5 nm) functionalized with a fluorescent tag, which can be found in the intercellular spaces of porcine skin stratum granulosum [25].

On the contrary, Zhang and colleagues proved that small Quantum Dots (QD) (QD655-COOH of 18 nm and QD565-COOH of 14 nm) applied on rat skin, which subsequently was flexed for a 60 minutes period, did not penetrate the skin at 8 and at 24 h after application [31].

5.2 Irritation

Mechanical friction on the skin exposed to some NPs can cause skin irritation. This was demonstrated in workers exposed to carbon fibers by Eedy, who reported skin onset of irritant contact dermatitis [48], and by Ema and colleagues, who reported same irritant effects using fullerene C60 NPs [49]. On the contrary, no dermal irritation was demonstrated in guinea pigs exposed to carbon nanotubes [50].

5.3 Sensitization

The NPs that can penetrate the epidermal layer may cause allergic reactions, due to the release of substances with notorious sensitizing potential, such as metals (e.g. nickel, cobalt, palladium), which can induce an allergic contact dermatitis or respiratory symptoms. Journeay and colleagues reported in 2014 a case of throat irritation, nasal congestion, facial flushing and skin reaction in a chemist exposed to nickel NPs [51].

Nowadays no data are available on NPs allergenic potential, even if it is well known that NPs may cause a high amount of ion's release, due to their wide surface area, and therefore may have a stronger sensitization potential. It is conceivable that metallic NPs containing cobalt, nickel or chromium could trigger allergic responses, while NPs containing gold or silver, which are known as non-allergenic substances, should not induce allergic phenomena.

On the contrary, it is noteworthy that fullerenes have been suggested to play a leading role in the prevention of the in-vitro and in-vivo IgE mediated allergic responses, by inhibiting

histamine release or by reducing nickel uptake after dermal application of creamy formulations [52].

6. Specific nanoparticles data

6.1 Carbon based nanomaterials

Carbon nanotubes (CNTs) are molecules composed entirely of carbon, which have cylindrical nanostructure. Them are quite large and cannot penetrate through the skin. Degim and colleagues investigated the application as permeation enhancers of 2-100 nm multi walled CNTs (MWCNT). Fluorescent microscopy analysis found MWCNTs only on the skin surface and not in the deeper layers [53].

Fullerenes are also molecules composed entirely of carbon but may have spherical, ellipsoid or tube-like structure. Fullerenes are smaller in size and their penetration through skin has been evaluated in Yorkshire weanling pigs: no penetration was revealed after application of fullerenes in mineral oil, while C60 (~ 1 nm) was detected in the stratum corneum when applied with solvents such as toluene, cyclohexane and, more than others, chloroform [54]. Rouse and colleagues evaluated Fullerenes penetration through flexed and unflexed porcine skin in vitro. Confocal microscopy confirmed dermal penetration in the flexed skin at 8 h, but no dermal penetration in unflexed skin was observed after 24 h [25].

Kato and colleagues dissolved fullerene-60 in a lipophilic squalene vehicle and applied three different doses on human skin for a 24 h period. Tissues were extracted with chloroform and analysed by high-performance liquid chromatography and Fullerene-60 was detected in the epidermis but not in the dermis [55].

6.2 Quantum dots (QDs)

QDs are nanocrystals made of semiconductor materials, usually composed of a CdSe core covered by a ZnS shell. They are characterized by fluorescence properties which allow to track them inside the skin. There are conflicting results in literature, but small QDs can penetrate the skin using a massage technique. Tang and coworkers demonstrated penetration and permeation of QDs through rat skin, since Cd was found inside liver and kidney after skin exposure, raising concern on QDs systemic toxicity [56]. Wang and colleagues demonstrated QDs penetration into the skin only after 8 hour skin exposure but not after 24 hours [57]. It is possible to summarize that QDs can permeate the skin, mostly when it is damaged or pretreated with UVB light, and that Cd can diffuse in internal organs. Size, pH, temperature and coating can influence this absorption profile. In table 1 QDs skin penetration studies results are reported.

6.3 Polystyrene nanoparticles

Polystyrene NPs are used in industrial application, in varnishes and in surface treatments. Alvarez-Roman and colleagues demonstrated that polystyrene NPs (diameters 20 and 200 nm) accumulated preferentially in the follicular openings of porcine skin, and that this localization was greater for smaller size particles [58]. Non-follicular structures did not offer an alternative penetration pathway for the polymer vectors, whose transport was clearly impeded

by the stratum corneum. Vogt and colleagues demonstrated that polystyrene NPs (40 nm) can translocate to the viable epidermis in damaged skin [59]. The study was conducted using human skin explants pretreated with cyanoacrylate skin surface stripping, which induces mild barrier disruption and open hair follicles orifices for shunt penetration. No penetration was detected using bigger size NPs.

Mahe and colleagues demonstrated in vivo that solid fluorescent 40 and 200 nm polystyrene nanoparticles (NPs) penetrated along the follicular duct of murine skin and diffuse into the perifollicular tissue, where them are taken up by epidermal and dermal DCs [60].

Wu and colleagues investigated on excised porcine skin in vitro three functionalized 100 nm NPs: cationic-amino (PS-NH3+), anionic-carboxyl (PS-CO2–) and anionic-poli-L lactide (PLL–). The cationic nanoparticles showed clear affinity for the negatively charged skin surface and were found in great amount into the SC. No penetration beyond the superficial SC was demonstrated for all of them [61].

Campbell and colleagues found penetration of 20-200 nm NPs only in depth of 2-3 μm of the stratum corneum, and the results were interpreted as infiltration along fissures in the stratum disjunctum [62].

6.4 Silica nanoparticles

Silica NPs are used as additives and fillers, inside foods, cosmetics, paints and are also investigated as drug carriers. Rancan and colleagues demonstrated that 42 nm silica NPs, applied on human skin explants, with a partially disrupted stratum corneum, were localized in hair follicles and can be internalized by epidermal and dendritic cells [19]. Bigger size NPs (75 nm and more) cannot penetrate the skin. Hirai and colleagues showed by TEM analysis that amorphous nanosilica particles (NSPs) with a diameter of 70 nm, applied for three days on mice in vivo, can penetrate the skin barrier, are transported to the lymph nodes, and potentially can be dispersed throughout the body via the lymphatic transport system [63]. However they did not perform further elemental analyses (including e.g. EDX or electron energy-loss spectroscopy) to assess the nature of the NPs visualized by TEM.

Staronovà and colleagues demonstrated in vitro that 25 nm silica NPs (103 nm hydrodynamic diameter) penetrated, but did not permeate through human skin [64]. Confocal images showed the presence of fluorescent SiO2 NPs in depths up to 160 μm, but the presence of the natural and narrow ridges in the skin may cause NPs presence on the surface of the SC or in the upper epidermis to show up on images at lower depths. So the observation of NPs below 100 μm requires confirmation with more exact measurement of the penetration depths and identification of specific skin strata.

Ostrowski and colleagues demonstrate in vivo that skin penetration of 55 ± 6 nm diameter (111 nm hydrodynamic diameter in ultrapure water) functionalized SiNPs (SiO2-NP AHAPS-SiO2-NP) was not observed after one or five consecutive days of topical application [65]. Penetration of AHAPS-SiO2-NP through the skin was not observed through intact nor damaged mice skin (tape stripped or showing allergic contact dermatitis). In conclusion, AHAPS-SiO2-NPs seem to not cross the normal or perturbed mouse skin.

6.5 Metal oxides

The use of TiO2 and ZnO NPSs inside skincare products is extremely common and the Australian Therapeutic Goods Administration estimated that in 2005 the 70% of all sunscreens containing TiO2 and the 30% of those containing ZnO were formulated with NPs [66]. Sunscreens use is highly recommended in order to prevent sunburn, skin cancer, photo aging and skin wrinkles. Sunscreens containing NPs may be more transparent resulting aesthetically more acceptable for the consumers.

Titanium dioxide skin penetration and its effects have been extensively studied, due to the wide use in sunscreens (table n. 2). The majority of studies did not report any penetration or permeation both in-vitro and in in-vivo studies on animals and on humans. Overall, it may be concluded that TiO2 NPs are localized only in the outer layer of the stratum corneum also when damaged or irradiated skin protocol was used. In a long-period NPs skin application protocol (56 days) Adachi and colleagues did not find any penetration of these NPs too [67]. Contrary to these results, Wu and colleagues demonstrated TiO2 nanoparticles not only in the stratum corneum but also in the viable epidermis using TEM analysis on pig ears after an exposure period of 30 days [61]. They did not, however, execute elemental analyses on the observed substances as Adachi and colleagues did. Jonaitis and colleagues pointed out that the observed significant increases in the titanium content in the liver, spleen, skin, subcutaneous muscle and other organs could be due to an oral contamination, which can definitely confound the results [68].

In an in vivo experiment on humans, Gulson and colleagues found Zn traces in the blood and urine of volunteers after 5 days of application of sunscreens containing ZnO NPs [69]. The detection method used was highly sensitive, but it is not known whether 68Zn was absorbed as ZnO or as soluble Zn. The Authors stated that Zn found in urine could be the result of ZnO released from Zn, but it can be hypothesized, in this case too, that even hand-mouth contamination could play a role.

Recently in vitro and in vivo studies were conducted with ZnO NPs applied on UVB damaged porcine skin, using four different sunscreen formulations. Results demonstrated that ZnO remained on the skin surface and did not enter into the viable epidermis [8].

Very few data are available on others metal oxides. A pilot study on Co3O4 NPs demonstrate that them are also very stable and do not enter deeply inside the skin, even when a damaged skin protocol is used [70].

Summarizing published data metal oxides NPs are generally very stable, do not release metal ions and can be considered as having low risk of skin penetration or permeation, which is possible only for those sized <10 nm (Table n. 3).

6.6 Gold nanoparticles

In vitro skin permeation of AuNPs was first studied by Sonavane in 2008 using rat skin samples applied on Franz static diffusion cells [34]. Three AuNPs sizes were tested (15 nm, 102 nm and 198 nm). AuNPs showed size-dependent permeation through the skin and Larese

and colleagues, using the same experimental method, confirmed that AuNPs of 12.6 nm can permeate, in a dose-dependent manner, also through intact and damaged human skin [71]. Gold concentration assessment into the skin revealed that it decreased from the superficial to deeper skin layers, and that the amount of metal found in damaged skin was significantly higher compared to the ratio in intact skin. The evaluation of abraded skin showed an increase of gold concentration only inside the skin but not in the receiving solution, therefore no flux permeation enhancement was demonstrated through damaged skin. This may be due to a strong interaction between AuNPs and skin cells or extracellular matrix, which might hinder the particle migration, or even to the short period of NPs skin application (24 h). Other authors reported data on AuNPs skin permeation, showing conflicting results. Some studies confirmed that smaller AuNPs can penetrate and even permeate the skin barrier, while other reports concluded that it is possible to observe penetration or permeation of the metal only through damaged skin. Lee and colleagues found a greater skin penetration for anionic AuNPs, which could potentially be mediated by interactions of the particles with negatively charged skin [41]. These findings are summarized in table 4.

6.7 Silver nanoparticles

AgNPs are widely used in many consumer products such as surgical and handling tools, food, clothing, cosmetics, contact lens cases, disinfectants and wound dressing. Skin exposure to AgNPS is highly due to their increasing inclusion into textiles, burn creams, jewelry, acupuncture needles, wound dressing and catheters. The Ag ions released from textiles and wound dressings can interact with the skin and penetrate it. Wijnhoven and colleagues evaluated silver release from wound dressings and the in vivo absorption of the metal, demonstrating an intoxication phenomena called “argyria” in the exposed people (as a result of Ag deposition on the basal lamina of the skin) and elevated serum and liver enzymes levels [72]. However Ag absorption through intact skin is low, since the majority of free Ag ions precipitated as Ag sulfide or chloride on the superficial layers of the stratum corneum of the skin.

Larese and coworkers demonstrated in vitro skin penetration of AgNPs of 25 nm, through intact and damaged human skin, using static diffusion cells [73]. TEM (Transmission Electron Microscopy) investigations confirmed the presence of AgNPs into the stratum corneum and the outermost surface of the epidermis but not inside the dermal layer. These results suggest that a fraction of the NPs were dissolved and diffused through the skin layers as elemental Ag. Bianco and colleagues confirmed that smaller AgNPs (19 nm) can penetrate and permeate fresh, cryopreserved and glycerolized human skin with higher amount for the third kind of skin, which is commonly used for burns treatment [74]. Published data are reported in table 5.

6.8 Other metals

Data of Co, Pt, Rh NPs skin penetration and permeation are reported in table n. 6, where a comparison with results obtained from silver and gold NPs is done.

Baroli and colleagues tested FeNPs (size: 6 nm) finding that they can penetrate into epidermis but cannot reach the dermal layer (results not shown) [2].

7. Comparison between nanoparticles and the bulk material counterpart

An important issue, which still has to be addressed, is to understand whether material in a nano size scale can penetrate the skin in a more efficient way and can have different toxicological effects compared to the homologous bulk materials.

Gulson and colleagues, Sadrieh and colleagues and Larese and colleagues performed studies to try to clarify this issue [68, 75-76]. Larese and co-workers used CoNPs and Co powder, and results showed that cobalt concentration inside intact and damaged skin and even cobalt permeation was higher when CoNPs were used, taking into account the differences in cobalt content between the donor solutions (Co powders and CoNPs). This result confirms that Co applied as NPs can permeate the skin in higher amount compared to bulk material.

8. Overall evaluation

Table 7 summarizes results taking in consideration type of NPs, critical size reported in studies, hazard, penetration, permeation and possible mechanism involved. For metal oxides the majority of studies did not demonstrated skin absorption and a critical size cannot be suggested. There is in vivo evidence of ZnO NPs skin absorption on volunteers but however this hazard can be considered very low [77]. FeO NPs can penetrate the skin but the hazard is negligible, considering available knowledge.

For gold the penetration and permeation was demonstrated when NPs size is around 12 nm. Bigger NPs failed to pass through the skin. Au is not a toxic metal and has been suggested as a carrier for drug delivery also through skin application. Silver NPs can pass through the skin probably in the form of ions, but its low toxicity is well known. Ag is a valid antiseptic agent and can be dangerous only when impaired skin undergoes a prolonged exposure to very high metal concentration [73].

Quantum dots can penetrate and permeate the skin when they are smaller than 12 nm and Cd can be found in internal organs. This can be dangerous because Cd is a toxic metal, which can cause kidney failure and lung cancer (for inhalation exposure). Exposure to Quantum dots must be controlled and evaluated for producers, researcher and consumers safety, due to the high risk related to Cd content.

Silica NPs can penetrate only the impaired skin barrier when their size is smaller than 42 nm, but the pathway and the mechanism of the release are not known yet.

NPs constituted of sensitizing metals such as Ni, Co, Pd can penetrate and permeate the skin but it is not clear if the permeation occur as ions or as NPs. Available data confirms an increased risk of sensitization in people exposed to nickel [77].

NPs constituted of very stable metals (Pt and Rh) can penetrate the skin only when this barrier is damaged and when NPs dimensions are very small (5 nm). Therefore these metals can be considered not toxic considering available knowledge.

9. Discussion and conclusions

On the basis of the available data it may be concluded that for some types of NPs both penetration and permeation through the skin have been shown, but for many NPs it is still uncertain.

Figure n. 1 summarized the available knowledge to understand how and in which way NPs can pass through the skin.

NPs intrinsic characteristics are crucial to define their capability to pass through the skin, and have to be evaluated in physiological solution and/or in synthetic sweat because size, charge, z-potential and shape are all parameters which can change dramatically when dried NPs are applied on the wet skin surface.

Even if the particle size is not the only parameter to take into account, it should be considered as a major determinant for the penetration of particles across the SC [2, 19]. Furthermore the role of zeta potential and charge is unclear in skin absorption while can be relevant in NPs interaction with cells in culture.

The second crucial aspect is the nature of NPs: metal and non-metal NPs behave in a different manner. Metal based NPs can easily release ions, as it has been demonstrate e.g. for silver, nickel and cobalt. This results in a high metal permeation through the skin, which however is probably due to soluble form more than NPs translocation.

Besides the penetration through the outermost rate-limiting barrier of the intact stratum corneum is the greater hindrance for NPs penetration, it has always to be considered that this layer could be impaired or disrupted and even that the transappendageal pathway can create a shunt for penetration of small NPs (diameter smaller than ~ 45 nm). NPs stored into hair follicles can be hence internalized by epidermal cells or mast cells and can activate the immune system. This is mostly important for metal NPs which can induce allergic reactions (for sensitizing metals) but it has been demonstrated for silica NPs [19] on impaired skin too.

Moreover ex vivo skin tests using Franz cells and similar techniques permit to obtain important information on penetration pathways, which can bridge experimental scenarios to the one which are commonly observed in occupational scenarios. This technique is widely used to study drug skin penetration [79] and allows to test products that can or cannot permeate the skin in a simple way. Its use to understand skin permeation of toxic chemicals enable researchers to define a joint protocol which can be useful as well to study NPs skin absorption. It is known that Franz cells technique evaluates, at least, passive diffusion and that it can underestimate what happens in real condition, where active diffusion can occur, but it is a reliable model to study skin diffusion and obtain valuable data such as flux and lag time permeation of the tested substance. One limitation of this technique could be the hyperhydration of the skin when experiments run up to 24 hours, but this issue has a relative importance, since in real condition skin permeation could be commonly increased when superficial impairment or skin flexion happened as well as for active transportation (probably more relevant for chemicals than for NPs). There are three main aspects that we strongly

suggest to consider in the evaluation of NPs safety profile summarizing the above mentioned aspects:

1. Size in physiological media:

the available data show that NPs ≤ 4 nm generally can penetrate and permeate the intact skin; NPs sized 4-20 nm can potentially permeate the intact and the damaged skin; NPs sized 21-45 nm can penetrate and permeate only damaged skin; NPs sized >45 nm cannot penetrate nor permeate the skin.

2. The hazard of NPs (see table n. 7):

a) TiO2 and ZnO NPSs cannot pass through the skin and exert pathological effects. As already known, they can be considered safe as regard skin absorption route;

b) AgNPs can penetrate and permeate the skin and their use inside wound dressing, when a large skin surface area is covered, or inside engineered textile, can cause a high silver skin absorption. This, exceptionally, may cause effects on internal organs;

c) AuNPs can penetrate the skin but there are conflicting results on their permeation potential. However Au is a noble metal, which is not toxic for human health;

d) NPs composed of sensitizing metals (Ni, Co, Pd) can be more hazardous for human health due to the high ions release and their localization into the hair follicles with a "reservoir effect".

3. The release of toxic metals in physiological condition (dissolution):

QDs can release Cd, metal NPs can effectively release metals ions leading to possible local or systemic effects.

Last but not least skin flexion and/or skin impairment of the outermost stratum corneum can influence NPs skin penetration and permeation. As a consequence in vitro data are very useful in order to simulate such conditions, which are very common in occupational exposure scenarios.

Skin contact with NPs can cause local or systemic effects. There are many different NPs and skin hazard must be evaluate taking into account their characteristics (size, composition, metal released, etc.) in real working condition as well as the area of exposure and the condition of the skin (flexed areas and/or damaged skin). Skin contamination must be avoided using personal protective equipment and workers must be informed that NPs, due to their small size, are able to penetrate into the skin and to be stored inside skin annexes, more in damaged or flexed areas. In nanotechnology industry as well as in research laboratories there is the need to improve the knowledge on the specific hazard related to NPs exposures for inhalation and for skin absorption, because it is well known that people underestimate the risk related to skin absorption.

Figures and tables

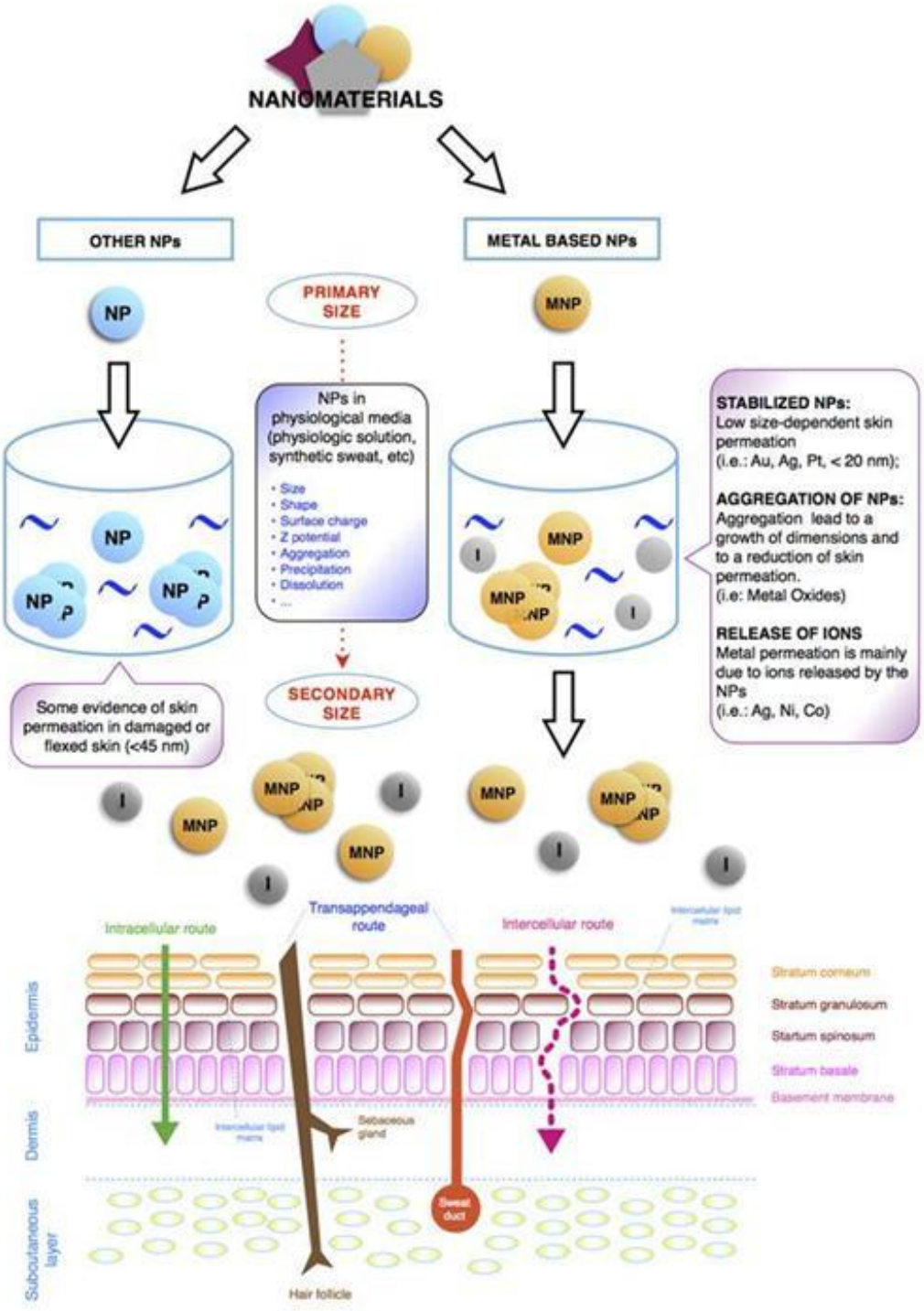

Figure N. 1 Skin absorption of nanomaterials. NP = nanoparticle (non metal), MNP = metal nanoparticles, I = ions released.

Table n. 1 Available data on QDs skin penetration and permeation

Authors	NPSs	Particles size (nm)	Particles shape	Skin type	Enhancement	Results
Ryman-Rasmussen 2006 [38]	QD-peg, amine, cooh	4.6 12 x 6	Spherical Elliptical	Porcine in vitro	-	Penetration: QD-peg, amine in E Permeation: QD-Cooh
Upadhyay et al. 2006 [80]	DT-QD-cooh	n.k.	nail-shaped	Mouse in vivo	Hypertermia	Penetration
Chu et al. 2007 [36]	QD-COOH	4.1	Spherical	Mouse in vitro and in vivo	-	Permeation
Mortensen et al. 2008, 2009 [81-82]	QD-COOH	20-33	Spherical	Mouse in vivo	- UV exposure	Low penetration but higher with UV exposure
Zhang et al. 2008 [26]	QD-peg	39 - 40	nail-shaped	Porcine in vitro	-	Penetration S.C.
Zhang and Monteiro-Riviere 2008 [31]	QD-COOH	4.6, 14 (H) 6 x 12, 18 (H)	Spherical Elliptical	Rat in vitro	- Flexion Tape-stripping Abrasion	No penetration No penetration No penetration Penetration
Gopee et al. 2009 [35]	QD peg	37	nail-shaped	Mouse in vivo	- Tape stripping Dermoabraded	No penetration No penetration Penetration
Gratieri et al. 2010 [83]	QD-COOH	4	spherical	Human in vitro	- Massage Tape stripping TS + massage	No penetration No penetration No penetration Penetration
Jeong 2010 et al. [84]	QD-peg-amine	7	spherical	Human in vivo Reconstructed human	occlusion -	Penetration S.C. Penetration S.C.
Ravichandran S. et al 2011[85]	QD ODA* capped	13.6 ± 0.4	n.k.	Human in vitro	Depilatory agent** Tape stripping	Penetration E. Penetration >> E
Prow 2012 et al. [86]	QD-peg, amine, cooh	35 (PEG) 14 (COOH) 15 (NH_2)	spherical	Human in vitro	- Tape stripping	Penetration of 35 PEG-QDs (PH 8.3) Penetration of all QDs types
Tang et al. 2013 [56]	QD-cooh	20	n.k.	Mouse in vivo	Shaved	Penetration Permeation
Wang et al. 2013 [57]	QD 630	24	n.k.	Mouse in vivo	-	Penetration at 8h – no penetration after 24 h
Mortensen et al. 2013 [38]	QD-cooh	14-15	spherical	Mouse in vivo	- UV exposure	Penetration and Permeation

E= epidermis, D= Dermis , S.C = stratum corneum, n.k. = not known, *ODA= octadecylamine, **containing thioglycolic acid, H = hydrodinamic diameter

Table n. 2 Titanium dioxide skin penetration studies

Authors	NPSs	Particles size (nm)	Skin type	Enhancement	Results
Tan et al. 1996 [87]	TiO_2	10-50	Human in vitro/ex vivo	Toluene	Penetration
Lademann et al. 1999 [88]	TiO_2	150-170	Human skin biopsy	-	No penetration
Bennat et al 2000 [89]	TiO_2	20	Human in vitro/in vivo	-	No penetration
Pflucker 2001 [90], Schulz 2002 [91]	TiO_2	20-100	Human in vivo	-	No penetration
Menzel 2004 [92]	TiO_2	Lanceolate shape 17-35 x 45-150	Porcine in vitro	-	Penetration
Kertész et al [93]	TiO_2	n.k.	Human grafts transplanted on SCID mouse	-	Penetration only in E
Gamer et al. 2006 [94]	TiO_2	30-60 x 10	Porcine in vitro	-	No penetration
Lekki et al. 2007 [95]	TiO_2	n.k.	Porcine and Human skin	Rubbed skin	No penetration
Kiss et al. 2008 [96]	TiO_2	Not specified	Human grafts on SCID mouse	-	No penetration
Mavon et al. 2007 [97]	TiO_2	20	Human in vitro and in vivo	-	No penetration
Pinheiro et al. 2007 [98]	TiO_2	Various size	Human in vivo	- Psoriatic	No penetration No penetration
Gontier et al. 2008 [99]	TiO_2	20-100	Porcine in vitro Human in vitro Human grafted on SCID mouse	- - -	No penetration No penetration No penetration
Zvyagin et al. 2008 [100]	TiO_2	20-70	Human in vitro	-	No penetration
Filipe et al. 2009 [101]	TiO_2	20	Human in vivo	-	No penetration
Wu et al 2009 [102]	TiO_2	Various sizes 4-10-25-60-90	Porcine in vitro Porcine in vivo	- Subcronic exp. 30 days	No penetration 4 nm: Penetration deep in E
Senzui et al.2010 [103]	TiO_2	35 coated	Porcine in vitro	- Tape stripping Hair removal	No penetration No penetration Penetration
Monteiro-Riviere 2011 [8]	TiO_2	fusiform shape 10 x 50	Porcine in vitro and in vivo	- UVB damaged	No penetration
Sadrieh et al. 2010 [75]	TiO_2	20-30 x 50-150 30-50 300-500	Porcine in vivo	Subcronic exp. 5 d/w for 20 days	No penetration
Bennett et al. 2012 [37]	TiO_2	27	Porcine in vitro	- photoinduced NPs disaggregation	No penetration Penetration

Miguel-Jeanjean et al. 2012 [104]	TiO_2	Needle-like 20-30 nm x 50-150	Porcine in vitro	- Damaged Irradiated Damaged+irradiated	No penetration No penetration No penetration No penetration
Adachi et al. 2013 [67]	TiO_2	Various size	Hairless rat in vivo	Subcronic exposure 56 days	No penetration

E = epidermis, SC = stratum corneum

Table n. 3 Skin penetration of metal oxides

Authors	NPSs	Particles size (nm)	Skin type	Enhancement	Results
Gamer et al. 2006 [94]	ZnO	80	Porcine in vitro	-	No penetration
Cross et al. 2007 [105]	ZnO	15 - 40	Human in vitro	-	No penetration
Zviagyn et al. 2008 [99]	ZnO	20 - 30	Human in vitro	-	No penetration
Roberts et al. 2008 [106]	ZnO	30	Human in vitro	-	No penetration
Durand et al. 2009 [107]	ZnO	< 200	Human in vitro	-	No penetration
Filipe et al.2009 [101]	ZnO	20-60	Human in vivo	-	No penetration
Kuo et al. 2009 [108]	ZnO	10	Mouse in vitro	Oleic acid + Ethanol	No penetration Penetration
Gulson et al. 2010 [69]	ZnO	19	Human in vivo	UVB damaged	Penetration
Szikszai et al. 2010 [109]	ZnO	80	Human in vitro	-	No penetration
Monteiro-Riviere 2011 [8]	ZnO	60-200 coated and uncoated	Porcine in vitro and in vivo	- UVB damaged	Penetration only in SC*
Baroli et al. 2007 [110]	Fe AOT coated Y-Fe_2O_3 TMAOH coated	5 6	Human in vitro	-	Penetration SC
Lee et al. 2010 [111]	Fe_3O_2	4-6-10	Mouse in vitro	Blade incision	Penetration
Van der Merwe et al. 2009 [112]	Magnesium oxide	7 x 100-200	Human in vitro	SLS	No penetration
Larese et al. [70]	Co_3O_4	30	Human in vitro	- Damaged skin	No penetration Penetration only in SC

*SC: stratum corneum, SLS: sodium lauryl sulphate, TMAOH-NPs: tetramethylammonium hydroxide, AOT: sodium bis (2-ethylhexyl) sulfosuccinate.

Table n. 4 Gold NPs skin penetration and permeation data

Authors	NPSs	Particles size (nm)	Skin type	Enhancement approach	Results
Sonavane et al. 2008 [34]	Au	15-102-198	Rat in vitro	-	Size dependent permeation
Graf et al. 2009 [112]	Au core/Si shell Si core/Au shell	94 -161 298	Human in vitro	-	Penetration SC
Huang et al. 2010 [114]	Au	5 (11.6 h.d.)	Mouse in vivo	-	Penetration
Seto et al. 2010 [115]	Au	4.6 ± 1.5 core (mean and SD) coated*	Human and Porcine in vitro Dermatomed	US and SLS	Penetration Penetration
Krishan et al. 2010 [116]	Au	10	Human in vitro	- Dermo asportation**	No penetration
Larese et al. 2011 [71]	Au	12.6	Human in vitro	- Dermal abrasion	Permeation Permeation
Labouta et al. 2011 [33]	Au	14.9 ± 1.8 in water 6.0 ± 0.8 in toluene	Human in vitro	- Toluene	No penetration Penetration in SC and E
Lee et al. 2013 [41]	Au nanorods	18 x 40 coated	HSEM in vitro Mouse in vitro	- -	Penetration of SC No penetration

*11-mercapto-1-undecanesulphonate ligand shell, ** by pulse electromagnetic field, US: ultrasound; SLS: sodium lauryl sulphate; h.d.: hydrodynamic diameter; HSEM: human skin equivalent model composed of multilayered human epidermal keratinocytes

Table n. 5 Silver NPs skin penetration and permeation data

Authors	NPSs	Particles size (nm)	Skin type	Enhancement approach	Results
Larese et al. 2007 [117]	Ag	9.8-48	Human in vitro	-	Metal penetration
Larese et al. 2009 [73]	Ag	25	Human in vitro	Intact and needle abraded skin	Penetration SC
Wijnhoven et al. 2009 [72]	Ag	various	Human in vivo	-	Metal penetration
Samberg et al. 2010 [118]	Ag	20-50	Porcine in vivo	Subchronic: 14 days	Penetration SC
Bianco et a. 2014 [119]	Ag	19	Human in vitro	Intact fresh, cryopreserved and glycerolized skin	Penetration

Table n. 6 In vitro skin permeation/penetration results of different metal NPs, using human skin

NPSs	Size (nm)	Concentration					Reference
		donor solution 24h (µg cm^{-2})	intact skin		damaged skin		
			receiving solution (ng cm^{-2})	skin (µg cm^{-2})	receiving solution (ng cm^{-2})	skin (µg cm^{-2})	
Ag	23	70	0.5	-	2.32	-	[73]
Au	12.6	15	60.8	-	55.2	-	[71]
Au	12.6	45	214	1.8	11.9	7.9	[71]
Co	80	1000	8.5	4.4	1870	12	[76]
Pd	13	600	98	0.7	1064	0.9	[120]
Rh	5.3	600	<LOD	0.4	760	7.4	[121]
Pt	5.8	600	<LOD	0.8	<LOD	1.7	[121]

Table n. 7 NPSs penetration, permeation and their hazard

NPSs	Critical size (nm)	Hazard	Penetration	Permeation	Possible mechanism
TiO_2	-	Very low?	No	No	-
ZnO	-	No	No	No	-
FeO	-	No	Yes	No	-
Au	12	No	Yes	Uncertain	-
Ag	70	Very low	Yes	Yes	Ions release
QDs (CdSe)	12	Possible	Yes	Yes	Cd release
Silica	42	Possible	Yes	No	To be studied
Co	80	Sensitizing	Yes	Yes	Ions release
Ni	77	Sensitizing	Yes	Yes	Ions release
Pd	13	Sensitizing	Yes	Yes	Ions release
Pt	5	Not known (no)	Very low (only in damaged skin)	No	-
Rh	5	Not known (no)	Very low (only in damaged skin)	No	-

Acknowledgments:

CEN WI001370xx - Workplace exposure - Guidance document of assessment of dermal exposure to manufactured nanoparticles.

Declaration of interest:

The authors report no conflicts of interest.

References

[1] Papakostas, D.; Rancan, F.; Sterry, W.; Blume-Peytavi, U.; Vogt, A. Nanoparticles in dermatology. Arch Dermatol Res. 2011, 303(8), 533-50.

[2] Baroli, B.; Ennas, M. G.; Loffredo, F.; Isola, M.; Pinna, R.; Lopez-Quintela, A. Penetration of metallic nanoparticles in human full-thickness skin. J. Invest. Dermatol. 2007, 127, 1701–1712.

[3] Crosera, M.; Bovenzi, M.; Maina, G.; Adami, G.; Zanette, C.; Florio, C.; Filon Larese, F. Nanoparticle dermal absorption and toxicity: a review of the literature. Int Arch Occup Environ Health. 2009, 82(9), 1043-55.

[4] Schneider, M.; Stracke, F.; Hansen, S.; Schaefer, U.F. Nanoparticles and their interactions with the dermal barrier. Dermatoendocrinol. 2009, 4, 197-206.

[5] Lane, M.E. Nanoparticles and the skin--applications and limitations. J Microencapsul. 2011, 28(8), 709-16.

[6] Poland, C.A.; Read, S.A.K.; Varet, J.; Carse, G.; Christensen, F.M.; Hankin, S.M. Dermal Absorption of Nanomaterials; Part of the "Better control of nano" initiative 2012-2015. The Danish Environmental Protection Agency. 2013. ISBN No.978-87-93026-50-6

[7] Monteiro-Riviere, N.A. Structure and Function of Skin. In: Toxicology of the Skin – Target Organ Series. (N. A. Monteiro-Riviere; Ed.); 2010.Vol. 29; Chap. 1; pp. 1-18. Informa Healthcare; New York; NY.

[8] Monteiro-Riviere, N.A.; Wiench, K.; Landsiedel, R.; Schulte, S.; Inman, A.O.; Riviere, J.E. Safety Evaluation of Sunscreen Formulations Containing Titanium Dioxide and Zinc Oxide Nanoparticles in UVB Sunburned Skin: An In Vitro and In Vivo Study. Toxicol Sci. 2011, 123(1), 264-80.

[9] Holbrook, K.A.; Odland, G.F. Regional differences in the thickness (cell layers) of the human stratum corneum: an ultrastructural analysis. J Invest Dermatol. 1974, 62(4), 415-22.

[10] Wolff-Schreiner, E. Ultrastructural cytochemistry of the epidermis. Int J Dermatol. 1977, 16, 77–102.

[11] Michaels, A.S.; Chandrasekaran, S.K.; Shaw. J. E. Drug permeation through human skin: Theory and in vitro experimental measurement. AIChE J. 1975, 21, 985–996.

[12] Elias, P.M. Epidermal lipids, barrier function and desquamation. J Invest Dermatol. 1983, 80 (suppl.), 44S – 9S.

[13] Scheuplein, R.J. Mechanism of percutaneous absorption. I. Routes of penetration and the influence of solubility. J. Invest Dermatol. 1965, 45, 334-46.

[14] Scheuplein, R.J. Mechanism of percutaneous absorption. II. Transient diffusion and the relative importance of various routes of skin penetration. J. Invest. Dermatol. 1967, 48, 79-88.

[15] Lademann, J.; Patzelt, A.; Richter, H.; Antoniou, C.; Sterry, W.; Knorr, F. Determination of the cuticula thickness of human and porcine hairs and their potential influence on the penetration of nanoparticles into the hair follicles. J Biomed Opt. 2009, 14 (2), 021014

[16] Blume-Peytavi, U.; Massoudy, L.; Patzelt, A.; Lademann, J.; Dietz, E.; Rasulev, U.; Garcia Bartels, N. Follicular and percutaneous penetration pathways of topically applied minoxidil foam. Eur J Pharm Biopharm. 2010, 76(3), 450–453.

[17] Knorr, F.; Lademann, J.; Patzelt, A.; Sterry, W.; Blume-Peytavi, U.; Vogt, A. Follicular transport route – research progress and future perspectives. Europ J Pharm Biopharm. 2009, 71, 173-180.

[18] Lademann, J.; Otberg, N.; Richter, H.; Weigmann, H.J.; Lindemann, U.; Schaefer, H.; Sterry, W. Investigation of follicular penetration of topically applied substances. Skin Pharmacol Appl Skin Physiol. 2001, 14(Suppl 1), 17–22.

[19] Rancan, F.; Gao, Q.; Graf, C.; Troppens, S.; Hadam, S.; Vogt, A. Skin penetration and cellular uptake of amorphous silica nanoparticles with variable size; surface functionalization and colloidal stability. ACS Nano. 2012, 8, 6829-684.

[20] Rancan, F.; Vogt, A. Getting under the skin: what is the potential of the transfollicular route in drug delivery? Ther Deliv. 2014, 5(8), 875-7.

[21] Elsner, P. Irritant dermatitis in the workplace. Dermatol. Clin. 1994, 12, 461–467.

[22] Fluhr, J.W.; Dickel, H.; Kuss, O.; Weyher, I.; Diepgen, T.L.; Berardesca, E.I. Impact of anatomical location on barrier recovery; surface ph and stratum corneum hydration after acute barrier disruption. Br. J . Dermatol. 2002, 146, 770-776.

[23] Kubo, A.; Nagao, K.; Armagal, M. Epidermal barrier dysfunction and cutaneous sensitization in atopic diseases. J Clin Inves.t 2012, 122, 440-447.

[24] Tinkle, S.S.; Antonini, J.M.; Rich, B.A.; Roberts, J.R.; Salmen, R.; DePree, K.; Adkins, E.J. Skin as a route of exposure and sensitization in chronic beryllium disease. Environ. Health Perspect. 2003, 111, 1202-1208.

[25] Rouse, J.G.; Yang, J.; Ryman-Rasmussen, J.P.; Barron, A.R.; Monteiro-Riviere, N.A. Effects of mechanical flexion on the penetration of fullerene amino acid-derivatized peptide nanoparticles through skin. Nano Lett. 2007, 7, 155-160.

[26] Zhang, L.W.; Yu, W.W.; Colvin, V.L.; Monteiro-Riviere, N.A. Biological interactions of quantum dot nanoparticles in skin and in human epidermal keratinocytes. Toxicol. Appl. Pharmacol. 2008. 228, 200-211.

[27] Ramos-e-Silva, M.; Jacques, Cd. Epidermal barrier function and systemic diseases. Clin Dermatol. 2012, 30(3), 277-9.

[28] Quandt, S.A.; Newman, J.C.; Pichardo-Geisinger, R.; Mora, D.C.; Chen, H.; Feldman, S.R.; Arcury, T.A. Self-reported skin symptoms and skin-related quality of life among latino immigrant poultry processing and other manual workers. Am J Ind Med. 2013. doi: 10.1002/ajim.22291.

[29] Oberdörster, G.; Maynard, A.; Donaldson, K.; Castranova, V.; Fitzpatrick, J.; Ausman, K.; Carter, J.; Karn, B.; Kreyling, W.; Lai, D.; Olin, S.; Monteiro-Riviere, N.; Warheit, D.; Yang, H.; ILSI Research Foundation/Risk Science Institute Nanomaterial Toxicity Screening Working Group. Principles for characterizing the potential human health effects from exposure to nanomaterials: elements of a screening strategy. Part Fibre Toxicol. 2005, 6, 2-8.

[30] Watkinson, A.C.; Bunge, A.L.; Hadgraft, J.; Lane, M.E. Nanoparticles do not penetrate human skin- a theoretical perspective. Pharm Res. 2013, 30(8), 1943-6.

[31] Zhang, L.W.; Monteiro-Riviere, N.A. Assessment of quantum dot penetration into intact; tape stripped; abraded and flexed rat skin. Skin Pharmacol. Physiol. 2008, 21, 166-180.

[32] Monteiro-Riviere, N.A. and Larese Filon, F. Effects of Engineered Nanomaterials on Skin. In Adverse Effects of Engineered Nanomaterials (Eds. B Fadeel; A. Pietroiusti; and A Shvedova); Elsevier; NY; 2012, Chapter 11; 185- 207.

[33] Labouta, H.I.; Schneider, M. Interaction of inorganic nanoparticles with the skin barrier: current status and critical review. Nanomedicine. 2013, 9(1), 39-54.

[34] Sonavane, G.; Tomoda, K.; Sano, A.; Ohshima, H.; Terada, H.; Makino, K. In vitro permeation of gold nanoparticles through rat skin and rat intestine: Effect of particle size. Colloids Surf. 2008, B 65, 1-10.

[35] Gopee, N.V.; Roberts, D.W.; Webb, P.; Cozart, C.R.; Siitonen, P.H.; Latendresse, J.R.; Warbitton, A.R.; Yu, W.W.; Colvin, V.L.; Walker, N.J.; Howard, P.C. Quantitative determination of skin penetration of PEG-coated CdSe quantum dots in dermabraded but not intact SKH-1 hairless mouse skin. Toxicol Sci. 2009, 111(1), 37-48.

[36] Chu, M.; Wu, Q.; Wang, J.; Hou, S.; Miao, Y.; Peng, J.; et al In vitro and in vivo transdermal delivery capacity of quantum dots through mouse skin. Nanotechnology. 2007, 18, 455103. doi:10.1088/0957-4484/18/45/455103.

[37] Bennett, S.W.; Zhou, D.; Mielke, R.; Keller, A.A. Photoinduced disaggregation of TiO_2 nanoparticles enables transdermal penetration. PLoS One. 2012, 7 (11), e48719. doi: 10.1371/journal.pone.0048719.

[38] Ryman-Rasmussen, J.P.; Riviere, J.E.; Monteiro-Riviere, N.A. Penetration of intact skin by quantum dots with diverse physicochemical properties. Toxicol. Sci. 2006, 91, 159–165.

[39] Mortensen, L.J.; Jatana, S.; Gelein, R.; De Benedetto, A.; De Mesy Bentley, K.L.; Beck, L.A.; Elder, A.; Delouise, L.A. Quantification of quantum dot murine skin penetration with UVR barrier impairment. Nanotoxicology. 2013, 7(8), 1386-98.

[40] Leroueil, P.R.; Hong, S.; Mecke, A.; Baker, J.R. Jr; Orr, B.G.; Banaszak Holl, M.M. Nanoparticle interaction with biological membranes: does nanotechnology present a Janus face? Acc Chem Res. 2007, 40(5), 335-42.

[41] Lee, O.; Jeong, S.H.; Shin, W.U.; Lee, G.; Oh, C.; Son, S.W. Influence of surface charge of gold nanorods on skin penetration. Skin Res Technol. 2013, 19(1), e390-6.

[42] Kim, B.; Han, G.; Toley, B.J.; Kim, C.K.; Rotello, V.M.; Forbes, N.S. Tuning payload delivery in tumour cylindroids using gold nanoparticles. Nat Nanotechnol, 2010, 5(6), 465-72.

[43] Hsieh, S.F.; Bello, D.; Schmidt, D.F.; Pal, A.K.; Rogers, E.J. Biological oxidative damage by carbon nanotubes: fingerprint or footprint? Nanotoxicology. 2012, 6 (1), 61-76.

[44] Altunbek, M.; Baysal, A.; Çulha, M. Influence of surface properties of zinc oxide nanoparticles on their cytotoxicity. Colloids Surf B Biointerfaces. 2014, 1, 121:106-13. doi: 10.1016/j.colsurfb.2014.05.034.

[45] Meding, B. Differences between the sexes with regard to work-related skin diseases. Contact Dermatitis. 2000, 43, 65-71.

[46] Dickel, H.I.; Kuss, O.; Schmidt, A.; Kretz, J.; Diepgen, T.L. Importance of irritant contact dermatitis in occupational skin disease. Am J Clin Dermatol. 2002, 3 (4), 283-9.

[47] Pichardo-Geisinger, R.; Muñoz-Ali, D.; Arcury, T.A.; Blocker, J.N.; Grzywacz, J.G.; Mora, D.C.; Chen, H.; Schulz, M.R.; Feldman, S.R.; Quandt, S.A. Dermatologist-diagnosed skin diseases among immigrant Latino poultry processors and other manual workers in North Carolina; USA. Int J Dermatol. 2013, 52(11), 1342-8.

[48] Eedy, D.J. Carbon fibre induced airborne irritant contact dermatitis. Contact Dermatitis 1996, 35, 362-363.

[49] Ema, M.; Matsuda, A.; Kobayashi, N.; Naya, M.; Nakanishi, J. Dermal and ocular irritation and skin sensitization studies of fullerene C60 nanoparticles. Cutan Ocul Toxicol. 2013, 32(2), 128-34.

[50] Kishore, A.S.; Surekha, P.; Murthy, P.B. Assessment of the dermal and ocular irritation potential of multi-walled carbon nanotubes by using in vitro and in vivo methods. Toxicol. Lett. 2009, 191, 268-274.

[51] Journeay, W.S.; Goldman, R.H. Occupational handling of nickel nanoparticles: a case report. Am J Ind Med. 2014, 57(9), 1073-6.

[52] Vermula, P.K.; Anderson, R.R.; Karp, J.M. Nanoparticles reduce nickel allergy by capturing metal ions. Nat. Nanotechnol. 2011, 5, 291-5.

[53] Degim, I.T.; Burgess, D.J.; Papadimitrakopoulos, F. Carbon nanotubes for transdermal drug delivery. J Microencapsul. 2010, 27(8), 669-81.

[54] Xia, X.R.; Monteiro-Riviere, N.A.; Riviere, J.E. Skin penetration and kinetics of pristine fullerenes (C60) topically exposed in industrial organic solvents. Toxicol. Appl. Pharmacol. 2010, 242, 29-37.

[55] Kato, S.; Aoshima, H.; Saitoh, Y.; Miwa, N. Biological safety of LipoFullerene composed of squalane and fullerene-C60 upon mutagenesis; photocytotoxicity; and permeability into the human skin tissue. Basic Clin Pharmacol Toxicol. 2009, 104(6), 483-7.

[56] Tang, L.; Zhang, C.; Song, G.; Jin, X.; Xu, Z. In vivo skin penetration and metabolic path of quantum dots. Sci China Life Sci. 2013, 56(2), 181-8.

[57] Wang, L.; Qin, G.; Geng, S.; Dai, Y.; Wang, J.Y. Preparation of zein conjugated quantum dots and their in vivo transdermal delivery capacity through nude mouse skin. J Biomed Nanotechnol. 2013, 9(3), 367-76.

[58] Alvarez-Román, R.; Naik, A.; Kalia, Y.N.; Guy, R.H.; Fessi, H. Skin penetration and distribution of polymeric nanoparticles. J Control Release. 2004, 99(1), 53-62.

[59] Vogt, A.; Combadiere, B.; Hadam, S.; Stieler, K.M.; Lademann, J.; Schaefer, H.; Autran, B.; Sterry, W.; Blume-Peytavi, U. 40 nm, but not 750 or 1,500 nm nanoparticles enter epidermal CD1a+ cells after transcutaneous application on human skin. J Invest Dermatol. 2006, 126(6),1316-22.

[60] Mahe, B.; Vogt, A.; Liard, C.; Duffy, D.; Abadie, V.; Bonduelle, O.; Boissonnas, A.; Sterry, W.; Verrier, B.; Blume-Peytavi, U.; Combadiere, B. Nanoparticle-based targeting of vaccine compounds to skin antigen-presenting cells by hair follicles and their transport in mice. J Invest Dermatol. 2009, 129(5), 1156-64.

[61] Wu, X.; Landfester, K.; Musyanovych, A.; Guy, R.H. Disposition of charged nanoparticles after their topical application to the skin. Skin Pharmacol Physiol. 2009, 23(3), 117-23.

[62] Campbell, C.S.; Contreras-Rojas, L.R.; Delgado-Charro, M.B.; Guy, R.H. Objective assessment of nanoparticle disposition in mammalian skin after topical exposure. J Control Release. 2012, 162(1), 201-7.

[63] Hirai, T.; Yoshikawa, T.; Nabeshi, H.; Yoshida, T.; Akase, T.; Yoshioka, Y.; Itoh, N.; Tsutsumi, Y. Dermal absorption of amorphous nanosilica particles after topical exposure for three days. Pharmazie. 2012, 67(8), 742-3.

[64] Staroňová, K.; Nielsen, J.B.; Roursgaard, M.; Knudsen, L.E. Transport of SiO_2 nanoparticles through human skin. Basic Clin Pharmacol Toxicol. 2012. 111(2), 142-4.

[65] Ostrowski, A.; Nordmeyer, D.; Boreham, A.; Brodwolf, R.; Mundhenk, L.; Fluhr, J.W.; Lademann, J.; Graf, C.; Rühl, E.; Alexiev, U.; Gruber, A.D. Skin barrier disruptions in tape stripped and allergic dermatitis models have no effect on dermal penetration and

systemic distribution of AHAPS-functionalized silica nanoparticles. Nanomedicine. 2014, 10(7), 1571-81.

[66] Faunce, T.; Murray, K.; Nasu, H.; Bowman, D. Sunscreen safety: the precautionary principle; the Australian Therapeutic Goods Administration and nanoparticles in sunscreens. Nanoethics 2008, 2, 231-240.

[67] Adachi, K.; Yamada, N.; Yoshida, Y.; Yamamoto, O. Subchronic exposure of titanium dioxide nanoparticles to hairless rat skin. Exp Dermatol. 2013, 22(4), 278-83.

[68] Jonaitis, T.S.; Card, J.W.; Magnuson, B. Concerns regarding nano-sized titanium dioxide dermal penetration and toxicity study. Toxicol Lett. 2010, 192(2), 268-9.

[69] Gulson, B.; McCall, M.; Korsch, M.; Gomez, L.; Casey, P.; Oytam, Y.; Taylor, A.; McCulloch, M.; Trotter, J.; Kinsley, L.; Greenoak, G. Small amounts of zinc from zinc oxide particles in sunscreens applied outdoors are absorbed through human skin. Toxicol. Sci. 2010, 118(1), 140-149.

[70] Larese, F.; Crosera, M.; Mauro, M.; Bianco, C.; Adami, G.; Bovenzi, M. Human skin penetration of cobalt oxide nanoparticles through intact and damaged skin. Nanotox - International Nanotoxicology Congress. 23th -26th April 2014; Antalya; Turkey; pag 103

[71] Larese Filon, F.; Crosera, M.; Adami, G.; Bovenzi, M.; Rossi, F.; Maina, G. Human skin penetration of gold nanoparticles through intact and damaged skin. Nanotoxicology 2011, Early online 1-9 DOI 10.3109/ 1743390. 2010.551428.

[72] Wijnhoven, S.W.P.; Peijnenburg, W.J.G.M.; Herberts, C.A.; Hagens, W.I.; Oomen, A.G.; Heugens, E.H.W.; Roszek, B.; Bisschops, J.; Gosens, I.; Van De Meent, D.; Dekkers, S.; De Jong, W.H.; Van Zijverden, M.; Sips, A.J.A.M.; Geertsma, R.E. Nano-silver: a review of available data and knowledge gaps in human and environmental risk assessment. Nanotoxicology 2009, 3(2), 109-138.

[73] Larese Filon, F.; D'Agostin, F.; Bovenzi, M.; Crosera, M.; Adami, G.; Romano, C.; Maina, G. Human skin penetration of silver nanoparticles through intact and damaged skin. Toxicol. 2009, 255, 33-37.

[74] Bianco, C.; Adami, G.; Crosera, M.; Larese, F.; Casarin, S.; Castagnoli, C.; Stella, M.; Maina, G. Silver percutaneous absorption after exposure to silver nanoparticles: a comparison study of three human skin graft samples used for clinical applications. Burns 2014, 40(7), 1390-6.

[75] Sadrieh, N.; Wokovich, A.M.; Gopee, N.V.; Zheng, J.; Haines, D.; Parmiter, D.; Siitonen, P.H.; Cozart, C.R.; Patri, A.K.; McNeil, S.E.; Howard, P.C.; Doub, W.H.; Buhse, L.F. Lack of significant dermal penetration of titanium dioxide from sunscreen formulations containing nano- and submicron-size TiO2 particles. Toxicol Sci. 2010, 115(1), 156-66.

[76] Larese Filon, F.; Crosera, M.; Timeus, E.; Adami, G.; Bovenzi, M.; Ponti, J.; Maina, G. Human skin penetration of cobalt nanoparticles through intact and damaged skin. Toxicol In Vitro. 2013, 27(1), 121-7.

[77] Gulson, B.; Wong, H.; Korsch, M.; Gomez, L.; Casey, P.; McCall, M.; McCulloch, M.; Trotter, J.; Stauber, J.; Greenoak, G. Comparison of dermal absorption of zinc from different sunscreen formulations and differing UV exposure based on stable isotope tracing. Sci Total Environ. 2012, 420, 313-8.

[78] Journeay, W.S. and Goldman, R.H. Occupational handling of nickel nanoparticles: a case report. A J Indust Med 2014, doi: 10.1002/agim.22344.

[79] Franz, T.J. Percutaneous absorption on the relevance of in vitro data. J Invest Dermatol. 1975, 64(3), 190-5.

[80] Upadhyay, P. Enhanced transdermal-immunization with diptheria-toxoid using local hyperthermia. Vaccine. 2006, 24(27-28), 5593-8.

[81] Mortensen, L.J.; Oberdörster, G.; Pentland, A.P.; Delouise, L.A. In vivo skin penetration of quantum dot nanoparticles in the murine model: the effect of UVR. Nano Lett. 2008, 8(9), 2779-87.

[82] Mortensen, L.; Zheng, H.; Faulknor, R.; De Benedetto, A.; Beek, L.; DeLouise, L.A. Increased in vivo skin penetration of quantum dots with UVR and in vitro quantum dots cytotoxicity. From Conference Volume 7189. Proc. SPIE 7189; Colloidal Quantum Dots for Biomedical Applications IV; 718919-12 (March 03; 2009); doi:10.1117/12.809215

[83] Gratieri, T.; Schaeter, U.F.; Jing, L.; Gao, M.; Lopez, R.F.V; Schneider, M. Penetration of quantum dot particles through human skin. J Biomed Nanotechnol. 2010, 6, 586-95.

[84] Jeong, S.H.; Kim, J.H.; Hi, S.M.; Lee, J.P.; Sohn, K.H. Assessment of penetration of quantum dots through in vitro and in vivo human skin using the human skin equivalent model and the tape stripping method. Biochem Biophys Research Commun. 2010, 394, 612-5.

[85] Ravichandran, S.; Mortensen, L.J.; DeLuise, L.A. Quantification of human skin barrier function and susceptibility to quantum dot skin penetration. Nanotoxicology. 2011, 5 (4), 675-86.

[86] Prow, T.W.; Monteiro-Riviere, N.A.; Inman, A.O.; Grice, J.E.; Chen, X.; Zhao, X.; Sanchez, W.H.; Gierden, A.; Kendall, M.A.; Zvyagin, A.V.; Erdmann, D.; Riviere, J.E.; Roberts, M.S. Quantum dot penetration into viable human skin. Nanotoxicology. 2012, 6(2), 173-85.

[87] Tan, M.H.; Commens, C.A.; Bumett, L.; Snitch, P.J.. A pilot study on the percutaneous absorption of microfine titanium dioxide from sunscreens. Australian J Dermatol. 1996, 37, 185-7.

[88] Lademann, J.; Weigmann, H.; Rickmeyer, C.; Barthelmes, H.; Schaefer, H.; Mueller, G.; Sterry, W. Penetration of titanium dioxide microparticles in a sunscreen formulation into the horny layer and the follicular orifice. Skin Pharmacol Appl Skin Physiol. 1999, 12(5), 247-56.

[89] Bennat, C.; Müller-Goymann, C.C. Skin penetration and stabilization of formulations containing microfine titanium dioxide as physical UV filter. Int J Cosmet Sci. 2000, 22(4), 271-83.

[90] Pflücker, F.; Wendel, V.; Hohenberg, H.; Gärtner, E.; Will, T.; Pfeiffer, S.; Wepf, R.; Gers-Barlag, H. The human stratum corneum layer: an effective barrier against dermal uptake of different forms of topically applied micronised titanium dioxide. Skin Pharmacol Appl Skin Physiol. 2001, 14 Suppl 1, 92-7.

[91] Schulz, J.; Hohenberg, H.; Pflücker, F.; Gartner, E.; Will, T.; Pfei Ver, S.; Wepf, R.; Wendel, V.; Gers-Barlag, H.; Wittern, K.P. Distribution of sunscreens on skin. Adv. Drug Deliv. Rev. 2002, 54 (S1), S157–S163..

[92] Menzel, F.; Reinert, T.; Vogt, J.; Butz, T. Investigations of percutaneous uptake of ultrafine TiO2 particles at the high energy ion nanoprobe LIPSION. Nuclear Instruments and Methods in Physics Research Section B: Beam Interactions with Materials and Atoms 2004, 219-220, 82-86.

[93] Kertész, Z.; Szikszai, Z.; Gontier, E.; Moretto, P.; Surlève-Bazeillec, G.E.; Kissd, B.; Juhászd, I.; Hunyadid, J.; Kissa, Á.Z. Nuclear microprobe study of TiO2-penetration in the epidermis of human skin xenografts. Nuclear Instruments and Methods in Physics Research Section B: Beam Interactions with Materials and Atoms. 2005, Volume 231; Issues 1–4; Pages 280–285.

[94] Gamer, A.D.; Leibolt, E.; van Ravenzwaay, B. The in-vitro absorption of microfine zinc oxide and titanium dioxide through porcine skin. Toxicol in vitro 2006, 20, 301-307.

[95] Lekki, J.; Stachura, Z.; Dabroś, W.; Stachura, J.; Menzel, F.; Reinert, T.; Butz, T.; Pallon, J.; Gontier, E.; Ynsa, M.D. et al. On the follicular pathway of percutaneous uptake of nanoparticles: ion microscopy and autoradiography studies. Nucl. Instrum. Methods Phys. Res. B. 2007, 260, 174–177.

[96] Kiss, B.; Bíró, T.; Czifra, G.; Tóth, B.I.; Kertész, Z.; Szikszai, Z.; Kiss, A.Z.; Juhász, I.; Zouboulis, C.C.; Hunyadi, J. Investigation of micronized titanium dioxide penetration in human skin xenografts and its effect on cellular functions of human skin-derived cells. Exp Dermatol. 2008, 17(8), 659-67.

[97] Mavon, A.; Miquel, C.; Lejeune, O.; Payre, B.; Moretto, P. In vitro percutaneous absorption and in vivo stratum corneum distribution of an organic and mineral sunscreen. Skin Pharmacol. Physiol. 2007, 20, 10-20.

[98] Pinheiro, T.; Pallon, J.; Alves, L.C.; Verissimo, A.; Filipe, P.; Silva, J.N.; Silva, R. The influence of corneocyte structure on the interpretation of permeation profiles of nanoparticles across the skin. Nuclear instrument Meth. Phys. Res. B. 2007, 260, 119-23.

[99] Gontier, E.; Ynsa, M.D.; Bíró, T.; Hunyadi, J.; Kiss, B.; Gáspár, K.; Pinheiro, T.; Silva, J.N.; Filipe, P.; Stachura, J.; Dabros, W.; Reinert, T.; Butz, T.; Moretto, P. and Surlève-Bazeille, J.E. Is there penetration of titania nanoparticles in sunscreens through skin? A comparative electron and ion microscopy study. Nanotoxicology. 2008, 2 (4); 218-231.

[100] Zvyagin, A.V.; Zhao, X.; Gierden, A.; Sanchez, W.; Ross, J.A.; Roberts, M.S. Imaging of zinc oxide nanoparticle penetration in human skin in vitro and in vivo. J Biomed Opt. 2008, 13(6), 064031. doi: 10.1117/1.3041492.

[101] Filipe, P.; Silva, J.N.; Silva, R.; Cirne de Castro, J.L.; Marques Gomes, M.; Alves, L.C.; Santus, R.; Pinheiro, T. Stratum corneum is an effective barrier to TiO2 and ZnO nanoparticle percutaneous absorption. Skin Pharmacol Physiol. 2009, 22 (5), 266-75.

[102] Wu, J.; Liu, W.; Xue, C.; Zhou, S.; Lan, F.; Bi, L.; Xu, H.; Yang, X.; Zeng, F.D. Toxicity and penetration of TiO2 nanoparticles in hairless mice and porcine skin after subchronic dermal exposure. Toxicol Lett. 2009, 191(1), 1-8.

[103] Senzui, M.; Tamura, T.; Miura, K.; Ikarashi, Y.; Watanabe, Y.; Fuji, M. Study on penetration of titanium dioxide (TiO2) nanoparticles into intact and damaged skin in vitro. J Toxicol Sci 2010, 35, 107- 13.

[104] Miquel-Jeanjean. C.; Crépel, F.; Raufast, V.; Payre, B.; Datas, L.; Bessou-Touya, S.; Duplan, H. Penetration study of formulated nanosized titanium dioxide in models of damaged and sun-irradiated skins. Photochem Photobiol. 2012, 88(6), 1513-21.

[105] Cross, S. E.; Innes, B.; Roberts, M.; Tsuzuki, T.; Robertson, T. A.; McCormick, P.. Human skin penetration of sunscreen nanoparticles: In-vitro assessment of a novel micronized Zinc Oxide formulation. Skin Pharmacol. Physiol. 2007, 20, 148-154.

[106] Roberts, M.S.; Roberts, M.J.; Robertson, T.A.; Sanchez, W.; Thorling, C.; Zhou, Y. In vitro and in vivo imaging of xenobiotic transport in human skin and in the rat liver. J Biophotonics 2008, 1, 478-93.

[107] Durand, L.; Habran, N.; Henschel, V.; Amighi, K. In vitro evaluation of the cutaneous penetration of sprayable sunscreen emulsions with high concentrations of UV filters. Int J Cosmet Sci. 2009, 31(4), 279-92.

[108] Kuo, T.R.; Wu, C.L.; Hsu, C.T.; Lo, W.; Chiang, S.J.; Lin, S.J. et al. Chemical enhancer induced changes in mechanism of transdermal delivery of zinc oxide nanoparticles. Biomaterials 2009, 30, 3002-8.

[109] Szikszai, Z.; Kertész, Z.; Bodnár, E.; Majora, I.; Borbíróc, I.; Kissa, A.Z.; Hunyadi, J. Nuclear microprobe investigation of the penetration of ultrafine zinc oxide into

intact and tape-stripped human skin. Nuclear Instruments and Methods in Physics Research Section B: Beam Interactions with Materials and Atoms. 2010, 268 (11–12), 2160–2163.

[110] Baroli, B.; Ennas, M.G.; Loffredo, F.; Isola, M.; Pinna, R.; López-Quintela, M.A. Penetration of metallic nanoparticles in human full-thickness skin. J Invest Dermatol. 2007, 127(7), 1701-12.

[111] Lee, S.E.; Choi, K.J.; Menon, G.K.; Kim, H.J.; Choi, E.H.; Ahn, S.K.; Lee, S.H. Penetration pathways induced by low-frequency sonophoresis with physical and chemical enhancers: iron oxide nanoparticles versus lanthanum nitrates. J Invest Dermatol 2010, 130, 1063-72.

[112] van der Merwe, D.; Tawde, S.; Pickrell, J.A.; Erickson, L.E. Nanocrystalline titanium dioxide and magnesium oxide in vitro dermal absorption in human skin. Cutan Ocul Toxicol. 2009, 28(2), 78-82.

[113] Graf, C.; Meinke, M.; Gao, Q.; Hadam, S.; Raabe, J.; Sterry, W.; Blume-Peytavi, U.; Lademann, J.; Rühl, E.; Vogt, A. Qualitative detection of single submicron and nanoparticles in human skin by scanning transmission x-ray microscopy. J Biomed Opt. 2009, 14(2), 021015.

[114] Huang, Y.; Yu, F.; Park, Y.S.; Wanh, J.; Shin, M.C.; Chung, H.S.; Yang, V.C. Coadministration of protein drugs with gold nanoparticles to enable percutaneous delivery. Biomaterials 2010, 31(34), 9086-91.

[115] Seto, J.E.; Polat, B.E.; Lopez, R.F.V.; Blankschtein, D.; Langer, R. Effects of ultrasound and sodium lauryl sulphate on the transdermal delivery of hydrophilic permeants: comparative in vitro studies with full-thickness and split-thickness pig and human skin. J Control Release 2010, 145, 26-32.

[116] Krishnan, G.; Edwards, J.; Chen, Y.; Benson, H.A. Enhanced skin permeation of naltrexone by pulsed electromagnetic fields in human skin in vitro. J Pharm Sci. 2010, 99(6), 2724-31.

[117] Filon, F.L.; D'Agostin, F.; Crosera, M.; Adami, G.; Rosani, R.; Romano, C.; Bovenzi, M.; Maina, G. [In vitro percutaneous absorption of silver nanoparticles]. G Ital Med Lav Ergon. 2007, 29(3 Suppl), 451-2.

[118] Samberg, M.E.; Oldenburg, S.J.; Monteiro-Riviere, N.A. Evaluation of silver nanoparticle toxicity in skin in vivo and keratinocytes in vitro. Environ Health Perspect. 2010, 118(3), 407-13.

[119] Bianco, C.; Adami, G.; Crosera, M.; Larese, F.; Casarin, S.; Castagnoli, C.; Stella, M.; Maina, G. Silver percutaneous absorption after exposure to silver nanoparticles: a comparison study of three human skin graft samples used for clinical applications. Burns 2014. 40(7), 1390-6.

[120] Larese Filon, F.; Crosera, M.; Adami, G.; Comiati,; Bovenzi M; Maina G. Skin absorption of palladium nanoparticles: a new possible risk in the nanotechnology industry. 6th International Conference on Occupational and Environmental Skin to Chemicals; 2nd - 3rd June 2014; Amsterdam; Pag. 88.

[121] Larese Filon, F.; Mauro, M.; Crosera, M.; Bovenzi, M. Poster: "Platinum and Rhodium nanoparticles skin absorption" Thematic workshop on Toxicology related topics eco- nano-; University of Nova Gorica; 13th -14th June 2013.